Park optimization and wake interaction study at Bockstigen offshore wind power plant

Dissertation in partial fulfilment of the requirements for the degree of

MASTER OF SCIENCE WITH A MAJOR IN ENERGY TECHNOLOGY WITH FOCUS ON WIND POWER

UPPSALA
UNIVERSITET

Dept. of Earth Sciences, Campus Gotland
Uppsala University

Jan Borràs Morales

9 February 2015

PARK OPTIMIZATION AND WAKE INTERACTION STUDY AT BOCKSTIGEN OFFSHORE WIND POWER PLANT

Dissertation in partial fulfilment of the requirements for the degree of

MASTER OF SCIENCE WITH A MAJOR IN ENERGY TECHNOLOGY WITH FOCUS ON WIND POWER

Uppsala University
Department of Earth Sciences, Campus Gotland

Approved by:

Supervisor, Stefan Ivanell

Examiner, Simon-Philippe Breton

9 February 2015

Abstract

Losses for wake effects in offshore wind farms represent about 10% to 20% of the park annual energy production. Several analytical wake models have been developed and implemented to predict the power deficit of a wake-affected wind turbine. Validating and parameterizing the wake models available in the industry is essential to better predict the wake losses and thus maximize the energy yield of future offshore developments.

In this study, a wake model validation is undertaken for the three models available in the commercial software WindSim. Data from Horns Rev wind farm is used to that purpose. Next, the models that show the best agreement with the observations are parameterized to better describe the power losses of a future offshore wind farm at Bockstigen. To finish with, an optimization sensitivity study is carried out and a final optimal layout is determined according to the seabed depth.

Key words: Wake, Wind power, Offshore, Analytical models, Experimental validation, Atmospheric stability, Layout optimization.

Acknowledgements

This work could never have been completed without the generous help and guidance of several professionals connected to Uppsala University, the Danish Technical University, and WindSim AS; nor without the interest and economical support of Bockstigen AB.

First of all, I would like to truly thank Andreas Wickman, a talented professional and enthusiastic entrepreneur, who quickly showed interest on doing this study, and allocated funds for a scholarship to support it. I am also indebted to Hans Bergström, who provided crucial data on wind resource assessment, and gave me priceless support and generous explanations, being always easy to reach.

Next, I would like to thank my supervisor Stefan Ivanell for his guidance and enthusiasm for this project. Although he is a very busy man, he always managed to have few minutes of concise feedback. I also thank Kurt S. Hansen for his explanations and to provide me with the useful AMOK tool, and Jens N. Sørensen for his enlightening guidance at an early stage of the project.

I wish to express my best gratitude and appreciation to Arne R. Gravdahl for giving me the opportunity to do an internship at WindSim AS headquarters, and to make me feel as a crew member during my stay. I feel sincerely grateful to Bele, Di, Matteo, Rui, and to the rest of WindSim team, who showed unlimited support while using their software and gave me priceless guidance in order to deliver the best output of this project.

I will always be indebted to Nikos for his enthusiastic feedback and empowering support. He is not only a bright mind but also a close, cheerful friend. Thanks for being there during those difficult moments. You can't imagine how much it meant to me!

Last, but not least, and from the bottom of my heart, I would like to give the warmest embrace to my family for their unconditional support, and especially to my grandma who at her 90s gladly offered me her new laptop to run some simulations.

Table of Contents

Abstract i

Acknowledgements ii

List of Figures v

List of Tables xii

1. Introduction 1

2. Literature review 1
   - 2.1. Atmospheric Stability 5
   - 2.2. Atmospheric turbulence and Turbulent Kinetic Energy 7
   - 2.3. Sea roughness 10
   - 2.4. Analytical wake models implemented in WindSim 11
   - 2.5. Adjustments of the wake decay constant 15

Part I. Bockstigen offshore wind farm 18

3. Introduction to Bockstigen offshore wind farm 18

4. Methodology – Wind resource assessment and wake analysis 21
   - 4.1. Data filtering and recorded periods 21
   - 4.2. WindSim modelling of Bockstigen 23

5. Results – Wind resource assessment and wake analysis 25
   - 5.1. Havsmast dataset 25
   - 5.2. Kustmast dataset 35
   - 5.3. Correlation Havsmast–Kustmast 36
   - 5.4. Long-term predicted climatology at Bockstigen 39
   - 5.5. Wind turbine classification 43
   - 5.6. Power performance and wake effects at Bockstigen 45

6. Discussion – Data not valid for wake models validation 48

Part II. Wake models validation at Horns Rev 49

7. Introduction to Horns Rev wind farm 49

8. Methodology – Wake models validation 53
   - 8.1. Simulation cases 53
   - 8.2. WindSim modeling set-up 54

9. Results – Wake models validation 59
   - 9.1. Results case 270° with 7D spacing 59
   - 9.2. Results case 221° with 9,4D spacing 65
   - 9.3. Results case 312° with 10,4D spacing 68

10. Discussion 71

Part III. Bockstigen layout optimization 73

11. Introduction – Layout optimization 73

12. Methodology – Layout optimization 75

  12.1. Parameterization optimisation for the 1st turbine downwind 75
  12.2. Directrices with maximum and minimum energy content 77
  12.3. Effect of spacing distance inside an array 79
  12.4. Downwind separation distance 80
  12.5. Effect of staggering 81

13. Results – Optimized layout 83

14. Discussion – Optimized layout 85

15. Conclusions 89

16. References 91

Annex I – Perl code of filtering script 95

Annex II – Sea temperature fluctuation event 97

Annex III – Roughness classification tables 100

Annex IV – Sector-wise correlation between Havsmast and Kustmast 101

Annex V – Modifying the Q1 file 103

Annex VI – Results analytical models: Case 270° with 7D spacing. 104

Annex VII – Results analytical models: Case 221° with 9,4D spacing. 111

Annex VIII – Results analytical models: Case 312° with 10,4D spacing. 118

Annex IX – Power Deficit at the 1st turbine downwind 125

Annex X – Simulated and experimental vertical wind profiles at Bockstigen 127

List of Figures

Figure 1. Conceptual structure of a wake, defining the near, intermediate and far wake regions. Source: Moskalenko et al. (2010). 3

Figure 2. Power deficit distribution as function of normalized wind direction for 7D spacing. The wake centreline is at 0º, which corresponds to a wind direction of 270º. Source: Risø Final Report WP8, Barthelmie et al. (2011). 4

Figure 3. Turbulence intensity measured from cup anemometers at 60 m.a.s.l. at Horns Rev and its related turbulent Kinetic Energy. Source: Hasager et al., *12MW Horns Rev experiment*, (2007) 8

Figure 4. Evolution with the distance of the total turbulence intensity at hub height though a large wind farm cluster. The straight line shows the calculated value for an infinitely large wind farm. Source: (Vermeer et al., 2003). 9

Figure 5. Added turbulence intensity I_{add} calculated from three experimental models (see legend) and compared to experimental measurements. Source: (Vermeer et al., 2003). 10

Figure 6. Mean Monin-Obukhov length, mean friction velocity, wind speed at 15 m high, and mean roughness length calculated for different stability classes at Horns Rev. Source: (Peña and Gryning, 2008). 11

Figure 7. Schematic definition of Jensen's wake model and its parameters (Katic et al. 1986). 11

Figure 8. Coordinate system and basic variables of Larsen's wake model. x is the stream direction, x_0 the turbine rotor position, and r the radius inside a wake section. The wake boundary is proportional to $x^{\frac{1}{3}}$. Source: (Larsen, 1988). 13

Figure 9. In-wake vertical velocity profiles for 2D, 4D, 6D and 8D downwind. The results obtained for Ishihara's model (red), Larsen's (yellow), and Jensen's (green) are plotted next to the experimental data (blue triangles). Source: (Ishihara et al., 2004). 15

Figure 10. Velocity deficit (left) and wake decay constant k (right) at 7D downwind for several stabilities h/L and roughness lengths: $z_0 = 0{,}0002$ (circles), $z_0 = 0{,}002$ (diamonds), $z_0 = 0{,}002$ (crosses), $z_0 = 0{,}2$ (squares). Source: (Peña and Rathmann, 2013). 15

Figure 11. Simulation of the planetary boundary layer (PBL) height, wind speed at hub height, and wind farm roughness length for an offshore cluster. Source: (Barthelmie et al., 2011). 16

Figure 12. Power deficit 3,8D, 7D and 10,4D downstream as a function of turbulence intensity. Source: Risø Final Report WP8, Barthelmie et al. (2011). 17

Figure 13. Situation map of Näsudden cape in the island of Gotland, Sweden, (left) and the location of Bockstigen offshore wind farm 4,6 km in front of Näsudden cape (right). Source: (Ronsten et al., 2000). 18

Figure 14. Park layout with five turbines in V and the met mast 'havsmast' in the centre. 19

Figure 15. Overhead view of Bockstigen offshore wind farm and Näsudden cape. Photo: Gunnar Britse. 20

Figure 16. Boundary layer depth over the Baltic sea. Bullets show the observations with radiosoundings. Source: (Hasager et al., 2007). 21

Figure 17. Screenshot of Havsmast raw dataset with consecutive writing errors on the day 2002-9-03 starting at 00:50 hours. 22

Figure 18. Data coverage of Havsmast, Kustmast and power output per turbine after filtering. 23

Figure 19. The blue guidelines define the undisturbed wind sectors. 26

Figure 20. Overview of Havsmast wake-affected sectors, directions of wake centrelines and the park layout. 27

Figure 21. Monthly recovery rate of Havsmast anemometer measurements at 45 m height. 27

Figure 22. Havsmat wind rose 45 m height with wind speed bins. All available but filtered data is used. The wake-affected sectors are shaded in orange, and their displayed mean wind speed might be lower than the real value. 28

Figure 23. Havsmat energy rose at 9, 23, 37, 45 m and calculated at the hub height 40 m. All available but filtered data is used. 29

Figure 24. Histogram and Weibull distribution for all available Havsmast data (left) and for free-wind sectors only (right) at a height of 45 m. 29

Figure 25. Atmospheric turbulence intensity by wind speed bin at 45 m height. Mean TI values (green) and their relevant representative values $\mathrm{TIr} = \mathrm{TI} + \sigma\mathrm{TI}$ (blue). 30

Figure 26. Histogram of turbulence intensity at Bockstigen at 40 m height. Source: (Hansen, 2005). 30

Figure 27. Values of sea roughness length by sector at Bockstigen. Wake-affected sectors are shaded in orange. 31

Figure 28. Sea roughness binned by measured wind speed at 45 m in height. Only data from free wind sectors is used. 32

Figure 29. Atmospheric stability by sector at Bockstigen using AMOK tool. Neutral conditions are classified as $|1/L| < 0{,}005$, stable as $1/L > 0{,}005$, and unstable as $1/L < -0{,}005$. All available data is used. 33

Figure 30. Atmospheric stability during the months of January at Bockstigen. Results obtained using AMOK tool. 34

Figure 31. Atmospheric stability during the months of May at Bockstigen. Results obtained using AMOK tool. 34

Figure 32. WindSim model of Bockstigen terrain elevation (left) and roughness length (left). The grey dot indicates Havsmast location........ 24

Figure 33. WindSim grid in xy-direction (left) and z-direction (right) for Bockstigen. 25

Figure 34. Monthly recovery rate of Kustmast anemometer measurements at 60 m height. 35

Figure 35. Histogram and Weibull distribution for all available Kustmast data. 35

Figure 36. Average wind speed ratio between Havsmat anemometer at 45 m and Kustmast anemometer at 53 m high. Source: (Ganander et al., 2001) 36

Figure 37. Scatter plot of Havsmast wind direction versus Kustmast wind direction during the concurrent period of both datasets. Two trends can be clearly seen. 37

Figure 38. Scatter plot of Havsmast versus Kustmast wind directions for the period 9/2001 – 1/2003. 38

Figure 39. Scatter plot of Havsmast wind direction versus Kustmast wind direction without considering the discarded data (left) and after applying the offset to the data of the second concurrent period (right). 39

Figure 40. Kustmast wind rose before applying the filtering and correction descried above (left) and after (right). 39

Figure 41. The location of the MERRA grid point (green pin) closest to Bockstigen (blue pin) is 57ºN 18ºE. Source: (Gmao.gsfc.nasa.gov, 2014). 40

Figure 42. Errors obtained testing Linear Least Squares (red), Total Least Squares (blue), Variance Ratio (green), Weibull Fit (orange), Speed Sort (pink), Vertical Slice (brown), and Matrix Time Series (purple) algorithms. 40

Figure 43. Energy roses of Kustmast Transferred to site dataset and its 4-year predicted dataset using MERRA data from 1999 to 2003. Dark green and dark blue represent MERRA dataset. 41

Figure 44. Long-term predicted energy rose for Kustmast transferred to site dataset using 30 years of MERRA data (left), and energy rose for MERRA dataset for the same 30-year period (right). 41

Figure 45. Histogram and Weibull fit for Bockstigen long-term predicted climatology at a height of 85 m. 42

Figure 46. Wind rose showing wind speed bins of Bockstigen long-term predicted climatology at a height of 85 m. 42

Figure 47. Energy rose of Bockstigen long-term predicted climatology at a height of 85 m with 360 directional bins. 43

Figure 48. Gumbel best-fit using Periodic Maxima method with square values preconditioning used to obtain 50-year extreme wind speed at Bockstigen at 85 m.. 43

Figure 49. Bockstigen park layout showing the location of its five units, directions with wake effects, and its distance between units in rotor diameters D = 37 m. 45

Figure 50. Filtering of the recorded power values of turbine 2 by graphical means. 47

Figure 51. Experimental power curves using undisturbed measurements for each turbine.48

Figure 52. Danish map showing the location of Horns Rev wind farm. Source: (Hasager et al., 2007). 49

Figure 53. Horns Rev wind farm layout, with 80 turbines Vestas V80 2MW, aligned in a matrix-like layout with 7D spacing between rows and columns. Source: (Hansen, 2008a). 49

Figure 54. Wake effect cases at Horns Rev. Cases with flow from 270º (top), flow from 221º (middle), and flow from 312º (bottom). Source: (Hansen, 2008a). 51

Figure 55. Mean turbulence intensity extracted from free wind speed measurements from two years previous to the park construction, and sorted by flow case. (Source: Deliverable D8.1, Hansen, 2008)... 52

Figure 56. The top of the oceanic boundary layer is obtained by measuring the concentration of aerosols. The dark blue line shows the boundary layer height Source: Hasager et al., *12MW Horns Rev experiment*, (2007). 53

Figure 57. Velocity field obtained using Larsen's wake model with free stream velocity of 6 m/s, ambient turbulence of 6%, and wake influence distances of 50D (top) and 100D downwind (bottom)... 56

Figure 58. Turbulence intensity values obtained after convergence using GCV solver for surface roughness z0 = 0,0002 m (top) and z0 = 0,001 m (bottom). The same KEIN value of 0,1313 has been inputted.. 58

Figure 59. Park overview with Jensen's (top), Larsen's (middle), and Ishihara's (bottom) wake models for the flow case 270º with 7D spacing. 60

Figure 60. Jensen's (top), Larsen's (bottom-left), and Ishihara's (bottom-right) wake widths at 7D downstream of the first turbine. Flow case 270º at 6 m/s..................... 60

Figure 61. Normalised power of the first 8 units downstream for flow case 270º at 6 m/s. Experimental values are plotted next to Jensen's wake model results with k = 0,085. 61

Figure 62. Normalised power of the first 8 units downstream for flow case 270º at 6 m/s. Experimental values are plotted next to Larsen's wake model results with TI = 7%. . 61

Figure 63. Normalised power of the first 8 units downstream for flow case 270º at 10 m/s. Experimental values are plotted next to Ishihara's wake model results with TI = 8%. 62

Figure 64. Turbulence intensity over the domain for flow case 270º. Its value increases downwind from 6,6% to 7,6%. A higher level or surface roughness, 0,002 m, and KEIN of 0,14 have been used to achieve the desired effect. 63

Figure 65. Normalised power of the first 8 units downstream for flow case 270º at 6 m/s. Experimental values are plotted next to Larsen's wake model results with increasing level of TI = 6,6 – 7,6%. 63

Figure 66. Park overview with Jensen's (top) and Ishihara's (bottom) wake models for the flow case 221º with 9,4D spacing. 65

Figure 67. Larsen's (left) and Ishihara's (right) wake widths at 9,4D downstream of the first turbine. Flow case 221º at 6 m/s. 66

Figure 68. Normalised power of the first 5 units downstream for flow case 222º at 10 m/s. Experimental values are plotted next to Jensen's wake model results with k = 0,07. 66

Figure 69. Normalised power of the first 5 units downstream for flow case 222º at 8 m/s. Experimental values are plotted next to Larsen's wake model results with TI = 5,5%. 67

Figure 70. Normalised power of the first 5 units downstream for flow case 222º at 8 m/s. Experimental values are plotted next to Ishihara's wake model results with TI = 5,5%. 67

Figure 71. Park overview with Jensen's (top), Larsen's (middle), and Ishihara's (bottom) wake models for the flow case 312º with 10,4D spacing. 68

Figure 72. Larsen's (left) and Ishihara's (right) wake widths at 10,4D downstream of the first turbine. Flow case 312º at 6 m/s. 69

Figure 73. Normalised power of the first 5 units downstream for flow case 312º at 10 m/s. Experimental values are plotted next to Jensen's wake model results with k = 0,07. 69

Figure 74. Normalised power of the first 5 units downstream for flow case 312º at 10 m/s. Experimental values are plotted next to Larsen's wake model results with TI = 6%. 70

Figure 75. Normalised power of the first 5 units downstream for flow case 312º at 10 m/s. Experimental values are plotted next to Ishihara's wake model results with TI = 14%. 70

Figure 76. Power deficit calculated with Jensen's (top), Larsen's (middle) and Ishihara's (bottom) at 7D, 9,4D and 10,4D downstream. The results are obtained with the parameter that better approximates to experimental data. 76

Figure 77. Drawing indicating the angular distance between a figurative wake centreline at 228º (in purple) and the neighbouring sectors centreline. The drawing only shows sectors 210º to 240º of a 36-sector wind rose. 76

Figure 78. Seabed area that has been scanned with sonar and its depth is known. Distances are in m. 74

Figure 79. Power curve and thrust coefficient of Vestas V117-3,3MW IIA turbine. 74

Figure 80. Energy content per wake directrix (mirrored energy rose), averaged using 72 sectors. 36º–216º is the directrix with the maximum energy content, and 96º–276º the directrix with the minimum energy content. 78

Figure 81. Schematic layout for the first array of turbines with a maximum spacing distance inside the array of 5,8D (left), and with a minimal spacing distance of 3,8D (right). The array is aligned to 158º–338º. Turbine location is represented with a triangle and Bockstigen climatology location with a dot. 79

Figure 82. Schematic layout showing the two arrays separated 10D, with 5,8D of inside-array spacing and not staggered. Turbine location is represented with a triangle and Bockstigen climatology location with a dot. 80

Figure 83. Annual wake losses relative to the downwind spacing between arrays. Results are plotted for Larsen's and Jensen's wake models. 81

Figure 84. Wind resource map showing the annual mean wind speed at Bockstigen taking into account the wake effects of the 1st array of turbines. The scanned seabed extension is drawn in white. The separation between arrays (dashed white) is 8D. The maximum energy content directrix 36º–216º (dashed magenta) and the range of sectors with the highest energy content, 200º to 240º, are shown. The minimum energy content directrix 96º–276º (solid green) is also plotted. 82

Figure 85. Positions of a turbine situated on the 2nd array (light grey) that have been used to run energy simulations. The positions are spaced 0,5D. The separation between arrays (dashed white) is 8D. The maximum energy content directrix 36º–216º (dashed magenta) and the range of sectors with the highest energy content, 200º to 240º, are shown. The minimum energy content directrix 96º–276º (dashed green) is also plotted. 82

Figure 86. Wake losses of a single turbine downwind for different staggering positions (dashed lines). Total park losses (first array of turbines plus single turbine downwind) are also shown (solid lines). Results using Larsen's model are plotted in blue and using Jensen's in green. 83

Figure 87. Turbine location and sea bed depth of the optimized layout. The seabed contour lines and turbine coordinates are not shown due to confidentiality reasons. . 84

Figure 88. Power deficit of downwind rows of turbines at Horns Rev, classified by atmospheric stability. Source: (Hansen, 2008b). 85

Figure 89. Wind rose at Horns Rev during 1999-2002, previous to the park construction (left), and during 2005-2007, after the park construction (right). Source: (Hansen et al., 2012). 87

Figure 90. Correlation of wind speed (left) and wind veer (right) for an onshore wind direction, sector 50º, with land effects. 101

Figure 91. Correlation of wind speed (left) and wind veer (right) for an offshore direction, sector 230º. 101

Figure 92. Correlation of wind speed (left) and wind veer (right) for wake direction 100º (4.8D distance). 102

Figure 93. Correlation of wind speed (left) and wind veer (right) for wake direction 300º (5.4D distance). 102

Figure 94. Vertical wind profiles plotted on a logarithmic chart for 36 sectors at Havsmast. Green dots show anemometer measurements and orange line the wind profile simulated using WindSim. Sea roughness: 0,0002 m. Neutral atmosphere. 127

Figure 95. Vertical wind profiles plotted on a logarithmic chart for 36 sectors at Havsmast. Green dots show anemometer measurements and orange line the wind profile simulated using WindSim. Sea roughness: 0,002 m. Neutral atmosphere. 128

List of Tables

Table 1. Atmospheric stability classification by different stability parameters. Source: (Ashrafi and Hoshyaripour, 2008). 7

Table 2. Atmospheric stability classes using Monin-Obukhov length according to Risø final report WP8. Source: (Barthelmie et al., 2011). 7

Table 3. Data coverage and concurrent period of Havsmast and Kustmast datasets.......... 22

Table 4. Havsmast free wind sectors. The limit wake guidelines are calculated by assuming a wake width of ±15° plus 5° of margin. 25

Table 5. Atmospheric stability classification at Bockstigen using Bulk Richardson Number. 32

Table 6. Stability classification at Bockstigen using AMOK tool. 33

Table 7. Parameters used to model the grid and simulate the wind fields.......... 24

Table 8. Correlation coefficients between wind speeds at Havsmast 45 m and Kustmast 60 m high. Havsmast free-wind sectors are also correlated individually.......... 36

Table 9. Correlation between Havsmast and Kustmast wind direction records during three concurrent periods. 37

Table 10. Wind turbine classification according to IEC 61400-1.......... 44

Table 11. Wake-affected and free wind sectors per turbine unit. The wake-affected sectors are obtained considering a wake width of ±10°, and the free wind sectors are obtained assuming there are no wake effects beyond ±20°. 46

Table 12. Undisturbed sectors for both Havsmast and the relevant turbine. 46

Table 13. Power curve and thrust curve of a Horns Rev turbine. Source: (Hansen, 2008a). 50

Table 14. Atmospheric classification at Horns Rev during 2005. Source: (Hansen, 2008a). 52

Table 15. Cases that are simulated for each flow direction 270°, 221°, 312°. 53

Table 16. Parameters used to model the grid and simulate the wind fields.......... 54

Table 17. Jensen's wake decay constant k and its relevant wake roughness z0.......... 55

Table 18. Optimal parameters for Jensen's, Larsen's and Ishihara's wake model for the flow cases at 6, 8 and 10 m/s. 77

Table 19. Wake models and parameters used on the park layout optimization. 77

Table 20. Annual wake losses using Larsen's and Jensen's models for an array with maximum and minimum spacing. 79

Table 21. Foundation water depth for the optimized layout. Turbine location (coordinates) are not included for confidentiality reasons. 84

Table 22. Turbine gross AEP, net AEP, and wake losses percentage under unstable conditions for the optimized layout. 84

Table 23. Annual stability classification and relevant wake losses for Horns Rev and Bockstigen wind farms. Annual losses under neutral and stable conditions are scaled from Horns Rev data (values in blue). The annual overall losses at Bockstigen is the weighted sum of the wake losses under each atmospheric condition. Values between brackets show results using Jensen's wake model, and without brackets Larsen's. 87

Table 24. Surface roughness classification for non-complex terrain. Source: (Wieringa, 1992). 100

Table 25. Surface roughness classification used in KNMI-HYDRA. Source: (Verkaik et al., 2003). 100

1. Introduction

Wind power deployment has experienced a steady growth in the power generation market since 2000. In Europe, the wind power installed capacity has had an annual increase of 10%, and it currently accounts for the 13% of the overall power generation installed capacity (EWEA, 2014a). At the end of 2013, the wind power accumulated installed capacity was 117,3 GW, with 110,7 GW onshore and 6,6 GW offshore.

Offshore wind power development started slowly. In 2001 only 51 MW were installed, slightly over 1% of the total wind power capacity connected to the grid during that year. During the following years, the offshore penetration has increased dramatically, reaching in 2013 the 14% of the total wind power installed capacity with 1.567 MW commissioned during that year.

Only in Europe, the European Wind Energy Agency forecasts that offshore installations will reach 23,5 GW by 2020 (EWEA, 2014b). Worldwide, Douglas-Westwood predicts an average growth of 3,2 GW per year until 2022, a growth boosted by the development of larger offshore wind turbines (Douglas-Westwood, 2013).

Offshore wind farms benefit from excellent wind conditions, but the limited availability of locations with appropriate water depth and the costs of transmission lines force turbines to be erected in clusters, maximizing the use of shallow areas and reducing the submarine cable length. Therefore, only wind turbines placed at the edge of a cluster will benefit of those excellent wind conditions, being the rest of downwind turbines exposed to wake effects.

The energy losses caused by wake effects can be higher than 20% of the annual energy production, and strongly depends on the turbine spacing and the atmospheric conditions. The park power deficit under stable atmosphere can be between 50% and 70% higher than under unstable conditions (Peña and Rathmann, 2013; Wharton et al., 2012).

Several analytical wake models have been developed and implemented in commercial software. Validating the models that are already available in the industry and calibrating their parameters to better fit experimental observations is very important for offshore development. Better optimizing offshore wind farm layouts will support the market growth, as it will help minimizing the park extension while maximizing its energy yield.

2. Literature review

Offshore wind farms benefit of great wind resources. In most cases annual mean wind speeds are higher than onshore, vertical wind shear lower, and there are no obstacles that interfere with the wind. The only disturbance present offshore is the wake from upwind turbines within the same cluster. What is more, the combined wake of an offshore wind farm can affect a nearby wind farm downstream. Satellites measurements have helped to determine that the average velocity deficit downwind an offshore wind farm is about 11% (Christiansen and

Hasager, 2005), and the wind speed recovery distance ranges from 2 to 14 km (Frandsen et al., 2004).

Wake effects have significant impact on Annual Energy Production (AEP), generating losses that range from 10% —as in the case of Middelgrunden wind farm, to 20% or even higher — as in Lillgrund wind farm (Barthelmie et al., 2010).

Several studies have been carried out to quantify the impact of wake effects at offshore wind farms, being Horns Rev, Nysted and Lillgrund the wind farms among the most studied and documented (Barthelmie and Jensen, 2010; Barthelmie et al., 2004, 2009; Gaumond et al., 2013; Hansen, 2008a; Hasager et al., 2007; Peña and Gryning, 2008).

Wake structure

Moskalenko et al. (2010) have clearly defined a conceptual wake and its internal regions. The wake structure can be divided in the near wake, the intermediate wake and the far wake as shown in Figure 1.

(a) Near wake: has about 1-2 rotor diameters (D) distance downwind. The wake starts expanding immediately while the pressure inside it gradually recovers and the wind speed continues to reduce. By the end of the near wake, 2 to 2,25D, the maximum velocity deficit occurs (Wharton et al., 2012).
(b) Intermediate wake: its length is about 2 to 3D. The wake velocity starts to recover, starting from the wake boundary, and creates a turbulent mixing layer. The velocity at the wake centerline remains constant until the mixing layer meets the center.
(c) Far wake: starts around 5D downwind and stretches for more than 5D. The velocity at the wake centerline increases steadily and asymptotically towards the free wind speed. The mixing layer generates an almost constant velocity profile, but has higher turbulence intensity than the free, undisturbed wind (Barthelmie et al., 2011, p.135) (Vermeer et al., 2003).

The wake expands downstream as a function of several atmospheric and orographic characteristics. Quoting Barthelmie et al. (2010), its expansion is a 'function of the ambient turbulence, turbine-generated turbulence, wind speed, wind direction, atmospheric stability, and the point at which the wake impacts the ground'. The wake expansion appears to be the same downwind of stall-regulated turbines than downwind of pitch-regulated turbines (Barthelmie et al., 2009).

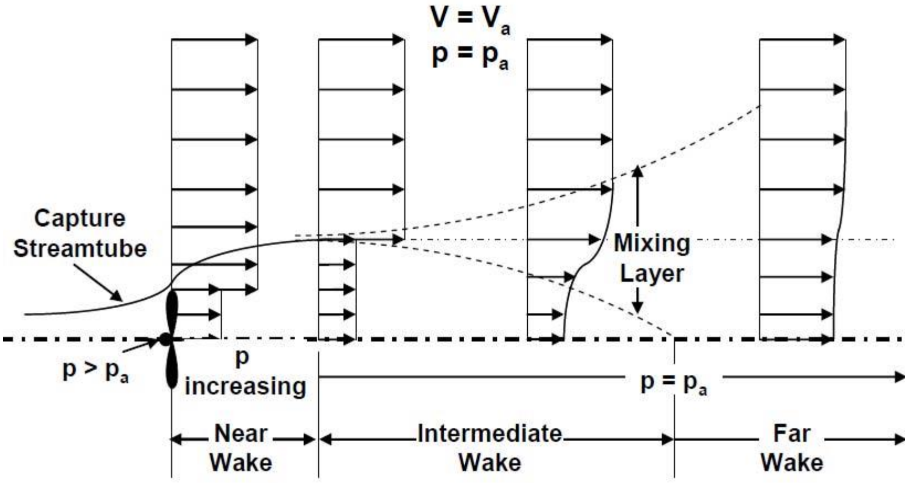

Figure 1. Conceptual structure of a wake, defining the near, intermediate and far wake regions. Source: Moskalenko et al. (2010).

To avoid the wake velocity deficit, offshore arrays are aligned towards directions with low wind frequency, and maintain a downwind distance (spacing) that guarantees an optimal wind speed recovery. There are park layouts with turbine spacing that range from 4D to 12D downwind, being 7-10D a common praxis offshore. Theoretically, the higher the downwind distance the lower the AEP losses, but in some cases a park with 10,5D spacing may show the same power losses than another with only 7D (Barthelmie et al., 2010).

Wake width

The width of a wake can be measured using SoDARs (Sonic Detection And Ranging), LIDARs (Laser Imaging Detection and Ranging), permanent met masts, or simply by analysing the power deficit of a wake-affected turbine in relation to the wind direction. Barthelmie et al. (2010) define the wake width as the ‘distance on each side of the centreline at which the power deficit is within ±5% of the free-stream power’.

After analysing SCADA data (Supervisory Control And Data Acquisition system) from Nysted and Horns Rev wind farms Barthelmie et al. prove the wake width to be the same over offshore conditions. The maximum power deficit occurs when the wind direction coincide with the array direction. The array direction ±1° includes only the wake centreline, half of the wake is comprised within ±5°, extending to ±10° includes most of the wake, and beyond ±15° also includes non-wake conditions.

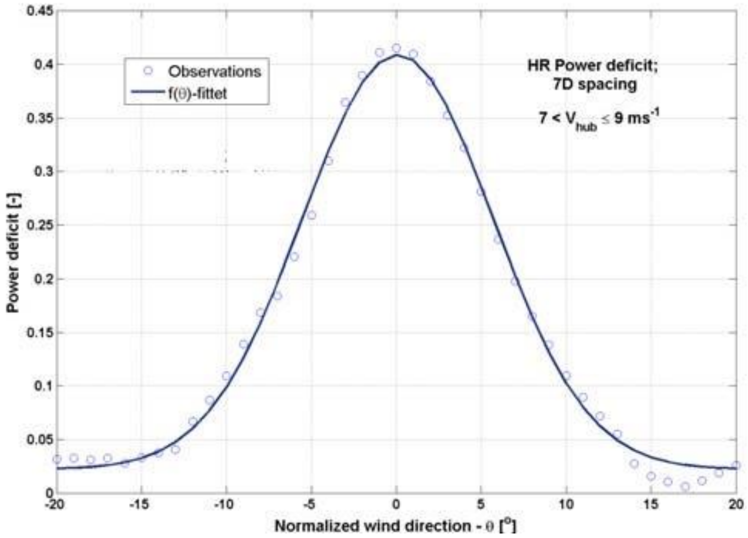

Figure 2. Power deficit distribution as function of normalized wind direction for 7D spacing. The wake centreline is at 0°, which corresponds to a wind direction of 270°. Source: Risø Final Report WP8, Barthelmie et al. (2011).

Wake models

Wake models started to develop during 1980s with the purpose to provide optimization tools to wind farm planning. There are mainly two types of models, analytical and field models. Analytical models explain the wake physics from geometrical or mathematical approximations to fluid dynamic physics (Frandsen, 1992; Jensen, 1983; Larsen, 1988). They are simple and run fast in personal computers. Although they cannot completely define the wake physics (specially the near wake region remains not defined), they are calibrated to give accurate results in the far wake section, where most downwind turbines interact with wakes.

Field models, or CFD-type models, calculate the flow field and its properties all over a domain. They can describe more accurately the flow physics by solving Reynolds-Averaged Navier-Stokes (RANS) equations. Even though they are more complete, field models have a wide range of physical description detail, ranging from light computer-intensive to very computer-demanding simulations that can only run in computer clusters. Starting from the simplest we find 2D wake models (Ainslie, 1988), parabolized 3D models, fully elliptic 3D models using actuator disc, and moving onto Detached Eddy Simulations (DES) or Large Eddy Simulations (LES) we find the most advanced models that use actuator line or real aerofoil profiles (Sørensen, 2011). For a comprehensive wake modelling review the reader is referred to Vermeer et al. (2003).

General results indicate analytical wake models used to underestimate power losses while field models tended to overestimate power losses (Barthelmie et al., 2011, p. 68). Several studies have been carried out to validate, calibrate and compare the output from different wake models. As an example, T. Sørensen and Thøgersen (2008) have calibrated the wake models implemented in the commercial software WindPRO to better meet offshore conditions. VanLuvanee (2006) validated the same against experimental data from Horns Rev wind farm. Barthelmie et al. (2004, 2006, 2009, 2011) have compared and validated most analytical with CFD-type wake models. However, still there is no a clear preference: meaning that CFD-type do not outperform analytic models and as such analytical models are still an attractive option for their simplicity and fair accuracy. As in all tested conditions no model, field or analytical, outperforms the rest, therefore one may conclude that further research has to be performed.

2.1. Atmospheric Stability

The atmospheric stability has a substantial influence on the wake recovery ratio. The in-wake velocity deficit is larger and the wake recovery slower under stable atmosphere in comparison to unstable atmosphere. In addition the effect of stability is much higher than the effect due to surface roughness (Peña and Rathmann, 2013).

Peña and Rathmann (2013) compile in their report that 'the annual mean array efficiency reduces from 91,5% under unstable to 85,3% under stable atmospheric conditions'. Similar results are shown by Wharton et al. (2012) in which the power losses are reported to be only 16% during unstable conditions whereas under stable atmosphere they reached 24%.

Fortunately, in a long term, most atmospheric stability conditions at wind turbine sites are generally close to neutral. For onshore sites atmospheric stability it neutral with a small tendency to the stable side, and for offshore to the unstable side (Peña and Rathmann, 2013). The stability conditions over the North Sea, though, appear not to follow that trend and they slightly lean towards stable atmosphere (Peña and Hahmann, 2012). For a formulation to estimate the average long-term stability of a site the reader can refer to Peña and Hahmann (2012).

Classifying the atmospheric stability of a site can be done by computing either the Monin-Obukhov length L or the bulk Richardson Number R_B. The bulk Richardson Number has an advantage over the Monin-Obukhov length: it can be simply calculated from observations of wind speed and potential temperature at two different heights. The expression of R_B reads as:

$$R_B = \frac{g\frac{\Delta\bar{\theta}_z}{\Delta z_\theta}}{\bar{\theta}_{ref}\left(\frac{\Delta\bar{U}_z}{\Delta z_U}\right)^2} = \frac{g\frac{(\bar{\theta}_{z_2}-\bar{\theta}_{z_1})}{z_2-z_1}}{\bar{\theta}_{z3}\left(\frac{\bar{U}_{z_4}-\bar{U}_{z_3}}{z_4-z_3}\right)^2}$$

where g is the gravitational acceleration, $\bar{\theta}_z$ the time averaged potential temperature at a height z, $\bar{U}_z$ the time averaged horizontal wind speed at height z, $z_2 > z_1$ the heights of the measured potential temperatures, and $z_4 > z_3$ the heights of measured wind speeds.

The Richardson Number is used in several studies to assess the atmospheric conditions onshore but specially offshore (Barthelmie et al., 2004; Christiansen and Hasager, 2005; Hansen, 2008a; Peña and Hahmann, 2012; Vermeer et al., 2003).

The Bulk Richardson Number is closely related to the Monin-Obukhov length L (Stull, 1988, p.177):

- Stable conditions: $R_B > 0{,}25$; $z/L = \frac{R_B}{1-5R_B}$
- Neutral conditions: $R_B \approx 0$; $z/L \approx 0$
- Unstable conditions: $R_B < 0$; $z/L \approx R_B$; or $R_B = \frac{z}{L}\left(1-16\frac{z}{L}\right)^{1/2}$

where z is the reference height. Peña and Hahmann (2012) refer to a simpler, updated relation between R_B and L for stable and unstable conditions:

- Stable conditions: $R_B > 0{,}2$; $z/L = \frac{C_1 R_B}{1 - C_2 R_B}$
- Unstable conditions: $-1 < R_B < 0$; $z/L = C_1 R_B$

with $C_1 = 10$ and $C_2 = 5$.

The Richardson Number, however, has a downside: the accuracy of temperature sensors is often not high enough for a correct stability categorization. Common values to classify the atmosphere as neutral are $|R_B| > 0{,}05$ (Barthelmie et al., 2004; Vermeer et al., 2003)[1]. Considering the case of temperature sensors with an absolute error of ±0,1 °C, the calculated potential temperature difference will have an uncertainty of ±0,2 °C. When applied to standard met tower heights, this uncertainty is large enough to alter R_B from the stable ($R_B > 0{,}05$) to the unstable region ($R_B < -0{,}05$) or vice versa.

A more solid approach for offshore applications is to calculate R_B using the sea temperature —as an approximation of the surface temperature T_s (Ott, 2012):

$$R_B = \frac{g \cdot z_{ref}\left(\bar{\theta}_{z_t} - T_s\right)}{T_s \bar{U}_{z_u}{}^2}$$

where z_{ref} is the reference height, and z_u and z_t the heights of wind speed and temperature measurements. It is possible to compute Monin-Obukhov stability parameter from R_B. The expression for Monin-Obukhov intensive length $1/L$, or its form z/L, which is more convenient than L reads as follows:

$$\frac{z_{ref}}{L} = R_B \left(\log\frac{z_u}{z_0} - \psi_m\left(\frac{z_u}{L}\right)\right)^2 \Big/ \left(\log\frac{z_t}{z_0} - \psi_h\left(\frac{z_t}{L}\right)\right)$$

with z_0 the roughness length, and ψ_m and ψ_h stability functions for the heat flux, which are both functions of $1/L$. It is obvious that the equation above cannot be solved for $1/L$, as several parameters are a function of $1/L$; the solution has to be found though an iterative process. Risø National Laboratory, at Technical University of Denmark, has developed a useful tool that calculates $1/L$ and the sea roughness z_0 using Charnock's relation (see part 2.3 for more details) for all time series of an offshore met mast with measurements of wind speed, air temperature and sea temperature (Ott, 2012).

The values applied to classify the atmospheric stability vary notably from one publication to another. Ashrafi and Hoshyaripour (2008) have arranged a stability classification table comparing the values of different stability parameters. Monin-Obukhov length and Richardson Numbers are always negative for unstable and positive for stable conditions. How to define the neutral region is always left to the authors criterion. In Table 1, Ashrafi and Hoshyaripour tabulate a standard value for neutral atmosphere $|L| > 10^5$.

Table 1. Atmospheric stability classification by different stability parameters. Source: (Ashrafi and Hoshyaripour, 2008).

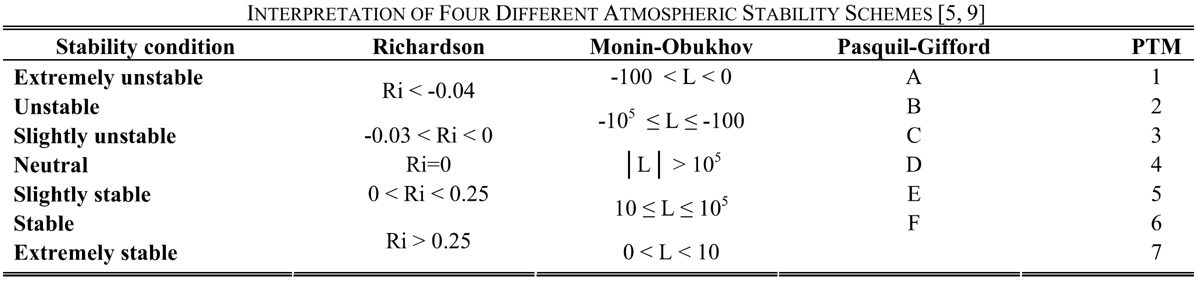
INTERPRETATION OF FOUR DIFFERENT ATMOSPHERIC STABILITY SCHEMES [5, 9]

Stability condition	Richardson	Monin-Obukhov	Pasquil-Gifford	PTM
Extremely unstable	Ri < -0.04	-100 < L < 0	A	1
Unstable		$-10^5 \leq L \leq -100$	B	2
Slightly unstable	-0.03 < Ri < 0		C	3
Neutral	Ri=0	$\lvert L \rvert > 10^5$	D	4
Slightly stable	0 < Ri < 0.25	$10 \leq L \leq 10^5$	E	5
Stable	Ri > 0.25		F	6
Extremely stable		0 < L < 10		7

Barthelmie et al. (2011), in their Risø final report WP8, define also seven stability classes but the criterion for neutral atmosphere drops radically to $|L| > 500$ (see Table 2). Same values were used by Peña and Gryning (2008) when they computed the sea roughness in relation to the atmospheric stability.

Table 2. Atmospheric stability classes using Monin-Obukhov length according to Risø final report WP8. Source: (Barthelmie et al., 2011).

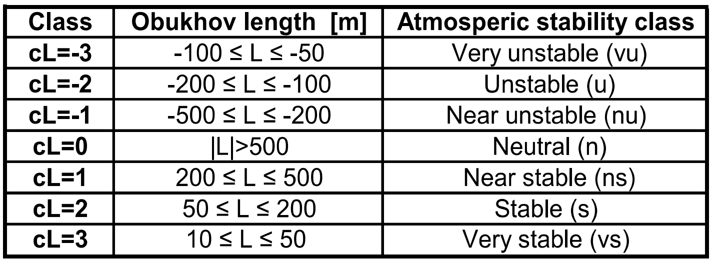

Class	Obukhov length [m]	Atmosperic stability class
cL=-3	-100 ≤ L ≤ -50	Very unstable (vu)
cL=-2	-200 ≤ L ≤ -100	Unstable (u)
cL=-1	-500 ≤ L ≤ -200	Near unstable (nu)
cL=0	|L|>500	Neutral (n)
cL=1	200 ≤ L ≤ 500	Near stable (ns)
cL=2	50 ≤ L ≤ 200	Stable (s)
cL=3	10 ≤ L ≤ 50	Very stable (vs)

In an earlier publication, Barthelmie and Jensen (2010) used a little higher criterion for neutral atmosphere, $|L| > 1000$. And more recently, Hansen et al. (2014) have defined neutral stability conditions at Horns Rev by using a much lower value, $|L| > 200$.

2.2. Atmospheric turbulence and Turbulent Kinetic Energy

Hasager et al. (2007), in their study "12MW Horns Rev experiment", reported data collected during an experimental campaign at Horns Rev. The campaign included wind measurements using LiDARs and SoDARs, and those measurements were compared with data obtained from cup anemometers from permanent met masts.

One of the outputs of that campaign is the assessment of the ambient turbulence intensity (TI) at Horns Rev. In a later stage, Hansen et al. (2012) classified the turbulence intensity at Horns Rev by atmospheric stability. Figure 3 shows the measured turbulence intensity as a function of the wind speed. The turbulence intensity at Horns Rev during the measurement period goes from 8 to 7% in the range of wind speeds from 6 to 10 m/s, and corroborates the typical values for offshore sites of 6-8% (Barthelmie et al., 2006).

---

[1] Other publications, such as Christiansen and Hasager (2005), use much higher values to categorize neutral atmospheres (i.e. $-0.4 \leq R_B \leq 0.1$). In any case, R_B is still too sensitive due to the uncertainty from temperature measurements.

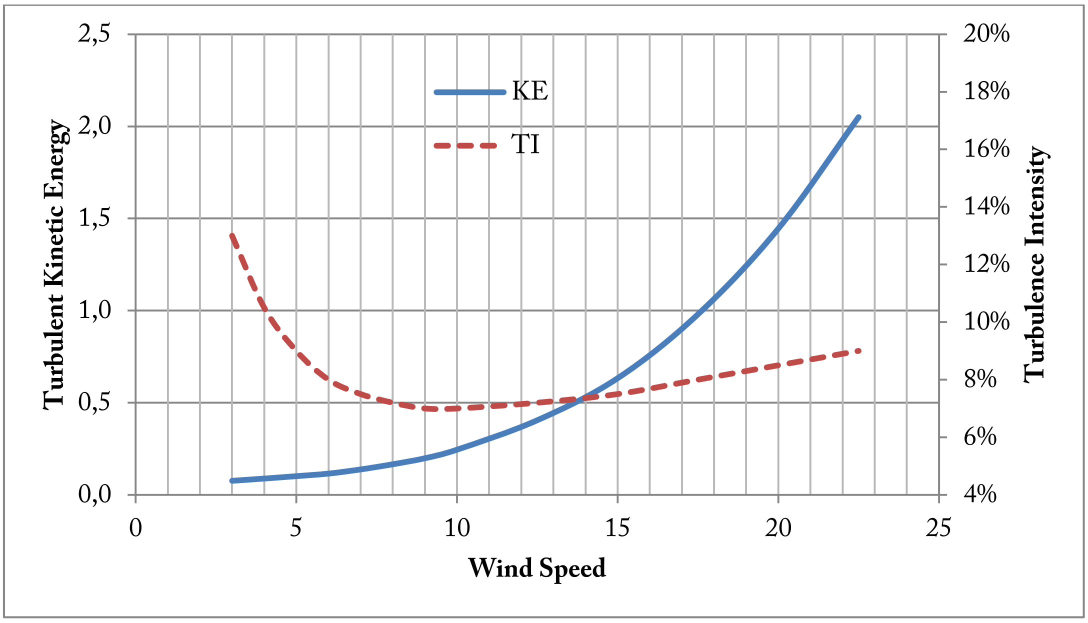

Figure 3. Turbulence intensity measured from cup anemometers at 60 m.a.s.l. at Horns Rev and its related turbulent Kinetic Energy. Source: Hasager et al., *12MW Horns Rev experiment*, (2007).

Hasanger et al. also propose a model to deduce the atmospheric turbulence from the friction velocity, where the turbulence is assumed to be proportional in the surface layer to the friction velocity: $\sigma_u = c \cdot u_*$, with $c = \sim 2{,}5$ —this concept was first introduced by Frandsen (1992). Combining the previous expression with the logarithmic wind profile, a variation in height of the turbulence intensity can be expressed as:

$$TI = TI(z) = \frac{c \cdot \kappa}{\ln\left(\frac{z}{z_0}\right)}$$

where κ is the Von Karman constant and z_0 the surface roughness length. Using the above expression to calculate the turbulence intensity at hub height at Horns Rev, using $z_0 = 0{,}0001\ m$, the results are a very accurate and consistent with the measurements: 7,4% at 70 m height.

The atmospheric turbulence intensity can be easily related to the turbulent kinetic energy. The general expression for turbulent kinetic energy (KE) reads as follows:

$$KE = \frac{1}{2}(\sigma_u^2 + \sigma_v^2 + \sigma_w^2)$$

being $\sigma_u, \sigma_v, \sigma_w$ the 10-min standard deviation of the wind speed components in x, y, z directions. If isotropic turbulence is assumed ($\sigma_u = \ \sigma_v = \sigma_w$) the KE expression reduces to:

$$KE = \frac{1}{2}(1^2 + 1^2 + 1^2)\sigma_u^2 = \frac{3}{2}\sigma_u^2$$

When anisotropic turbulence is considered, σ_v and σ_w are assumed to be proportional to σ_u. Some common values are $\sigma_v = 0{,}8\sigma_u$, $\sigma_w = 0{,}5\sigma_u$ (Barthelmie et al., 2011, Appendix A). The anisotropic expression for KE results in:

$$KE = \frac{1}{2}(1^2 + 0{,}8^2 + 0{,}5^2)\sigma_u^2 = 0{,}945\sigma_u^2 = k\sigma_u^2$$

In fact, for anisotropic turbulence KE is proportional to σ_u^2 by a constant $k < \frac{3}{2}$, with the exception of $k = \frac{3}{2}$ for isotropic turbulence.

Turbulent kinetic energy (KE) and turbulence intensity (TI) are closely related through σ_u. From the TI definition:

$$TI = \frac{\sigma_u}{\overline{U}} \qquad \Longrightarrow \qquad KE = k \cdot TI^2 \overline{U}^2$$

where $\overline{U}$ is the 10-min mean wind speed.

2.2.1. *Added turbulence intensity*

The turbulence inside a wake increases with the distance downwind. An easy way to quantify the added turbulence due to the mechanical disturbance of the free wind is to define the total turbulence intensity (in the wake region) as the addition of the free wind or ambient turbulence I_{amb} and an added turbulence I_{add}. The following expression shows how these two can be added to obtain the total turbulence intensity:

$$TI_{total} = \sqrt{I_{amb}^2 + I_{add}^2}$$

Measurements in wakes show that I_{add} has the same magnitude in x-, y-, and z-direction, being a fully isotropic turbulence as opposite to the anisotropic ambient turbulence (Barthelmie et al., 2011, p. 135).

The decay of the added turbulence intensity is slower than the recovery of the velocity deficit (Vermeer et al., 2003). Figure 4 shows the evolution, with the downwind distance, of the total TI within a large wind farm.

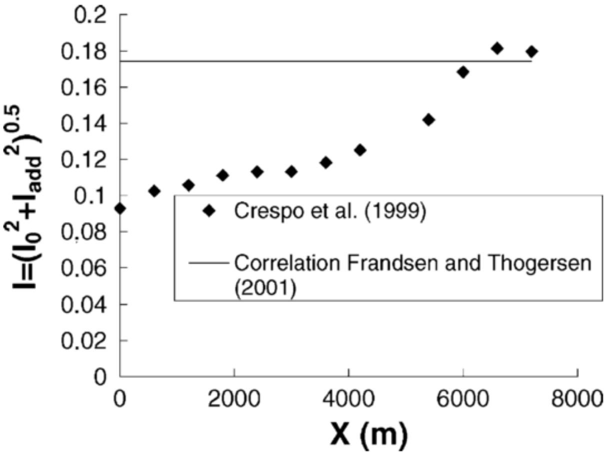

Figure 4. Evolution with the distance of the total turbulence intensity at hub height though a large wind farm cluster. The straight line shows the calculated value for an infinitely large wind farm. Source: (Vermeer et al., 2003).

Vermeer et al. (2003) have done a comprehensive compilation of I_{add} turbulence models and they have compared them with experimental data. Their study conclude that the best fit of

I_{add} for the far wake region is obtained by Crespo and Hernández's experimental expression (Crespo and Hernández, 1996):

$$I_{add} = 0{,}73a^{0{,}83}I_{amb}^{-0{,}0325}\left(\frac{D}{x}\right)^{0{,}32}$$

where a is the induction factor. Other authors relate I_{add} to the turbine thrust coefficient, C_T, or to the wind speed at the hub height. The commercial software WindPRO has also implemented a model based on the free- and added- turbulent kinetic energy.

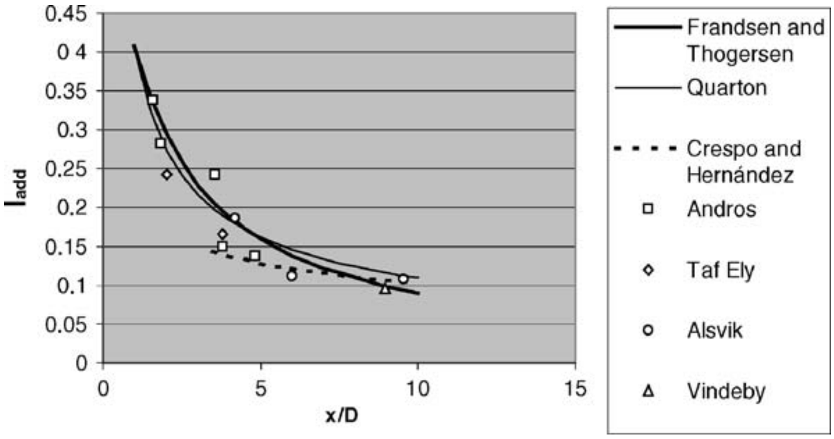

Figure 5. Added turbulence intensity I_{add} calculated from three experimental models (see legend) and compared to experimental measurements. Source: (Vermeer et al., 2003).

2.3. Sea roughness

To assess the sea surface roughness several publications refer to Charnock's relation, such as Verkaik et al. (2003), Barthelmie et al. (2006), Hasager et al. (2007), or Peña and Hahmann (2012), either in its simple or extended form:

$$z_0 = \alpha_c \frac{{u_*}^2}{g}; \qquad \text{or} \qquad z_0 = \alpha_c \frac{{u_*}^2}{g} + \beta_c \frac{\nu}{u_*}$$

where $\alpha_c = 0{,}012 \sim 0{,}035$ (α_c has the higher values for shallow waters), $\beta_c = 0{,}12$, g is the gravitational acceleration, and ν the kinematic viscosity. Ott et al. (2011) describe in their report that Charnock's relation is only valid at medium wind speeds. At high wind speeds the sea roughness length actually decreases, the opposite of what obtained from Charnock's relation.

Peña and Gryning (2008) have applied Charnock's equations to compute the sea roughness at Horns Rev under different atmospheric stabilities.

Stability class	L interval [m]	$\bar{L}$ [m]	$\bar{u}_*$ [m s^{-1}]	u_{15} [m s^{-1}]	$\bar{z}_0$ [m]	Profiles
Stable	$50 \leq L \leq 200$	94	0.20	6.76	0.5×10^{-4}	80
Neutral	$-500 \geq L \geq 500$	-1253	0.47	12.61	2.7×10^{-4}	1253
Unstable	$-300 \leq L \leq -150$	-175	0.33	9.45	1.3×10^{-4}	886
Very unstable	$-150 \leq L \leq -50$	-79	0.25	7.29	0.8×10^{-4}	940

Figure 6. Mean Monin-Obukhov length, mean friction velocity, wind speed at 15 m high, and mean roughness length calculated for different stability classes at Horns Rev. Source: (Peña and Gryning, 2008).

2.4. Analytical wake models implemented in WindSim

2.4.1. Jensen's wake model

A simple analytical wake model for cluster efficiency was presented firstly by Jensen (1983) and further developed three years after by Katic et al. (1986). Jensen's model is based on a linearity assumption: the wake expands linearly downwind[2].

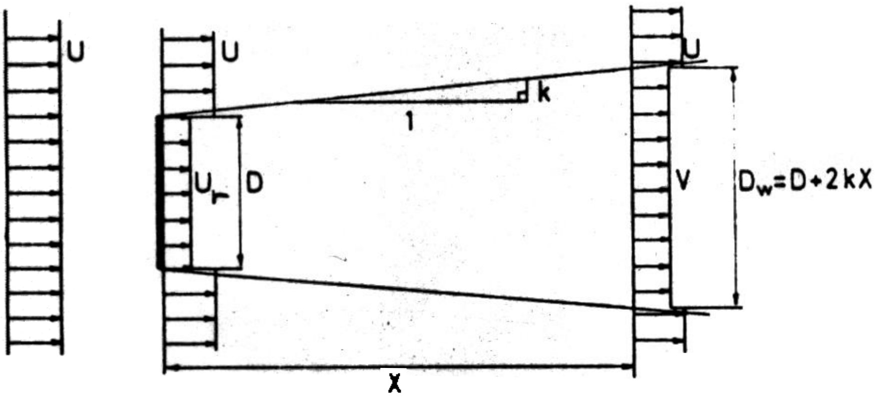

Figure 7. Schematic definition of Jensen's wake model and its parameters (Katic et al. 1986).

The expression of the wake velocity deficit reads:

$$\frac{U_{def}}{U_\infty} = 1 - \frac{U_w}{U_\infty} = \frac{\left(1 - \sqrt{1 - C_T}\right)}{(1 + 2k_w x/D)^2}$$

where U_w is the in-wake velocity, U_∞ the free wind speed, C_T the thrust coefficient, k_w the wake decay constant, x the distance downwind, and D the rotor diameter. The wake expansion downwind is defined by the following expression:

$$D_w = D + 2k_w x$$

where D_w is the wake diameter as a function of the downwind distance x.

In order to obtain a simple model the wake behaviour is simplified: the in-wake speed profile is considered constant, it starts expanding just after the rotor, and its initial diameter is set to be the same as the rotor diameter. Those assumptions, together with the linearity assumption, give a poor fit of the near wake region but they allow the model to be surprisingly consistent with experimental data for more than 4D downwind.

---

[2] Although the author states that the equations are derived from the momentum balance over a control volume, they are actually not. The equations are derived from the mass balance. For a wake model completely derived from the momentum balance the reader is referred to Frandsen's model (Frandsen et al., 2006).

Jensen developed an expression for the velocity deficit of an array with n wind generators (including its asymptotic value), and Katic generalized the model applicability to any layout configuration by assuming that the velocity deficit resulting from the merging of two other wakes can be calculated by the sum of squares.

$$U_{def\_resultant} = \sqrt{{U_{def\_1}}^2 + {U_{def\_2}}^2}$$

Frandsen (1992) proposed, by semiempirical means, an expression to obtain the wake decay constant k_w as a function of the surface roughness:

$$k_w = \frac{1}{2 \cdot \ln(h/z_0)}$$

where h is the hub height and z_0 the surface roughness length. The wake decay constant can be further adjusted to fit characteristic atmospheric stability for a long-term energy production (Peña and Rathmann, 2013). The wake decay constant is related to the atmospheric stability by including the stability function for momentum in its expression:

$$k_w \approx \frac{u_{*free}}{u_{h_{free}}} = \frac{\kappa}{\ln(h/z_0) - \psi_m(h/L)}$$

where κ is the Von Karman constant and $\psi_m(h/L)$ is the stability function for momentum, which is a function of h/L with L the Monin-Obukhov length.

Using the above-presented expression the wake decay constant can be adjusted to fit the annual characteristic atmospheric stability of a particular site. As seen previously in section 2.1 the annual offshore conditions over the North Sea are slightly stable. The wake decay constant can be therefore adjusted to fit more accurately the power losses under those conditions.

2.4.2. Larsen's wake model

Larsen developed a solid physical approach to an analytical wake model by assuming that the 'wake region behind a wind turbine can be described by Prandtl's turbulent boundary layer equations' (Larsen, 1988). The model combines the boundary layer equations with the continuity equation, and quantifies the velocity deficit as a function of the downwind position and the radial position from the wake centreline $U_{def} = U_{def}(x, r)$. Therefore, the wake speed profile is not constant as in Jensen's model.

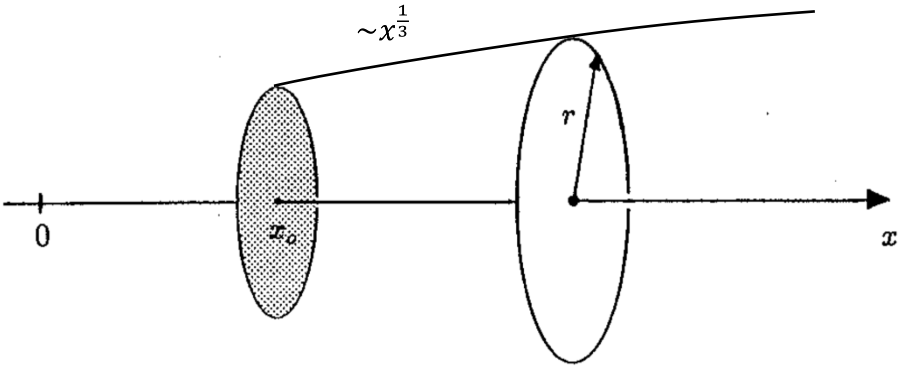

Figure 8. Coordinate system and basic variables of Larsen's wake model. x is the stream direction, x_0 the turbine rotor position, and r the radius inside a wake section. The wake boundary is proportional to $x^{\frac{1}{3}}$. Source: (Larsen, 1988).

Larsen derived two solutions, one simplifying the equations to their first order and another to their second other. The model obtained for the first order solution is shown here as its equations are implemented in the commercial software WindSim. The in-wake velocity deficit U_{def} and the wake expansion radius downwind r_o have the following expressions:

$$\frac{U_{def}}{U_\infty} = \frac{1}{9}\left(C_T A x^{-2}\right)^{\frac{1}{3}}\left\{r^{\frac{3}{2}}\left(3c_1^2 C_T A x\right)^{-\frac{1}{2}} - \left(\frac{35}{2\pi}\right)^{\frac{3}{10}}\left(3c_1^2\right)^{-\frac{1}{5}}\right\}^2$$

$$r_0 = \left(\frac{105}{2\pi}\right)^{\frac{1}{5}} c_1^{\frac{2}{5}}\left(C_T A x\right)^{\frac{1}{3}}$$

with U_∞ the free stream velocity, C_T the thrust coefficient, A the rotor area, x the axial distance (the downwind distance is $x - x_0$), r the radius inside a wake section, and c_1 a constant related to the Prandtl mixing length. The expression of c_1 is obtained from imposing conditions. In its first publication (Larsen, 1988) the wake diameter is imposed to be equal to the rotor diameter D at the turbine position x_0. Then,

$$c_1 = \left(\frac{D}{2}\right)^{\frac{5}{2}}\left(\frac{105}{2\pi}\right)^{-\frac{1}{2}}\left(C_T A x_0\right)^{-\frac{5}{6}}$$

where x_0 is the turbine rotor position in reference to the coordinate system used. Its expression was originally derived analytically by imposing the in-wake velocity at a certain distance downwind to match an experimental value. However, in 2003 Larsen derived a new, experimental expression that relates the relative rotor position x_0 to the experimental wake radius 9,5D downstream (Larsen et al., 2003):

$$x_0 = \frac{9{,}5D}{\left(\frac{2R_{w_{9,5}}}{D_{eff}}\right)^3 - 1}$$

with D_{eff} the effective rotor diameter, $D_{eff} = D\sqrt{\frac{1+\sqrt{1-C_T}}{2\sqrt{1-C_T}}}$, and $R_{w_{9,5}}$ the experimental value of the wake radius 9,5D downwind. The expression of c_1 is also updated using D_{eff} instead of D. The experimental value of the wake radius $R_{w_{9,5}}$ is parameterised as a function of the atmospheric turbulence intensity TI:

$$\begin{cases} R_{w_{9,5}} = \frac{1}{2}\left[R_{nb} + \min(h;\ R_{nb})\right] \\ R_{nb} = \max\left(1{,}08D;\ 1{,}08D + 21{,}7D(TI - 0{,}05)\right) \end{cases}$$

where h is the hub height. This whole set of equations is also well explained in the EMD Wake Models report (Thøgersen, 2012). As x_0 is a function of the atmospheric turbulence intensity TI, c_1 will also be and thus the wake expansion radius r_o and the in-wake velocity deficit U_{def}.

2.4.3. Ishihara's wake model

The wake model developed by Ishihara et al. (2004) aims to obtain one universal model able to describe the wake effects in both onshore and offshore applications. The ambient turbulence intensity in those applications varies significantly, and consequently the model must incorporate it. Furthermore, as the authors state in their publication, in onshore cases the higher level of ambient turbulence helps the wake to recover quicker for any thrust coefficient (C_T). However, in offshore cases, the low ambient turbulence gives lower recovery rates when C_T is low; and only for large C_T there is enough mechanical turbulence generated inside the wake that facilitates higher recoveries.

Ishihara's model is derived from the momentum equation and uses a similarity velocity profile. It takes into account both the ambient and the added turbulence into its wake recovery rate. The expression for the velocity deficit, as a function of the downwind position x and the radial position from the wake centreline r, $U_{def} = U_{def}(x, r)$, reads as follows:

$$\begin{cases} \dfrac{U_{def}}{U_\infty} = \dfrac{C_T^{\frac{1}{2}}}{32}\left(\dfrac{1{,}666}{k_1}\right)^2 \left(\dfrac{x}{D}\right)^{-p} e^{-\frac{r^2}{b^2}} \\ b(x) = \dfrac{k_1 C_T^{\frac{1}{4}}}{0{,}833} D^{1-\frac{p}{2}} x^{\frac{p}{2}} \end{cases}$$

with U_∞ the free stream speed, C_T the thrust coefficient, D the rotor diameter, and p the parameter that defines the wake recovery and it is assumed to be a function of the turbulence:

$$p = k_2(I_a + I_w)$$

$$I_w = k_3 \frac{C_T}{\max(I_a; 0{,}03)}\left\{1 - e^{-4\left(\frac{x}{10D}\right)^2}\right\}$$

where I_a is the ambient turbulence (previously referred as TI), and I_w is the mechanical turbulence generated inside the wake. The constants in the set of equations have the following values: $k_1 = 0{,}27$, $k_2 = 6{,}0$, $k_3 = 0{,}004$. It is worth to mention that, as I_w is a function of the downstream distance x, the wake recovery parameter p will also vary with the downstream distance.

Ishihara et al. claim that the model they have developed also describes accurately the vertical velocity profiles inside a wake.

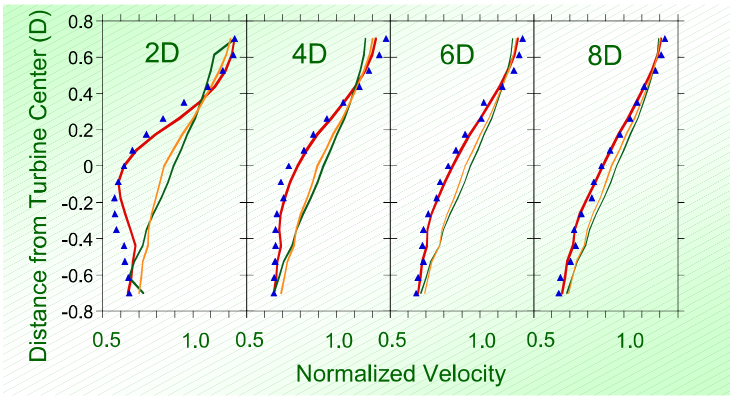

Figure 9. In-wake vertical velocity profiles for 2D, 4D, 6D and 8D downwind. The results obtained for Ishihara's model (red), Larsen's (yellow), and Jensen's (green) are plotted next to the experimental data (blue triangles). Source: (Ishihara et al., 2004).

2.5. Adjustments of the wake decay constant

The commercial software WindPRO recommends to use wake decay values within the range of 0,04 ~ 0,075 for its Jensen's (PARK) model; with 0,04 suitable for offshore and 0,075 for onshore sites (Sørensen and Thøgersen, 2008). However, the wake decay depends strongly on the atmospheric conditions and site orography. According to Sørensen and Thøgersen, some onshore sites have the best fit to the power loss with a value of 0,03 instead of the common 0,075. On the other end, in some cases the standard offshore value of 0,04 has also proved to be too low.

2.5.1. Effect of atmospheric stability on the wake decay constant

It has been introduced in part 2.4.1 that the wake decay constant in the Jensen's model can be expressed as a function of the atmospheric stability. In an enlightening publication Peña and Rathmann (2013) compare the Jensen's wake decay constant modified by atmospheric stability with the results from Frandsen's infinite wind farm boundary layer (IWFBL) model.

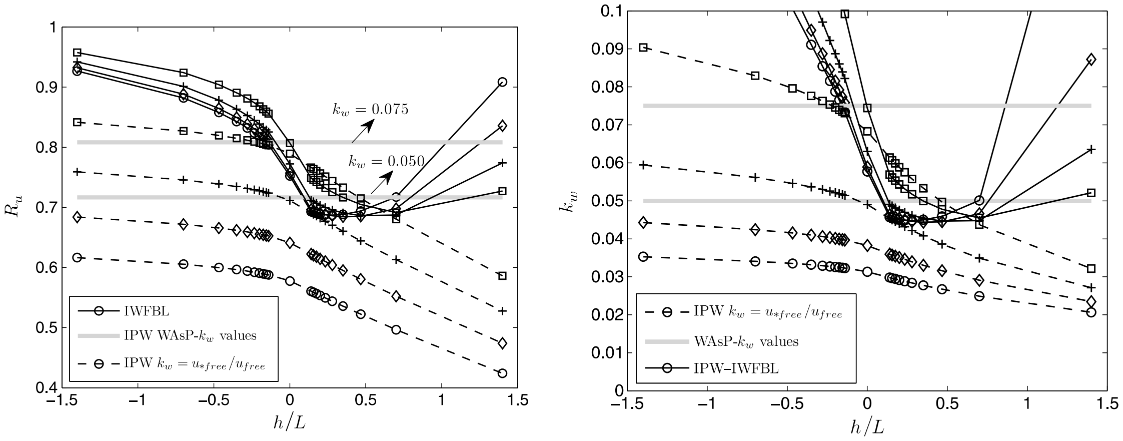

Figure 10. Velocity deficit (left) and wake decay constant k (right) at 7D downwind for several stabilities h/L and roughness lengths: $z_0 = 0{,}0002$ (circles), $z_0 = 0{,}002$ (diamonds), $z_0 = 0{,}002$ (crosses), $z_0 = 0{,}2$ (squares). Source: (Peña and Rathmann, 2013).

The in-wake velocity recovers quicker under unstable than under stable conditions. The wake decay constant will therefore be larger for unstable than for stable conditions. The stability-corrected k_w plotted in Figure 10 shows more realistic values than Frandsen's IWFBL, which shows unrealistically high values for stable and unstable conditions. The values Peña et al. obtained for stability-corrected k_w are higher than what recommended for unstable conditions with large roughness lengths, and lower than what recommended for stable conditions in all roughness cases.

2.5.2. *Wind farm roughness length and the wake decay constant*

The wake decay constant can be expressed as a function of the surface roughness as seen in part 2.4.1. A concept that extends its applicability is the variation of the roughness length throughout the wind farm. In the Deliverable D8.4 of the UpWind WP8 Final Report (Barthelmie et al., 2011) Frandsen models a wind farm as a whole and calculates its roughness length. One of the outputs of his model is a varying value of the roughness length over the farm cluster and several kilometers downwind.

Inside the cluster it is found that the wind farm roughness increases from 0.01 to ~0.5 m. The author estimates the wind farm roughness at Nysted from the experimental measurements and obtains a value of $z_{0\_wf} = 0{,}68$ m.

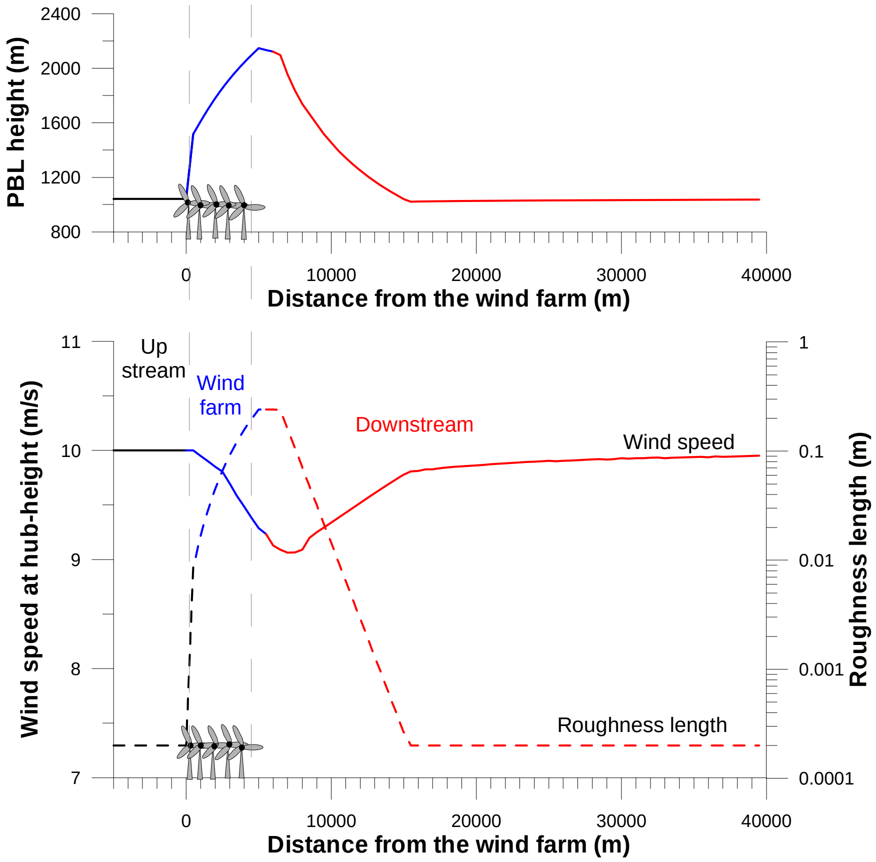

Figure 11. Simulation of the planetary boundary layer (PBL) height, wind speed at hub height, and wind farm roughness length for an offshore cluster. Source: (Barthelmie et al., 2011).

If the model introduced by Frandsen proves to be accurate enough to define the surface roughness variation inside and downwind any cluster, it could be used in combination with the expression of the wake decay as a function of the surface roughness (see 2.4.1) to obtain a k_w that would better fit to each segment of a wind farm cluster and to farm-to-farm wake effects.

2.5.3. *Contribution: wake decay constant as a function of TI*

As a simple step forward towards adjusting the wake decay constant to the site conditions, k_w can also be related to the atmospheric turbulence intensity TI. Using Frandsen's semiempirical expression for k_w (see 2.4.1) and Hasager et al. formulation of TI as a function of height (see section 2.2) it can be derived an expression for k_w as a function of TI:

$$\begin{cases} TI \approx c\dfrac{u_*}{u_h} = \dfrac{c \cdot \kappa}{\ln(h/z_0)} \\ k_w = \dfrac{1}{2\ln(h/z_0)} \end{cases} \Rightarrow \quad k_w \approx \frac{TI}{2c \cdot \kappa}$$

where u_h is the free wind speed at hub height, h the hub height, $\kappa = 0{,}4$ the Von Karman constant, and $c = {\sim}2{,}5$ a constant —Prospathopoulos and Evangelos use $c = 2{,}4135$ in their Deliverable 8.3 of Risø Final Report WP8 (Barthelmie et al., 2011, p.134).

According to this simple expression the wake decay constant k_w is directly proportional to the turbulence intensity, which is consistent with the literature as Peña and Rathmann (2013) assume $k_w \approx u_*/u_h$ and Hasager et al. (2007) assume $TI \approx c \cdot u_*/u_h$.

The above presented expression for $k_w = k_w(TI)$ should be tested with experimental data to see if it has good agreement between the wake recovery and the atmospheric turbulence —for example with the data presented in Figure 12. The expression can be easily extended to take into account the added turbulence inside the park, or to read the varying level of TI over a site from the output of a CDF model. This way k_w will adjust as TI varies, which could prove to be very useful over complex terrain or inside turbine clusters.

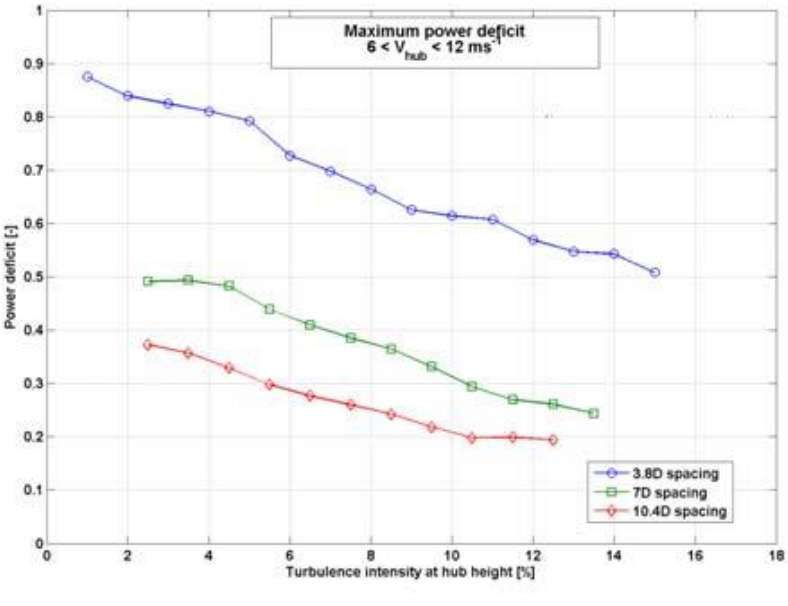

Figure 12. Power deficit 3,8D, 7D and 10,4D downstream as a function of turbulence intensity. Source: Risø Final Report WP8, Barthelmie et al. (2011).

Part I. Bockstigen offshore wind farm

3. Introduction to Bockstigen offshore wind farm

Bockstigen offshore wind farm was the first offshore wind farm in Sweden. It was commissioned in March 1998 and consists of five stall-regulated turbines Wind World W3700-500kW, which were modified to operate at a semi-variable speed. The wind farm installed capacity is 2,5 MW, but initially it was restricted to 2,2 MW due to limitations on the grid connection.

Bockstigen was developed as a demonstration project with the purpose to evaluate offshore foundation loads, offshore power production, to study wake effects and to acquire meteorological data for offshore wind resource mapping.

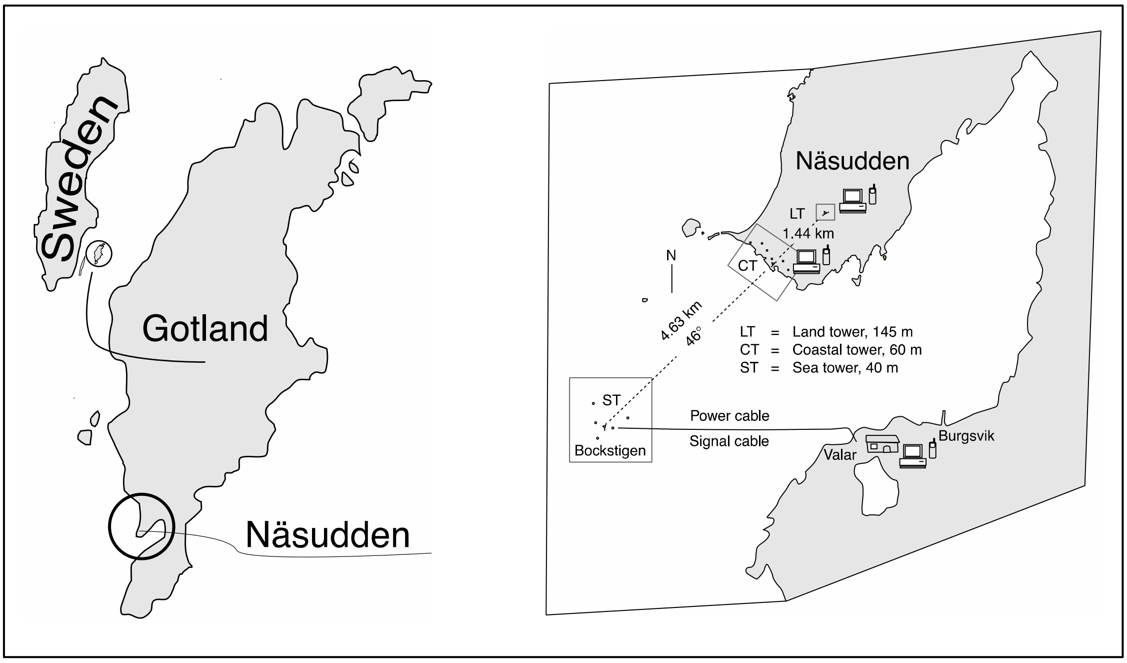
Sweden
Gotland
Näsudden
Näsudden
LT
1.44 km
CT
N
4.63 km
46°
LT = Land tower, 145 m
CT = Coastal tower, 60 m
ST = Sea tower, 40 m
ST
Bockstigen
Power cable
Signal cable
Valar
Burgsvik

Figure 13. Situation map of Näsudden cape in the island of Gotland, Sweden, (left) and the location of Bockstigen offshore wind farm 4,6 km in front of Näsudden cape (right). Source: (Ronsten et al., 2000).

The first reports were published only a few years after commissioning, reporting and analysing the early acquired data (Ganander et al., 2001; Ronsten et al., 2000). Few years later Ronsten (2006) provides a report analysing power performance and park (wake) effects at Bockstigen. However, Barthelmie et al. (2004) studied in more detail the wake effects of offshore wind farms, comparing the experimental data of four sites: Vindeby, Bockstigen, Horns Rev, and

Middelgrunden. Unfortunately, the results obtained from Bockstigen 'were inconclusive and data from this site were not used further'. Most probably, the reason of that conclusion is the high level of uncertainty associated with nacelle anemometer measurements, different power curve for each unit, and yaw misalignment (see Chapters 4 and 5.6 for a complete analysis).

The park layout was designed in a V-shape arrangement, with its vertex pointing towards SSW. The five turbines are erected on monopiles drilled 10 m into the seabed rock, in an area that only has 5 to 6 m depth. All turbines hub height is 41 m and they have 37 m of rotor diameter.

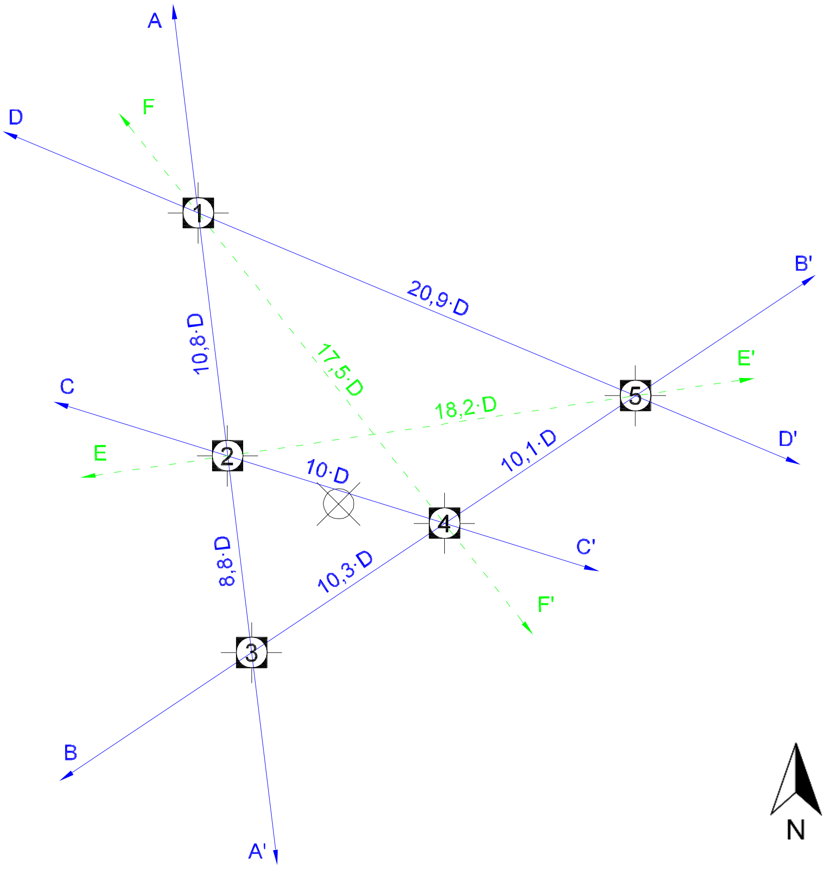

Figure 14. Park layout with five turbines in V and the met mast 'havsmast' in the centre.

The site was equipped with permanent met masts offshore and onshore in order to compare offshore and onshore wind speeds and profiles. An offshore met tower 'Havsmast' of 40 m height was installed at the centre of the park layout (see Figure 14), and was extended to 45 m height. Unfortunately there are no undisturbed wind measurements at the site, the mast was erected in 1999 after the park was constructed.

Havsmast was instrumented with the following equipment:

- combined cup/wind vane anemometers (MIUU-type) mounted in pairs on booms at 180º, in order to filter tower effects, at the heights of 9, 23, and 37 m;
- one Vaisala cup anemometer mounted at 45 m height;
- four PT-100 thermometers at 6, 15, 25, and 35 m;
- and an air humidity sensor at 7 m height.

A costal met mast 'Kustmast' of 60 m height was located on the southern coast of Näsuden, only 4 km away from the site. There is some concurrent data available from both Havsmast and Kustmast, for more information see Section 4.1. Kustmast was instrumented with the following equipment:

- combined cup/wind vane anemometers (MIUU-type) mounted at 10, 20, 35, and 53 m on booms oriented towards the predominant wind direction (southwest);
- one Vaisala cup anemometer mounted at 60 m height;
- thermometers mounted at 10, 20, 35, and 53 m;
- and an air humidity sensor at 10 m height.

Further northeast, in the centre of Nässuden peninsula, there was situated an onshore met mast 'Landmast' with 145 m high. The tower had two systems implemented, one with MIUU technology, measuring wind speed, direction and temperature at five different heights; and another based on SMHI with measurements of wind speed, direction and temperature at seven different heights, including the top anemometer at 145 m (Ronsten et al., 2000).

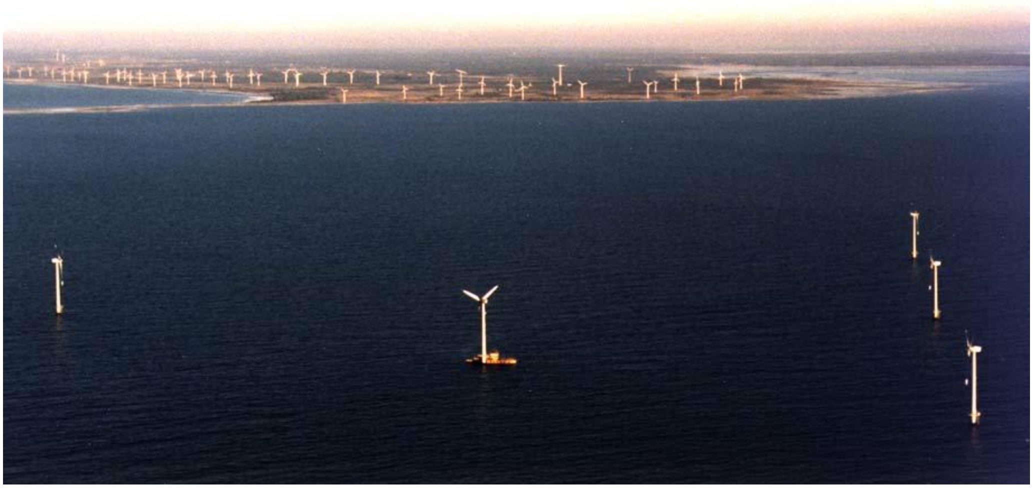

Figure 15. Overhead view of Bockstigen offshore wind farm and Näsudden cape. Photo: Gunnar Britse.

The boundary layer depth over the Baltic sea has been also object of study. Hasager et al. (2007) compile and compare the measurements performed with radiosoundings with analytical models. As a result, the average boundary layer height can be estimated to be around 400 to 500 m, as it is appreciated in Figure 16.

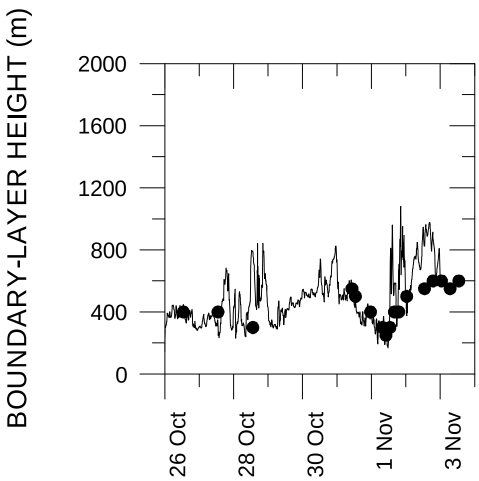

Figure 16. Boundary layer depth over the Baltic sea. Bullets show the observations with radiosoundings. Source: (Hasager et al., 2007).

4. Methodology – Wind resource assessment and wake analysis

4.1. Data filtering and recorded periods

Hans Bergström has kept the meteorological records from both met masts Havsmast and Kustmast. He has been very helpful not only providing them for this study, but also filtering Havsmast dataset to avoid tower effects. Havsmast has anemometers mounted in pairs at 9, 23, and 37 m. Only the most-upwind observations are used for each height.

Havsmast and Kustmast datasets still need to be checked and filtered using a commercial software for wind resource assessment. The filtering and checking is performed following guidelines of Brower (2012) p. 121-123 and Jain (2011) p. 97-98.

10-min means of wind speed and temperature are filtered using realistic maximum and minimum values for Bockstigen: 0 ≤ wind speed ≤ 35 m/s, -30 ≤ temperature ≤ 30 °C. All recorded data fall within those limits. Maximum hourly temperature fluctuation is also checked, paying special attention to the recorded sea temperature, as its value strongly influences the atmospheric stability.

The wind speed values are compared (correlated) between them to see if any anemometer is not performing. The wind speed variation in height is also checked to determine the existence of low-level jets (with negative wind shear) to filter out those cases when assessing the surface roughness.

Kustmast, but specially Havsmast dataset present plenty of recording mistakes. There are gaps with no logged data —most probably due to sensor failure or a power loss of the datalogger. There are also plenty of repeated values, new records that have exactly the same values than the previous entry, a clear sign of a writing error created by the logging system. Figure 17. Screenshot of Havsmast raw dataset with consecutive writing errors on the day 2002-9-03 starting at 00:50 hours.

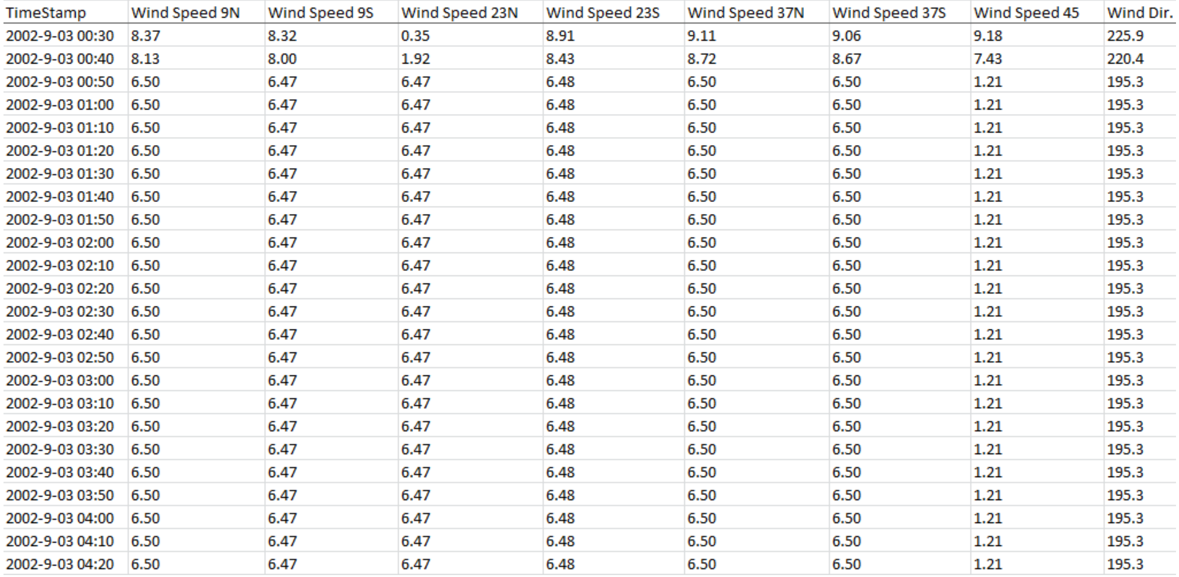

TimeStamp	Wind Speed 9N	Wind Speed 9S	Wind Speed 23N	Wind Speed 23S	Wind Speed 37N	Wind Speed 37S	Wind Speed 45	Wind Dir.
2002-9-03 00:30	8.37	8.32	0.35	8.91	9.11	9.06	9.18	225.9
2002-9-03 00:40	8.13	8.00	1.92	8.43	8.72	8.67	7.43	220.4
2002-9-03 00:50	6.50	6.47	6.47	6.48	6.50	6.50	1.21	195.3
2002-9-03 01:00	6.50	6.47	6.47	6.48	6.50	6.50	1.21	195.3
2002-9-03 01:10	6.50	6.47	6.47	6.48	6.50	6.50	1.21	195.3
2002-9-03 01:20	6.50	6.47	6.47	6.48	6.50	6.50	1.21	195.3
2002-9-03 01:30	6.50	6.47	6.47	6.48	6.50	6.50	1.21	195.3
2002-9-03 01:40	6.50	6.47	6.47	6.48	6.50	6.50	1.21	195.3
2002-9-03 01:50	6.50	6.47	6.47	6.48	6.50	6.50	1.21	195.3
2002-9-03 02:00	6.50	6.47	6.47	6.48	6.50	6.50	1.21	195.3
2002-9-03 02:10	6.50	6.47	6.47	6.48	6.50	6.50	1.21	195.3
2002-9-03 02:20	6.50	6.47	6.47	6.48	6.50	6.50	1.21	195.3
2002-9-03 02:30	6.50	6.47	6.47	6.48	6.50	6.50	1.21	195.3
2002-9-03 02:40	6.50	6.47	6.47	6.48	6.50	6.50	1.21	195.3
2002-9-03 02:50	6.50	6.47	6.47	6.48	6.50	6.50	1.21	195.3
2002-9-03 03:00	6.50	6.47	6.47	6.48	6.50	6.50	1.21	195.3
2002-9-03 03:10	6.50	6.47	6.47	6.48	6.50	6.50	1.21	195.3
2002-9-03 03:20	6.50	6.47	6.47	6.48	6.50	6.50	1.21	195.3
2002-9-03 03:30	6.50	6.47	6.47	6.48	6.50	6.50	1.21	195.3
2002-9-03 03:40	6.50	6.47	6.47	6.48	6.50	6.50	1.21	195.3
2002-9-03 03:50	6.50	6.47	6.47	6.48	6.50	6.50	1.21	195.3
2002-9-03 04:00	6.50	6.47	6.47	6.48	6.50	6.50	1.21	195.3
2002-9-03 04:10	6.50	6.47	6.47	6.48	6.50	6.50	1.21	195.3
2002-9-03 04:20	6.50	6.47	6.47	6.48	6.50	6.50	1.21	195.3

Figure 17. Screenshot of Havsmast raw dataset with consecutive writing errors on the day 2002-9-03 starting at 00:50 hours.

To keep data usability and comparability, in case of missing or erroneous data from one sensor the whole record line is filtered out. A script in perl is developed to filter the entries with writing errors (see Annex I for the script code). The script filters out the lines that have the same value recorded in the same channel for a specific number of consecutive occurrences. When filtering the dataset using the wind speed channels, no more than 30 min with the same value are accepted (maximum 3 repetitive values); or when filtering by wind speed no more than 1 hour with the same value is accepted (maximum 6 repetitions).

The filtering script has proved to work faultlessly: after filtering the dataset based with the value of one channel using no more than 6 repeated values, the clean dataset is filtered again reducing the number of repeated values to 5. No new writing mistakes are found, ensuring that all blocks with writing mistakes have already been filtered out.

After the filtering, Havsmast and Kustmast datasets have the following coverage:

Table 3. Data coverage and concurrent period of Havsmast and Kustmast datasets.

Periods:	**Havsmast**	**Kustmast**
Recorded period:	10-1999 to 01-2003	11-1998 to 08-2001
Recorded period in months:	39,7	33,7
Equivalent recorded period after filtering:	24,6	19,5
Concurrent period:	10-1999 to 08-2001	
Equivalent	8,6 months	

Although Havsmast and Kustmast have 23 concurrent months in the logging period, there is only 8,6 months of equivalent recorded period after data filtering.

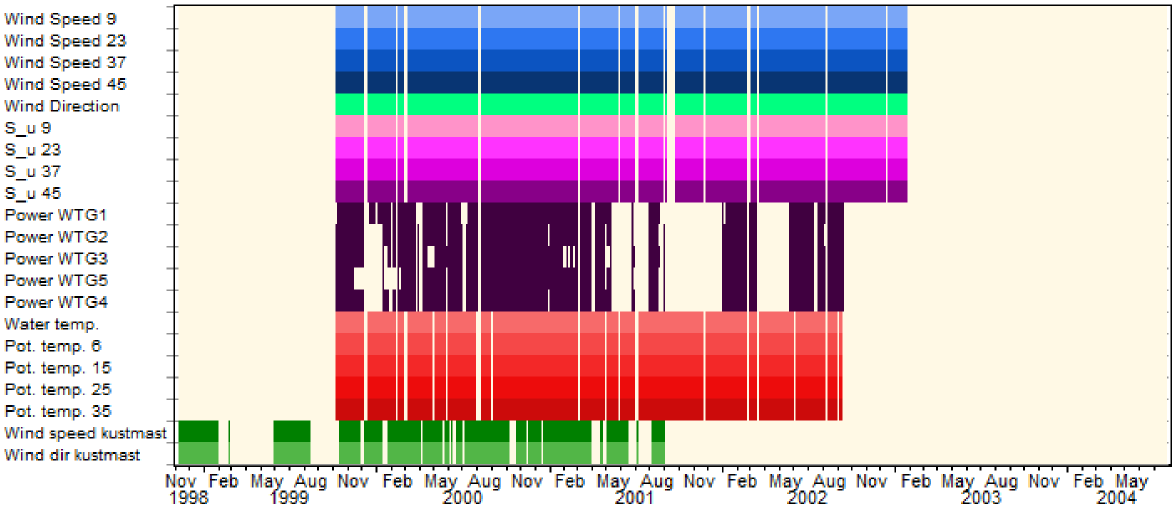

Figure 18. Data coverage of Havsmast, Kustmast and power output per turbine after filtering.

The measurements of water temperature are completely disregarded for any purpose in this study. The registered temperature fluctuates beyond any physical explanation. Annex II compiles an event where, whilst the air temperature at 6 m height remains considerably steady during day and night, the water temperature drops by more than 8 ºC and rises again more than 10 ºC in less than 48 hours.

An explanation to such an extreme behaviour could be the proximity to the site of warm waters from a shallow area next to the shore, and cold waters from a deeper offshore area. A change in direction of the sea currents might bring water from one area or the other that will generate a sudden increase or decrease of the observed water temperature at the site.

Another explanation could be related to the installed dump loads at the bottom of the towers. Those release heat when part of the generated power cannot be transferred to the grid, and that heat could warm up quickly the water temperature. In any case, the water temperature observations are not used in this study.

4.2. WindSim modelling of Bockstigen

To create a model in WindSim a file with elevation data and surface roughness in needed. The terrain is downloaded from ASTER Global Digital Elevation Model (Gdem.ersdac.jspacesystems.or.jp, 2014). The land cover available online does not capture correctly the coast line at Näsudden. The terrain roughness is defined following the roughness classification published by Wieringa (1992), with sea roughness of 0,0002 m and forest roughness of 1 m (see Annex III).

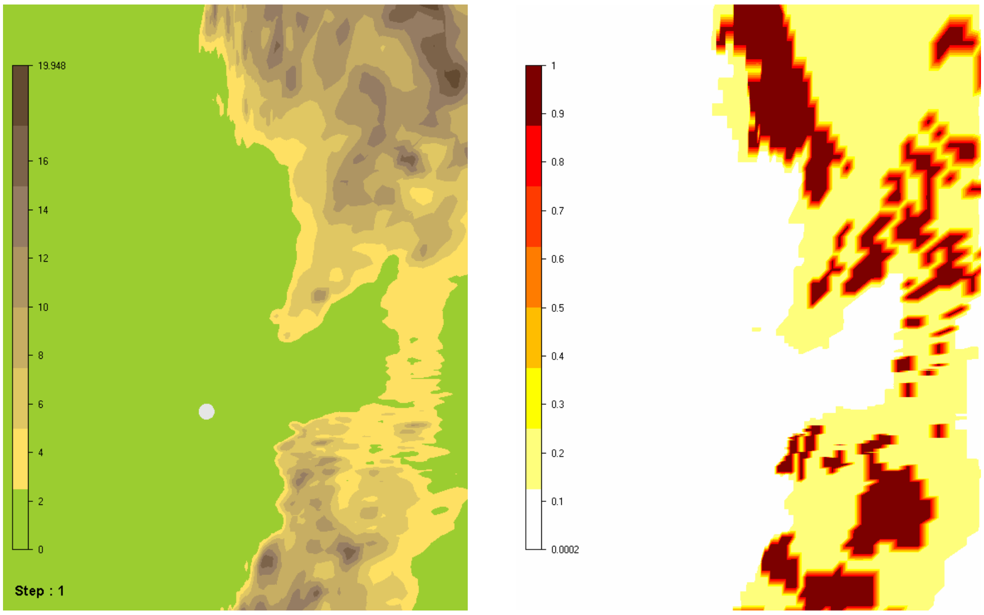

Figure 19. WindSim model of Bockstigen terrain elevation (left) and roughness length (left). The grey dot indicates Havsmast location.

The model grid is created using refinement around the site area to have a higher resolution and better assess the wake effects. The refinement area is defined a little larger than the park layout according to WindSim Best Practices guidelines, making sure to have at least 500 m (15 cells in this case) from the refinement boundaries to the nearest turbine or met mast location.

Table 4. Parameters used to model the grid and simulate the wind fields.

Grid modelling		**Wind fields simulation**	
Terrain extension:	23 km x 30 km	Boundary layer height:	400 m
Resolution in refinement area:	30 m	Boundary condition on top:	No-friction wall
Maximum grid xy-spacing:	617 m	Number of sectors:	36
Height model above terrain:	800 m	Air density:	1,225
Number of cells in z-direction:	30	Thermal stability:	Disregarded
Height distribution factor:	0,05	Turbulence model:	Standard k-ε
Height 10th node above the ground:	94 m	Solver:	GCV
Total number of cells:	1,2 M		

The distribution of cells in z-direction is adjusted in order to have more cells below the turbines hub height. The terrain extension is set to 23 by 30 km in order to include the land effects from sectors 0° to 180°, and at the same time provide a clearance from the model boundaries to the site location of more than 2 km. The parameters used in the model are listed in Table 4.

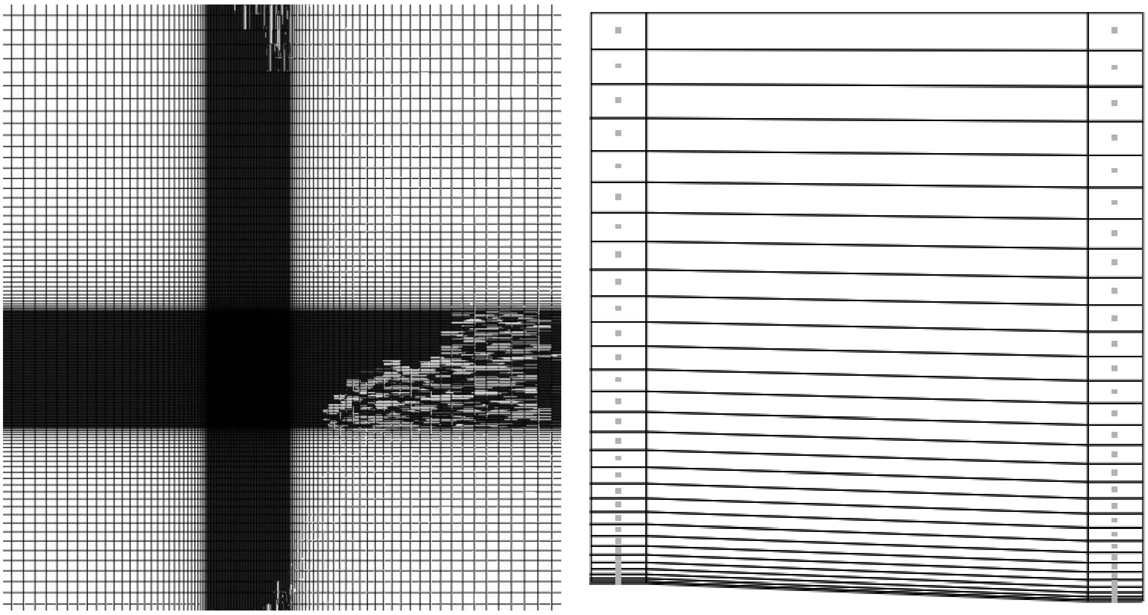

Figure 20. WindSim grid on the xy-plane (left) and z-direction or height (right) for Bockstigen.

4.2.1. Surface roughness sensibility study

A surface roughness sensibility study is carried out, checking whether the vertical profiles match better the observations by using the standard sea roughness value, 0,0002 m, or using a higher one, 0,002 m, closer to the empirical roughness values obtained in part 5.1.4. For the 36-sector vertical profile comparison see Annex X.

As a result, the model with higher sea roughness, 0,002 m, fits better the observations from free-wind sectors, especially it has a good agreement with sectors 230°, 240°, 250°, 260°, which are free-wind sectors with higher energy content. However, contrary of what it is expected, the model with standard sea roughness, 0,0002 m, is the most appropriate for sectors between the shore and the wind farm.

5. Results – Wind resource assessment and wake analysis

5.1. Havsmast dataset

5.1.1. Free wind sectors

Due to the unusual location of the met mast in the centre of the park layout, the wind measurements are affected by wakes in several sectors. Figure 21 shows the boundary directions that separate undisturbed wind from wake affected directions. The undisturbed directions have been obtained assuming a wake width of ±20°, 5° wider than the empirical wake width value to ensure that no wake effects are captured but only free-wind conditions (see Chapter 2 for the wake width definition). The free wind sectors are transcribed into Table 5.

Table 5. Havsmast free wind sectors. The limit wake guidelines are calculated by assuming a wake width of ±15° plus 5° of margin.

Limit wake guidelines	Havsmast free wind sectors
349,3 + 5º : 55º - 5º	355º ≤ FWS1 ≤ 360º, 0º ≤ FWS1 ≤ 50º
115,5 + 5º : 195,3º - 5º	120º ≤ FWS2 ≤ 190º
225,3º + 5º : 278,3 - 5º	230º ≤ FWS3 ≤ 273º

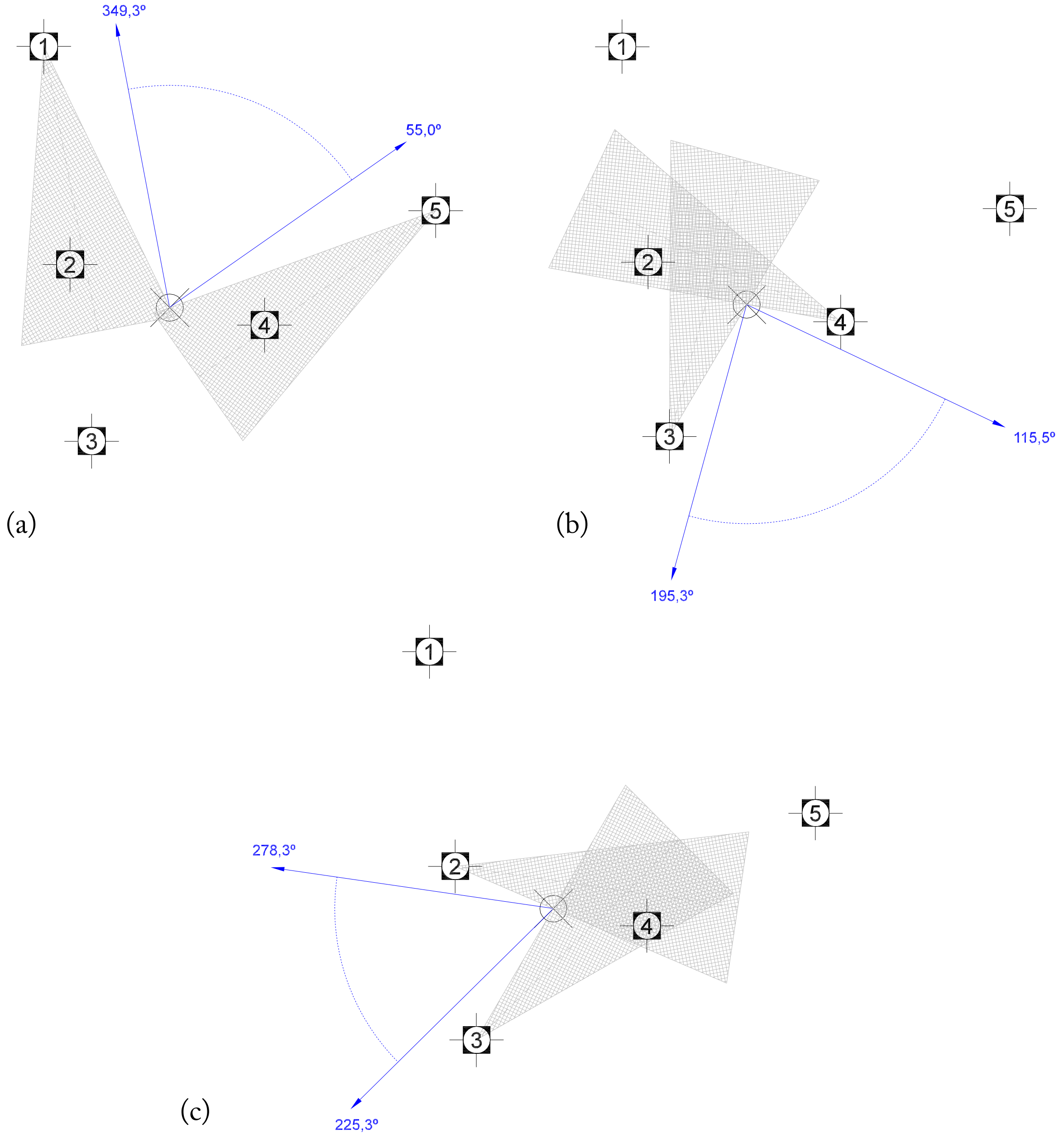

(a)

(b)

(c)

Figure 21. The blue guidelines define the undisturbed wind sectors.

There are five main directions from which Havsmast receives the wake centrelines from turbines 1 to 5. These wake centrelines are at 334º, 293º, 210º, 100º, and 70º for turbines 1 to 5 respectively. Figure 22 shows an overlay of the wake-affected sectors, wake centreline directions, together with the park layout.

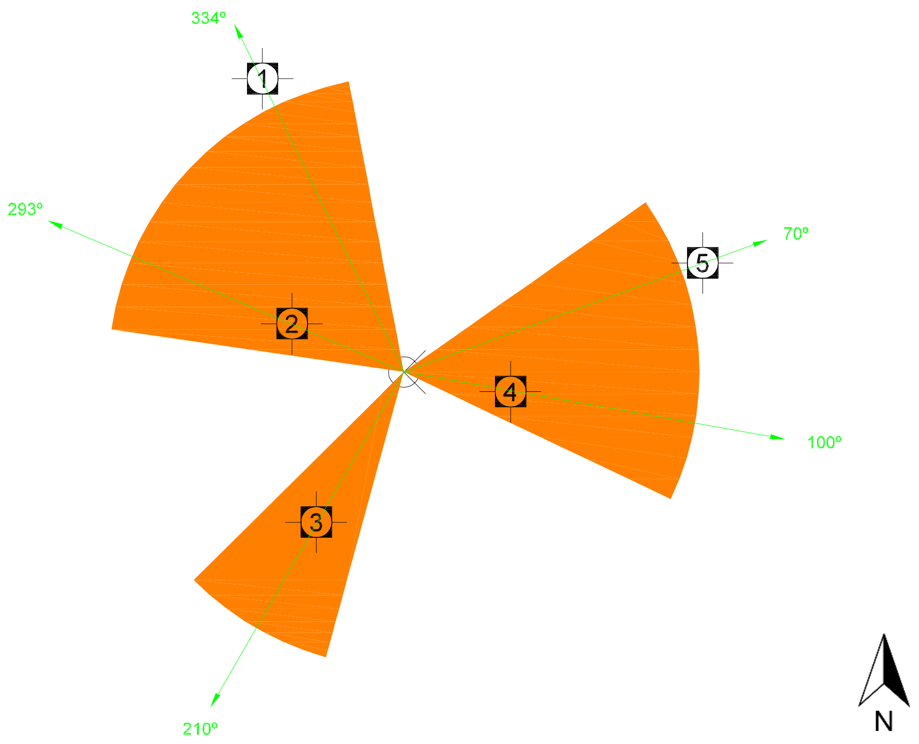

Figure 22. Overview of Havsmast wake-affected sectors, directions of wake centrelines and the park layout.

5.1.2. *Wind rose and energy rose*

There is not one complete year of continuous data after filtering Havsmast dataset. The monthly recovery rate after data filtering is shown in Figure 23.

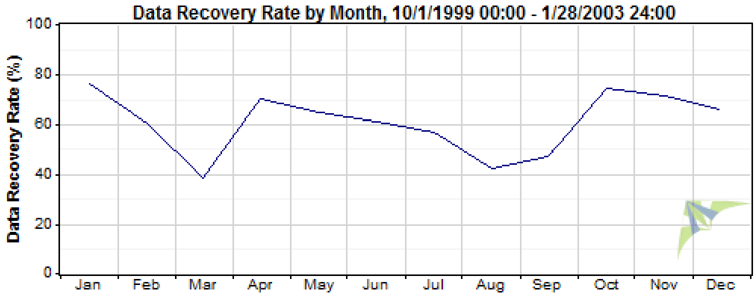

Figure 23. Monthly recovery rate of Havsmast anemometer measurements at 45 m height.

The recovery rate is higher than 60% in the majority of months, only in the months of March, August and September it drops to levels lower than 50%. Seasonal effects might be under-represented for those months, influencing the sector-wise frequency distribution and mean wind speed. However, the overall good recovery ratio makes the wind rose of Figure 24 rather representative.

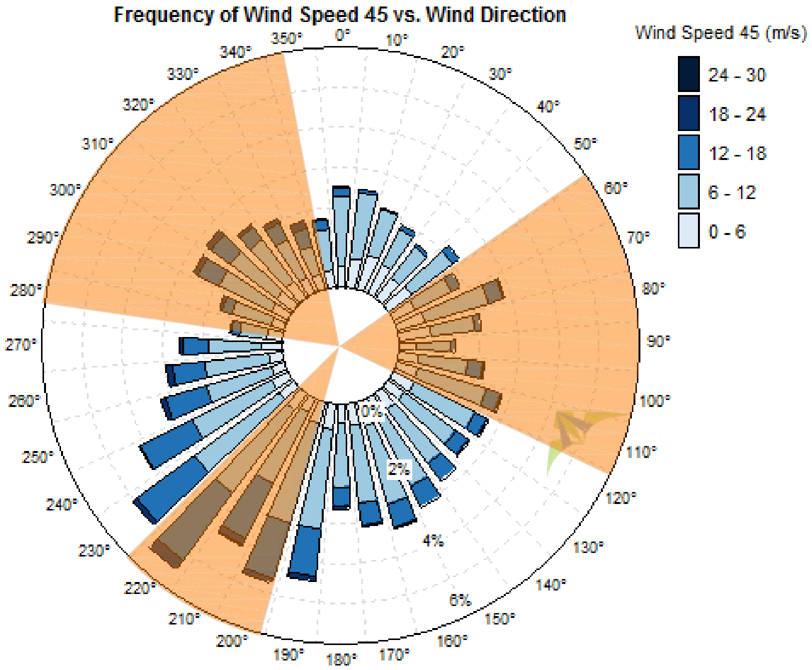

Figure 24. Havsmat wind rose 45 m height with wind speed bins. All available but filtered data is used. The wake-affected sectors are shaded in orange, and their displayed mean wind speed might be lower than the real value.

The wind rose shown in Figure 24 is not completely characteristic of the site climate because of very low and uneven sector-wise recovery ratios.

The energy roses at 9, 23, 37, 40 and 45 m high are shown in Figure 25. It can be appreciated that the correlation between measurements at different heights is very high. When comparing sectors 200º to 220º from the energy rose with the frequency rose it can be noticed that the small gap at 210º is much larger in the energy rose. This might be due to effect of having filtered out records with higher wind speeds at this sector than at the rest. In any case, it is clear that the main wind energy content comes from Southern-Southwesterly sectors.

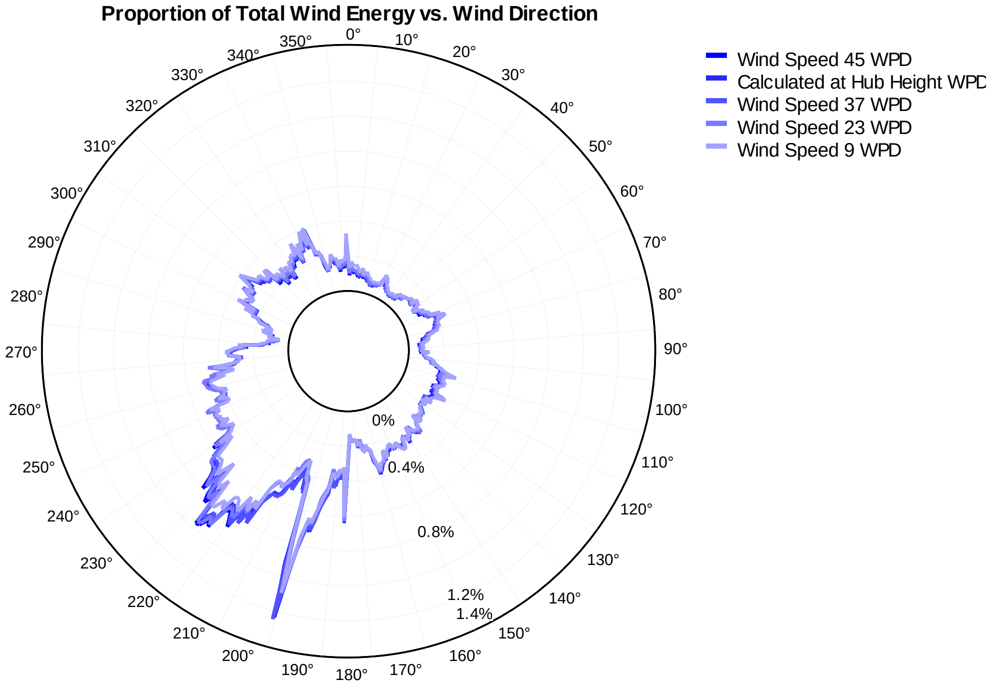

Figure 25. Havsmat energy rose at 9, 23, 37, 45 m and calculated at the hub height 40 m. All available but filtered data is used.

In spite of the low recovery ratio, the histogram of the filtered data fits surprisingly well with a Weibull distribution, revealing that the data filtering has presumably not affected more one wind speed bin than another. Figure 26 shows the Weibull fit for all available data and data only from free-wind sectors.

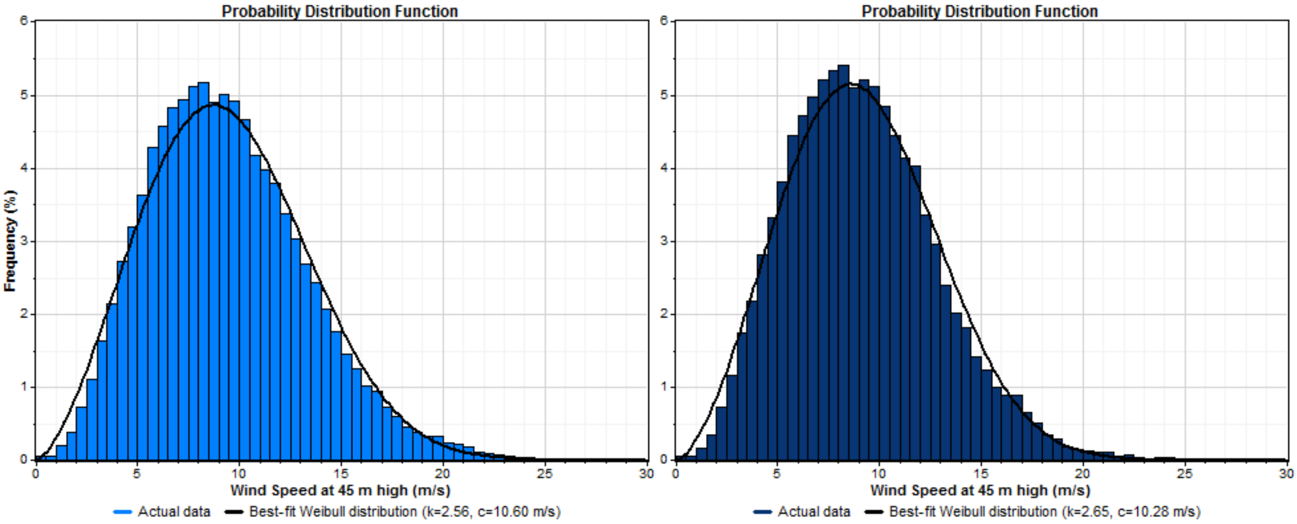

Figure 26. Histogram and Weibull distribution for all available Havsmast data (left) and for free-wind sectors only (right) at a height of 45 m.

The annual mean wind speed at 45 m is 9,24 m/s, an unrealistically high value at that height. A reason for such a high annual wind speed could be that sectors with low energy content have been filtered out more intensively.

5.1.3. Atmospheric turbulence

It has been introduced in part 2.2.1 that wakes generate mechanical turbulence that add to the atmospheric turbulence downstream. To obtain the level of atmospheric turbulence at Bockstigen only measurements from free-wind sectors are used.

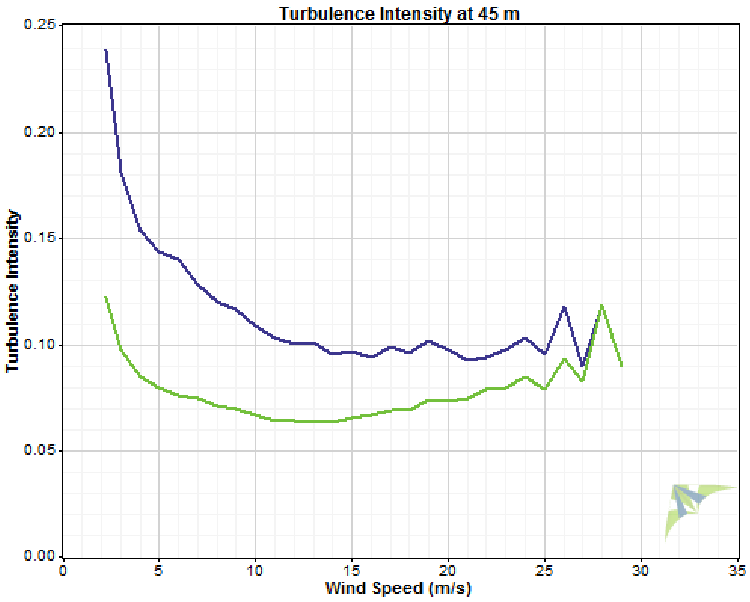

Figure 27. Atmospheric turbulence intensity by wind speed bin at 45 m height. Mean TI values (green) and their relevant representative values $TI_r = TI + \sigma_{TI}$ (blue).

The mean turbulence intensity has its maximum value at low wind speeds as expected. Its value remains within 6% and 8% from 5 to 23 m/s, the majority of operational wind speeds. These values are consistent with what has been published in the past. Figure 28 shows the turbulence intensity distribution at 40 m height, with the largest probability for values in the range of 5% to 8% (Hansen, 2005).

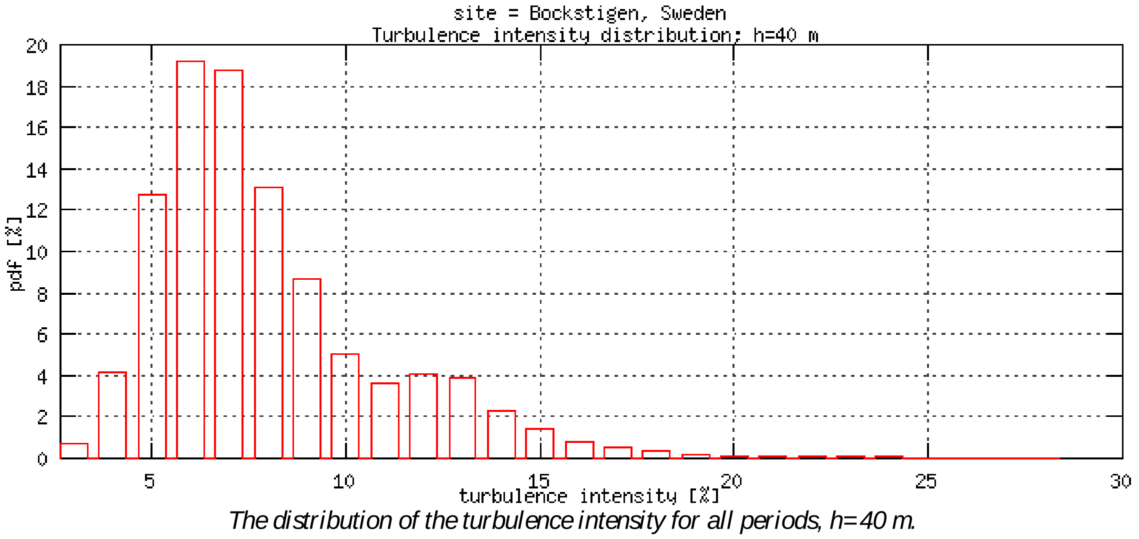

The distribution of the turbulence intensity for all periods, h=40 m.

Figure 28. Histogram of turbulence intensity at Bockstigen at 40 m height. Source: (Hansen, 2005).

5.1.4. Surface roughness

It is possible to obtain the sea roughness from the wind speed measurements at different heights by fitting a logarithmic profile. A value of roughness length is computed for each entry of Havsmast dataset.

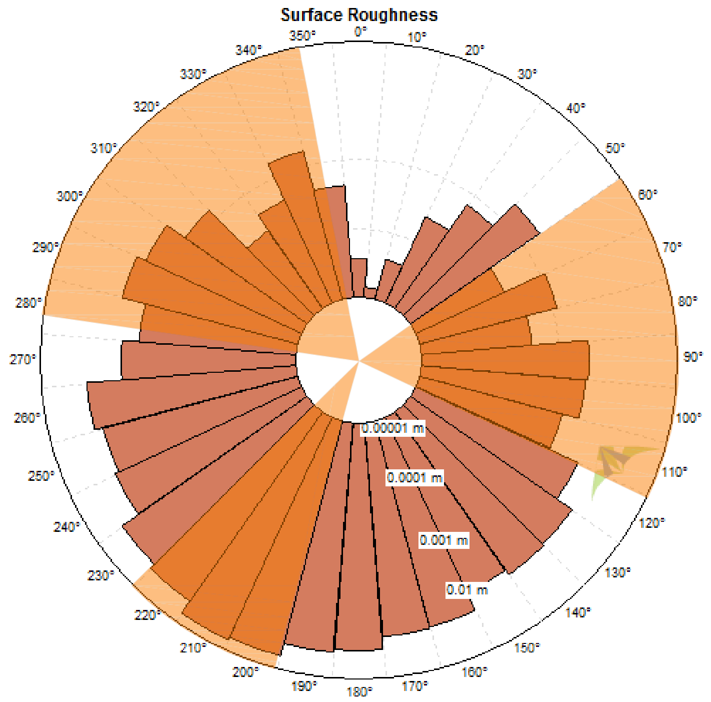

Figure 29. Values of sea roughness length by sector at Bockstigen. Wake-affected sectors are shaded in orange.

Figure 29 shows the mean of the roughness length values binned by sector. Wake-affected sectors are disregarded in this discussion as the wake velocity deficit modifies the vertical wind speed profiles, giving not accurate roughness length values. Opposite to what expected, the sea roughness of sectors with land effects, 0° to 50° for example, present lower values than undisturbed offshore sectors, 230° to 270° for instance (see Figure 19 for the situation of land in reference to Havsmast). This higher roughness values in offshore-facing sectors could be related to higher wind speeds from those sectors that would generate large waves.

As introduced in Section 2.3, the sea roughness increases with the wind speed. The roughness length binned by wind speed is plotted in Figure 30. Only data from free-wind sectors is used. Values of ~0,01 m are achieved from 12 to 28 m/s. When compared to sea roughness classification, standard values fall between 0,0001 and 0,003 m (Jain, 2011, p. 35). Hence the obtained values are too high. A reason for that could be that the measurements from the anemometers at lower heights are affected by the surface layer, or they suffer excessive presence of water droplets, or simply they are underperforming. Another reason might be that the met tower height is too low to capture the complete vertical profile, inducing too much uncertainty when fitting a logarithmic profile.

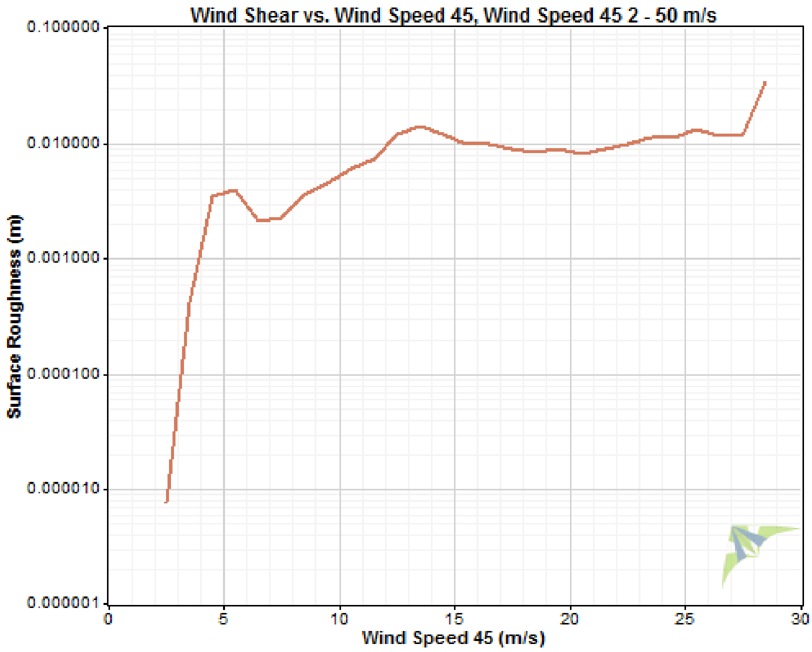

Figure 30. Sea roughness binned by measured wind speed at 45 m in height. Only data from free wind sectors is used.

5.1.5. *Atmospheric stability at Bockstigen*

The atmospheric stability at the site can be calculated since there are available wind speed and temperature observations at different heights. The Bulk Richardson Number is the first stability parameter that is computed for each entry of Havsmast dataset. To avoid air temperature measurements to be affected by the surface temperature, measurements at heights too close to the ground should be disregarded. The Bulk Richardson Number is then calculated using the expression introduced in Section 2.1, temperature measurements at 15 and 35 m height, and wind measurements at 23 and 45 m height.

Using only data from free wind sectors, the obtained Richardson Numbers enable us to classify the atmospheric conditions. The results are classified in Table 6 using two different criteria sets.

Table 6. Atmospheric stability classification at Bockstigen using Bulk Richardson Number.

Stability classification:	**Cases using as neutral conditions $\lvert R_i \rvert > 0,05$**	**Cases using as neutral conditions $-0,4 \leq \lvert R_i \rvert \leq 0,1$**
Stable:	33.300 (78,5%)	31.171 (73,5%)
Neutral:	4.416 (10,4%)	9.631 (22,7%)
Unstable:	4.702 (11,1%)	1.616 (3,8%)

In spite of thermometer accuracy or different criteria applied to classify the stability, it is clear that the Richardson Number describes stable atmosphere in the majority of cases. However, half of the data has been disregarded as wind measurements from some sectors are disturbed by wake effects.

A better approach to the stability classification is to use the Monin-Obukhov stability parameter. The advantage of using Risø AMOK tool (Ott, 2012) is that only the observation of one wind speed is required, together with the air temperature at one height and the sea surface temperature. This provides less uncertainty when calculating the vertical gradients of temperature and velocity, making the tool more robust even in sectors with disturbed wind.

Using AMOK tool at Bockstigen with air temperature the registered temperature at 35 m high, surface temperature the air temperature at 6 m high (it is not the optimal but it avoids the problematic with the sea temperature described in Section 4.1), and wind speed the anemometer measurements at 45 m high. The use of air temperature measurements to assess the surface temperature may be more accurate according to Motta et al. (2005) study.

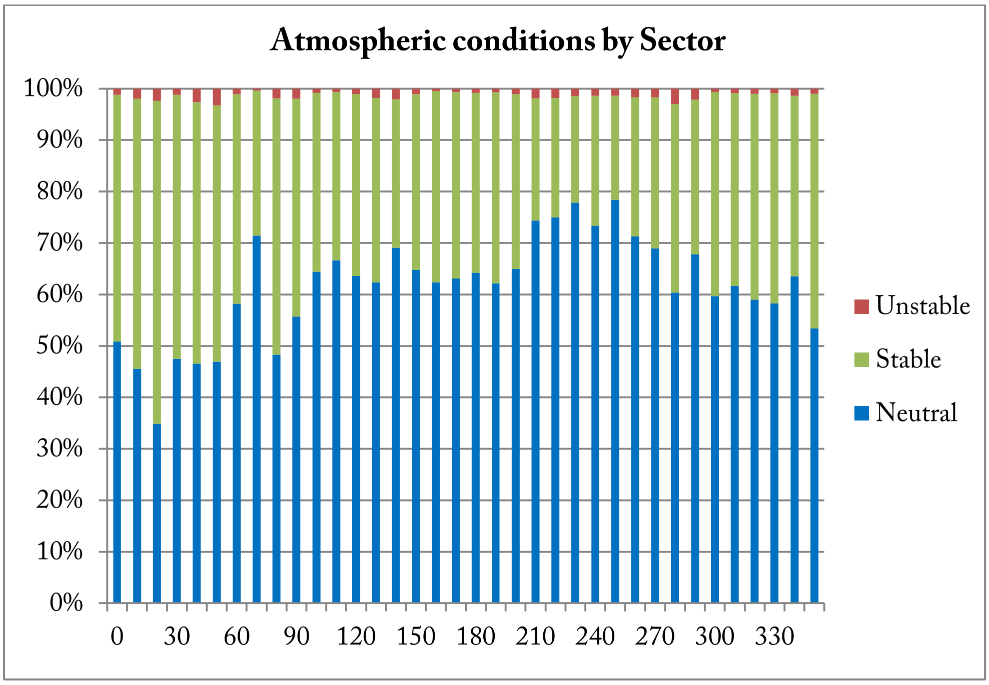

Figure 31. Atmospheric stability by sector at Bockstigen using AMOK tool. Neutral conditions are classified as $|1/L| < 0{,}005$, stable as $1/L > 0{,}005$, and unstable as $1/L < -0{,}005$. All available data is used.

The obtained Monin-Obukhov length is classified in Figure 31 according to the classification used by Hansen et al. (2014) in a similar study performed over Horns Rev. The neutral conditions are defined as $|L| > 200$ m, or what it is the same, $|1/L| < 0{,}005$.

It is noticeable that using AMOK tool describes the atmospheric stability as Neutral in the majority of cases, 64,5%, a completely different situation of what obtained with the Richardson Number. The reason of such a difference might rely on the uncertainty associated with each method. The Bulk Richardson Number is more sensible to thermometer accuracy, and might classify events that should fall into the neutral definition as stable.

Table 7. Stability classification at Bockstigen using AMOK tool.

Stability classification:	**With neutral conditions $|1/L| < 0{,}005$**
Stable:	30.331 (34,1%)
Neutral:	57.360 (64,5%)
Unstable:	1.198 (1,3%)

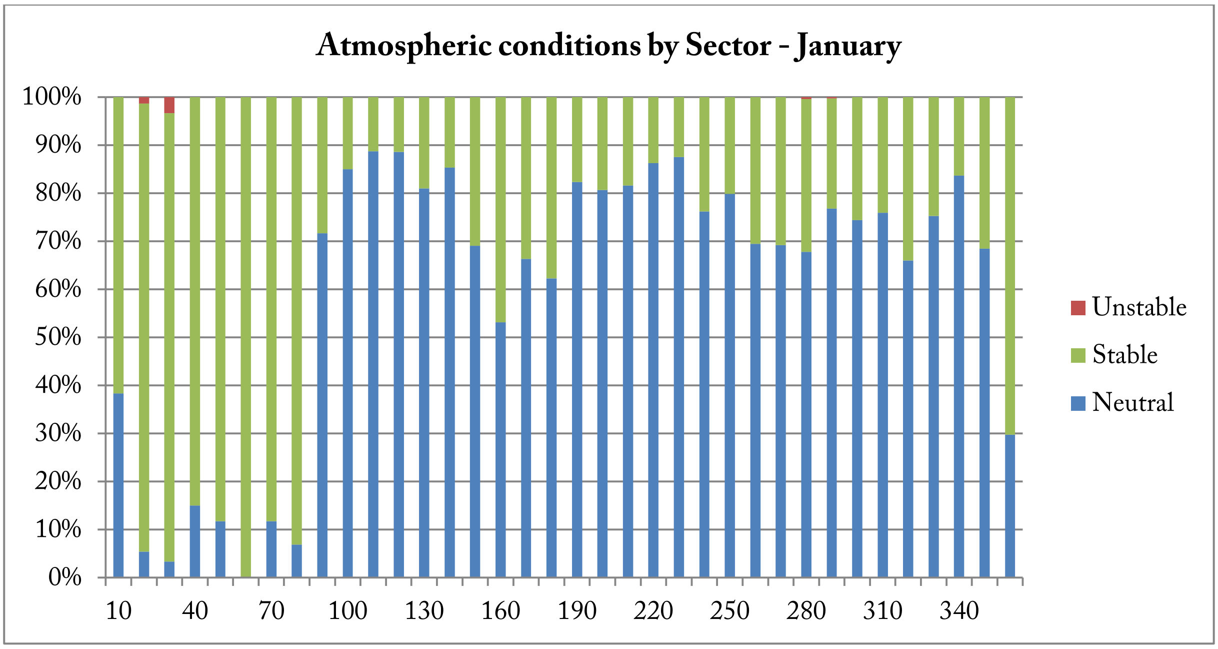

Figure 32. Atmospheric stability during the months of January at Bockstigen. Results obtained using AMOK tool.

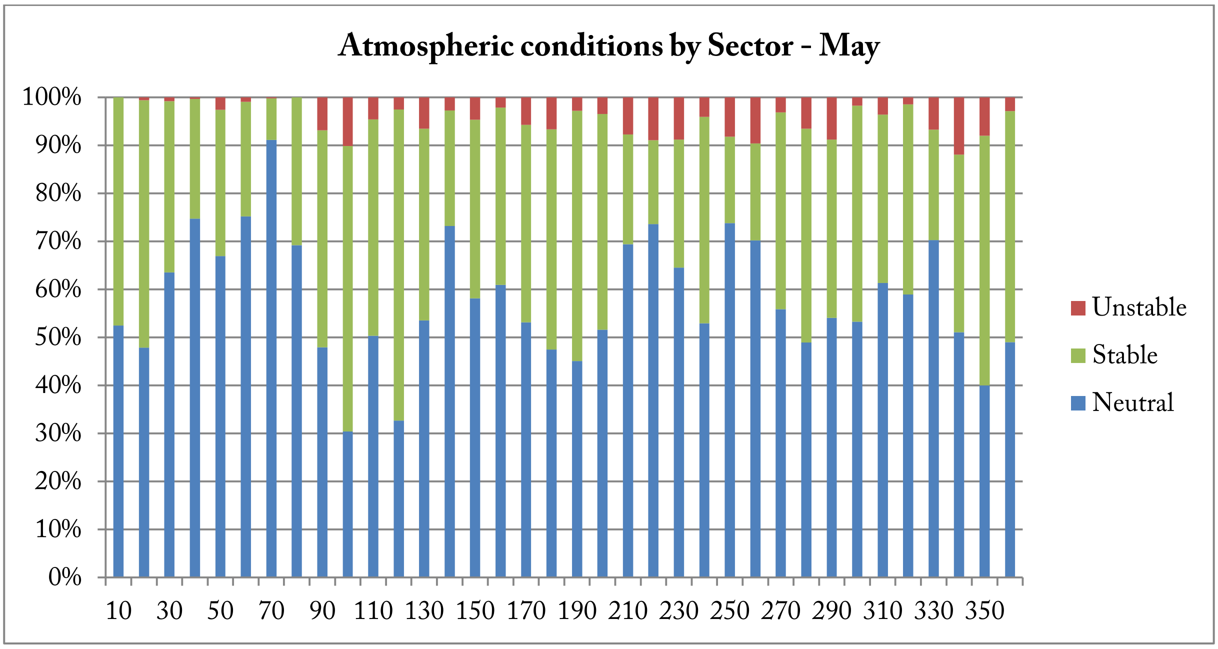

Figure 33. Atmospheric stability during the months of May at Bockstigen. Results obtained using AMOK tool.

Seasonal changes in stability can also be easily studied with the intensive Monin-Obukhov length. Figure 33 and Figure 19 show the stability conditions during the months of January and May respectively. It is remarkable that, during January, sectors 0º to 80º are completely stable whereas the rest of sectors have a wide majority of neutral cases (sectors 0º to 80º are land-affected, which have colder surface during winter than open sea sectors). During May, though, the situation is partly inverted: sectors 0º to 80º have majority of neutral cases, and sectors 90º to 350º have significantly more presence of unstable conditions (open sea sectors will suffer the effect of warm sea water whilst land-affected sectors will not).

5.2. Kustmast dataset

The recovery rate of Kustmast dataset is a little lower than the recovery of Havsmast. Still, the percentage is higher than 50% for all months excepting April, September and October (see Figure 34).

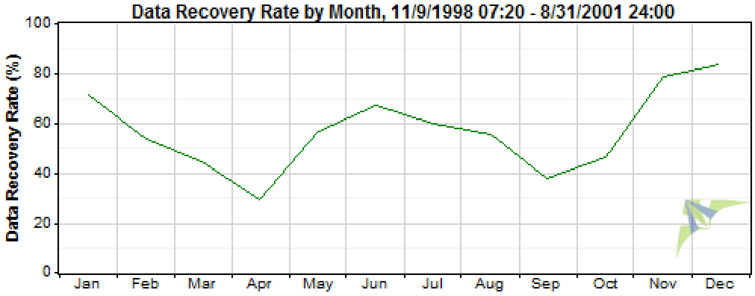

Figure 34. Monthly recovery rate of Kustmast anemometer measurements at 60 m height.

The wind rose obtained from this dataset can also be considered representative to a certain degree. However, the equipment mounted on Kustmast was adjusted or changed a few times during the monitoring campaign. To obtain a 'correct' windrose the wind direction signal has to be filtered and offsetted. See Section 5.3 for its correction procedure and results.

The wind histogram and its Weibull distribution, obtained without taking into account the wind direction (without direction bins), are still valid and representative of the site wind conditions. The wind histogram and Weibull distribution are plotted in Figure 35.

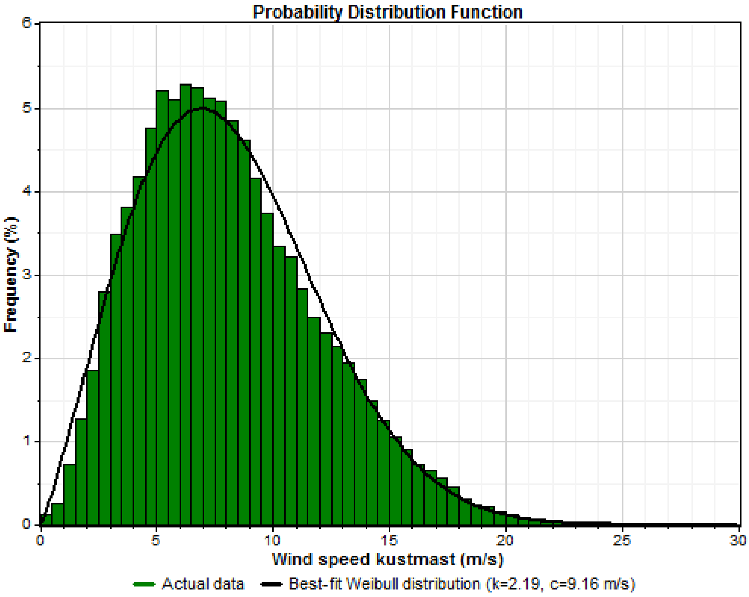

Figure 35. Histogram and Weibull distribution for all available Kustmast data.

Although there were some turbines situated near the Kustmast location during the measurement campaign, this dataset offers higher quality measurements and less uncertainty than Havsmast dataset. Figure 36 clearly indicates the wake cases for Havsmast and Kustmast. Not only Kustmast has less wake effects (just from three nearby obstacles), they happen at directions 20°, 70°, and 340°, directions with low wind energy content.

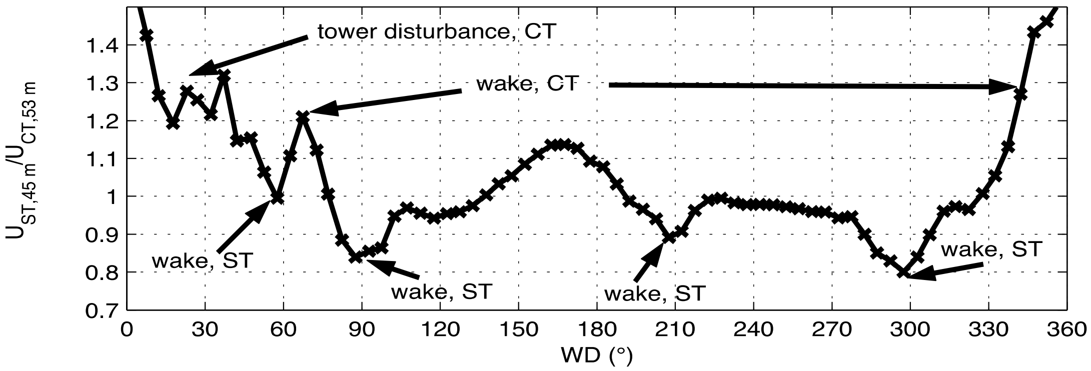

Figure 36. Average wind speed ratio between Havsmat anemometer at 45 m and Kustmast anemometer at 53 m high. Source: (Ganander et al., 2001)

5.3. Correlation Havsmast–Kustmast

The measured wind speed at Havsmast at 45 m in height has a very good correlation coefficient with the Kustmast measured wind speed at 60 m in height:

Table 8. Correlation coefficients between wind speeds at Havsmast 45 m and Kustmast 60 m high. Havsmast free-wind sectors are also correlated individually.

Data considered	Correlation coefficient
All sectors:	0,8794
Only free sectors:	0,8915

For a comparison of the correlation between free-wind sectors and wake-affected sectors see Annex IV.

However, when analysing the correlation between the wind directions of both datasets, its correlation shows more than one trend. Figure 37 displays a scatter plot of both wind directions during the concurrent period. Due to the proximity of the two measurement locations, the recorded wind directions should have a direct correlation, i.e. a slope of 1 in the scattered plot.

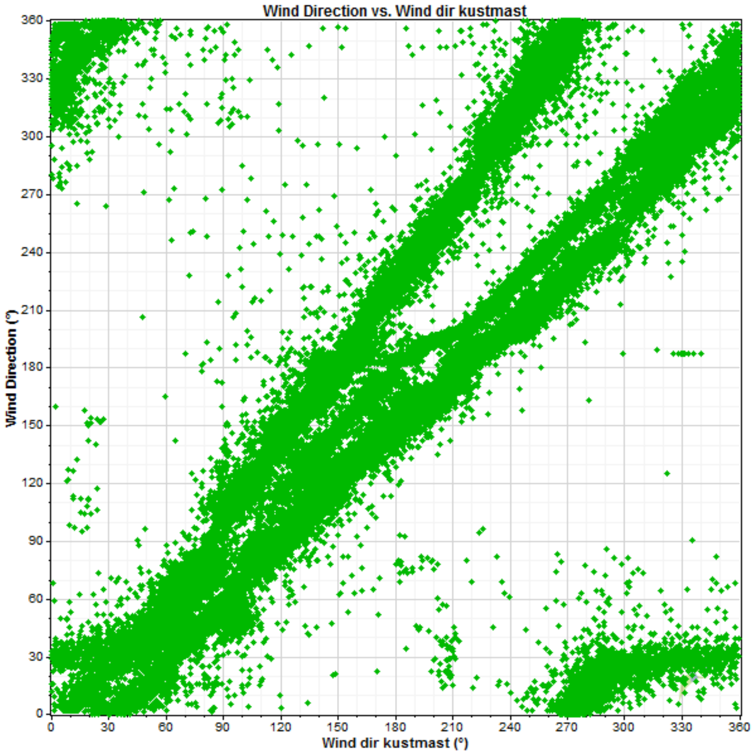

Figure 37. Scatter plot of Havsmast wind direction versus Kustmast wind direction during the concurrent period of both datasets. Two trends can be clearly seen.

Looking for elements that may have disturbed the measurements, the scatter plot is filtered by sector, wind speed, and period. The correlation by sector and at different wind speeds presents the same dual trend. Only when filtering by period its effect becomes clear.

There are three consecutive concurrent periods that have been identified, each one showing a really good correlation coefficient within that period:

Table 9. Correlation between Havsmast and Kustmast wind direction records during three concurrent periods.

Period	Correlation coef.	Offset value	Scaling value
10/1999 – 3/2000	0,9776	0,15º	0,94
4/2000 – 9/2001	0,9366	-22,5º	0,94
9/2001 – 1/2003	0,9745	-23,9º	1,38

As discussed above, the slope of the fitted line (scaling value) should be very close to 1 due to the proximity of the measurement locations. For this reason, all data from Kustmast that belongs to the period 9/2001 – 1/2003 is disregarded as it shows a ratio of almost 1,4. Analysing more closely this period, it is clear that there are measuring errors from the Kustmast wind vane. This can be seen in the lower-right corner of Figure 38, where at a wind direction of 30º in the Havsmast there is a wide range of wind directions recorded at the Kustmast (ranging from 270º to 360º).

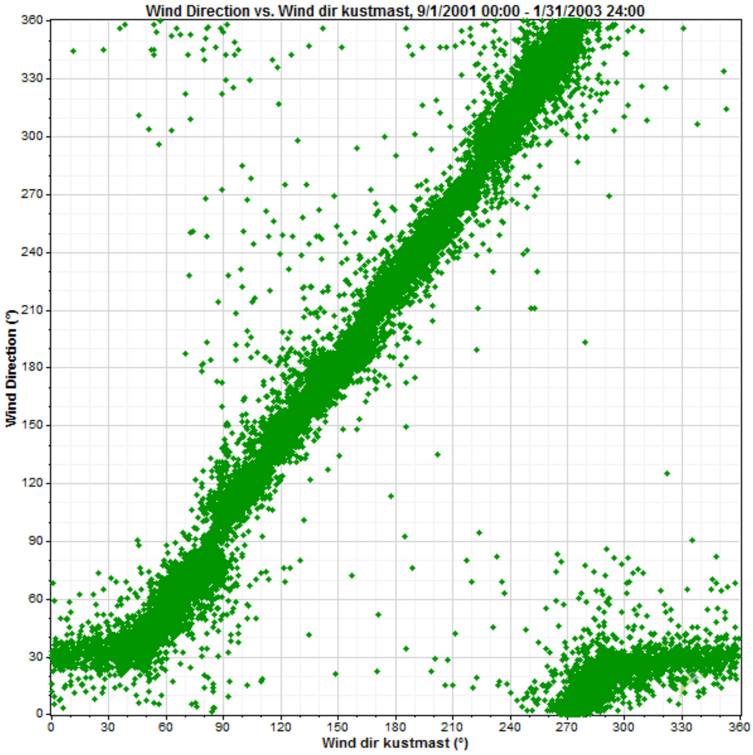

Figure 38. Scatter plot of Havsmast versus Kustmast wind directions for the period 9/2001 – 1/2003.

The data recorded during the period 10/1999 – 3/2000 has a scaling factor of 0,94 (very close to 1) and the wind veer between the two met mast positions can be considered null as their offset in only 0,15º. This is consistent with the location and terrain orography, as Kustmast and Havsmast are only 4,6 km separated, and there are no geological formations between them that would introduce wind veer.

On the next concurrent period, 4/2000 – 9/2001, Kustmast wind vane might have suffered a misalignment and shows a large offset when correlating both wind directions. The scaling factor has exactly the same value as in the previous period, but the offset value rises to -22,5º. A wind veer of 22,5º between the two met mast locations is very unrealistic. A correction in the measured wind direction is applied for this period. Assuming that there is no wind veer between both locations, an offset of -22,5º is applied to the Kustmast measurements. The results of the filtering and offsetting are shown in Figure 39.

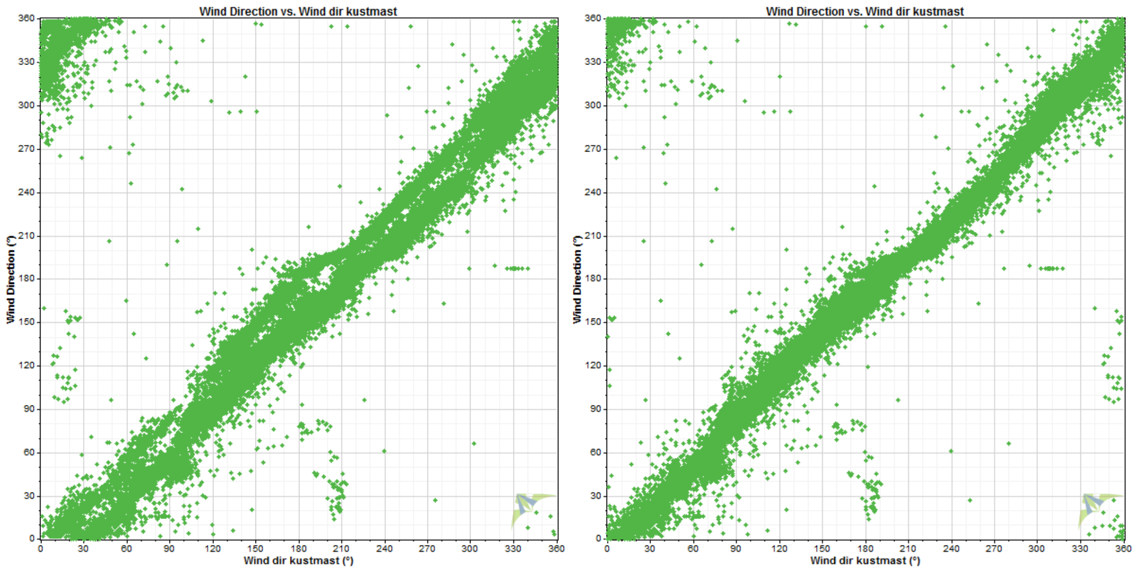

Figure 39. Scatter plot of Havsmast wind direction versus Kustmast wind direction without considering the discarded data (left) and after applying the offset to the data of the second concurrent period (right).

The Kustmast wind rose before and after applying the filtering and correction are shown in Figure 40.

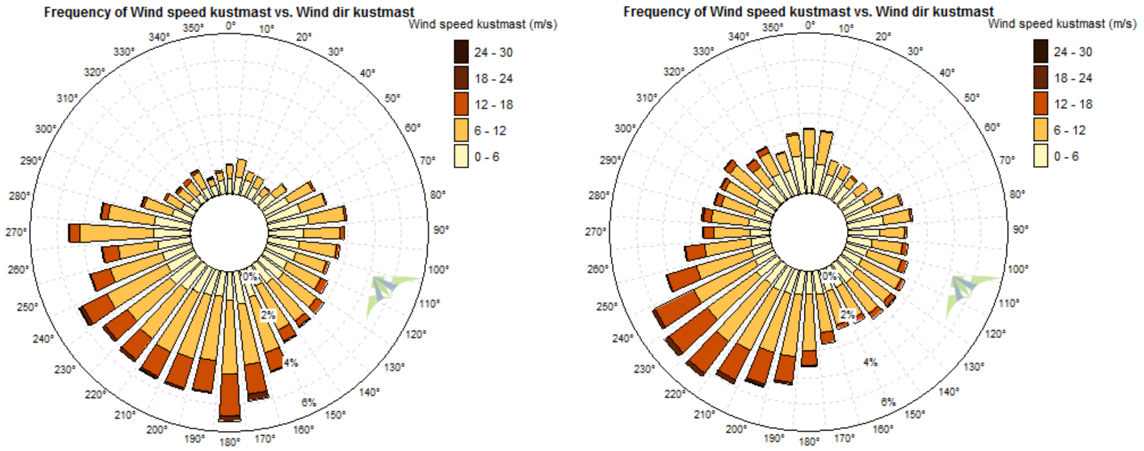

Figure 40. Kustmast wind rose before applying the filtering and correction descried above (left) and after (right).

5.4. Long-term predicted climatology at Bockstigen

The wind measurements recorded by Havsmast are wake affected and present a high level of uncertainty. It has been seen in Section 5.2 that Kustmast have reduced wake effects (and thus less uncertainty), and in Section 5.3 that it has a very high correlation coefficient with Havsmast. For these reasons Kustmast will be used to assess the wind climate at Bockstigen.

Kustmast time series are transferred to Bockstigen using WindSim. Kustmast measurements are at 60 m height above the ground level, but its transferred meteorology is calculated at 50 m in height for ease its long-term correlation.

Thirty years of historical data are downloaded from MERRA as a reference to correlate and long-term predict the transferred meteorology from Kustmast. MERRA is a reanalysis database with more than 30 years of historic data freely available for download. It has grid points worldwide with 0,5° latitudinal and 0,66° longitudinal spacing. For each grid point, a dataset comprises hourly values of wind speed and direction (among others) at 50 m above the ground starting from 1979 (Gmao.gsfc.nasa.gov, 2014). The nearest grid point to Bockstigen is shown in Figure 41. Luckily is placed offshore, 9,7 km southwest from the site, so it will be a good reference for the site climate.

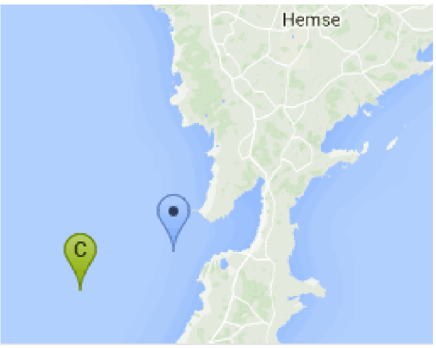

Figure 41. The location of the MERRA grid point (green pin) closest to Bockstigen (blue pin) is 57°N 18°E. Source: (Gmao.gsfc.nasa.gov, 2014).

The Kustmast transferred-to-site climatology and the selected MERRA dataset have 19,5 months of concurrent data (complete Kustmast recorded period) and present good correlation coefficients: 76,2% for wind speed and 90,0% for wind direction. MERRA data from three consecutive decades (1980 to 2010) is used to long-term predict the site climatology. Different correlation algorithms are tested. Matrix method with 1 direction bin proves to perform the best as it is shown in Figure 42, and thus it is used to long-term predict.

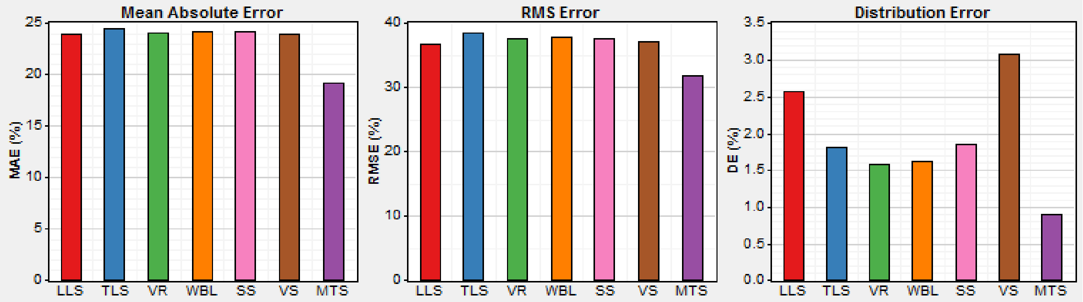

Figure 42. Errors obtained testing Linear Least Squares (red), Total Least Squares (blue), Variance Ratio (green), Weibull Fit (orange), Speed Sort (pink), Vertical Slice (brown), and Matrix Time Series (purple) algorithms.

With the aim to fill in the missing blanks in Kustmast dataset over the measuring campaign period, the transferred Kustmast dataset is first correlated and predicted for the same years of the concurrent measurements: 1999 – 2003. The wind roses and energy roses for the transferred Kustmast and for its 4-year predicted dataset are shown in Figure 43. Both energy roses show very similar energy content for the majority of the 36 sectors, indicating that MERRA dataset offers a good agreement with the local observations. Only the main wind direction appears to be shifted: MERRA has the sector with high energy content at 230° while Kustmast at 220°.

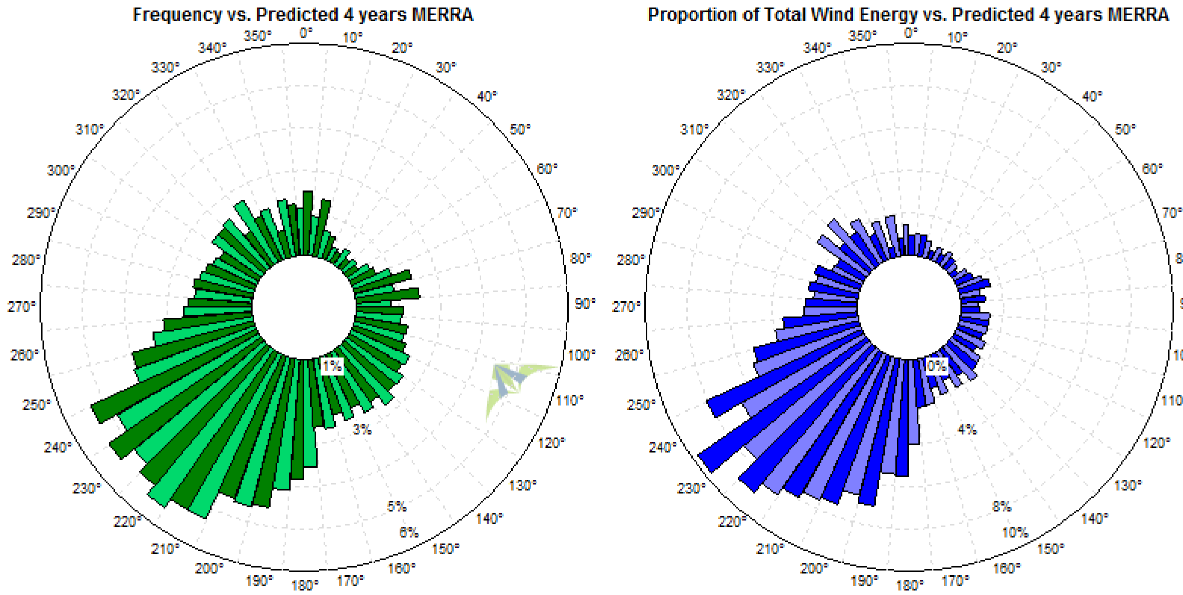
Frequency vs. Predicted 4 years MERRA

Proportion of Total Wind Energy vs. Predicted 4 years MERRA

Figure 43. Energy roses of Kustmast Transferred to site dataset and its 4-year predicted dataset using MERRA data from 1999 to 2003. Dark green and dark blue represent MERRA dataset.

The annual mean wind speed at 50 m high obtained from the transferred Kustmast, 30-year long-term predicted dataset is 7,9 m/s, and its main wind direction comes from 231º. There is a clear shift in the main wind direction when compared to the original 30-year long MERRA dataset, which its main direction is from 217º. This shift can be appreciated in Figure 44, and demonstrates that the long-term predicted dataset preserves the characteristics of the local climate.

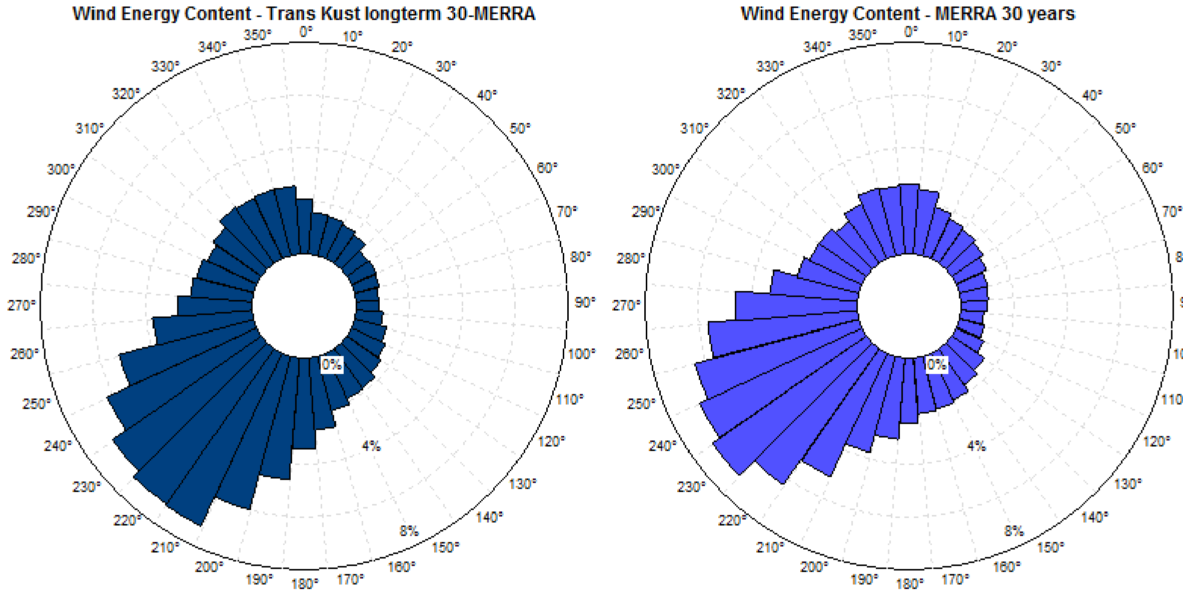
Wind Energy Content - Trans Kust longterm 30-MERRA

Wind Energy Content - MERRA 30 years

Figure 44. Long-term predicted energy rose for Kustmast transferred to site dataset using 30 years of MERRA data (left), and energy rose for MERRA dataset for the same 30-year period (right).

To perform the park layout optimization of Chapter 0 it will be necessary to know the wind resources at 85 m above the sea level (assumed hub height of this case study). The Kustmast transferred to site, long-term predicted dataset is transferred to 85 m in height using

WindSim. The model with higher sea roughness, 0,002 m, is used to perform the climatology transferring as it provides the best agreement with observations for the sectors with higher energy content (see part 4.2.1). Figure 45 shows the Weibull distribution at Bockstigen at a height of 85 m.

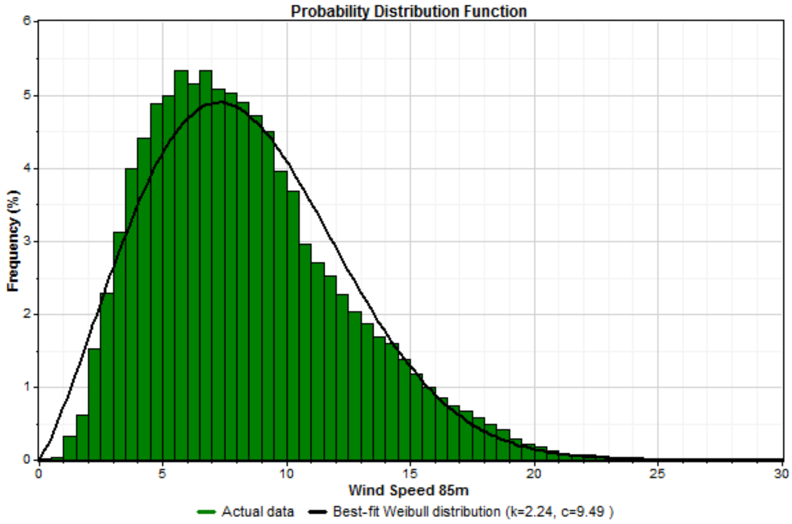

Figure 45. Histogram and Weibull fit for Bockstigen long-term predicted climatology at a height of 85 m.

The wind and energy roses are shown in Figure 46. The main wind direction is the same as the reference dataset at 50 m high, 231º, but the annual mean wind speed is 8,38 m/s.

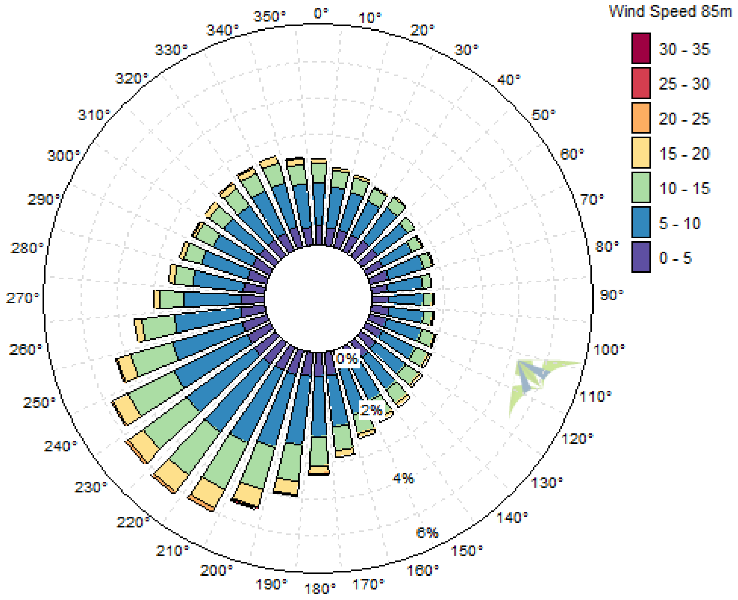

Figure 46. Wind rose showing wind speed bins of Bockstigen long-term predicted climatology at a height of 85 m.

The main wind direction to consider for wake interaction analysis is not only direction 231º. It can be seen in Figure 47 that sectors 210º – 230º have very similar level of energy content. Therefore, the wake effect minimization shall be carried out considering those sectors as main wind direction sectors.

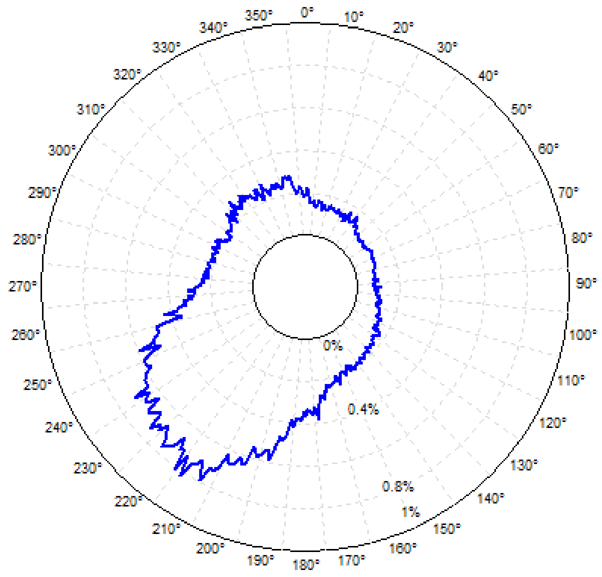

Figure 47. Energy rose of Bockstigen long-term predicted climatology at a height of 85 m with 360 directional bins.

5.4.1. *Extreme wind speed at Bockstigen*

The extreme wind speed in a 50-year period is calculated using the Periodic Maxima method, preconditioning the data with square values and using 4-months maxima. All 30-year predicted data at 85 m high are used. The Gumbel best-fit is shown in Figure 48. The obtained extreme wind speed is 33,8 m/s.

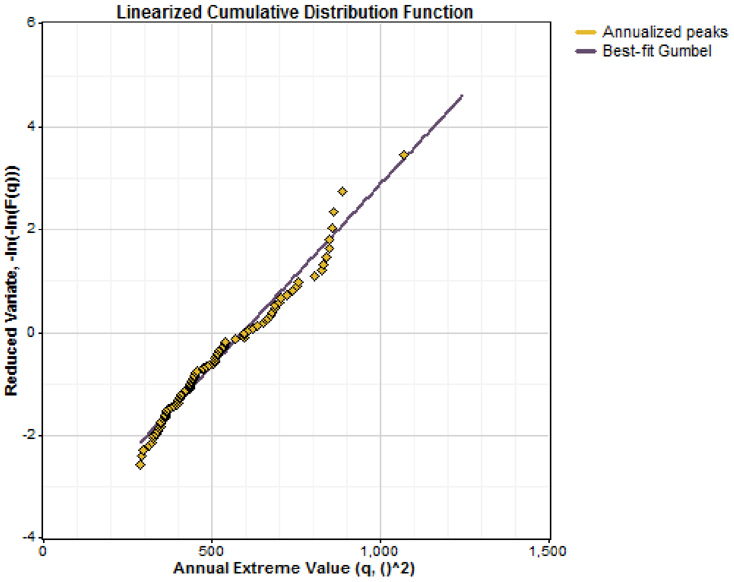

Figure 48. Gumbel best-fit using Periodic Maxima method with square values preconditioning used to obtain 50-year extreme wind speed at Bockstigen at 85 m.

5.5. Wind turbine classification

When transferring the climatology from Kustmast to Bockstigen the wind speed standard deviation, and hence the atmospheric turbulence, is lost. Only the atmospheric turbulence measured by Havsmast can be used as reference. In Figure 27 it can be seen that the level of turbulence intensity at 45 m high is quite low, as usual in offshore site. The representative value at 15 m/s is lower than 10%. As the turbulence intensity decreases in height, it can be assured that at a hub height of 85 m the turbulence level will be lower than 10%.

However, the added turbulence intensity due to wake effects has to be taken into account. It has been seen in part 2.2.1 that the total turbulence intensity can increase up to 18% inside a wind farm cluster, but data indicating at which wind speed that turbulence intensity is measured is missing. In any case, the turbulence intensity supported by downwind units will be always higher than the atmospheric turbulence, and therefore the turbulence classification for offshore sites must always be considered A (see Table 10 below).

Considering the 50-year extreme wind speed calculated in part 5.4.1, 33,8 m/s, the site classification is assessed as class IIA.

Table 10. Wind turbine classification according to IEC 61400-1

Wind turbine classes	**I**	**II**	**III**
50-year extreme wind (m/s)	50	42,5	37,5
A *TI*(15m/s)	16%		
B *TI*(15m/s)	14%		
C *TI*(15m/s)	12%		

5.6. Power performance and wake effects at Bockstigen

5.6.1. Wake directions and free wind sectors

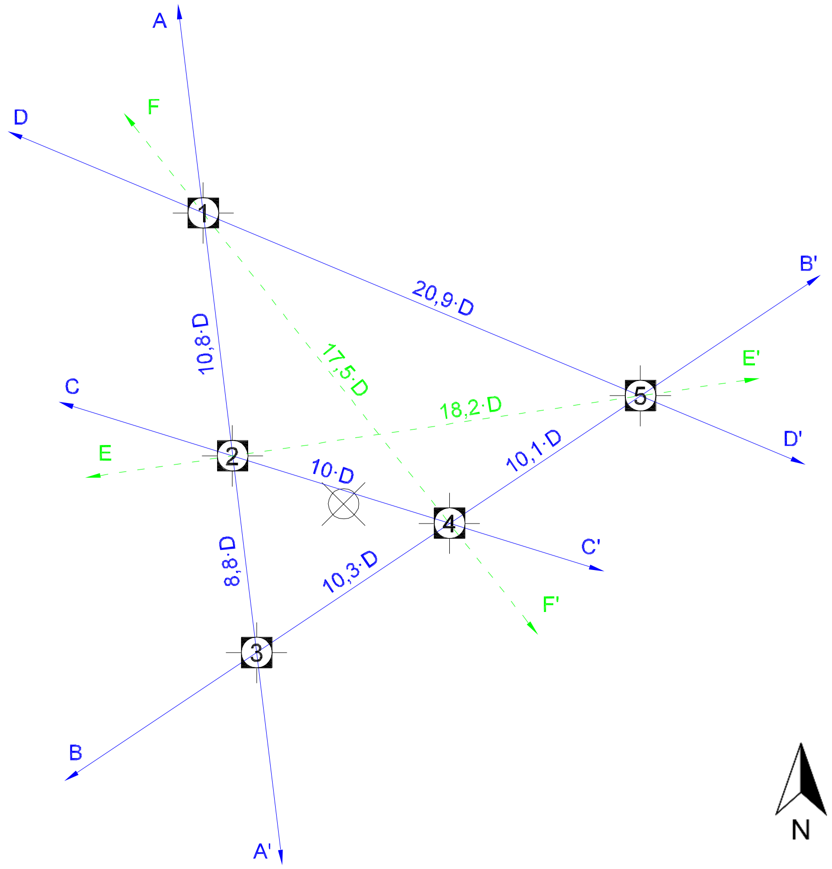

Figure 49. Bockstigen park layout showing the location of its five units, directions with wake effects, and its distance between units in rotor diameters $D = 37$ m.

At Bockstigen wind farm there are wind directions with one and two wake effects interfering with downwind turbines. These directions come from the arrangement of the park layout as shown in Figure 49.

The directions with wake effects are:

- A–A': 353,1–173,1°
- B–B': 236,1–56,1°
- C–C': 287,3–107,3°
- D–D': 292,7–112,7°
- E–E': 261,6–81,6°
- F–F': 321,6–141,6°

only directions A–A' and B–B' encounter two wakes interacting with a downwind unit.

Each turbine is affected in a different manner by wakes when changing wind direction. As introduced in Chapter 1 the wake width is about ±15°. Assuming linear expansion, it can be ensured that there are wake effects within ±10°, and there shall be free wind conditions beyond ±20°.

Table 11. Wake-affected and free wind sectors per turbine unit. The wake-affected sectors are obtained considering a wake width of ±10°, and the free wind sectors are obtained assuming there are no wake effects beyond ±20°.

Turbine	Wake-affected sectors	Free wind sectors		
WTG 1	D’: 112,7 ± 10°	≤ D’ - 20° ≈ 92°	≥ D’ + 20° ≈ 133°	193° ≤ S1 ≤ 360°,
	F’: 141,6 ± 10°	≤ F’ - 20° ≈ 121°	≥ F’ + 20° ≈ 162°	0° ≤ S1 ≤ 92°
	A’: 173,1 ± 10°	≤ A’ - 20° ≈ 153°	≥ A’ + 20° ≈ 193°	
WTG 2	E’: 81,6 ± 10°	≤ E’ - 20° ≈ 61°	≥ E’ + 20° ≈ 102°	13° ≤ S1 ≤ 61°
	C’: 107,3 ± 10°	≤ C’ - 20° ≈ 87°	≥ C’ + 20° ≈ 128°	128° ≤ S2 ≤ 153°
	A’: 173,1 ± 10°	≤ A’ - 20° ≈ 153°	≥ A’ + 20° ≈ 193°	193° ≤ S3 ≤ 333°
	A: 353,1 ± 10°	≤ A - 20° ≈ 333°	≥ A + 20° ≈ 13°	
WTG 3	B’: 56,1 ± 10°	≤ B’ - 20° ≈ 36°	≥ B’ + 20° ≈ 76°	13° ≤ S1 ≤ 26°
	A: 353,1 ± 10°	≤ A - 20° ≈ 333°	≥ A + 20° ≈ 13°	76° ≤ S2 ≤ 333°
WTG 4	B’: 56,1 ± 10°	≤ B’ - 20° ≈ 36°	≥ B’ + 20° ≈ 76°	342 ≤ S1 ≤ 36°
	B: 236,1 ± 10°	≤ B - 20° ≈ 216°	≥ B + 20° ≈ 256°	76 ≤ S2 ≤ 216°
	C: 287,3 ± 10°	≤ C - 20° ≈ 267°	≥ C + 20° ≈ 307°	256 ≤ S3 ≤ 267°
	F: 321,6 ± 10°	≤ F - 20° ≈ 301°	≥ F + 20° ≈ 342°	
WTG 5	B: 236,1 ± 10°	≤ B - 20° ≈ 216°	≥ B + 20° ≈ 256°	313 ≤ S1 ≤ 360°,
	E: 261,6 ± 10°	≤ E - 20° ≈ 241°	≥ E + 20° ≈ 282°	0 ≤ S1 ≤ 216°
	D: 292,7 ± 10°	≤ D - 20° ≈ 272°	≥ D + 20° ≈ 313°	

5.6.2. *Experimental power curves*

To obtain the experimental power curve per each turbine, data from Table 5 and Table 11 has to be crossed. Only data within the free wind sectors of Havsmast can be used together with data free of wake effects of the relevant turbine to create the power curve. The unusual location of the met mast in the centre of the park layout provides only few gaps where both datasets are undisturbed. Table 12 shows the available sectors per turbine.

Table 12. Undisturbed sectors for both Havsmast and the relevant turbine.

Turbine	Undisturbed sectors for turbine and met mast (for obtaining power curve)		
Free Met Mast (Ref.)	355° ≤ FWS1 ≤ 360°, 0° ≤ FWS1 ≤ 50°	120° ≤ FWS2 ≤ 190°	230° ≤ FWS3 ≤ 273°
WTG 1	355° ≤ FS1 ≤ 50°	-	230° ≤ FS2 ≤ 273°
WTG 2	13° ≤ FS1 ≤ 50°	128° ≤ FS2 ≤ 153°	230° ≤ FS3 ≤ 273°
WTG 3	13° ≤ FS1 ≤ 26°	120° ≤ FS2 ≤ 190°	230° ≤ FS3 ≤ 273°
WTG 4	355° ≤ FS1 ≤ 36°	120° ≤ FS2 ≤ 190°	256° ≤ FS3 ≤ 267°
WTG 5	355° ≤ FS1 ≤ 50°	120° ≤ FS2 ≤ 190°	-

To obtain the power curve the production data has also to be filtered out of outsiders and idle or downtime states, which otherwise will have a strong influence on the results. The 10-min mean power records are filtered graphically to keep only the entries with a measured power within approximately ±50% of the nominal power at that wind speed. Figure 50 shows the experimental power measurements versus the wind speed at hub height, with the disregarded measurements marked in red.

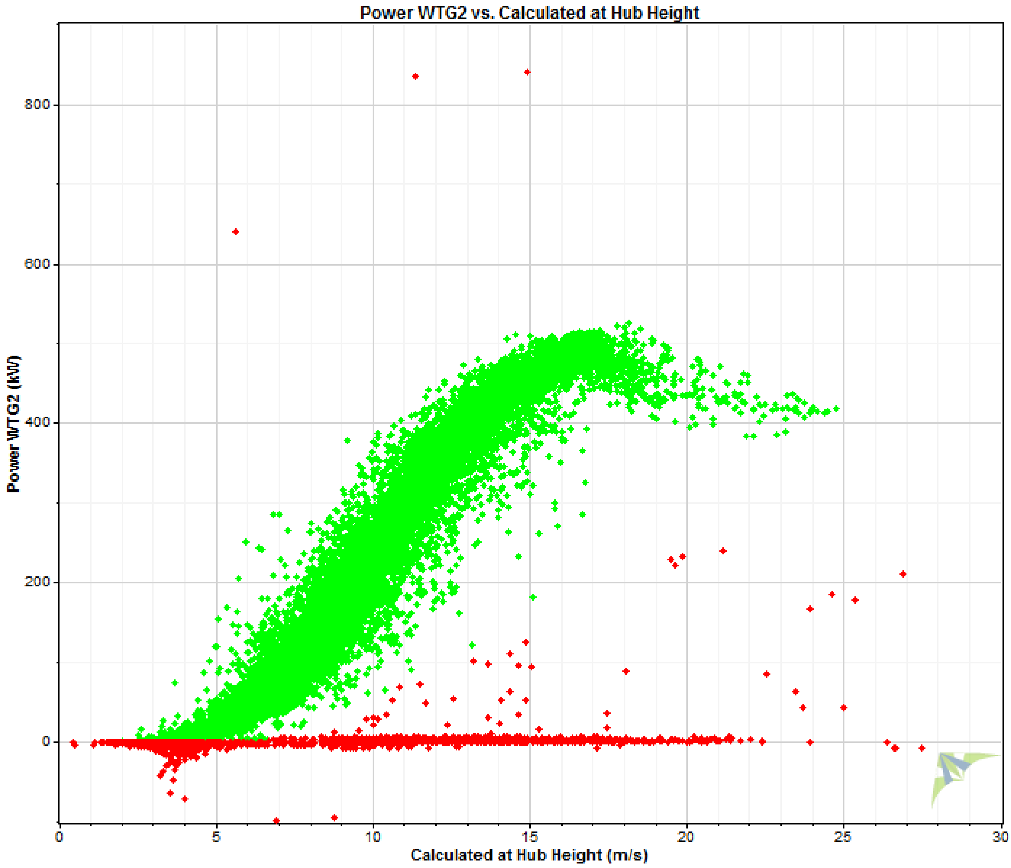

Figure 50. Filtering of the recorded power values of turbine 2 by graphical means. Green dots are valid 10-min averaged observations and red dots are invalid data.

The experimental power curve of each wind turbine is plotted in Figure 51. Although all turbines are the same model and operate under the same conditions, their power curves differ remarkably. Although all units seem to deliver their maximum power at the same rated wind speed of 16 m/s, their maximum power varies from 480 (turbine 2) to 560 kW (turbine 1). The results presented here are consistent with those obtained by Ganander et al. (2001).

Few reasons could be considered to explain such a big difference in power output: some turbines underperform and some others outperform the rated power, or maybe some turbines suffer from a major yawing misalignment, seeing less wind than the rest. One could also consider that the wind speed conditions vary significantly throughout the site. However, this cannot be true in all cases, for example turbines 2 and 4 are the closest to Havsmast nevertheless their power curves differ significantly.

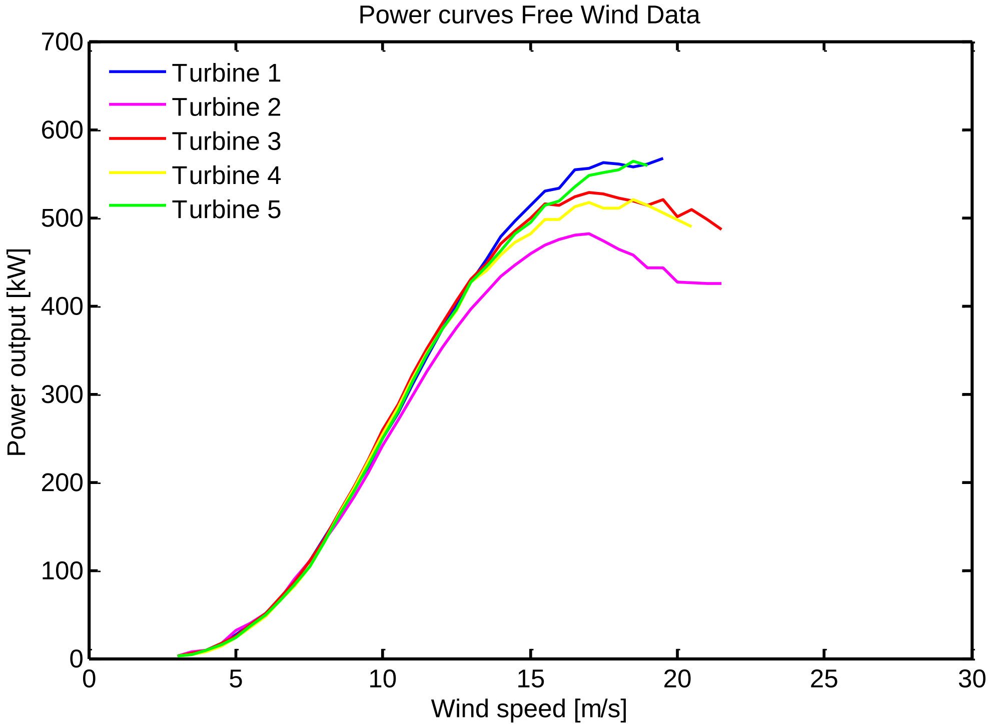

Figure 51. Experimental power curves using undisturbed measurements for each turbine.

6. Discussion – Data not valid for wake models validation

The data available from Bockstigen have a high level of uncertainty. The wind measurements from Havsmast present wake effects that are not easy to remove, the filtered dataset have a lot of blank periods generated by recording errors, the power output and nacelle anemometer measurements are not accurate enough to use to obtain power curves, some turbines might be underperforming or suffer yawing misalignment. All together, in consequence, makes the available data not suitable for validating any wake model. Experimental data from another offshore wind farm shall be used for that purpose.

Part II. Wake models validation at Horns Rev

7. Introduction to Horns Rev wind farm

Horns Rev offshore wind farm is located on the Danish North sea, about 15 km west from the seaside town of Blåvanshuk. It consists of 80 units Vestas V80 2MW, with hub height of 70 m and rotor diameter *D* of 80 m. The total installed capacity is 160 MW.

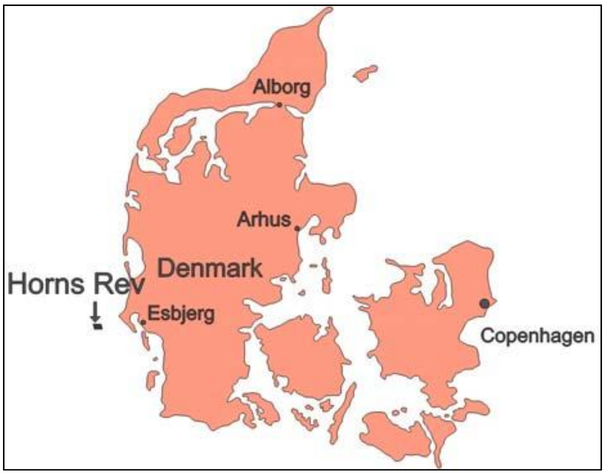
Alborg
Arhus
Denmark
Horns Rev
Esbjerg
Copenhagen

Figure 52. Danish map showing the location of Horns Rev wind farm. Source: (Hasager et al., 2007).

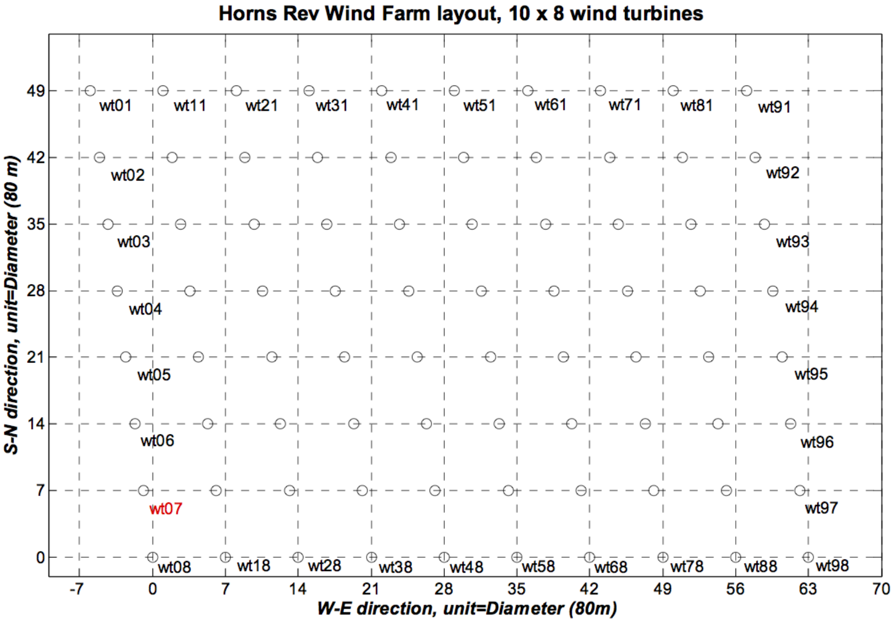
Horns Rev Wind Farm layout, 10 x 8 wind turbines
S-N direction, unit=Diameter (80 m)
W-E direction, unit=Diameter (80m)
49
42
35
28
21
14
7
0
-7
0
7
14
21
28
35
42
49
56
63
70
wt01
wt11
wt21
wt31
wt41
wt51
wt61
wt71
wt81
wt91
wt02
wt92
wt03
wt93
wt04
wt94
wt05
wt95
wt06
wt96
wt07
wt97
wt08
wt18
wt28
wt38
wt48
wt58
wt68
wt78
wt88
wt98

Figure 53. Horns Rev wind farm layout, with 80 turbines Vestas V80 2MW, aligned in a matrix-like layout with 7D spacing between rows and columns. Source: (Hansen, 2008a).

The turbines are arranged in a matrix-like layout, with 8 arrays aligned East-West with 10 units in each array. The spacing between arrays (rows) and between units of the same array (columns) is the same, 7 rotor diameters (7D). Figure 53 shows the wind farm layout.

Intrinsically, a matrix-like arrangement has some directions with noticeable wake effects. Three main wake cases have been studied by Hansen (2008), who classified atmospheric observations and park performance for the following main wake directrices:

- flow from 270º with 7D spacing;
- flow from 221º with 9,4D;
- and flow from 312º with 10,4D spacing.

The three main wake directrices are plotted in Figure 54. In their study, the power losses are tabulated for three free stream wind velocities: 6, 8 and 10 m/s. The atmospheric stability is also studied and there are some recorded measurements under stable, neutral and unstable conditions. Unfortunately, in Hansen's publication there are only enough records to perform a wake model validation under unstable conditions. Although there are few records under stable and neutral conditions those are only at 6 m/s and for the wake centerline, and their related power deficit is not tabulated.

For this wake validation study it is therefore used the measured power deficit under unstable conditions (for the original experimental values the reader is referred to the original publication Hansen, 2008).

The turbine power curve used to model the power losses is also provided by Hansen in his paper. The V80 units of Horns Rev have a specific power curve (see Table 13).

Table 13. Power curve and thrust curve of a Horns Rev turbine. Source: (Hansen, 2008a).

Wind Speed [m/s]	Power [kW]	Thrust Coefficient	Wind Speed [m/s]	Power [kW]	Thrust Coefficient
4	66.6	0.818	15	1997	0.249
5	154	0.806	16	1999	0.202
6	282	0.804	17	2000	0.167
7	460	0.805	18	2000	0.140
8	696	0.806	19	2000	0.119
9	996	0.807	20	2000	0.102
10	1341	0.793	21	2000	0.088
11	1661	0.739	22	2000	0.077
12	1866	0.709	23	2000	0.067
13	1958	0.409	24	2000	0.060
14	1988	0.314	25	2000	0.053

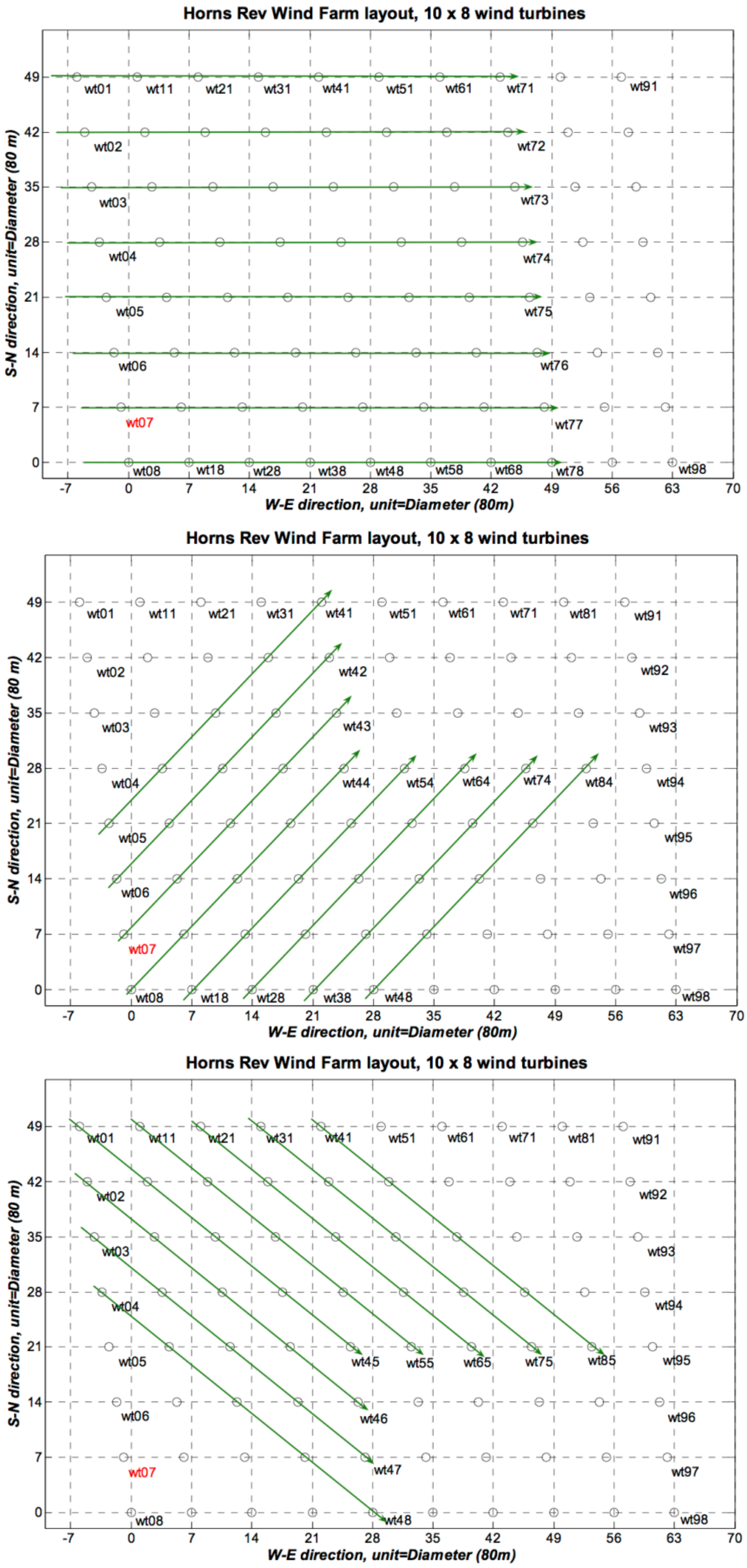
Horns Rev Wind Farm layout, 10 x 8 wind turbines
S-N direction, unit=Diameter (80 m)
W-E direction, unit=Diameter (80m)
-7
0
7
14
21
28
35
42
49
56
63
70
wt01
wt02
wt03
wt04
wt05
wt06
wt07
wt08
wt11
wt18
wt21
wt28
wt31
wt38
wt41
wt42
wt43
wt44
wt45
wt46
wt47
wt48
wt51
wt54
wt55
wt58
wt61
wt64
wt65
wt68
wt71
wt72
wt73
wt74
wt75
wt76
wt77
wt78
wt81
wt84
wt85
wt91
wt92
wt93
wt94
wt95
wt96
wt97
wt98

Figure 54. Wake effect cases at Horns Rev. Cases with flow from 270º (top), flow from 221º (middle), and flow from 312º (bottom). Source: (Hansen, 2008a).

7.1.1. *Atmospheric turbulence at Horns Rev*

It has been seen in Section 2.2 that the atmospheric turbulence at Horns Rev changes with the wind speed. Yet, when considering the study cases with 6, 8 and 10 m/s the atmospheric turbulence can be considered constant to 7% (see Figure 3).

This value is consistent with Figure 56, which shows similar turbulence intensity values measured at sectors 270º, 221º and 312º. Although the turbulence intensity value stretches more in one sector than another, for comparison purposes a mean atmospheric turbulence intensity of 7% is used in all three simulated wake directions.

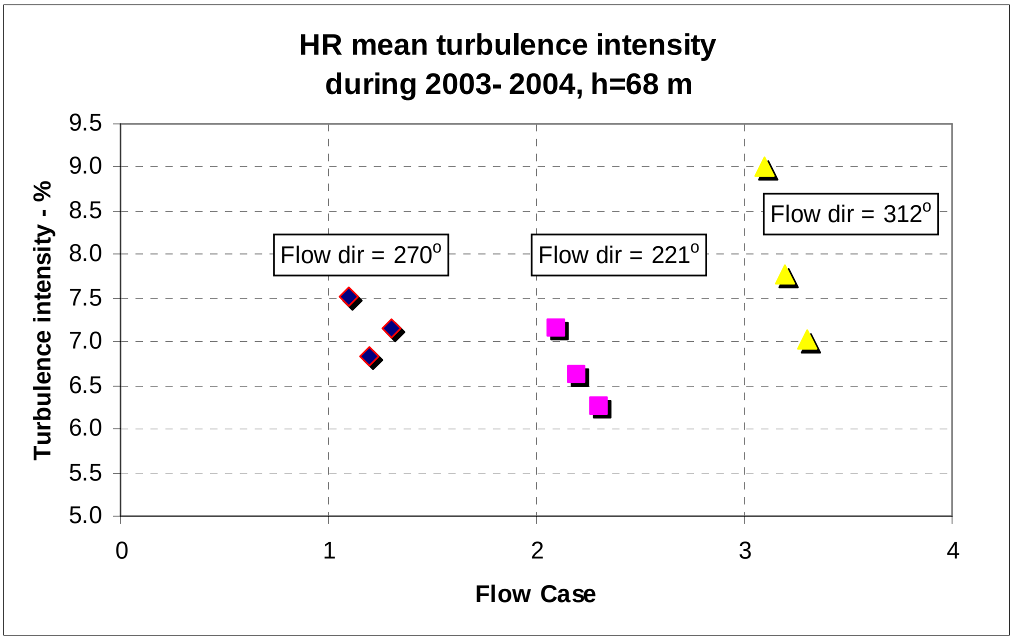

Figure 55. Mean turbulence intensity extracted from free wind speed measurements from two years previous to the park construction, and sorted by flow case. (Source: Deliverable D8.1, Hansen, 2008).

7.1.2. *Atmospheric stability at Horns Rev*

Hansen (2008) has also studied the atmospheric stability during 2005. The atmospheric conditions were classified into four types using the bulk Richardson number based on air/air temperature measurements. Table 14 shows the annual stability percentages obtained.

Table 14. Atmospheric classification at Horns Rev during 2005. Source: (Hansen, 2008a).

Atmospheric conditions	**Intensive Monin-Obukhov length**	**Total hours**	**Percentage**
Very unstable	$1/L < -0{,}32$	1.920 hours	22,3%
Unstable	$-0{,}32 < 1/L < -0{,}053$	1.881 hours	21,8%
Near neutral	$-0{,}053 < 1/L < +0{,}053$	2.618 hours	30,4%
Stable	$1/L > 0{,}053$	2.187 hours	25,4%
	Total:	8.606 hours	

7.1.3. *Sea roughness at Horns Rev*

The sea roughness is assessed from the literature. It has been already introduced in Section 2.3 that the sea roughness at Horns Rev has been object of study. The value used here is extracted from Figure 6 considering neutral atmosphere: 0,0002 m.

7.1.4. *Boundary layer depth at Horns Rev*

The boundary layer depth over Horns Rev was measured during the Danish Galathea expedition in 2006 (Hasager et al., 2007). The results show an average depth of 400 m.

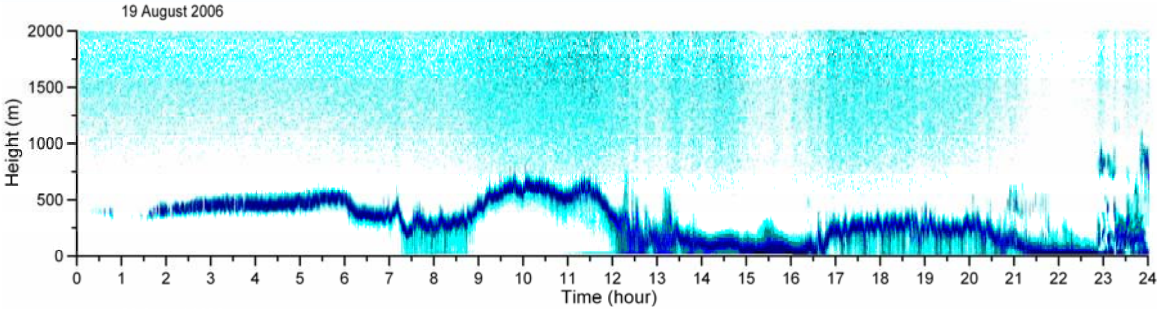

Figure 56. The top of the oceanic boundary layer is obtained by measuring the concentration of aerosols. The dark blue line shows the boundary layer height Source: Hasager et al., *12MW Horns Rev experiment*, (2007).

8. Methodology – Wake models validation

8.1. Simulation cases

There are data available (velocity deficit and power losses) for the three main wake directions described in Figure 54, and they are classified into three wind speeds, 6, 8, and 10 m/s, which give a total of nine flow cases to simulate. For each flow case, there are three analytical wake models to test, and each wake model has one main parameter to adjust.

The validation is performed adjusting the relevant parameter and comparing the simulated power output with the experimental power output of the specific flow case. Although all reference data are under slightly unstable conditions, only neutral conditions are simulated. Thus, the wake parameters obtained during the validation will reflect the best match for slightly unstable conditions.

Table 15. Cases that are simulated for each flow direction 270°, 221°, 312°.

Wake model	Wind Speed at 70 m	Atmospheric conditions	Directional variation	Wake decay or Turbulence Intensity
Jensen	6; 8; 10 m/s	Neutral	±15°, every 1°	0,04; 0,05; 0,06; 0,07; 0,08; 0,085
Larsen	6; 8; 10 m/s	Neutral	±15°, every 1°	5%; 5,5%; 6%; 6,5%; 7%; 7,5%; 8%
Ishihara	6; 8; 10 m/s	Neutral	±15°, every 1°	8%; 10%; 12%; 14%; 16%; 18%

Table 15 indicates the cases that are simulated for each flow direction: 270°, 221°, 312°. In order to compare the results with the experimental values, a directional variation is performed around the main wake direction, with 1° steps until ±15°. The values obtained in those 31 directional variations around the wake centerline are averaged afterwards in bins of ±1°, ±5°,

±10°, and ±15°. The available experimental data has been binned in the same manner, thus the comparison between them is straightforward.

8.2. WindSim modeling set-up

The model terrain is created as a flat uniform surface with constant roughness length, simulating the flat sea surface. The grid is created using refinement around the site area following the same guidelines introduced in Section 4.2. The park extension in x-y directions is 5,5 by 4 km, but the terrain extension is set much larger, 15 by 9 km, in order to capture completely the wake recovery downwind, and to maintain a clearance of at least 2 km along the model boundaries. The parameters used in the model are listed in Table 16:

Table 16. Parameters used to model the grid and simulate the wind fields.

Grid modelling		**Wind fields simulation**	
Terrain extension:	15 km x 9 km	Boundary layer height:	400 m
Roughness length:	0,0002 m	Boundary condition on top:	No-friction wall
Resolution in refinement area:	25 m	Number of sectors:	36
Maximum grid xy-spacing:	345 m	Air density:	1,225
Height model above terrain:	800 m	Thermal stability:	Disregarded
Number of cells in z-direction:	30	Turbulence model:	Standard and Modif. k-ε
Height distribution factor:	0,05	Solver:	GCV and Segregated
Height 10th node above the ground:	91 m		
Total number of cells:	2,3 M		

To obtain the desired wind speed at hub height the wind speed above the boundary layer can be calculated from logarithmic profile to obtain 6 m/s at hub height. The following relation can be easily obtained from the logarithmic profile equation for neutral atmospheric conditions:

$$U_z = \frac{u_*}{\kappa} \ln\left(\frac{z}{z_0}\right)$$

$$U_1 = U_2 \cdot \ln\left(\frac{z_1}{z_0}\right) \Big/ \ln\left(\frac{z_2}{z_0}\right)$$

For the case with $U_2 = 6$ m/s, with a boundary layer height z_1 of 400 m, hub height z_2 of 70 m, and roughness length z_0 of 0,0002 m, the wind speed above the boundary layer U_1 to input to WindSim has a value of 6,819213 m/s.

WindSim does not admit to input a certain value of atmospheric turbulence intensity. Instead, the input value of KE at the boundary conditions can be adjusted. WindSim uses the following relation to calculate TI from the KE values obtained from the CFD results:

$$KE = \frac{3}{4} TI^2 \bar{U}^2$$

which might be obtained assuming anisotropic turbulence with $\sigma_v = \sigma_w = \frac{1}{2}\sigma_u$ (see Section 2.2). This expression can be used to calculate the relevant KE from a desired value of TI.

WindSim uses an analytical profile in height for KE at the boundary conditions and to initialise the model (Gravdahl, 1998):

$$KE = \frac{u_*^2}{\sqrt{c_\mu}}\left(1 - \frac{z}{BL}\right)^2$$

where z is the variable height, BL the boundary layer height, u_* the friction velocity, and $c_\mu = 0{,}0324$ is a constant in the turbulence model. Finding the right value of KE to input in order to achieve a specific level of turbulence intensity at the hub height is possible only for the first iteration. After that, the flow properties evolve until they converge to a solution and the value of KE will have changed.

However, a value of KE can be forced in the boundary conditions in WindSim, manually modifying the parameterization file Q1. To know more how to modify to Q1 file, see Annex V.

A trial-error process is undertaken to see how the atmospheric turbulence evolves downstream with a certain value of forced KE at the inlet. Fortunately, the model is flat and its behavior easy to predict.

The forced KE value at the inlet for the flow case of 6 m/s and 7% of turbulence intensity would be:

$$KE = \frac{3}{4} 0{,}07^2 6^2 = 0{,}1313\,\frac{\mathrm{m}^2}{\mathrm{s}^2}$$

It will be presented in Part 8.2.3 that the level of turbulence intensity varies significantly downstream. This problem can be easily solved by manually inputting a constant TI value to the analytical wake models that use TI as a parameter, instead of reading it from the model.

Following that procedure, only a constant wind field of 6, 8 and 10 m/s has to be obtained over the domain to perform the validation analysis. The simplest way of achieving it is initializing the model with logarithmic vertical profiles by running only one iteration using the Segregated solver.

8.2.1. Set-up of Jensen's wake model

Larsen's and Ishihara's models can read the value of TI from the wind database or use a manually inputted constant value. Jensen's model does not have TI implemented, its wake expands linearly according to a wake decay constant. In WindSim the wake decay is related to the surface roughness, which can be read from the terrain surface or inputted manually.

$$k_w = \frac{1}{2 \cdot \ln(h/z_0)}$$

Hence, to set a specific wake decay constant k_w its related wake roughness has to be calculated. Table 17 shows the values of k_w used and their related wake roughnesses.

Table 17. Jensen's wake decay constant k and its relevant wake roughness z_0.

Wake decay constant	**Wake roughness**
$k = 0{,}04$	$z_0 = 0{,}00026$

$k = 0{,}05$	$z_0 = 0{,}00317$
$k = 0{,}06$	$z_0 = 0{,}0168$
$k = 0{,}07$	$z_0 = 0{,}0553$
$k = 0{,}08$	$z_0 = 0{,}135$
$k = 0{,}085$	$z_0 = 0{,}195$

8.2.2. Wake influence range

It is not easy to assess which downstream influence distance may have each wake model. As seen in Chapter 2 wake effects can stretch several kilometres downwind. A comparison using 50D and 100D influence range is preformed using Larsen's model with 6% of ambient turbulence.

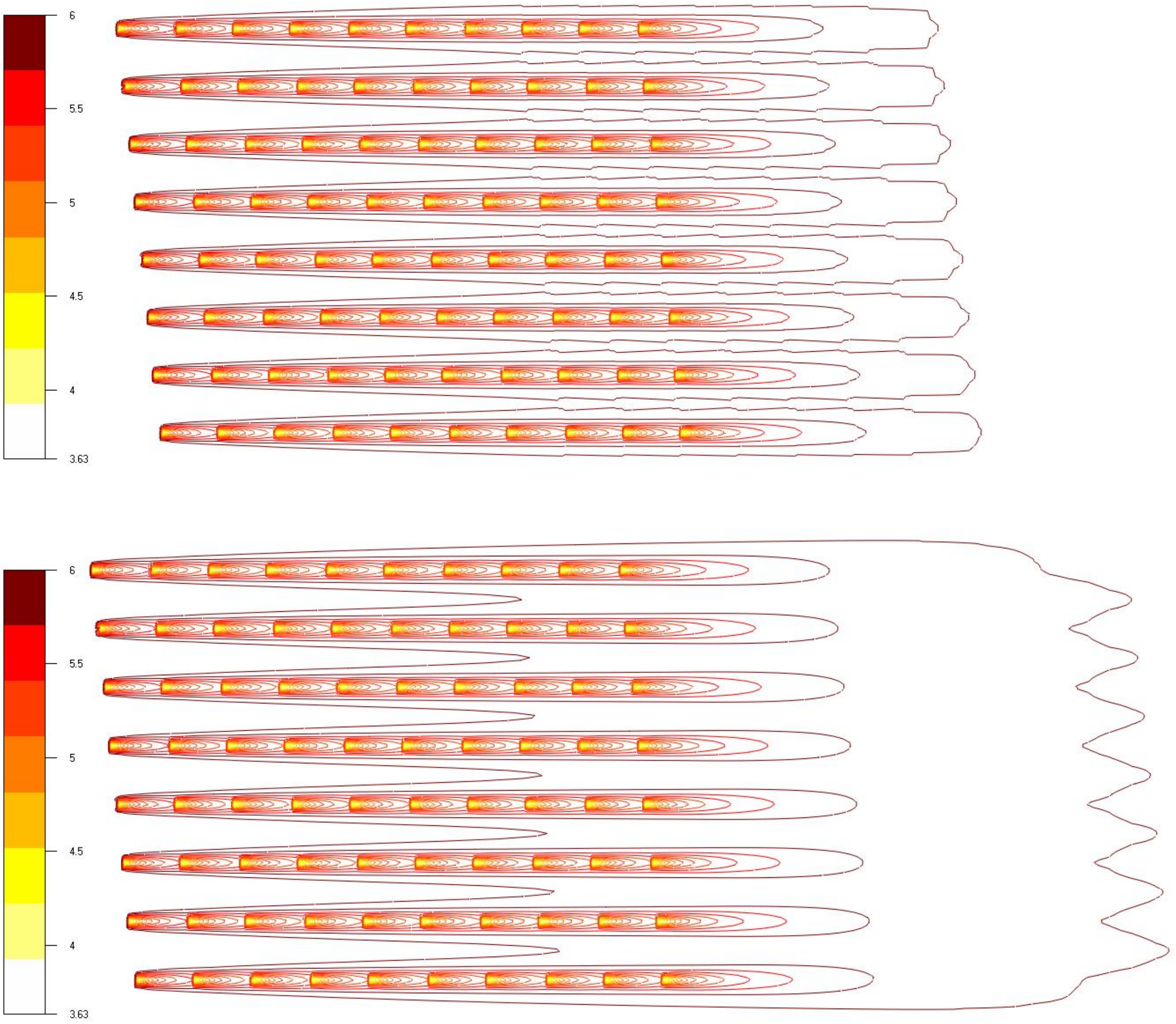

Figure 57. Velocity field obtained using Larsen's wake model with free stream velocity of 6 m/s, ambient turbulence of 6%, and wake influence distances of 50D (top) and 100D downwind (bottom).

For a wake influence of only 50D distance the wake development is not complete, there is not merging to neighbouring wakes as the wake expansion is stopped before its recovery has completed. Using 100D it can be appreciated complete wake length and merging between rows (see Figure 57). It is noticeable that, using Larsen's analytical model, the areas where neighbouring wakes merge get longer influence distances than the wake centrelines themselves.

8.2.3. Internal wake subcycle

The internal wake subcycle defines the number of divisions a sector is divided to calculate the wake effects. 1° changes on wind direction are imputed in the simulations, therefore divisions of 1° are set for the internal wake subcycle. As 36 sectors are used, which are 10° wide, 10 divisions are inputted.

A sensitivity analysis is carried out by comparing the results obtained using 5 or 10 divisions. The results do not show any differences for the tested case. Despite of having the same results, 10 divisions are used.

8.2.4. Simulation of increasing turbulence intensity

Inside a cluster mechanical created turbulence adds to the ambient turbulence (see part 2.2.1). When running GCV solver until convergence, TI 'fades' away downwind due to very low surface roughness over the sea (0,0002 m). Wake generated turbulence is not calculated nor added to the atmospheric turbulence intensity in the domain. To obtain a more realistic increase of TI within the cluster, a new model is set with higher roughness length.

Figure 58 shows a model with decreasing turbulence intensity, at hub height, in the flow direction, and another scenario with increasing turbulence intensity. The results of applying a similar approach to obtain a better wake recovery within the park are shown in part 9.1.1.

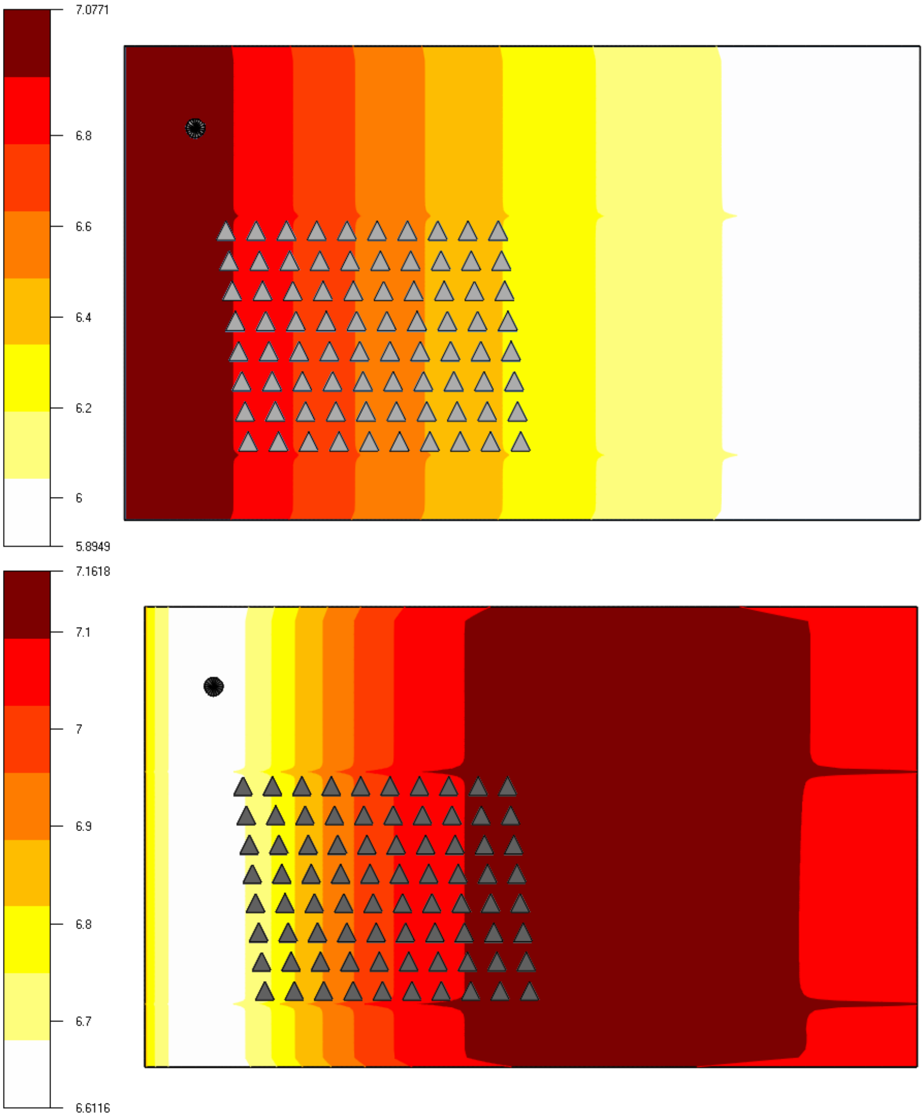

Figure 58. Turbulence intensity values obtained after convergence using GCV solver for surface roughness $z_0 = 0{,}0002$ m (top) and $z_0 = 0{,}001$ m (bottom). The same KEIN value of 0,1313 has been inputted.

9. Results – Wake models validation

9.1. Results case 270º with 7D spacing

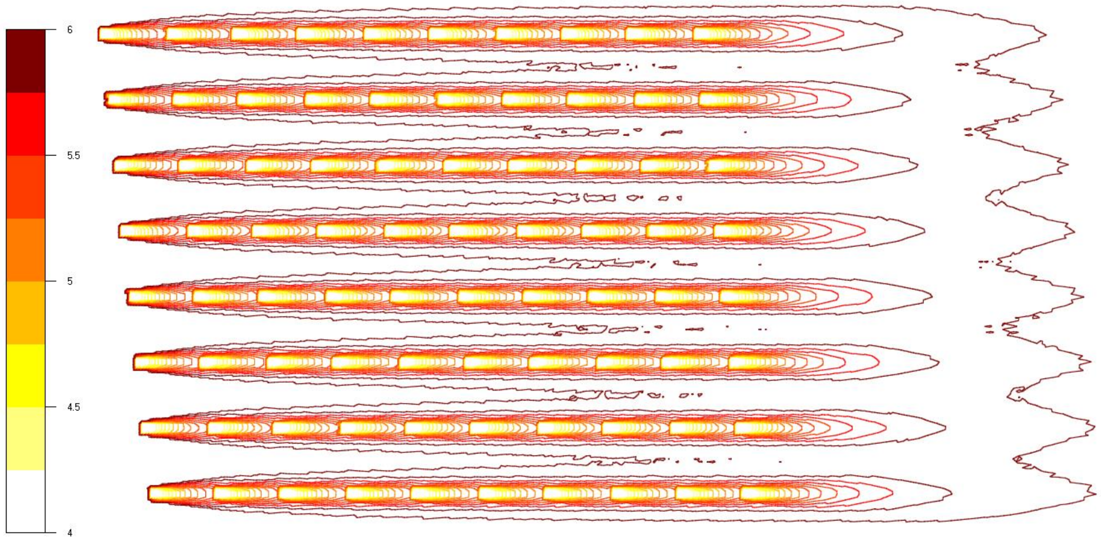

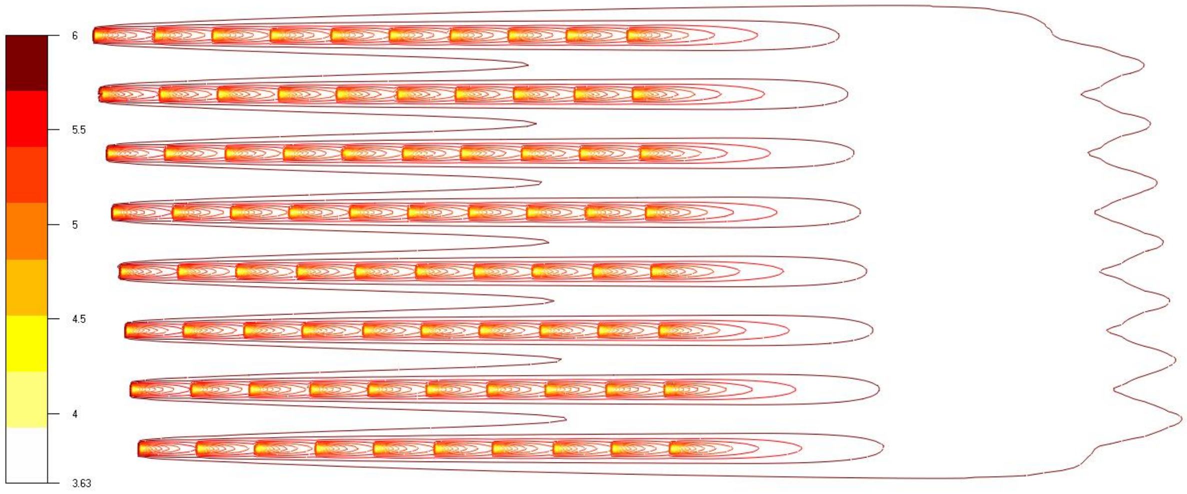

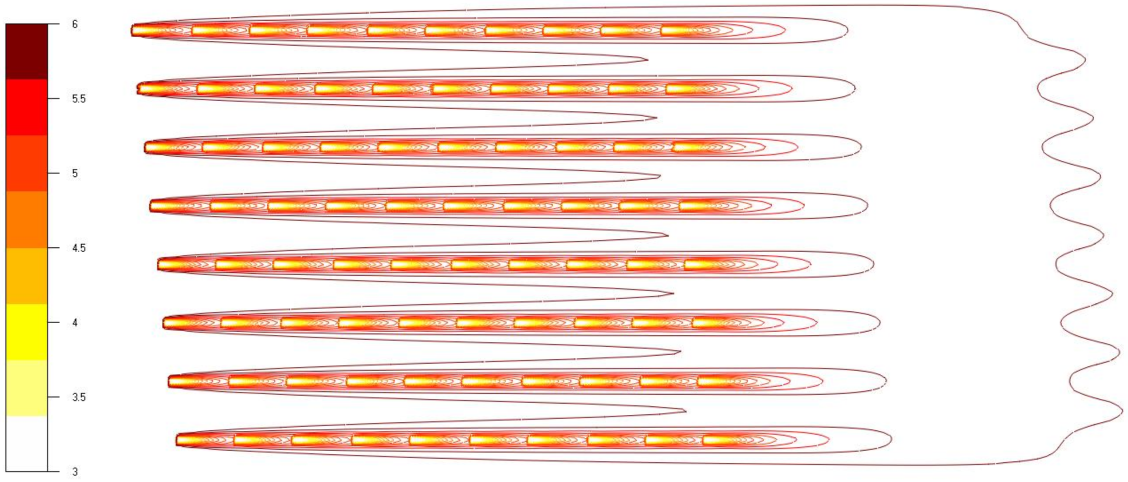

Figure 59. Park overview with Jensen's (top), Larsen's (middle), and Ishihara's (bottom) wake models for the flow case 270º with 7D spacing. Legend shows values in m/s.

Figure 59 shows a park overview with the complete wake development for the flow case 270º at 6 m/s using Jensen's, Larsen's and Ishihara's wake models. The wake width at 7D downwind of the first turbine is shown in Figure 60. While Larsen's and Ishihara's models present a wake width of about ±15º, Jensen's has a width of only ±8º for its largest wake decay.

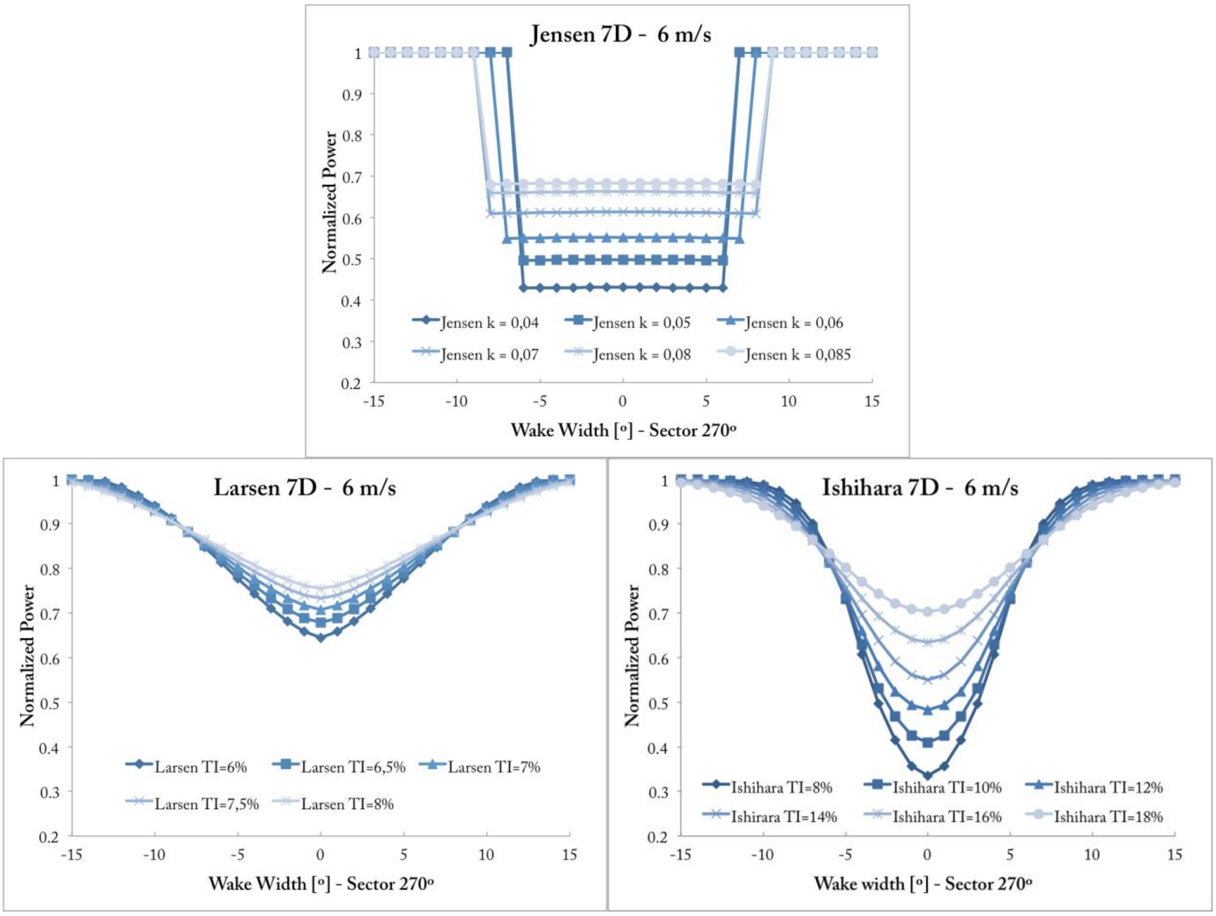

Figure 60. Jensen's (top), Larsen's (bottom-left), and Ishihara's (bottom-right) wake widths at 7D downstream of the first turbine. Flow case 270º at 6 m/s.

Only the most meaningful plot per wake model is shown in this section. The rest of the charts the following discussion refers to can be found in Annex VI.

At a wind speed of 6 m/s the results using Jensen's model with k = 0,085 show an excellent fit of the power losses at the wake centreline for the majority of units downwind (see Figure 61), precisely quantifying the power drop of the first turbine downwind (2nd column). Only results for units at the 4th and 5th columns are slightly higher than observations, showing lower power losses. At higher wind speeds, 8 and 10 m/s, k = 0,085 completely overshoots power losses. The wake decay constant has to be reduced to at least 0,07 to start matching experimental values.

The average losses for a wake width of ±15º are not well captured at 6 m/s for any tested k. At 8 and 10 m/s, however, the lowest plotted value k = 0,05 follows remarkably close the power deficit until the 6th column of turbines.

Larsen's model seems not to capture the quick recovery of the velocity deficit at the wake centreline at velocities of 6 and 8 m/s, and overestimates the power losses for the units at the end of the array. Only for the case of 10 m/s the predicted values seem to get closer to the observations. In any case, if the initial power drop at the 2nd column is to be precisely described, this model overestimates the power losses for the rest of the array.

The results obtained for the averaged values with a wake width of ±15° are far from experimental data. The estimated power losses are too low for any of the tested TI values. What is more, with the aim of achieving a good match with the values of wake ±15°, lower turbulence intensities are inputted to Larsen's model. Exactly the same values are found when using TI = 4% than when using TI = 5%, showing that this model is indifferent to lower TI values than 5%.

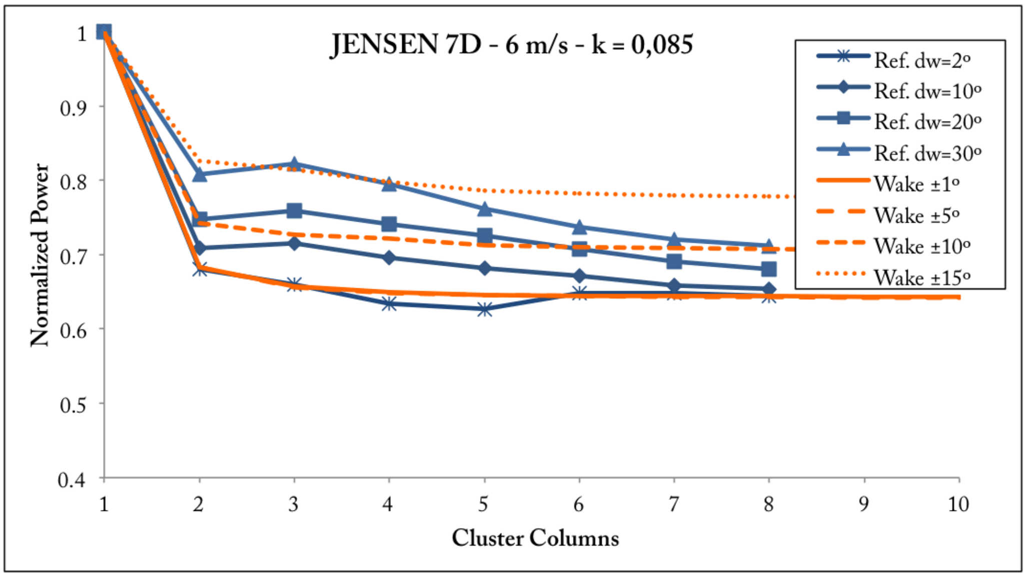

Figure 61. Normalised power of the first 8 units downstream for flow case 270° at 6 m/s. Experimental values are plotted next to Jensen's wake model results with *k* = 0,085.

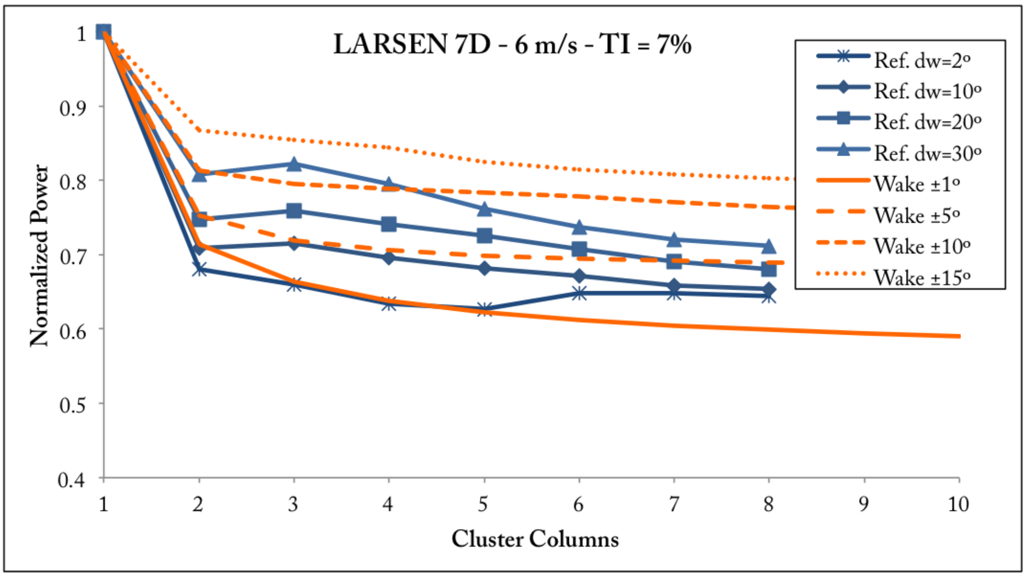

Figure 62. Normalised power of the first 8 units downstream for flow case 270° at 6 m/s. Experimental values are plotted next to Larsen's wake model results with TI = 7%.

Ishihara's averaged results with a width of ±15° seem to be the most accurate of the three models. They describe perfectly the power losses for a wake width of ±15° when using TI = 10% at 6 m/s and TI = 8% for 8 and 10 m/s. Unfortunately, the power deficit at the wake centreline is dramatically overshot at that level of ambient turbulence. A good agreement with experimental data is only obtained for values between 16% and 18%, which are unrealistic for offshore applications. See all the charts with the results from flow case 270° in Annex VI.

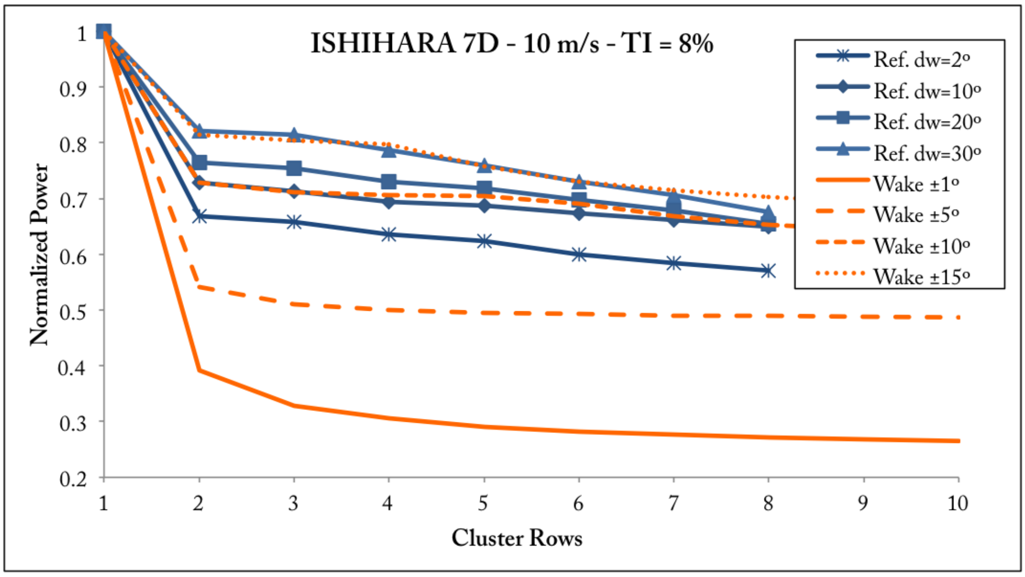

Figure 63. Normalised power of the first 8 units downstream for flow case 270° at 10 m/s. Experimental values are plotted next to Ishihara's wake model results with TI = 8%.

9.1.1. *Effect of increasing atmospheric turbulence downstream using Larsen's wake model*

Contrary to Ishihara's, Larsen's model has proved to use realistic turbulence intensity values to predict the experimental power losses. However, Larsen's model doesn't take into account mechanical added turbulence inside a cluster. A sensitivity study is here performed to see if Larsen's model would describe more accurately the observations.

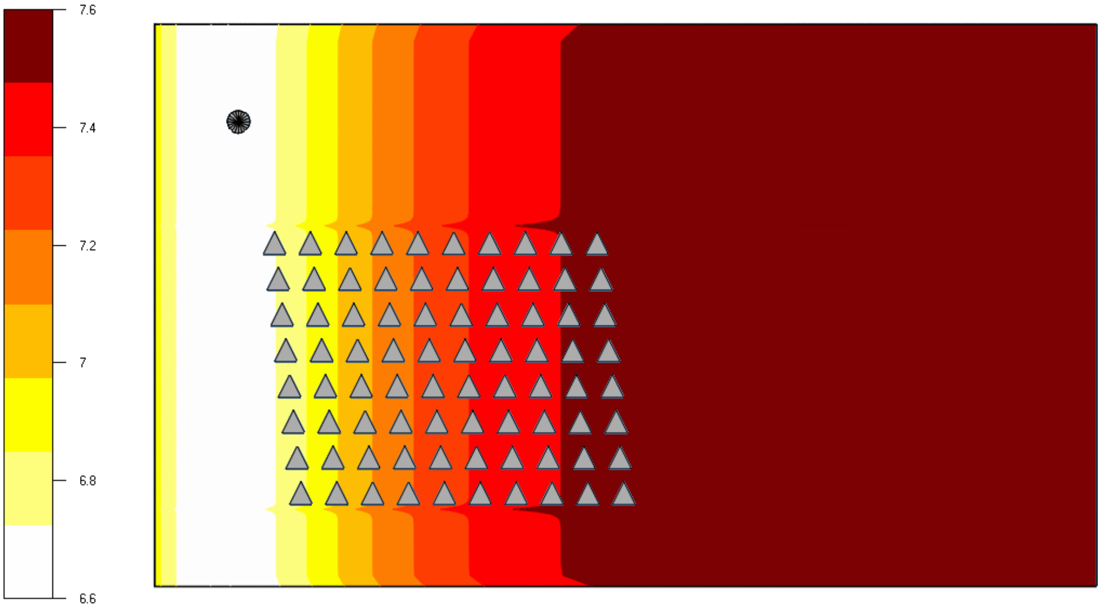

Figure 64. Turbulence intensity over the domain for flow case 270°. Its value increases downwind from 6,6% to 7,6%. A higher level or surface roughness, 0,002 m, and KEIN of 0,14 have been used to achieve the desired effect.

A model with a surface roughness ten times higher is set, z_0 = 0,002 m, and a larger value of turbulent kinetic energy is inputted, KEIN = 0,14. The result of it is a level of ambient turbulence increasing downwind over the domain (see Figure 64).

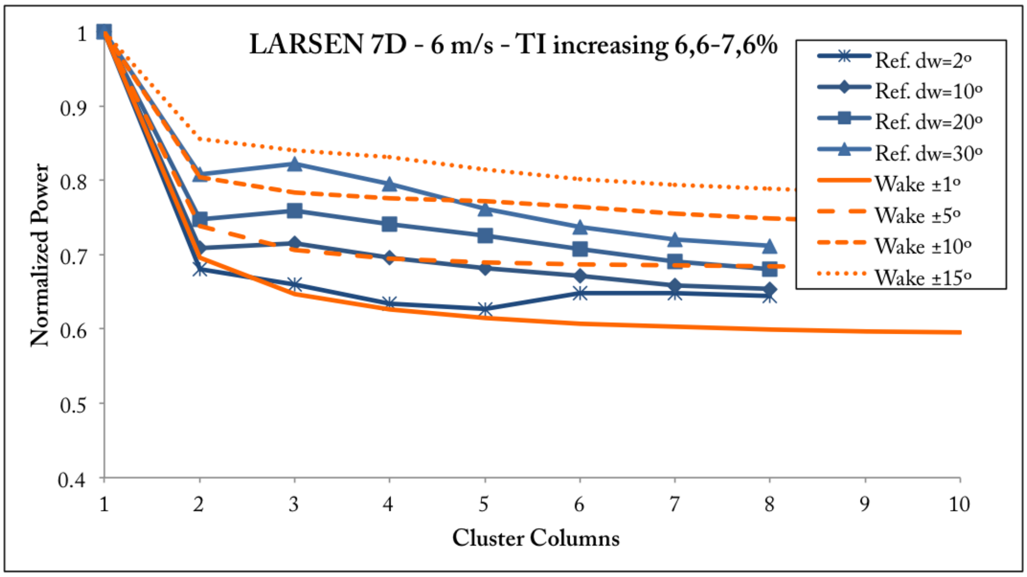

Figure 65. Normalised power of the first 8 units downstream for flow case 270° at 6 m/s. Experimental values are plotted next to Larsen's wake model results with increasing level of TI = 6,6 – 7,6%.

With increasing levels of turbulence, from 6,6% to 7,6%, Larsen's model captures better the power deficit at the 2nd column —almost the same result as using a constant value of TI of 6,5%— and follows much better the trend at columns 3, 4 and 5 than the case with constant TI of 7,5%. The results can be directly compared with the best fit obtained at 6 m/s using 7% TI, as shown in Figure 62. In both cases (increasing TI and TI of 7%), the wake recovery after the 5th column seems to be too slow.

At 6 m/s it appears that the simulated added mechanical turbulence is not high enough to match accurately the experimental data —which one could already expect as the levels of total turbulence intensity within a cluster can raise up to 18% (see part 2.2.1).

At a higher wind speeds, however, the effect of increasing TI downwind does not provide a better capturing of the power losses trend. The power deficit in those cases is almost constantly decreasing and the higher TI downwind simulates a quicker recovery. The figures for the flow cases at 8 ant 10 m/s can be found in Annex VI.

9.2. Results case 221º with 9,4D spacing

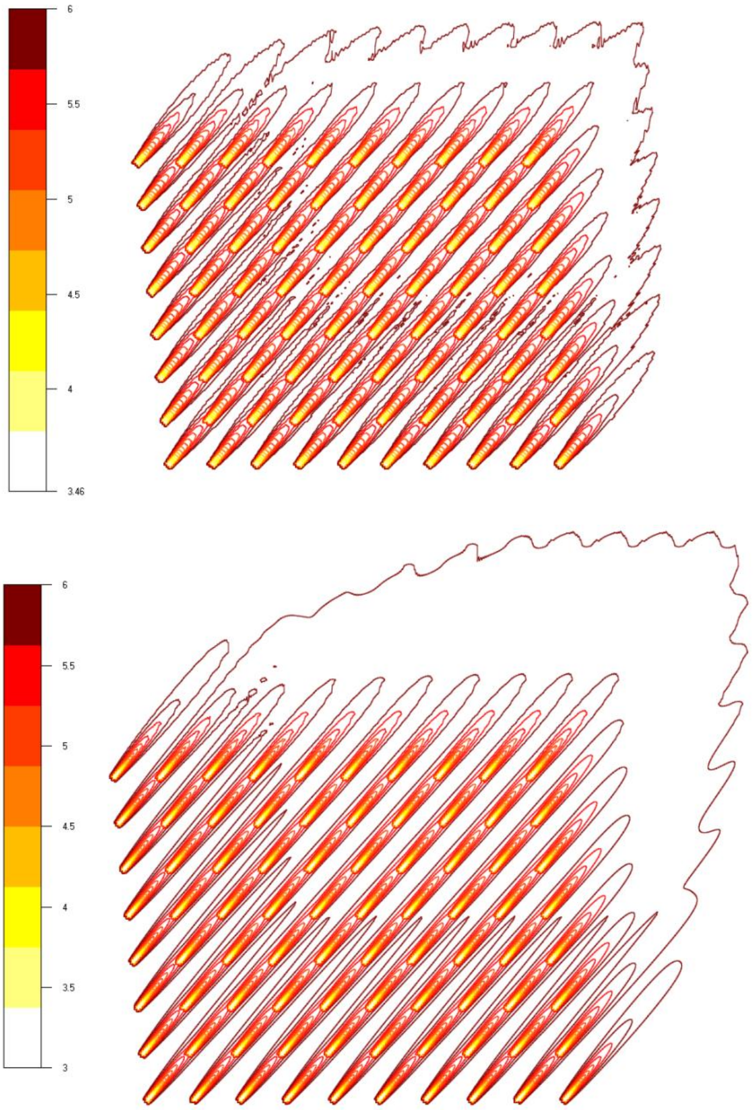

Figure 66. Park overview with Jensen's (top) and Ishihara's (bottom) wake models for the flow case 221º with 9,4D spacing. Legend shows values in m/s.

A park overview with a complete wake development for the flow case 221º is shown in Figure 66, comparing the results obtained with Jensen's and Ishihara's models. The wake width at 9,4D downwind of the first turbine is displayed in Figure 67, using Larsen's and Ishihara's models. There is 1º misalignment between the real wake centreline and the flow case direction compiled by Hansen, 2008. Maybe there is a yawing or a wind vane misalignment of 1º at Horns Rev. To compute correct averages, the modelled wake centreline is set to 222º, but the results are compared to the original data with the wake centreline at 221º.

In Figure 67 it can also be appreciated an additional power loss from -13º to -16º from the newly defined centreline 222º. This is due to the presence of a secondary wake directrix at 202º. The power losses related to this secondary are filtered out, defining a maximum wake width of ±13º from the newly defined centreline at 222º.

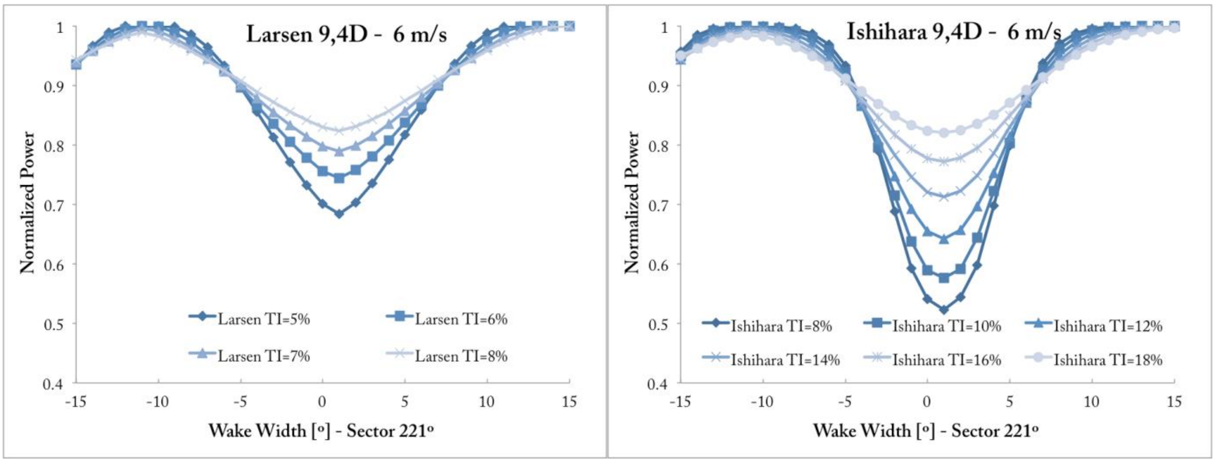

Figure 67. Larsen's (left) and Ishihara's (right) wake widths at 9,4D downstream of the first turbine. Flow case 221° at 6 m/s.

Only the most meaningful plot per wake model is shown in this section. The rest of the charts the following discussion refers to can be found in Annex VII.

For the three tested wind speeds, Jensen's wake width and power deficit are well captured at the first turbine downstream (2nd column) but the tendency of a constant decrease in power for the subsequent columns is not obtained; Jensen's model delivers an almost asymptotic (constant) value after the 2nd unit in the array (see Figure 68). Only for very low wake decay constants, k = 0,04, the regular increase in power losses is better captured for a wake width of ±13°, but the relevant values at the wake centreline completely over-predict the power losses.

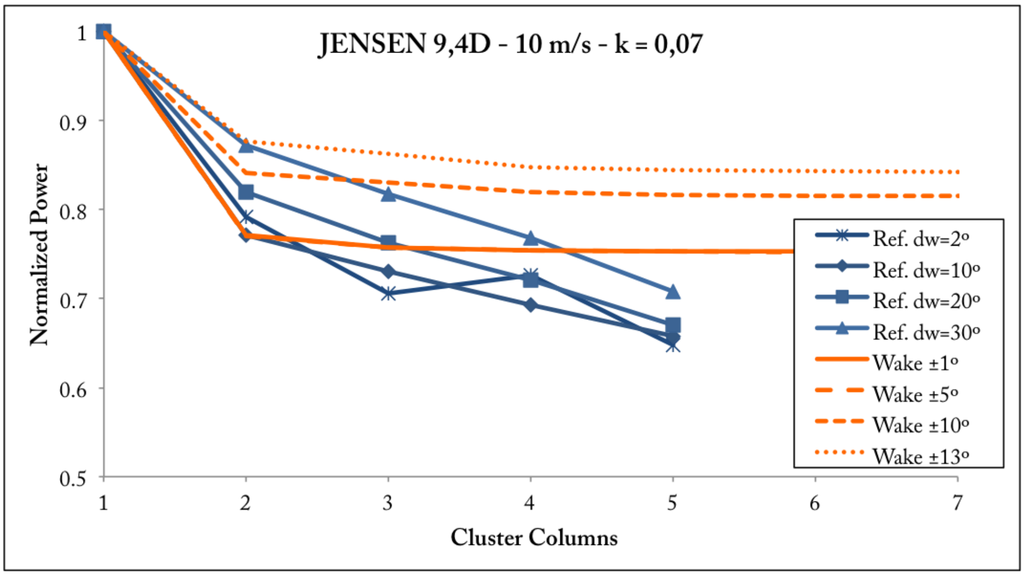

Figure 68. Normalised power of the first 5 units downstream for flow case 222° at 10 m/s. Experimental values are plotted next to Jensen's wake model results with k = 0,07.

Larsen's and Ishihara's models remarkably show the same results at a turbulence intensity of 5,5% and 14% respectively for all tested wind speeds (see Figure 69 and Figure 70). The results are very similar to Jensen's: the models do not capture the power drop at 4th and 5th columns but they have a better fit for turbines on the 3rd column. However, their wake widths seem not to match with experimental data, delivering lower power losses at a wake width of

±13° lower than the experimental average for ±15° —which, considering the difference in the bin range, averaging with ±13° should always give higher power deficits than using ±15°.

See all the charts with the results from flow case 270° in Annex VII.

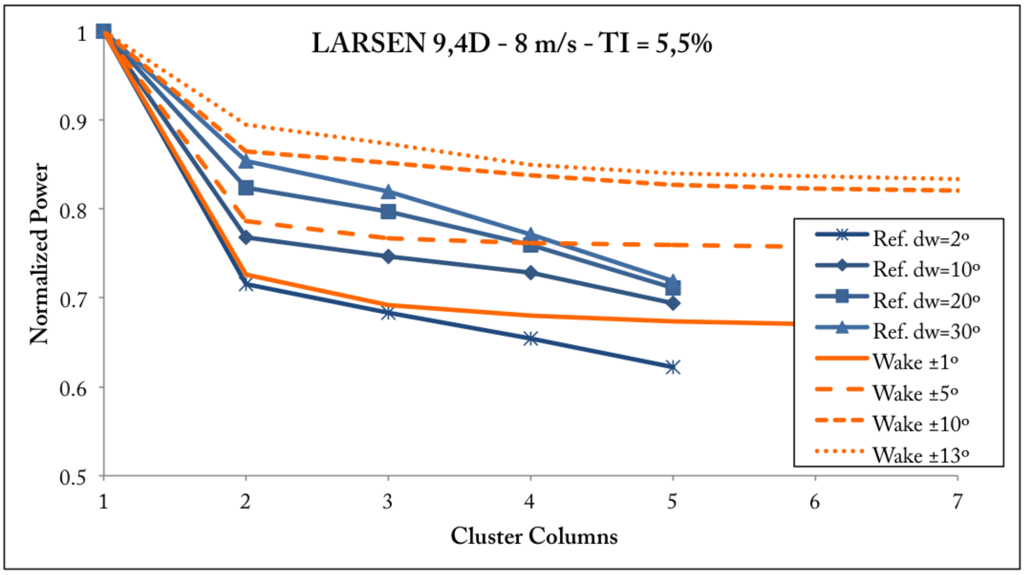

Figure 69. Normalised power of the first 5 units downstream for flow case 222° at 8 m/s. Experimental values are plotted next to Larsen's wake model results with TI = 5,5%.

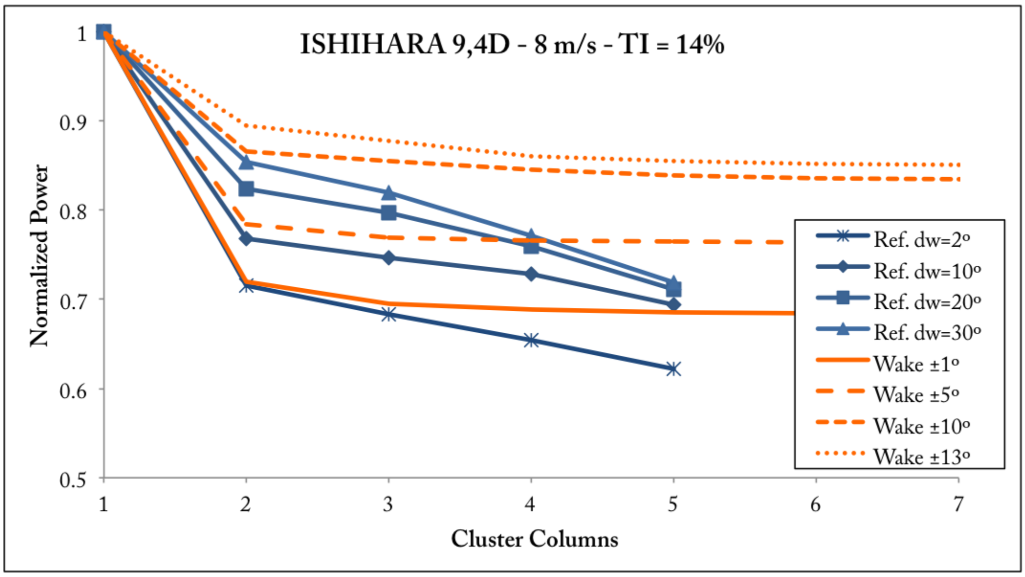

Figure 70. Normalised power of the first 5 units downstream for flow case 222° at 8 m/s. Experimental values are plotted next to Ishihara's wake model results with TI = 5,5%.

9.3. Results case 312° with 10,4D spacing

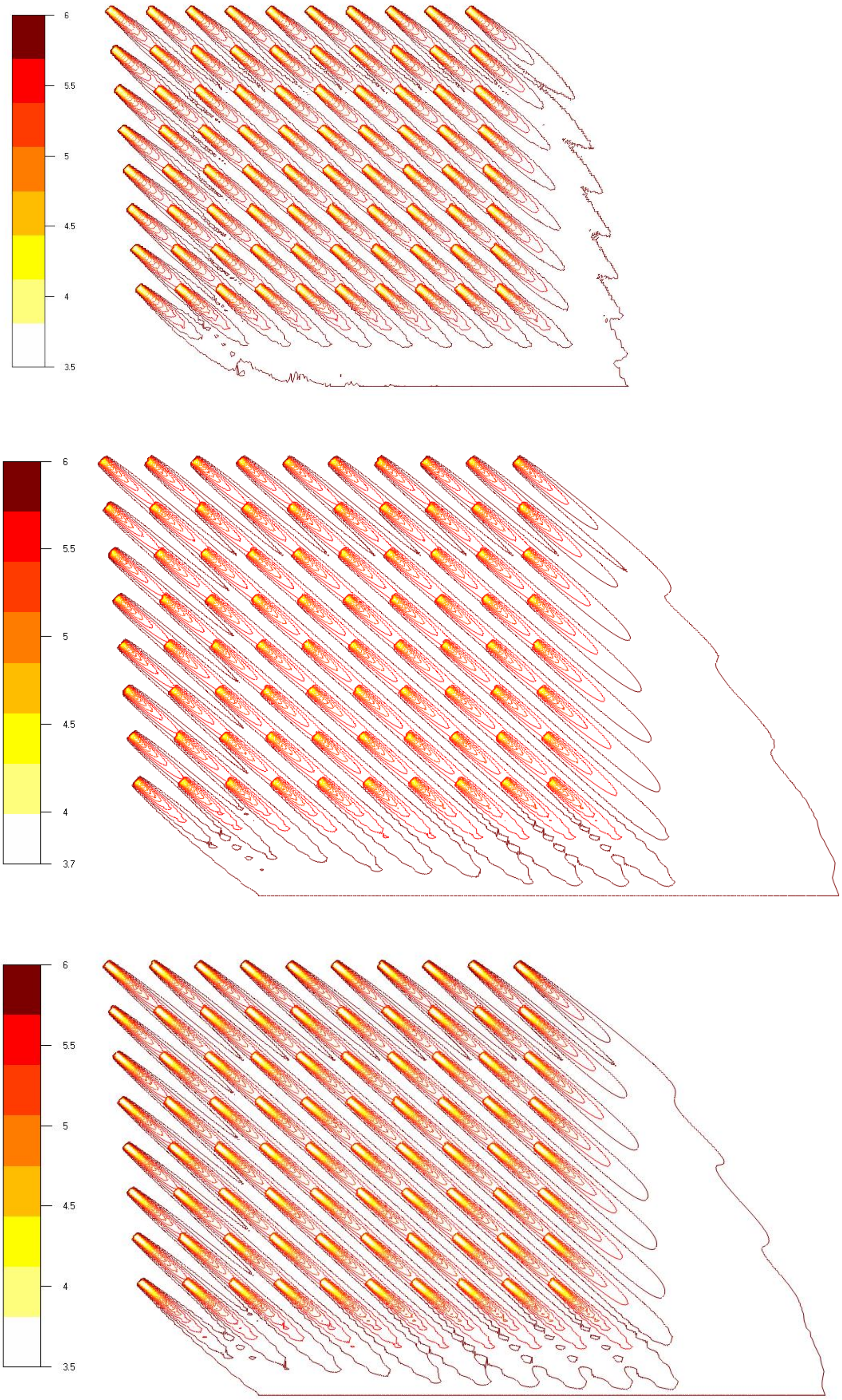

Figure 71. Park overview with Jensen's (top), Larsen's (middle), and Ishihara's (bottom) wake models for the flow case 312° with 10,4D spacing. Legend shows values in m/s.

Figure 71 shows a park overview with a complete wake development for the flow case 312º, using the three tested analytical wake models. Larsen's and Ishihara's wake widths are plotted in Figure 72, at 10,4D downstream of the first turbine and for the flow case 312º at 6 m/s. The power deficit comprised between +10º and +15º from the wake centreline belongs to wake effects of another wake directrix. Although not shown in Figure 72, Jensen's wake width shows exactly the same overlay between +10º and +15º. To avoid including effects from another wake into this flow case, the power deficit is averaged using a wake width of maximum ±10º from the wake centreline 312º.

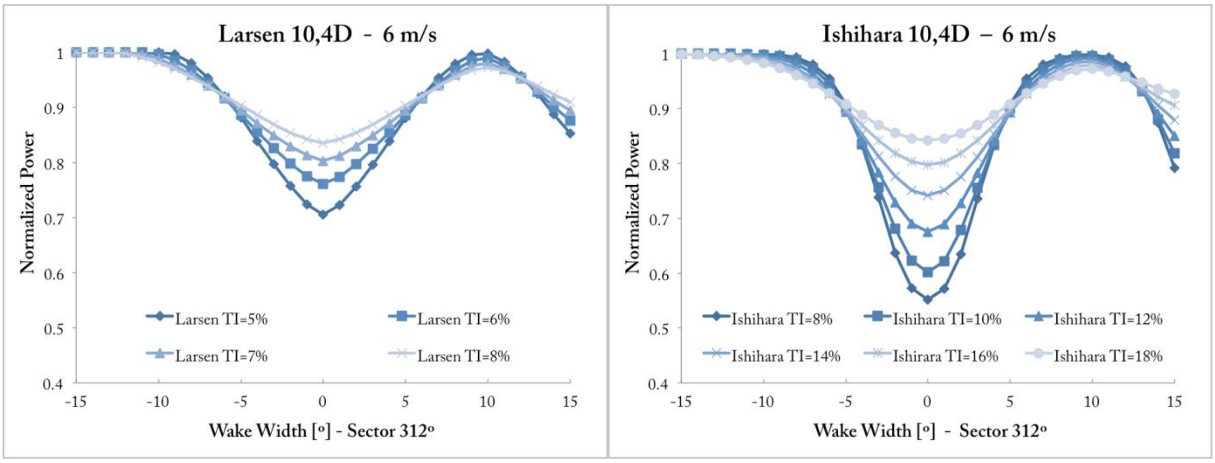

Figure 72. Larsen's (left) and Ishihara's (right) wake widths at 10,4D downstream of the first turbine. Flow case 312º at 6 m/s.

Only the most meaningful plot per wake model is shown in this section. The rest of the charts the following discussion refers to can be found in Annex VIII.

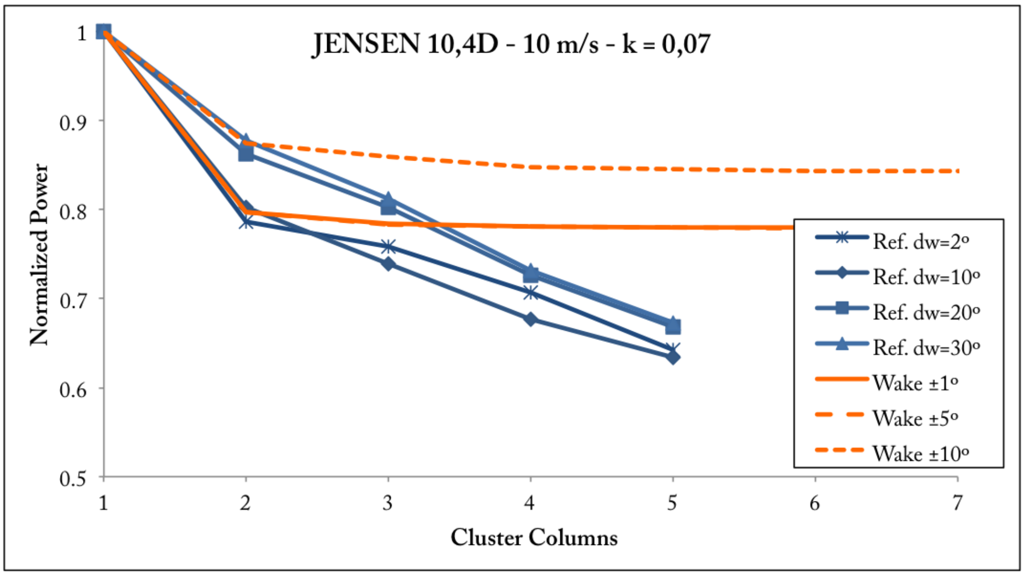

Figure 73. Normalised power of the first 5 units downstream for flow case 312º at 10 m/s. Experimental values are plotted next to Jensen's wake model results with k = 0,07.

Jensen's, Larsen's and Ishihara's results for any of the tested wind speeds define a wake width larger than what observations show. Jensen's seems to give the most accurate match of the wake width (see Figure 73), while Larsen's and Ishihara's models define respectively a larger wake width. However, none of the models is able to describe accurately the thin wake width that observations show at 8 m/s —see Annex VIII for the plotted results, keeping in mind that the averaged results for ±10° have to be compared with the observations of 20° width.

At 6 and 10 m/s, all models capture accurately the power drop of the turbines situated at the 2nd column, but they underestimate the power losses for the rest of the columns downstream.

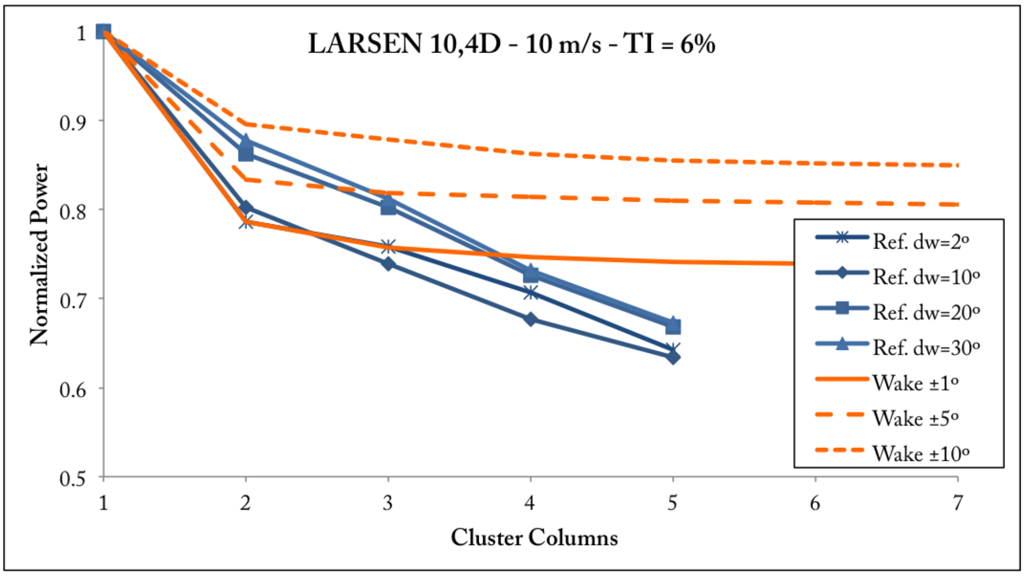

Figure 74. Normalised power of the first 5 units downstream for flow case 312° at 10 m/s. Experimental values are plotted next to Larsen's wake model results with TI = 6%.

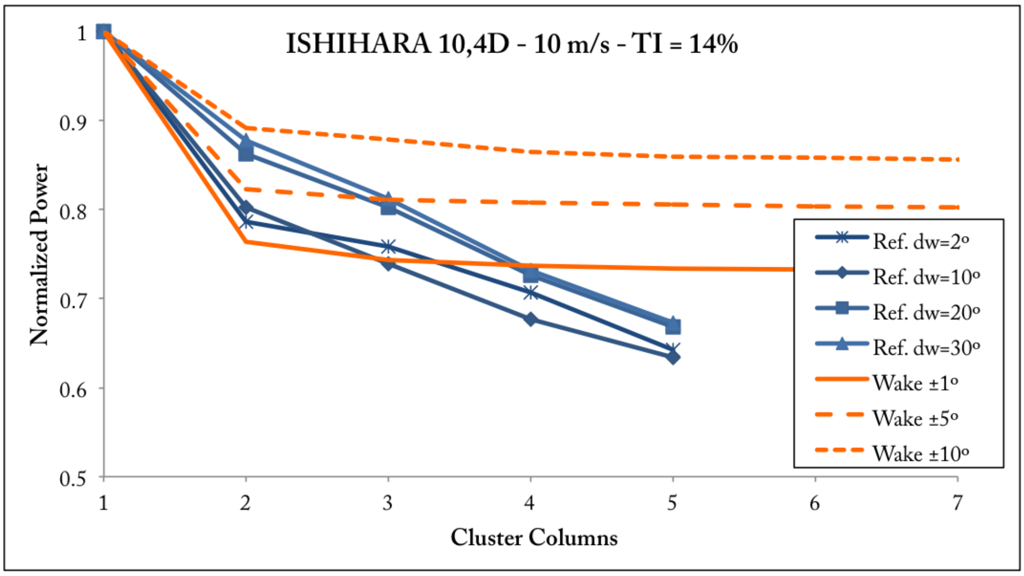

Figure 75. Normalised power of the first 5 units downstream for flow case 312° at 10 m/s. Experimental values are plotted next to Ishihara's wake model results with TI = 14%.

The observed power losses present a strange situation: the normalized power at the wake centreline for columns 3, 4, and 5, is larger than the normalized power averaged for ±5° (Ref. width 10°). Most likely the reduced number of occurrences registered under those conditions (Hansen, 2008a) might affect the averaging and give an apparently wrong value at the wake centreline. This might be one of the reasons why the tested models appear to have too large wake widths compared to observations. Nevertheless, it is noticeable in Figure 74 that

Larsen's modelled power losses at the wake centreline perfectly match the observations at the 2nd and 3rd column, which might be mere coincidence as the losses at the wake centreline should always be larger than its averaged value at ±5° in the far wake region.

10. Discussion

The overall results of the three tested models show a better agreement with experimental data for the flow case with 7D spacing than for 9,4D and 10,4D. As regards as the effect of the free stream wind speed, there array asymptotic value of power deficit is well characterized only at the lowest wind speed of 6 m/s for the cases with 7D and 9,4D spacing. At higher wind speeds, 8 and 10 m/s, and for any tested wind speed with 10,4D spacing, the experimental normalized power seems to have an almost constant decrease per each turbine downwind, which none of the models captures.

Jensen's wake decay values that better match with observations are unusually high for an offshore wind farm, meaning that the wake recovery at Horns Rev is quicker than what expected. The slightly unstable atmospheric conditions under which the measurements are obtained might partially explain this quicker wake recovery. However, the atmospheric turbulence intensity has common values for offshore sites, around 7%, and Larsen's wake model agrees quite well with observations when inputting turbulence intensity values lower than that, around 5-6%. The reason why Jensen's model has its best fit for wake decay values that are more common in onshore sites should be other than a higher wake recovery due to higher atmospheric turbulence under unstable conditions.

Ishihara's model requires unrealistically high levels of turbulence intensity to obtain similar levels of power deficit than observations. The TI values inputted to Ishihara's more than double the values used in Larsen's model. Ishihara's wake recovery does not show better results than Larsen's or Jensen's, even though the model accounts with added mechanical turbulence to calculate the wake decay. It could be that not enough added mechanical turbulence is calculated into that model, as results are almost the same than Larsen's model when inputting about the double the value of TI.

However, increasing the level of TI downstream and using Larsen's model does not provide a better fit to observations. Only for the case at 6 m/s there is a better agreement with the power drop of the first turbines downwind and the three subsequent units. But at 8 and 10 m/s the results obtained are further away from experimental data.

The simple wake model developed by Jensen fits remarkably well with experimental data. Despite of its 'top-hat' shape and a narrow wake width —narrower than the wake width obtained with the other two models— the power losses averaged using ±10° and ±15° match surprisingly well with observations.

It is difficult to assess which of the models performs the best, as some of them describe better the power deficit at the wake centreline, and some others for the average of ±15°. In any case, an Annual Energy Production (AEP) calculation shall be undertaken to determine which model matches better the overall park production, which is the ultimate purpose of wake modelling.

Part III. Bockstigen layout optimization

11. Introduction – Layout optimization

Bockstigen atmospheric stability conditions are neutral leaning towards stable conditions, as it has been seen in part 5.1.5. Hence, the study of power losses due to wake effect at Bockstigen could be carried out only considering neutral atmosphere. The available data and wake model parameterization, however, are performed under slightly unstable conditions. Therefore, any power generation calculated using the parameters obtained in Chapter 0 will underestimate the power losses, which according to the literature might be between 50% and 70% higher under stable conditions (see reference values in Section 2.1).

Having said that, it is important to mention that the reference data from Horns Rev wind farm is obtained under slightly unstable conditions, and the annual atmospheric stability at Bockstigen wind farm is slightly stable. The difference between the wake losses under those conditions is not expected to be that high.

In any case, the wind rose and thus the sector-wise energy content of Bockstigen define directions with higher and lower energy content. Turbine arrays shall be preferably aligned towards a direction with lower energy content in order to diminish the overall wake losses. Those layout leading directions, or directrices, will be the same under any atmospheric conditions. The optimization performed using the wake parameterization of Chapter 0 will minimize the power losses for slightly unstable conditions but also for slightly stable conditions. The optimal park layout obtained in this chapter will be optimal for any atmospheric conditions. Only the calculations of the Annual Energy Production (AEP) will differ.

11.1.1. Layout constrains and seabed extension

The layout for a future offshore wind farm at Bockstigen has been predefined as two parallel arrays to follow the seabed characteristics and to reduce the visual impact. The arrays have to be directed towards 158º–338º, and have 6 turbines per array.

The seabed has been scanned with sonar to map the water depth in detail. The scanned extension is shown in Figure 76. The sea depth absolute values are not shown due to confidentiality reasons.

The optimal layout must have 12 units located in two arrays, and must fulfil the following restrictions provided by the project developer:

- Minimum depth: 7 m
- Maximum depth: 12 m

- Maximum 3 turbines could be placed at a depth between 6 and 7 m, but shall be avoided.
- Up to 2 turbines can be placed at a depth between 12 and 14 m.

The optimal layout must satisfy the restrictions on the seabed depth and at the same time minimize the losses due to wake effects.

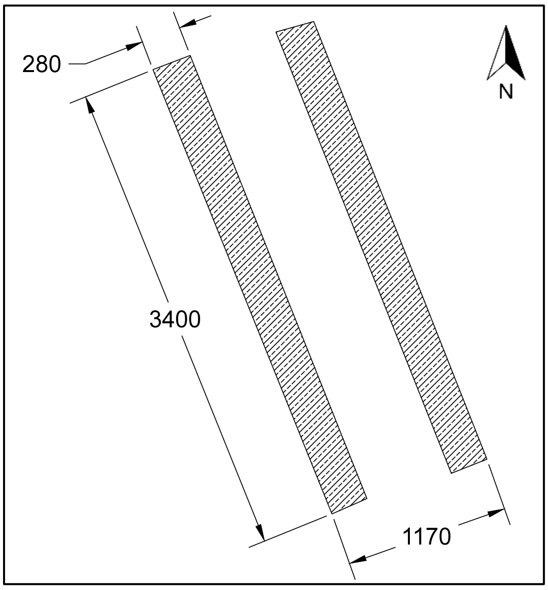

Figure 76. Seabed area that has been scanned with sonar and its depth is known. Distances are in m.

11.1.2. Wind turbine model

The turbine model selected is Vestas V117-3,3MW class IIA, which compiles with the atmospheric turbulence intensity and extreme winds assessed in Section 5.5. The power curve and thrust coefficient are shown in Figure 77.

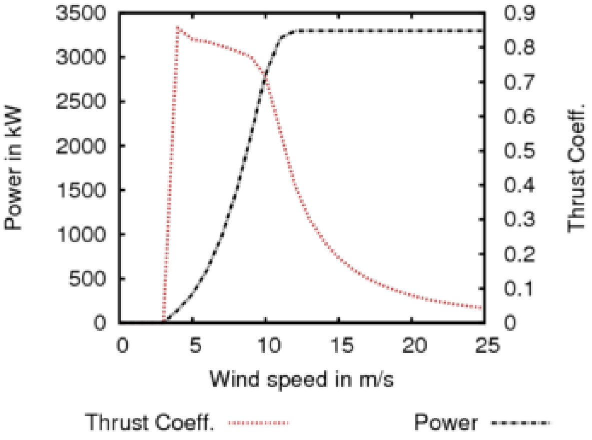

Figure 77. Power curve and thrust coefficient of Vestas V117-3,3MW IIA turbine.

12. Methodology – Layout optimization

12.1. Parameterization optimisation for the 1st turbine downwind

A parameterization optimization of each model is undertaken to achieve the best accuracy on defining the power losses at the 1st turbine downwind (2nd column of turbines).

Figure 78 shows the results obtained for the three tested models with the relevant parameter —either wake decay or atmospheric turbulence— that approximates the best to observations. For the charts at the wind speeds of 8 and 10 m/s, see Annex IX.

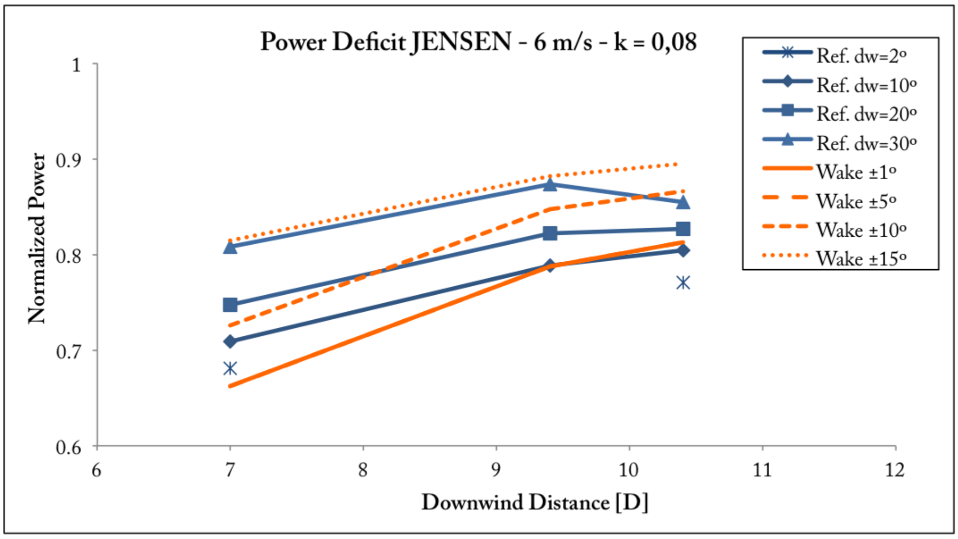

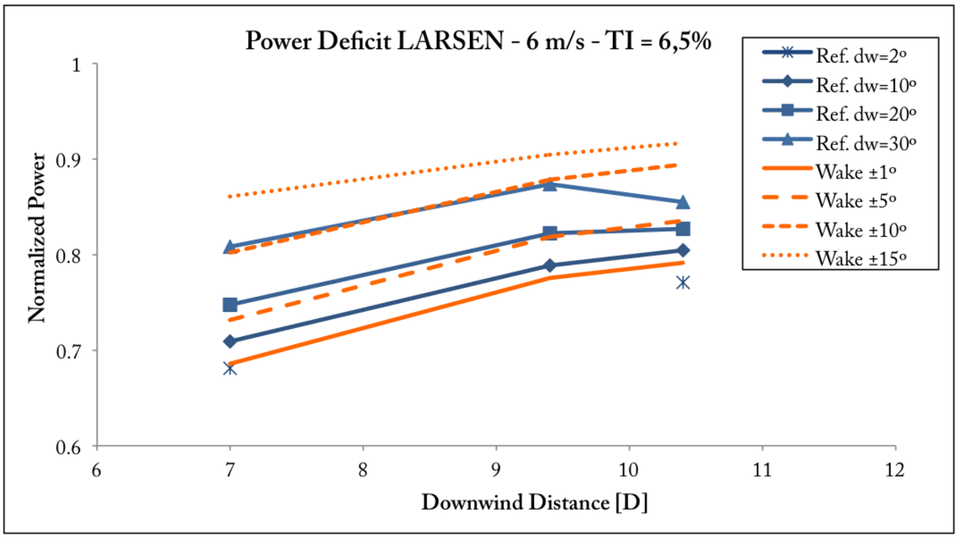

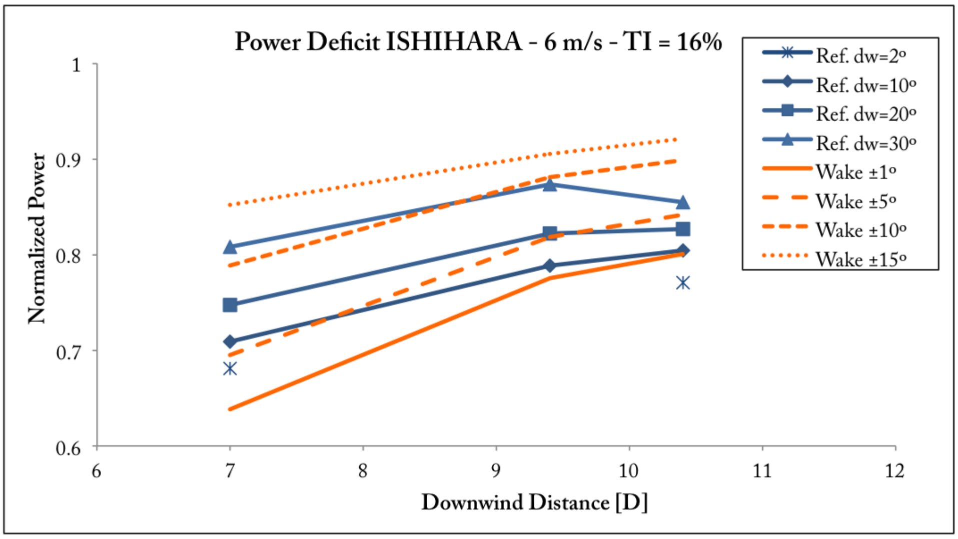

Figure 78. Power deficit calculated with Jensen's (top), Larsen's (middle) and Ishihara's (bottom) at 7D, 9,4D and 10,4D downstream. The results are obtained with the parameter that better approximates to experimental data.

The calculation of wake losses in the Annual Energy Production (AEP) will be done sector-wise using the frequency table characteristic of the site climate. Let's imagine there is wake interaction on direction 228°, and that 36 sectors are used (see Figure 79). Under these circumstances, sector 220° will take into account wake effects 8° shifted from the wake centreline, sector 230° with 2° shifted, and sector 240° with a shift of 12°. Sector 210° should not take into account any wake losses as the experimental wake width, usually around ±15°, is lower than 18°.

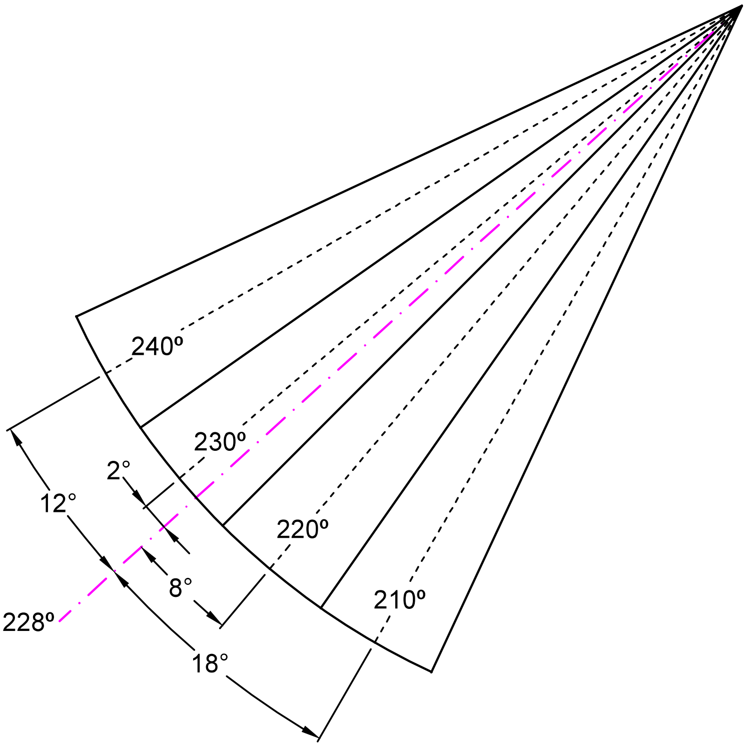

Figure 79. Drawing indicating the angular distance between a figurative wake centreline at 228° (in purple) and the neighbouring sectors centreline. The drawing only shows sectors 210° to 240° of a 36-sector wind rose.

The wake model used for AEP losses calculation has thus to describe accurately the power deficit at the wake centreline, and also for the averaged losses with a width of ±5°, ±10°, and ±15°.

The optimization of each model parameter is performed graphically. The parameter that describes the best both the experimental power deficit and the wake width is selected. Table 18 lists the optimal parameters for the three models at the three tested wind speeds:

Table 18. Optimal parameters for Jensen's, Larsen's and Ishihara's wake model for the flow cases at 6, 8 and 10 m/s.

Wake model:	**Jensen**	**Larsen**	**Ishihara**
Wind speed:	k_w	TI	TI
6 m/s	0,08	6,5%	~17%
8 m/s	0,07	5,5%	~15%
10 m/s	0,07	6%	16%

Ishihara's optimal value of turbulence intensity for 6 and 8 m/s is found to be between two of the tested values (16% and 18% for 6 m/s, and 14% and 16% for 8 m/s) so the estimated optimal TI shall be around ~17% and ~15% respectively.

In overall, Jensen's model shows an excellent fit to the wake width, matching remarkably well the averaged power losses with a wake width of ±15°. Larsen's model, however, presents a better description of the power losses and their recovery at the wake centreline. Only Ishihara's model (considering the tested TI values) doesn't seem to capture so accurately the wake width and the power losses at the wake centreline. It has to be mentioned, nevertheless, that Larsen's and Ishihara's model behave almost identically when inputting the right TI values to Ishihara's model. It might be the case that using the estimated values of 17% and 15% it would show the same fit to observations than Larsen's model.

To perform the proposed wind farm layout optimization either Jensen's or Larsen's model should be considered. There is no clear preference for one or another, therefore both wake models are utilized and compared in the park layout optimization carried out in this chapter.

The optimal parameters obtained at 10 m/s are used here as the experimental power deficit at that wind speed bin is the largest in absolute values, and consequently by describing better the power deficit at that wind speed the overall wake losses calculation will have the best accuracy. Table 19 lists the optimal parameters.

Table 19. Wake models and parameters used on the park layout optimization.

Wake model:	**Jensen**	**Larsen** TI
Parameter used:	$k_w = 0{,}07$ ($z_0 = 0{,}0553$)	$TI = 6\%$

12.2. Directrices with maximum and minimum energy content

When placing two wind turbines near each other park losses will arise, specifically for the directions that align both the turbines. Those directions are supplementary to each other and follow the line (directrix) that connects the two turbines. How much losses that will represent can be assessed by analysing the energy content of the sectors that belong to that directrix. Adding the energy content of a sector with its supplementary sector (energy of a sector plus the energy of the sector 180º from the former) an energy rose that describes the total energy content by array directrix is obtained. Turbine arrays, and thus wake directrices, should be aligned to directrices with the minimal energy content.

Figure 80 shows the directrix energy rose for Bockstigen climatology at 85 m in height. The directrix with the maximum energy content is 36º–216º. As expected, it falls between the sectors with the highest energy content, from 210º to 230º, as seen previously on Section 5.4. The sectors centred at this directrix with a width of ±15º accounts for 26,12% of the total energy content.

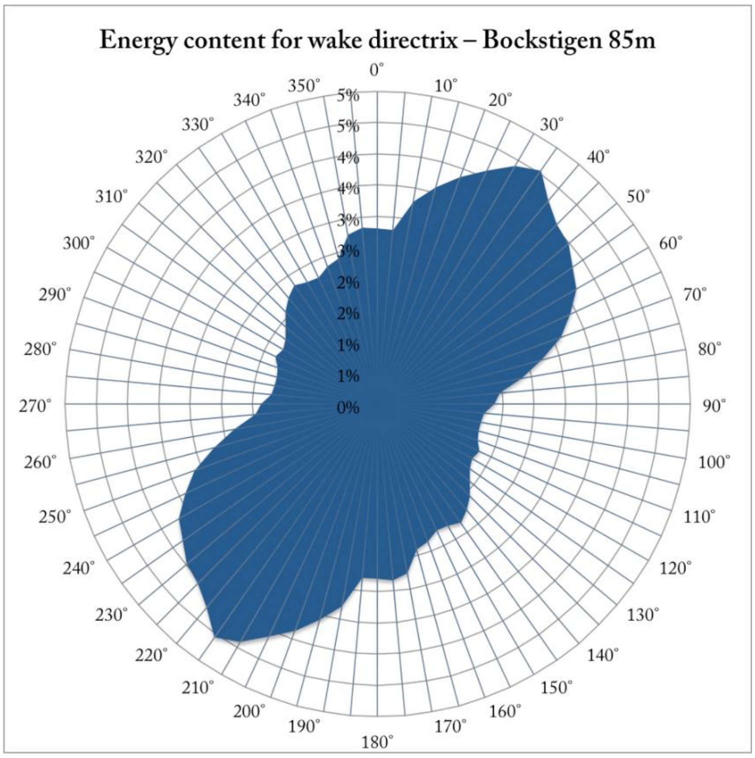

Figure 80. Energy content per wake directrix (mirrored energy rose), averaged using 72 sectors. 36º–216º is the directrix with the maximum energy content, and 96º–276º the directrix with the minimum energy content.

The directrix with the minimum energy content has direction 96º–276º. The sector ±15º wide centred at this directrix supports 11,08% of the total energy content, which is still significant. Two turbines aligned towards this direction will still have to be spaced enough to reduce the wake losses.

There is a second directrix with reduced energy content, following direction 150º–330º. The sector ±15º wide centred at this directrix accounts for 14,05% of the total energy content.

Turbine arrays should be aligned towards the directrix with minimal energy content, although this is not the case in this case study. Due to other constraints (such as visual impact or seabed characteristics) the turbine arrays are directed towards 158º–338º, which falls very close to the second directrix with minimal energy content. The sector centred at 158º–338º (design directrix) with a width of ±15º supports 14,79% of the total energy content.

12.3. Effect of spacing distance inside an array

Considering the seabed extension presented in Figure 76, with 3.400 m length, and that 6 units Vestas V117 are to be placed in each array, there is a maximum spacing distance inside the array of 680 m or approximately 5,8D (with a rotor diameter *D* of 117 m).

There is an area at the end of the array with water depth from 13 to 16 m. Excluding all that area, a minimal spacing distance between units is found to be around 450 m or 3,8D. Figure 81 shows a schematic layout for the first array with 5,8D and 3,8D spacing.

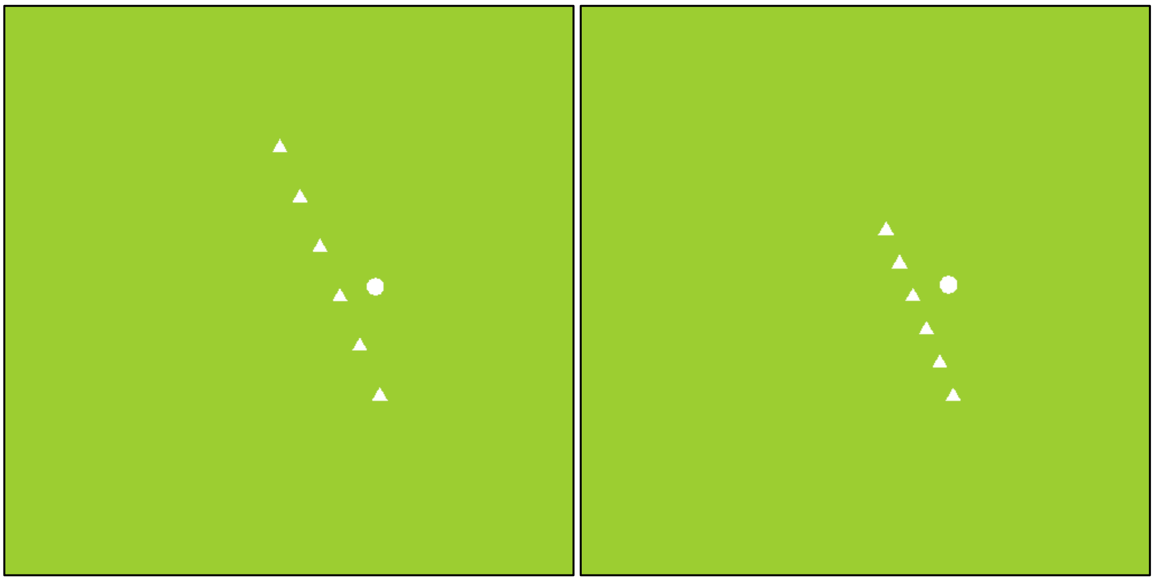

Figure 81. Schematic layout for the first array of turbines with a maximum spacing distance inside the array of 5,8D (left), and with a minimal spacing distance of 3,8D (right). The array is aligned to 158º–338º. Turbine location is represented with a triangle and Bockstigen climatology location with a dot.

The annual wake losses are computed using WindSim. The losses percentage using Larsen's and Jensen's models are listed in Table 20. There is a substantial increase when reducing the spacing distance. The losses increase 1 percentage point using Larson's and 1,3 percentage point using Jensen's wake model when reducing the spacing from 5,8D to 3,8D.

When reducing the spacing from 5,8D to 3,8D only between two turbines, the wake losses are not so significant: there is an increase of only 0,1 percentage point using Larsen's and a little over 0,1 percent point using Jensen's wake model. These small increments indicate that, once an array spacing has been defined, a turbine location can be moved within a rotor diameter distance along the array to an area with the desired water depth without incurring with a significant increase in wake losses.

Table 20. Annual wake losses using Larsen's and Jensen's models for an array with maximum and minimum spacing.

	Annual wake losses		
Wake model:	**5,8D**	**3,8D**	**One spacing at 3,8D, rest at 5,8D**
Larsen TI = 6%	1,40%	2,42%	1,51%

Jensen k = 0,07	1,74%	3,09%	1,87%

12.4. Downwind separation distance

To determine the wake losses generated by the presence of a second array of turbines the configuration with the minimal inside-array losses is used (inside-array spacing of 5,8D). When using the maximum inside-array spacing there is no place for staggering the units of the second array. Those turbines will be aligned at 90° downwind from the units of the first array, following the directrix 69°–249° (see Figure 82). According to Figure 80, the sector ±15° wide centred to that directrix accounts for 19,12% of the total energy content (much higher than the directrix with the minimum energy content 96°–276°) which make the losses calculated in this part a referent for the worst case scenario.

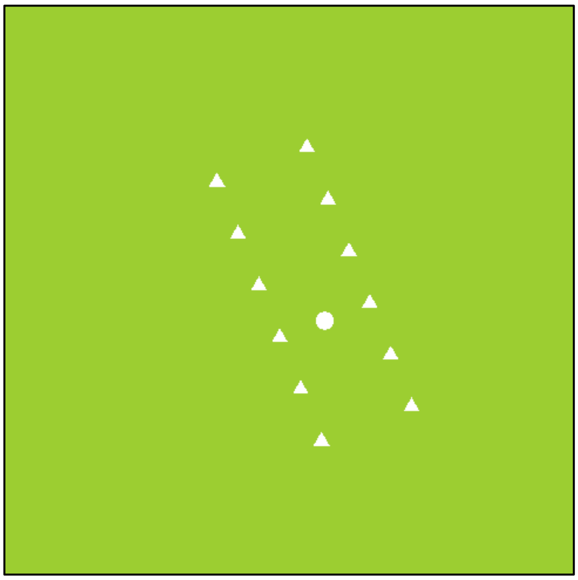

Figure 82. Schematic layout showing the two arrays separated 10D, with 5,8D of inside-array spacing and not staggered. Turbine location is represented with a triangle and Bockstigen climatology location with a dot.

Several simulations are undertaken, increasing the separation distance between arrays from 6D to 10D, being 10D the maximum possible distance within the seabed extension limitations. The results are shown in Figure 83. The wake losses decrease almost linearly when increasing the separation distance. They have a magnitude as high as 3,64% for a distance of 6D (using Jensen's model they would be 4,42%), and they slowly reduce to 2,95% (3,46% using Jensen's) for 10D.

The wake losses inside the arrays will have the same percentage as calculated on one single array of turbines, 1,40% using Larsen's model the maximum turbine spacing. Hence, at the separations considered, the array-to-array wake interaction generates a higher contribution to the total wake losses (representing 1,55% at 10D and up to 2,24% at 6D using Larsen's model).

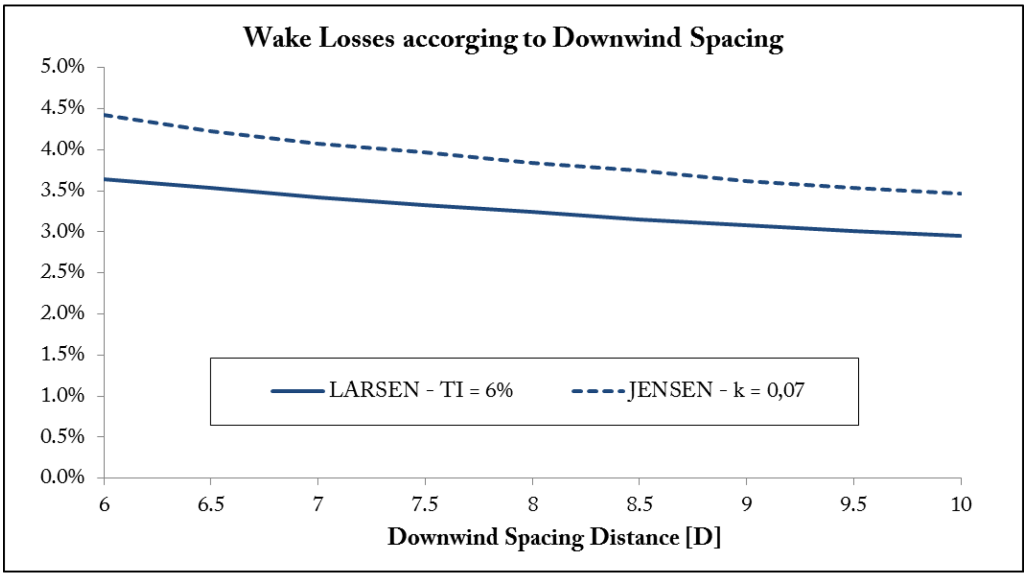

Figure 83. Annual wake losses relative to the downwind spacing between arrays. Results are plotted for Larsen's and Jensen's wake models.

12.5. Effect of staggering

Placing the turbines on the 2nd array staggered from the turbines on the 1st array will help to reduce the wake effects. Unfortunately, the optimal staggering angle cannot be obtained from the energy rose analysis performed in part 12.2. Figure 84 shows a wind resource map calculated with WindSim. The map displays the annual mean wind speed at Bockstigen after taking into account the wake effects from the 1st array of turbines (Larsen's model is used). The annual mean wind speed is a direct measure of the energy content, thus the turbines of the 2nd array must be located at spots with the highest annual mean wind speed possible.

Figure 84 also shows the directrix with the maximum energy content 36º–216º, including the sectors with the highest energy content, from 200º to 240º, and the directrix with the minimum energy content 96º–276º. The areas scanned to place the two turbine arrays are overlaid. It can be clearly seen that the area defined for the 2nd array is completely covered by wake effects generated from the sectors with the highest energy content (see radial arches in magenta). That is the reason why the directrix with the minimum energy content does not provide the optimal staggering angle.

There will still be an optimal staggering angle (at a given separation between arrays) because the distance between the turbine at the 2nd array and turbines on the 1st array will vary when staggering. Figure 85 shows the positions of a turbine at the 2nd array that have been used to run energy simulations.

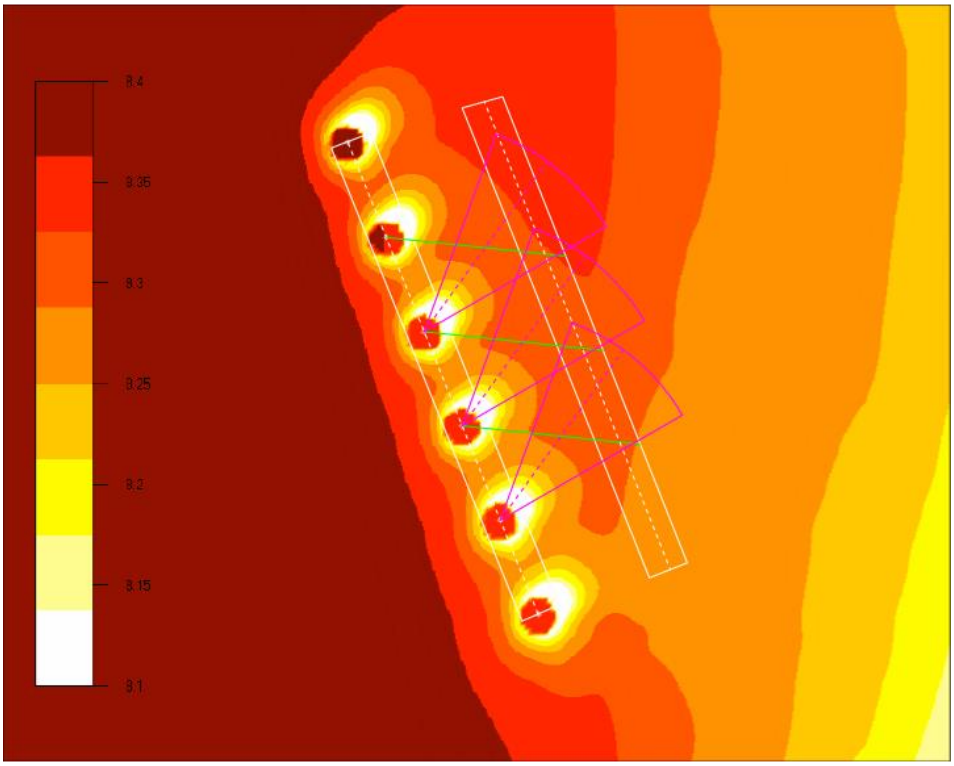

Figure 84. Wind resource map showing the annual mean wind speed at Bockstigen taking into account the wake effects of the 1st array of turbines. The scanned seabed extension is drawn in white. The separation between arrays (dashed white) is 8D. The maximum energy content directrix 36º–216º (dashed magenta) and the range of sectors with the highest energy content, 200º to 240º, are shown. The minimum energy content directrix 96º–276º (solid green) is also plotted.

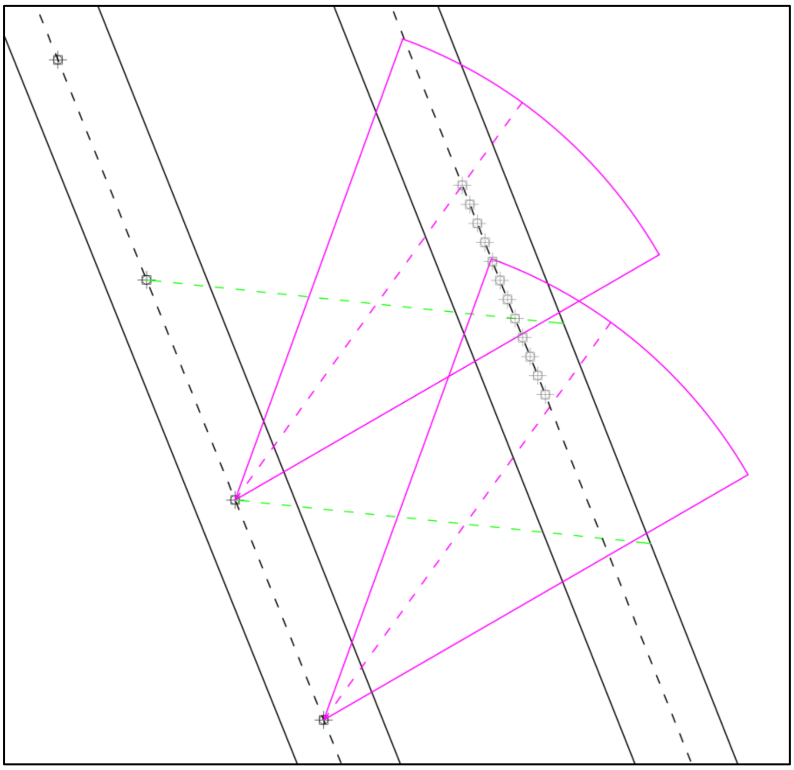

Figure 85. Positions of a turbine situated on the 2nd array (light grey) that have been used to run energy simulations. The positions are spaced 0,5D. The separation between arrays (dashed white) is 8D. The maximum energy content directrix 36º–216º

(dashed magenta) and the range of sectors with the highest energy content, 200º to 240º, are shown. The minimum energy content directrix 96º–276º (dashed green) is also plotted.

The results are plotted in Figure 86. As expected, the wake losses of the single turbine downwind remain almost constant whilst changing its staggering position. Jensen's model gives an erratic output due to its 'top hat' wake width. Larsen's model, in contrast, with a smooth Gaussian definition of the wake width, provides continuous results that show a small reduction at the third staggering position. That position is situated at 229º from the nearest upwind turbine, which, surprisingly enough, it is closer to the directrix with maximum energy content 36º–216º than to the directrix with minimum energy content 96º–276º.

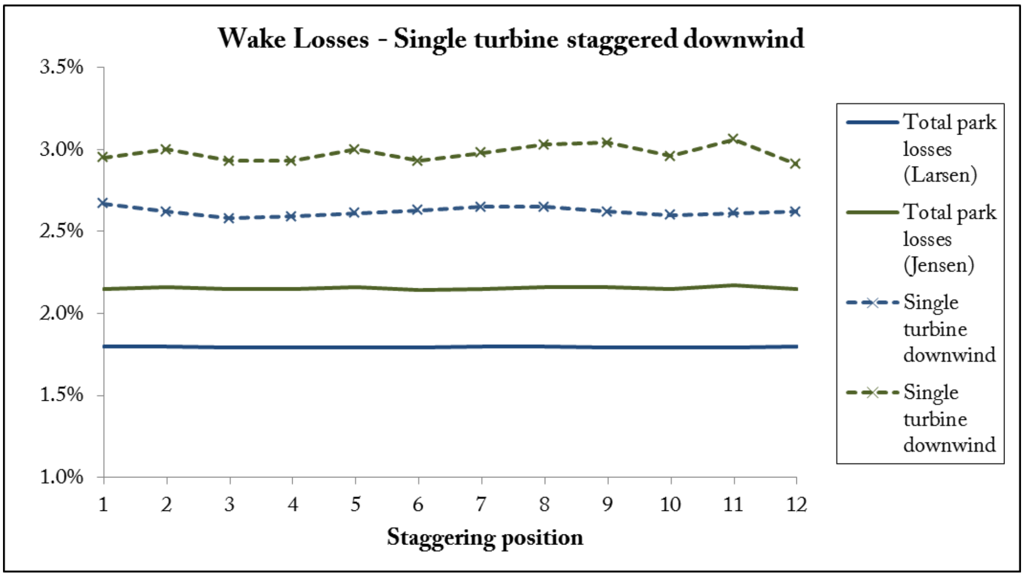

Figure 86. Wake losses of a single turbine downwind for different staggering positions (dashed lines). Total park losses (first array of turbines plus single turbine downwind) are also shown (solid lines). Results using Larsen's model are plotted in blue and using Jensen's in green.

Further analysing the wind resource map of Figure 84, over a separation distance between arrays of 3,9D the staggering effect is imperceptible.

13. Results – Optimized layout

Considering the effect of spacing inside the array, the effect of the separation distance between arrays, and the staggering effect, the layout is optimized by maximizing the separation distance between arrays and the inside-array spacing. No restrictions on staggering are considered, as its effects are almost imperceptible.

The optimization is started by placing the turbines at the maximum spacing and maximum distance between arrays. Next, those distances are progressively shortened to meet the constraints of water depth introduced in part 11.1.1.

The optimal layout is shown in Figure 87. The spacing inside the array varies from 5D to 6D, and the separation distance between arrays in 7D. The water depth of each turbine foundation is listed in Table 22.

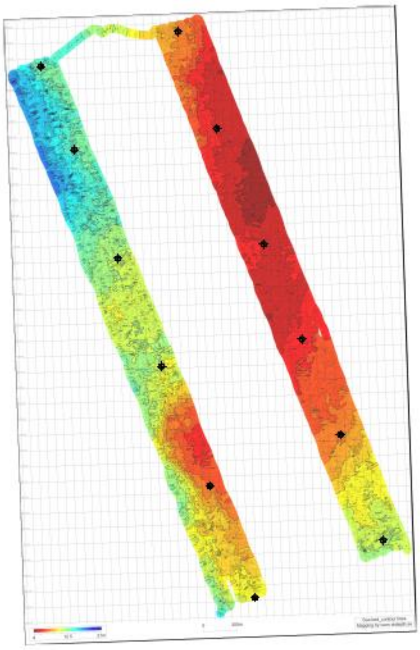

Figure 87. Turbine location and sea bed depth of the optimized layout. The seabed contour lines and turbine coordinates are not shown due to confidentiality reasons.

Table 21. Foundation water depth for the optimized layout. Turbine location (coordinates) are not included for confidentiality reasons.

Units 1st array	Foundation water depth [m]	Units 2nd array	Foundation water depth [m]
Turbine 11	13,5	Turbine 21	8,0
Turbine 12	13,5	Turbine 22	6,5
Turbine 13	12,0	Turbine 23	6,5
Turbine 14	11,0	Turbine 24	6,5
Turbine 15	7,5	Turbine 25	8,0
Turbine 16	10,5	Turbine 26	12,0

The Annual Energy Production and the wake losses percentage for each turbine and for the overall park are listed in Table 22, using Larsen's and Jensen's wake models. The individual wake percentage shows clearly that turbines located on the 2nd array have higher losses than those located on the 1st array. The overall park losses, however, present to be rather low, 3,5% using Larsen's and 4,2% using Jensen's wake model. The AEP calculation and wake losses have to be considered under unstable atmosphere since the wake parameters used have been calibrated with data recorded under unstable conditions.

Table 22. Turbine gross AEP, net AEP, and wake losses percentage under unstable conditions for the optimized layout.

Units 1st array	Gross AEP [MWh]	Net AEP [MWh] (Larsen)	Wake losses [%] (Larsen)	Net AEP [MWh] (Jensen)	Wake losses [%] (Jensen)
Turbine 11	14311,0	13988,6	2,25	13925,0	2,70
Turbine 12	14293,2	13821,7	3,30	13717,9	4,02

Turbine 13	14269,8	13796,2	3,32	13703,9	3,97
Turbine 14	14245,8	13777,2	3,29	13678,2	3,98
Turbine 15	14211,1	13776,7	3,06	13687,4	3,69
Turbine 16	14185,2	13895,4	2,04	13842,7	2,41
Units 2st array					
Turbine 21	14244,3	13728,5	3,62	13615,8	4,41
Turbine 22	14223,0	13585,4	4,48	13463,5	5,34
Turbine 23	14198,9	13547,8	4,59	13408,1	5,57
Turbine 24	14185,1	13533,4	4,59	13396,3	5,56
Turbine 25	14122,5	13513,9	4,31	13391,2	5,18
Turbine 26	14046,1	13640,6	2,89	13540,1	3,60
Total Park:	**170536,0**	**164605,4**	**3,48**	**163370,1**	**4,20**

14. Discussion – Optimized layout

The wake losses obtained with the optimized layout are, at a first sight, surprisingly low (3,5% ~ 4,2%) compared to what it is reported from other offshore wind farms, which are usually between 10% and 20% (see Chapter 2). Several reasons might help to explain those low values, starting from the number of rows or columns in the layout situated downwind, the annual atmospheric conditions at the site, or the site characteristic wind rose.

It has been seen in Chapter 0 that the power deficit continues increasing for downwind units for the majority of cases under unstable conditions. The wake recovery ratio is the quickest under unstable atmospheres; therefore, with slower wake recoveries under neutral or stable conditions, the power deficit increases with downwind units in a more pronounced manner. This can be easily seen in Figure 88. It can be stated that, in overall, offshore wind farms with more than 2 arrays will present larger wake losses than a wind farm with only 2 arrays of turbines.

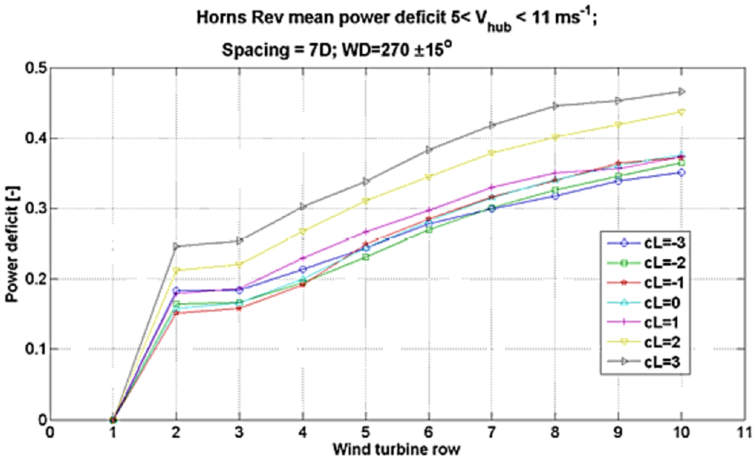

Figure 88. Power deficit of downwind rows of turbines at Horns Rev, classified by atmospheric stability. Source: (Hansen, 2008b).

Even if one assumes the losses of a wake-affected unit are the same as the losses of the 1st turbine downwind, the characteristics of the layout arrangement at Bockstigen will prove that the losses have to be lower. Horns Rev wind farm has similar spacing distances (7D x 7D) than the optimized layout for Bockstigen (5D~6D x 7D). Comparing the optimized layout with Horns Rev layout (see Figure 54) the percentage of wind turbines that are wake-affected change tremendously. Bockstigen may have 6/12 (50%) shadowed units for wind directions around ~270º, and 10/12 (83%) shadowed units for directions ~158º. At Horns Rev the shadowed units would be 72/80 (90%) for wind directions around ~270º, and 63/80 (79%) for directions ~221º and 312º.

The sectors with the highest energy content at Bockstigen are from 200º to 240º, which will hold 50% of wake-affected turbines compared to the 79%, or even 90%, of affected units that Horns Rev shows from its sectors with the highest energy content (see Figure 89). The difference in the ratio of shadowed units is from 58% to 80% times higher at Horns Rev than at Bockstigen, and thus the wake losses are expected to be at least from 58% to 80% times higher at Horns Rev than at Bockstigen.

In spite of having higher level of losses due to the presence of several arrays downwind, the annual wake losses percentage at Horns Rev can be taken as a reference value to assess the wake losses at Bockstigen by comparing the losses percentages under similar atmospheric conditions.

Bockstigen atmospheric stability has been studied in part 5.1.5. During the three years of recorded data, the atmospheric conditions were neutral in the majority of the cases, 64,5%, the atmosphere was stable 34,1% of the cases, and unstable only 1,3% of the time.

As introduced in part 7.1.2, Hansen (2008) studied the annual stability at Horns Rev. In Table 14 it is shown that, during 2005, there were unstable or very unstable conditions 44,1% of the time. 30,4% of the events were recorded under neutral and 25,4% under stable conditions.

L.E. Jensen (2007) has studied the overall park losses under neutral, stable and unstable conditions. Using all available data, Horns Rev shows an annual wake losses of 9,8%. The annual losses under unstable and neutral conditions are quite close, 8,5% and 11,1% respectively. Only under stable atmosphere the losses are significantly higher, 14,7%, which represent an increase of 73% compared to unstable conditions.

The wake model validation, and the subsequent park layout optimization, has been carried out using the available data from Horns Rev, which was recorded under unstable conditions. Taking the unstable data as reference, and assuming that the stability classification of Table 14 (for Horns Rev) and Table 7 (for Bockstigen) are representative of the site climate and have been obtained using similar stability criteria, it is possible to assess the overall annual wake losses at Bockstigen using the new optimized layout as listed in Table 23. Same methodology is used by Sørensen and Thøgersen (2008).

The annual wake losses at Bockstigen under neutral and stable atmospheres are scaled from Horns Rev data using the losses for unstable conditions as a reference. The annual overall wake losses are calculated as the weighted addition of the wake losses under each atmospheric condition. The annual overall wake losses of the optimized layout at Bockstigen are 5,1% when using Larsen's and 6,1% when using Jensen's wake model.

Table 23. Annual stability classification and relevant wake losses for Horns Rev and Bockstigen wind farms. Annual losses under neutral and stable conditions are scaled from Horns Rev data (values in blue). The annual overall losses at Bockstigen is the weighted sum of the wake losses under each atmospheric condition. Values between brackets show results using Jensen's wake model, and without brackets Larsen's.

Stability classification	**Stability at Horns Rev**	**Annual Wake losses**	**Stability at Bockstigen**	**Annual Wake losses At Bockstigen**
Unstable:	*44,1%*	*8,5%*	1,3%	3,5% (4,2%)
Neutral:	*30,4%*	*11,1%*	64,5%	4,6% (5,5%)
Stable:	*25,4%*	*14,7%*	34,1%	6,0% (7,3%)
Annual overall:	-	*9,8%*	-	**5,1% (6,1%)**

In any case, the wake losses under neutral and stable conditions might be assessed higher for the optimized layout than what they would be in reality because of lower wake recovery ratios under those conditions will only affect the 1st array of turbines downwind, eliminating the increasing power deficit effect for the succeeding downwind units. The values used in Table 23 for neutral and stable conditions have to be read as maximum losses coefficient for the worst-case scenario.

However, the annual overall losses obtained for the optimized layout (5,1% using Larsen's) are still low compared to the performance of other offshore wind farms. The characteristic wind rose at Bockstigen might have a lot to do with it. Comparing Horns Rev and Bockstigen energy roses (see Figure 47 and Figure 89) the sectors with the highest energy content at Bockstigen are mainly concentrated in one side, from 200º to 240º, opposite to what shows Horns Rev frequency rose, with the sectors with the largest percentage of high wind speeds widely spread from 210º to 330º.

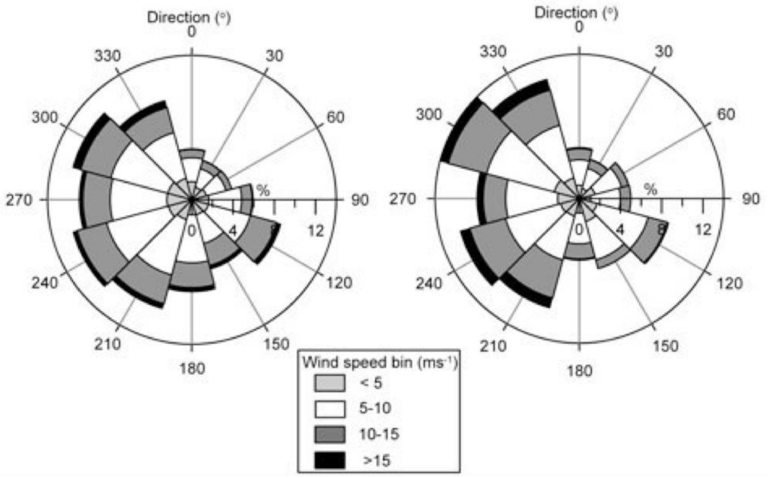

Figure 89. Wind rose at Horns Rev during 1999-2002, previous to the park construction (left), and during 2005-2007, after the park construction (right). Source: (Hansen et al., 2012).

The specific Bockstigen energy rose and the right choice to direct the two arrays in the layout towards directrix 158º–338º makes the wake effects to be lower for a single turbine located downwind of the 1st array. Considering the optimized layout of Figure 87, most of the turbines from the 2nd array are situated towards 90° from the nearest unit of the 1st array. According to the mirrored energy rose from Figure 80, directrix 90°–270° is one with the lowest energy content. The distance between a turbine from the 1st array and its downwind couple (on the 2nd array) is 7D.

Any downwind turbine will also receive important wake effects from the 1st-array unit situated south-west from it (see Figure 85). The directrix connecting them both has direction 37°–217°, and its separation distance is 8,8D. It has been seen in part 12.2 that the directrix with the maximum energy content is practically the same, with direction 36°–216°. Therefore, the layout arrangement geometrically compensates the wake effects, providing larger spacing downwind distances for the directions with the highest energy content and shorter spacing for directions with the lower energy content.

This geometrical compensation does not occur with Horns Rev layout and the its characteristic energy rose, which supports to explain the lower wake effects obtained at Bockstigen with the optimized layout.

15. Conclusions

The tested and validated analytical wake models have proved to be satisfactory defining the wake losses of an offshore wind farm. The models can be parameterized to capture the power deficit for specific atmospheric conditions, but can only describe precisely the power drop at the 1st turbine downwind (2nd in the array). The trend of the power deficit for the rest of downwind units in not well captured with any of the tested models. The three tested analytical models, Jensen's, Larsen's and Ishihara's, tend to achieve their asymptotic value too quickly.

The values of the wake parameters tuned during the validation with Horns Rev production data are quite realistic for Larsen's and Jensen's models. Ishihara's, however, requests to have inputted an unrealistically high value for the atmospheric turbulence intensity to give good agreement with the measurements (or at least the version implemented in WindSim does). This issue is found to be related with the wake width definition in each model. Jensen's wake width, despite of being defined as a 'top hat' shape, provides a surprisingly good fit to the experimental wake width when averaging the results with 1º step. Larsen's shows also a very good fit with experimental data, but Ishihara's completely overshoots the power deficit at the wake centerline, reason why this model requests a higher value of atmospheric turbulence to be inputted to start matching the experimental data.

Further research has to be undertaken, therefore, to develop a model that describes more accurately the power losses for the subsequent downwind units and the wake width, taking into account the cluster turbulence intensity and atmospheric stability.

When applying the validated and parameterised models to the layout optimization at Bocktigen both Jensen's and Larsen's models show consistent results. The calculated wake losses are valid under unstable atmospheric conditions as the validation study has been carried out with data from Horns Rev under those conditions. Analysing the annual stability at Bockstigen and Horns Rev, the park losses at Bockstigen can be scaled using the annual losses from Horns Rev as a reference.

The park losses obtained could seem to be too small for an offshore wind farm with about 7D of spacing distance. The results are proved to be correct after analysing the number of shadowed turbines, and the energy rose characteristics. For instance, Bockstigen optimized layout may have 50% of its 12 units affected by wakes when the wind blows from the main wind sector, whilst in Horns Rev the percentage is as high as 79% or 90%.

Atmospheric stability has manifested to play a key role in wake losses assessment. However, it has been seen that classifying accurately the atmospheric conditions of an offshore site is rather difficult; available measurements (especially temperature measurements) are not accurate enough, and the usage of different methods and several classification criteria makes the results unreliable, they cannot be contrasted with other publications and involve a high level of uncertainty. It is therefore crucial to develop a robust methodology classify the atmosphere, and define measuring equipment specifications to assess faultlessly the atmospheric stability at any site.

The focus of this investigation has been to identify an optimal layout of the Bockstigen generation II wind farm. By applying well-known wake models on existing wind farms, i.e., Horns Rev, methods have been calibrated to be used for this case. The work has further investigated the influence of stability. However, the focus has not been to calculate the AEP with a high accuracy, therefore the AEP discussed here should not be considered as a base for investment decisions.

16. References

Ainslie, J.F. (1988), "Journal of Wind Engineering and Industrial Aerodynamics, 27 (1988) 213-224", Vol. 27, pp. 213–224.

Ashrafi, K. and Hoshyaripour, G.A. (2008), "A Model to Determine Atmospheric Stability and its Correlation with CO Concentration", *World Academy of Science, Engineering and Technology*, Vol. 2 No. 8, pp. 143–148.

Barthelmie, R., Frandsen, S.T., Hansen, K., Schepers, J.G., Rados, K., Schlez, W., Neubert, A., et al. (2009), "Modelling the impact of wakes on power output at Nysted and Horns Rev", *EWEC 2009*, available at: http://www.gl-group.com/assets/technical/301_EWEC2009presentation.pdf.

Barthelmie, R., Frandsen, S.T., Rathmann, O., Hansen, K., Politis, E.S., Prospathopoulos, J., Schepers, J.G., et al. (2011), "Flow and wakes in large wind farms : Final report for UpWind WP8 Risø-R-Report", *Risø National Laboratory, Technical University of Denmark*, No. Risø-R-1765(EN).

Barthelmie, R. and Jensen, L.E. (2010), "Evaluation of wind farm effi ciency and wind turbine wakes at the Nysted offshore wind farm", No. June, pp. 573–586.

Barthelmie, R., Larsen, G., Pryor, S., Jørgensen, H., Bergström, H., Schlez, W., Rados, K., et al. (2004), "ENDOW(efficient development of offshore wind farms): modelling wake and boundary layer interactions", *Wind Energy*, Vol. 7 No. 3, pp. 225–245.

Barthelmie, R., Larsen, G.C., Frandsen, S.T., Folkerts, L., Rados, K., Pryor, S.C., Lange, B., et al. (2006), "Comparison of Wake Model Simulations with Offshore Wind Turbine Wake Profiles Measured by Sodar", *Journal of Atmospheric and Oceanic Technology*.

Barthelmie, R., Pryor, S.C., Frandsen, S.T., Hansen, K.S., Schepers, J.G., Rados, K., Schlez, W., et al. (2010), "Quantifying the Impact of Wind Turbine Wakes on Power Output at Offshore Wind Farms", *Journal of Atmospheric and Oceanic Technology*, Vol. 27 No. 8, pp. 1302–1317.

Brower, M.C. (2012), *Wind Resource Assessment: A Practical Guide to Developing a Wind Project*, Wiley, pp. 121–123.

Christiansen, M.B. and Hasager, C.B. (2005), "Wake effects of large offshore wind farms identified from satellite SAR", *Remote Sensing of Environment*, Vol. 98 No. 2-3, pp. 251–268.

Crespo, A. and Hernández, J. (1996), "Turbulence characteristics in wind-turbine wakes", *Journal of Wind Engineering and Industrial Aerodynamics*, Vol. 61, pp. 71–85.

Douglas-Westwood. (2013), "World Offshore Wind Market Forecast 2013-2022", available at: http://www.douglas-westwood.com/shop/shop-infopage.php?longref=1158.

EWEA. (2014a), "Wind in power. 2013 European statistics", European Wind Energy Association.

EWEA. (2014b), "Wind energy scenarios for 2020", European Wind Energy Association.

Frandsen, S. (1992), "On the wind speed reduction in the center of large clusters of wind turbines", *Journal of Wind Engineering and Industrial Aerodynamics*, Vol. 39, pp. 251–265.

Frandsen, S., Barthelmie, R., Pryor, S., Larsen, S. and Højstrup, J. (2004), "The necessary distance between large wind farms offshore - study", *Risø National Laboratory, Technical University of Denmark*, No. Risø-R-1518(EN).

Frandsen, S., Barthelmie, R., Pryor, S., Rathmann, O. and Larsen, S. (2006), "Analytical Modelling of Wind Speed Deficit in Large Offshore Wind Farms", *Wind Energy*, No. January, pp. 39–53.

Ganander, H., Ronsten, G. and Bergström, H. (2001), "Medium term evaluation of meteorological conditions, power performance and loads on the first Swedish offshore wind farm at Bockstigen", *EWEA Special Topic Offshore Conference*, Brussels, Belgium.

Gaumond, M., Réthoré, P.E., Ott, S., Peña, A., Bechmann, A. and Hansen, K.S. (2013), "Evaluation of the wind direction uncertainty and its impact on wake modeling at the Horns Rev offshore wind farm", *Wind Energy*, doi:10.1002/we.1625.

Gdem.ersdac.jspacesystems.or.jp. (2014), "ASTER Global Digital Elevation Model", available at: http://gdem.ersdac.jspacesystems.or.jp (accessed 27 October 2014).

Gmao.gsfc.nasa.gov. (2014), "GMAO MERRA: Modern Era Retrospective-Analysis for Research and Applications", available at: Gmao.gsfc.nasa.gov (accessed 27 October 2014).

Gravdahl, A.R. (1998), "Meso Scale Modeling with a Reynolds Averaged Navier Stokes Solver. Assessment of wind resources along the Norwegian coast.", *31st IEA Experts Meeting*, Denmark.

Hansen, K.S. (2005), "Bockstigen - Site documentation.", No. April, pp. 1–20.

Hansen, K.S. (2008a), "Data Wake measurements used in the model evaluation", *Risø National Laboratory, Technical University of Denmark*, No. Project UpWind, Deliverable D8.1.

Hansen, K.S. (2008b), "Guideline to wind farm wake analysis", *Risø National Laboratory, Technical University of Denmark*, No. Project UpWind, Appendix 7.

Hansen, K.S., Barthelmie, R.J., Jensen, L.E. and Sommer, A. (2012), "The impact of turbulence intensity and atmospheric stability on power deficits due to wind turbine wakes at Horns Rev wind farm", *Wind Energy*, Vol. 15 No. November 2011, pp. 183–196.

Hansen, K.S., Larsen, G.C. and Ott, S. (2014), "Dependence of offshore wind turbine fatigue loads on atmospheric stratification", *Journal of Physics: Conference Series*, Vol. 524 No. Torque, p. 012165.

Hasager, C.B., Peña, A., Mikkelsen, T., Courtney, M.S., Antoniou, I., Gryning, S.-E., Hansen, P., et al. (2007), "12MW Horns Rev experiment", *Risø National Laboratory, Technical University of Denmark*, No. Risø-R-1506(EN).

Ishihara, T., Yamaguchi, A. and Fujino, Y. (2004), "Development of a new wake model based on a wind tunnel experiment", *Global Wind Power*, Global Wind Power 2004, available at: http://windeng.t.u-tokyo.ac.jp/ishihara/posters/2004_gwp_poster.pdf (accessed 20 May 2014).

Jain, P. (2011), *Wind Energy Engineering*, McGraw Hill, pp. 97–98.

Jensen, L.E. (2007), "Analysis of array efficiency at horns rev and the effect of atmospheric stability", *Eurpoean Wind Energy Conference*, Milan.

Jensen, N.O. (1983), "A Note on Wind Generator Interaction", *Risø National Laboratory*, No. Risø-M-2411.

Katic, I., Højstrup, J. and Jensen, N.O. (1986), "A Simple Model for Cluster Efficiency", *European Wind Energy Conference and Exhibition*, Rome, pp. 407–410.

Larsen, G. (1988), "A Simple Wake Calculation Procedure".

Larsen, G.C., Madsen, H.A. and Sørensen, N.N. (2003), "Mean wake deficit in the near field", *European Wind Energy Conference and exhibition 2003*, Madrid, Spain.

Moskalenko, N., Rudion, K. and Orths, A. (2010), "Study of Wake Effects for Offshore Wind Farm Planning", *Modern Electric Power Systems*.

Motta, M., Barthelmie, R.J. and Vølund, P. (2005), "The influence of non-logarithmic wind speed profiles on potential power output at Danish offshore sites", *Wind Energy*, Vol. 8 No. 2, pp. 219–236.

Ott, S. (2012), "AMOK", DTU Wind Energy. Risø Campus.

Ott, S., Berg, J. and Nielsen, M. (2011), "Linearised CFD Models for Wakes", *Risø National Laboratory, Technical University of Denmark*, No. Risø–R–1772(EN).

Peña, A. and Gryning, S.-E. (2008), "Charnock ' s roughness length model and non-dimensional wind profiles over the sea", *Boundary-Layer Meteorology*, Vol. 128 No. 2, pp. 191–203.

Peña, A. and Hahmann, A.N. (2012), "Atmospheric stability and turbulence fluxes at Horns Rev-an intercomparison of sonic, bulk and WRF model data", *Wind Energy*, Vol. 15, pp. 717–731.

Peña, A. and Rathmann, O. (2013), "Atmospheric stability- dependent infinite wind- farm models and the wake- decay coefficient", *Wind Energy*, doi:10.1002/we.

Ronsten, G. (2006), *Power Performance and Park Efficiency of the Bockstigen Wind Farm*.

Ronsten, G., Thor, S.-E., Ganander, H., Johansson, H., Thiringer, T., Petru, T. and Bergström, H. (2000), "Evaluation of loads, power quality, grid interaction, meteorological conditions and power performance of the first Swedish offshore wind farm at Bockstigen", *Proceedings from Offshore Wind Energy in Meditteranean and Other Seas OWEMES2000*, Sicily, Italy.

Sørensen, J.N. (2011), "Lecture Note in LES in Marine Hydrodynamics and Offshore Wind Power Wind Turbine Aerodynamics".

Sørensen, T. and Thøgersen, M. (2008), "Adapting and calibration of existing wake models to meet the conditions inside offshore wind farms", *EMD International A/S.*, available at: http://www.risoe.dk/rispubl/NEI/NEI-DK-4960.pdf.

Stull, R.B. (1988), *An Introduction to Boundary Layer Meteorology*, Kluwer Academic Publishers, Dordrecht, Boston, London, p. 177.

Thøgersen, M.L. (2012), "Introduction to Wind Turbine Wake Modelling and Wake Generated Turbulence", *EMD International A/S*, No. WindPRO / PARK.

VanLuvanee, D. (2006), *Investigation of observed and modelled wake effects at Horns Rev using WindPRO*, *Technical University of Denmark Department of …*, available at: http://scholar.google.com/scholar?hl=en&btnG=Search&q=intitle:Investigation+of+Observed+and+Modeled+Wake+Effects+at+Horns+Rev+using+WindPRO#0 (accessed 12 May 2014).

Verkaik, J.W., Smits, A. and Royal, J.E. (2003), *KNMI-HYDRA Project. Phase report 9 Wind Climate Assessment of the Netherlands 2003*.

Vermeer, L.J., Sørensen, J.N. and Crespo, A. (2003), "Wind turbine wake aerodynamics", *Progress in Aerospace Sciences*, Vol. 39 No. 6-7, pp. 467–510.

Wharton, S., Lundquist, J.K. and Marjanovic, N. (2012), "Synergistic Effects of Turbine Wakes and Atmospheric Stability on Power Production at an Onshore Wind Farm".

Wieringa, J. (1992), "Updating the Davenport rou(jhness classification", *Journal of Wind Engineering and Industrial Aerodynamics*, Vol. 41-44, pp. 357–368.

Annex I – Perl code of filtering script

```
#!/usr/bin/perl

use strict;
use warnings;

print "File name to filter: ";
my $file = <STDIN>;
open(DATA, "<".$file) or die "Could not find $file";
chomp ($file);

print "Column Num. to filter: ";
my $col = <STDIN> -1;

print "Num. identical consecutive values to start filtering: ";
my $maxCons = <STDIN>;

my %valors = ('reference',,'new',,'lini',,'lfi',);
my @mach_lines;
my $consecutive = 1;
my $count = 0;

while (my $line = <DATA>) {
  my @array = split(';', $line);
  if ( $array[$col] ) {
    $valors{'new'} = $array[$col];
    if (  ($valors{'reference'}) eq 'new'){
      $valors{'reference'} = $valors{'new'};
      next
    }
    if ( $valors{'new'} eq $valors{'reference'}) {
      $consecutive++;
      if ($consecutive eq 2){
        $valors{'lini'} = $.-1;
      }
    }
    else {
      if ($consecutive >= $maxCons){
        $valors{'lfi'}=$.-1;
        my $val = $valors{'lini'};
        while ($val <= $valors{'lfi'}){
          push( @mach_lines, "$val");
          $val++;
        }
        $count = $count + $valors{'lfi'} - $valors{'lini'} +1;
      }
      $valors{'reference'}=$valors{'new'};
      $consecutive = 1;
    }
  }
}

# for the last evaluation in the loop
if ($consecutive >= $maxCons){
  $valors{'lfi'}=$.-1;
  my $val = $valors{'lini'};
  while ($val <= $valors{'lfi'}){
    push( @mach_lines, "$val");
    $val++;
    }
  $count = $count + $valors{'lfi'} - $valors{'lini'} +1;
}

$col++;
close(DATA);
print "--------------------\n";

if ($count ne 0) {

  open (DATA, "<".$file);
  my @file = split('\.', $file);
  my $extension ='.'.$file[-1];
  pop (@file);
  $file = join (' ', @file);
  my $output = $file.'_Column'.$col.'_filtered'.$extension;
  my $dumped = $file.'_Column'.$col.'_dumped_lines'.$extension;
  open(OUTPUT, ">$output");
  open (DUMPED, ">$dumped");

  my $i=0;

  while ( <DATA> ) {
    if ( $mach_lines[$i]) {
      if ( $. eq $mach_lines[$i] ) {
        print "Line: ".$.."\n";
        print DUMPED $_;
        $i++;
      }
      else {
        print OUTPUT $_;
      }
    }
    else {
      print OUTPUT $_;
    }
  }
  close (DATA);
  close (OUTPUT);
  close (DUMPED);
  print "$count issues have been found.\nOutput files created:\n";
  print "\t\"$output\"\n";
  print "\t\"$dumped\"\n";
}

if ($count eq 0) { print "No issues found in Column $col.\n";}
```

Annex II – Sea temperature fluctuation event

TimeStamp	Water temp.	Pot. temp. 6 m
25/08/2000 00:00	16,56	14,68
25/08/2000 00:10	16,52	14,51
25/08/2000 00:20	16,51	14,56
25/08/2000 00:30	16,52	14,63
25/08/2000 00:40	16,54	14,68
25/08/2000 00:50	16,50	14,57
25/08/2000 01:00	16,46	14,53
25/08/2000 01:10	16,46	14,26
25/08/2000 01:20	16,44	14,22
25/08/2000 01:30	16,43	14,41
25/08/2000 01:40	16,38	14,52
25/08/2000 01:50	16,35	14,63
25/08/2000 02:00	16,37	14,69
25/08/2000 02:10	16,39	14,75
25/08/2000 02:20	16,41	14,79
25/08/2000 02:30	16,39	14,83
25/08/2000 02:40	16,35	14,76
25/08/2000 02:50	16,35	14,68
25/08/2000 03:00	16,29	14,36
25/08/2000 03:10	16,26	14,62
25/08/2000 03:20	16,18	14,74
25/08/2000 03:30	16,12	14,16
25/08/2000 03:40	16,09	13,96
25/08/2000 03:50	16,07	14,38
25/08/2000 04:00	16,08	14,53
25/08/2000 04:10	16,04	14,63
25/08/2000 04:20	16,00	14,27
25/08/2000 04:30	15,95	14,11
25/08/2000 04:40	15,95	14,06
25/08/2000 04:50	15,80	14,37
25/08/2000 05:00	15,54	14,55
25/08/2000 05:10	15,05	14,74
25/08/2000 05:20	14,66	14,79
25/08/2000 05:30	13,40	14,77
25/08/2000 05:40	12,12	14,76
25/08/2000 05:50	11,89	14,79
25/08/2000 06:00	11,81	14,68
25/08/2000 06:10	11,71	14,46
25/08/2000 06:20	11,63	14,42
25/08/2000 06:30	11,53	14,36
25/08/2000 07:00	11,25	14,39
25/08/2000 07:10	11,22	14,41
25/08/2000 07:20	11,20	14,48
25/08/2000 07:30	11,31	14,53
25/08/2000 07:40	11,33	14,54
25/08/2000 07:50	11,30	14,58
25/08/2000 08:00	11,28	14,44
25/08/2000 08:10	11,25	14,70
25/08/2000 08:20	11,13	14,60
25/08/2000 08:30	10,99	14,42
25/08/2000 08:40	10,92	14,41
25/08/2000 08:50	10,89	14,45
25/08/2000 09:00	10,93	14,45
25/08/2000 09:10	10,97	14,46
25/08/2000 09:20	10,96	14,56
25/08/2000 09:30	11,06	14,52
25/08/2000 09:40	11,14	14,54
25/08/2000 09:50	11,32	14,67
25/08/2000 10:00	11,46	14,72
25/08/2000 10:10	11,55	14,66
25/08/2000 10:20	11,58	14,78
25/08/2000 10:30	11,52	14,83
25/08/2000 10:40	11,42	14,64
25/08/2000 10:50	11,40	14,69
25/08/2000 11:00	11,23	14,66
25/08/2000 11:10	11,11	14,64
25/08/2000 11:20	10,86	14,35
25/08/2000 11:30	10,76	14,43
25/08/2000 11:40	10,73	14,64
25/08/2000 11:50	10,70	14,69
25/08/2000 12:00	10,59	14,58
25/08/2000 12:10	10,51	14,41
25/08/2000 12:20	10,37	14,70
25/08/2000 12:30	10,33	14,75
25/08/2000 12:40	10,36	14,65
25/08/2000 12:50	10,16	14,68
25/08/2000 13:00	10,05	14,72
25/08/2000 13:10	9,96	14,48
25/08/2000 13:20	9,74	14,27
25/08/2000 13:30	9,52	14,72
25/08/2000 13:40	9,45	14,77
25/08/2000 13:50	9,28	14,83
25/08/2000 14:00	9,06	14,79
25/08/2000 14:10	9,04	14,95
25/08/2000 14:20	9,07	14,77
25/08/2000 14:30	8,95	14,89
25/08/2000 14:40	8,90	14,67
25/08/2000 14:50	8,98	14,72
25/08/2000 15:00	8,92	14,63
25/08/2000 15:10	8,73	14,67
25/08/2000 15:20	8,81	14,74
25/08/2000 15:30	8,83	14,93
25/08/2000 15:40	8,70	14,85
25/08/2000 15:50	8,60	14,99
25/08/2000 16:00	8,66	14,96
25/08/2000 16:10	8,76	14,96
25/08/2000 16:20	8,72	15,28
25/08/2000 16:30	8,76	15,24
25/08/2000 16:40	8,69	15,45
25/08/2000 16:50	8,55	15,54
25/08/2000 17:00	8,61	15,52
25/08/2000 17:10	8,71	16,30
25/08/2000 17:20	8,85	15,60
25/08/2000 17:30	8,77	15,40
25/08/2000 17:40	8,68	15,08
25/08/2000 17:50	8,74	15,46

25/08/2000 18:00	8,74	15,60
25/08/2000 18:10	8,63	15,55
25/08/2000 18:20	8,67	15,41
25/08/2000 18:30	8,79	15,56
25/08/2000 18:40	8,99	15,51
25/08/2000 18:50	9,49	16,03
25/08/2000 19:00	9,58	15,97
25/08/2000 19:10	9,53	15,99
25/08/2000 19:20	9,47	15,99
25/08/2000 19:30	9,39	15,93
25/08/2000 19:40	9,27	15,89
25/08/2000 19:50	9,30	15,85
25/08/2000 20:00	9,29	15,85
25/08/2000 20:10	9,41	15,81
25/08/2000 20:20	11,61	15,79
25/08/2000 20:30	13,48	15,52
25/08/2000 20:40	13,90	15,30
25/08/2000 20:50	14,07	15,36
25/08/2000 21:00	14,18	15,37
25/08/2000 21:10	14,28	15,31
25/08/2000 21:20	14,32	15,20
25/08/2000 21:30	14,34	15,19
25/08/2000 21:40	14,37	15,12
25/08/2000 21:50	14,38	15,02
25/08/2000 22:00	14,39	15,00
25/08/2000 22:10	14,37	14,96
25/08/2000 22:20	14,37	14,92
25/08/2000 22:30	14,36	14,86
25/08/2000 22:40	14,38	14,83
25/08/2000 22:50	14,40	14,97
25/08/2000 23:00	14,40	14,92
25/08/2000 23:10	14,40	14,90
25/08/2000 23:20	14,44	14,80
25/08/2000 23:30	14,69	14,79
25/08/2000 23:40	14,83	14,74
25/08/2000 23:50	14,89	14,63
26/08/2000 00:00	14,92	14,58
26/08/2000 00:10	14,92	14,46
26/08/2000 00:20	14,93	14,53
26/08/2000 00:30	14,98	14,46
26/08/2000 00:40	15,03	14,43
26/08/2000 00:50	15,04	14,34
26/08/2000 01:00	14,99	14,24
26/08/2000 01:10	14,96	14,02
26/08/2000 01:20	14,95	13,97
26/08/2000 01:30	14,95	13,97
26/08/2000 01:40	14,93	13,90
26/08/2000 01:50	14,92	13,92
26/08/2000 02:00	14,95	13,72
26/08/2000 02:10	14,93	13,66
26/08/2000 02:20	14,93	13,49
26/08/2000 02:30	14,92	13,59
26/08/2000 02:40	14,88	13,67
26/08/2000 02:50	14,88	13,97
26/08/2000 03:00	14,87	13,69
26/08/2000 03:10	14,88	13,42
26/08/2000 03:20	14,89	13,35
26/08/2000 03:30	14,89	13,25
26/08/2000 03:40	14,88	13,16
26/08/2000 03:50	14,90	13,18
26/08/2000 04:00	14,83	13,34
26/08/2000 04:10	14,71	13,28
26/08/2000 04:20	14,58	13,38
26/08/2000 04:30	14,48	13,60
26/08/2000 04:40	14,50	13,75
26/08/2000 04:50	14,33	13,74
26/08/2000 05:00	14,14	13,74
26/08/2000 05:10	13,93	13,75
26/08/2000 05:20	13,81	13,75
26/08/2000 05:30	13,74	13,87
26/08/2000 05:40	13,66	13,98
26/08/2000 05:50	13,61	14,10
26/08/2000 06:00	13,43	14,20
26/08/2000 06:10	13,29	14,20
26/08/2000 06:20	13,06	14,16
26/08/2000 06:30	12,89	14,09
26/08/2000 06:40	12,82	14,10
26/08/2000 06:50	12,70	14,24
26/08/2000 07:00	12,46	14,20
26/08/2000 07:10	12,17	14,22
26/08/2000 07:20	12,04	14,23
26/08/2000 07:30	11,78	14,32
26/08/2000 07:40	11,54	14,35
26/08/2000 07:50	11,38	14,43
26/08/2000 08:00	11,08	14,47
26/08/2000 08:10	10,94	14,52
26/08/2000 08:20	10,99	14,57
26/08/2000 08:30	11,22	14,64
26/08/2000 08:40	11,36	14,67
26/08/2000 08:50	10,87	15,05
26/08/2000 09:00	10,72	15,17
26/08/2000 09:10	10,92	15,25
26/08/2000 09:20	11,13	15,25
26/08/2000 09:30	11,27	15,23
26/08/2000 09:40	11,35	15,20
26/08/2000 09:50	11,53	14,85
26/08/2000 10:00	11,73	15,16
26/08/2000 10:10	12,06	15,21
26/08/2000 10:20	12,33	15,21
26/08/2000 10:30	12,69	15,26
26/08/2000 10:40	12,90	15,24
26/08/2000 10:50	13,27	15,29
26/08/2000 11:00	13,62	15,36
26/08/2000 11:10	13,84	15,41
26/08/2000 11:20	13,91	15,42
26/08/2000 11:30	14,20	15,47
26/08/2000 11:40	14,22	15,56
26/08/2000 11:50	14,13	15,53
26/08/2000 12:00	14,17	15,58
26/08/2000 12:10	14,51	15,54
26/08/2000 12:20	14,76	15,52
26/08/2000 12:30	14,79	15,35
26/08/2000 12:40	14,82	15,51
26/08/2000 12:50	15,00	15,61
26/08/2000 13:00	15,02	15,72
26/08/2000 13:10	15,14	15,80
26/08/2000 13:20	15,26	15,87
26/08/2000 13:30	15,28	15,91

26/08/2000 13:40	15,30	15,97
26/08/2000 13:50	15,36	16,01
26/08/2000 14:00	15,56	16,05
26/08/2000 14:10	15,67	16,07
26/08/2000 14:20	15,75	16,20
26/08/2000 14:30	15,75	16,31
26/08/2000 14:40	15,78	16,32
26/08/2000 14:50	15,79	16,25
26/08/2000 15:00	15,87	16,21
26/08/2000 15:10	16,00	16,20
26/08/2000 15:20	16,13	16,21
26/08/2000 15:30	16,14	16,21
26/08/2000 15:40	16,07	16,21
26/08/2000 15:50	16,07	16,21
26/08/2000 16:00	16,04	16,22
26/08/2000 16:10	16,07	16,27
26/08/2000 16:20	16,16	16,31
26/08/2000 16:30	16,16	16,30
26/08/2000 16:40	16,06	16,32
26/08/2000 16:50	16,03	16,38
26/08/2000 17:00	16,08	16,34
26/08/2000 17:10	16,21	16,34
26/08/2000 17:20	16,32	16,35
26/08/2000 17:30	16,40	16,37
26/08/2000 17:40	16,42	16,36
26/08/2000 17:50	16,38	16,33
26/08/2000 18:00	16,47	16,35

Annex III – Roughness classification tables

Table 24. Surface roughness classification for non-complex terrain. Source: (Wieringa, 1992).

Class	Surface	Landscape Description	z_0 (m)
1	Sea	Open sea, fetch at least 5 km	0.0002
2	Smooth	Mud flats, snow, little vegetation, no obstacles	0.005
3	Open	Flat terrain: grass few isolated obstacles	0.03
4	Roughly Open	Low crops: occasional large obstacles	0.1
5	Rough	High Crops: scattered obstacles	0.25
6	Very Rough	Orchards, bushes: numerous obstacle	0.5
7	Closed	Regular large obstacle coverage (suburban area, forest)	1.0
8	Chaotic	City centre with high and low rise building	>2

Table 25. Surface roughness classification used in KNMI-HYDRA. Source: (Verkaik et al., 2003).

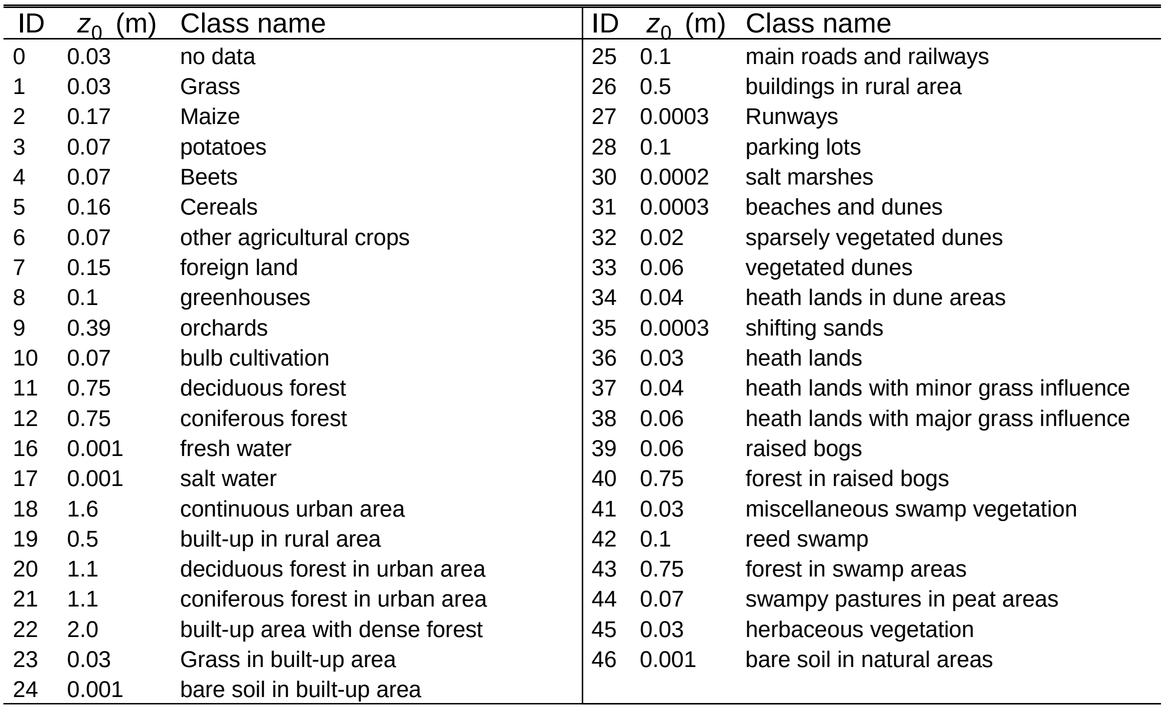

ID	z_0 (m)	Class name	ID	z_0 (m)	Class name
0	0.03	no data	25	0.1	main roads and railways
1	0.03	Grass	26	0.5	buildings in rural area
2	0.17	Maize	27	0.0003	Runways
3	0.07	potatoes	28	0.1	parking lots
4	0.07	Beets	30	0.0002	salt marshes
5	0.16	Cereals	31	0.0003	beaches and dunes
6	0.07	other agricultural crops	32	0.02	sparsely vegetated dunes
7	0.15	foreign land	33	0.06	vegetated dunes
8	0.1	greenhouses	34	0.04	heath lands in dune areas
9	0.39	orchards	35	0.0003	shifting sands
10	0.07	bulb cultivation	36	0.03	heath lands
11	0.75	deciduous forest	37	0.04	heath lands with minor grass influence
12	0.75	coniferous forest	38	0.06	heath lands with major grass influence
16	0.001	fresh water	39	0.06	raised bogs
17	0.001	salt water	40	0.75	forest in raised bogs
18	1.6	continuous urban area	41	0.03	miscellaneous swamp vegetation
19	0.5	built-up in rural area	42	0.1	reed swamp
20	1.1	deciduous forest in urban area	43	0.75	forest in swamp areas
21	1.1	coniferous forest in urban area	44	0.07	swampy pastures in peat areas
22	2.0	built-up area with dense forest	45	0.03	herbaceous vegetation
23	0.03	Grass in built-up area	46	0.001	bare soil in natural areas
24	0.001	bare soil in built-up area			

Annex IV – Sector-wise correlation between Havsmast and Kustmast

Correlation of Havsmast wind measurements at 45 m high and Kustmast at 60 m high using Linear Regression method in WindPRO. All sectors show a high degree of correlation, including the wake-affected sectors.

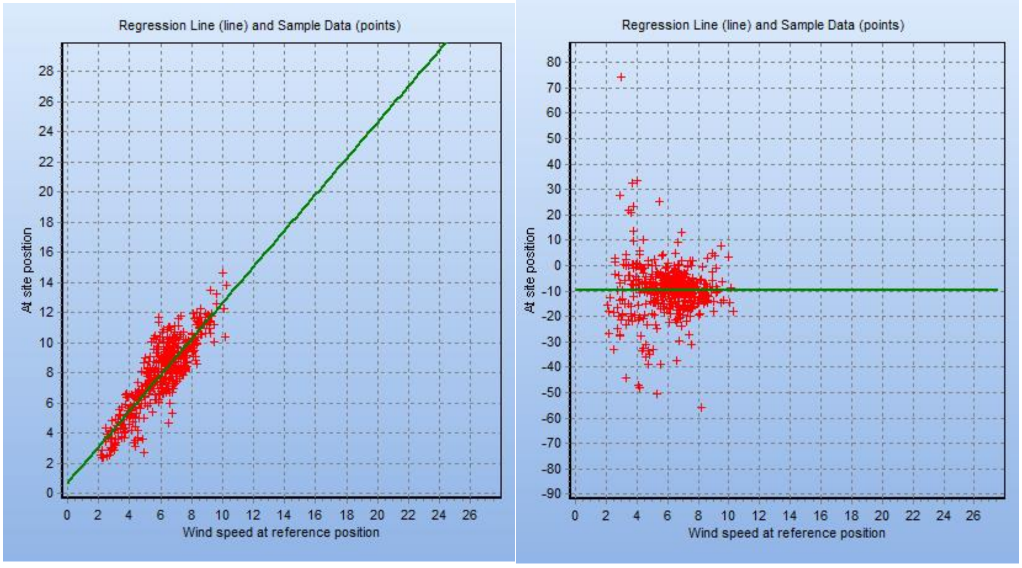

Figure 90. Correlation of wind speed (left) and wind veer (right) for an onshore wind direction, sector 50°, with land effects.

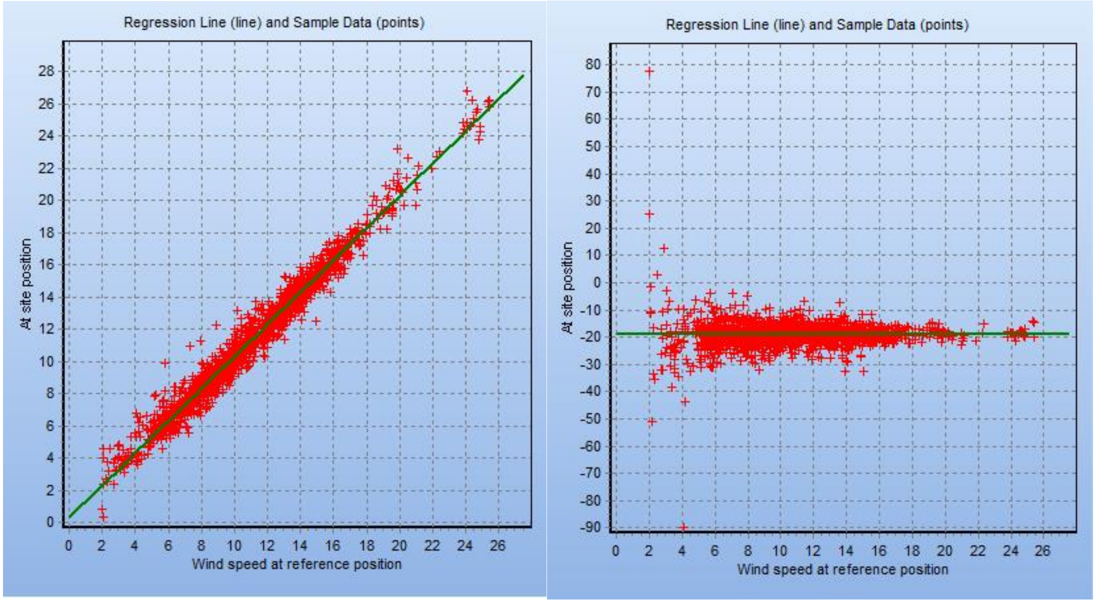

Figure 91. Correlation of wind speed (left) and wind veer (right) for an offshore direction, sector 230°.

Comparing onshore and offshore sectors, the wind direction has better correlation in offshore sectors (less std. dev.), while for onshore sectors it is clear the effect of mainland roughness with lower wind speeds and higher std. dev.

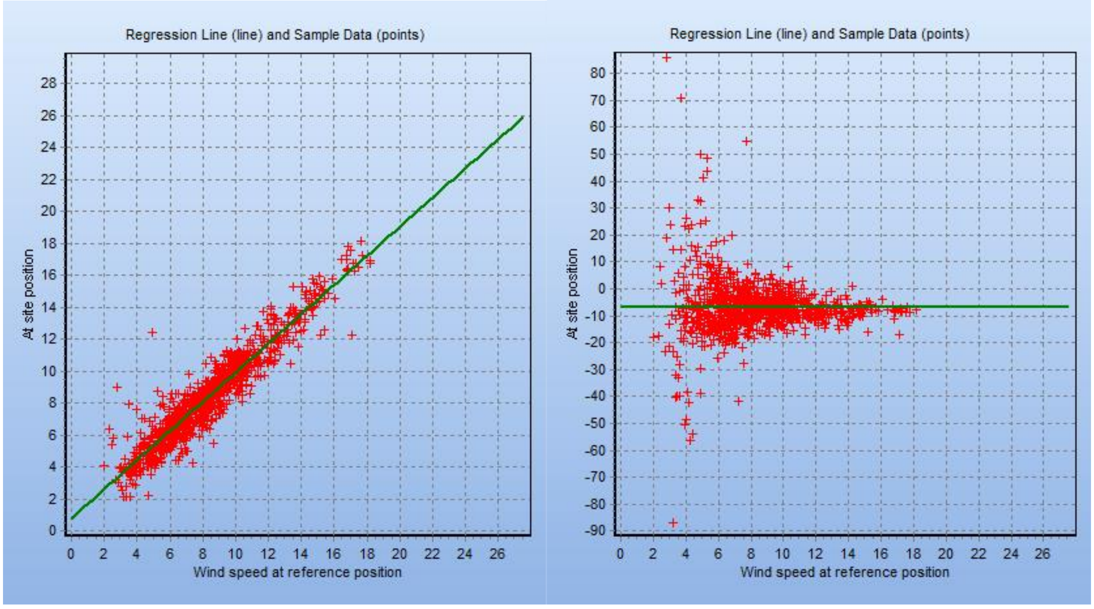

Figure 92. Correlation of wind speed (left) and wind veer (right) for wake direction 100º (4.8D distance).

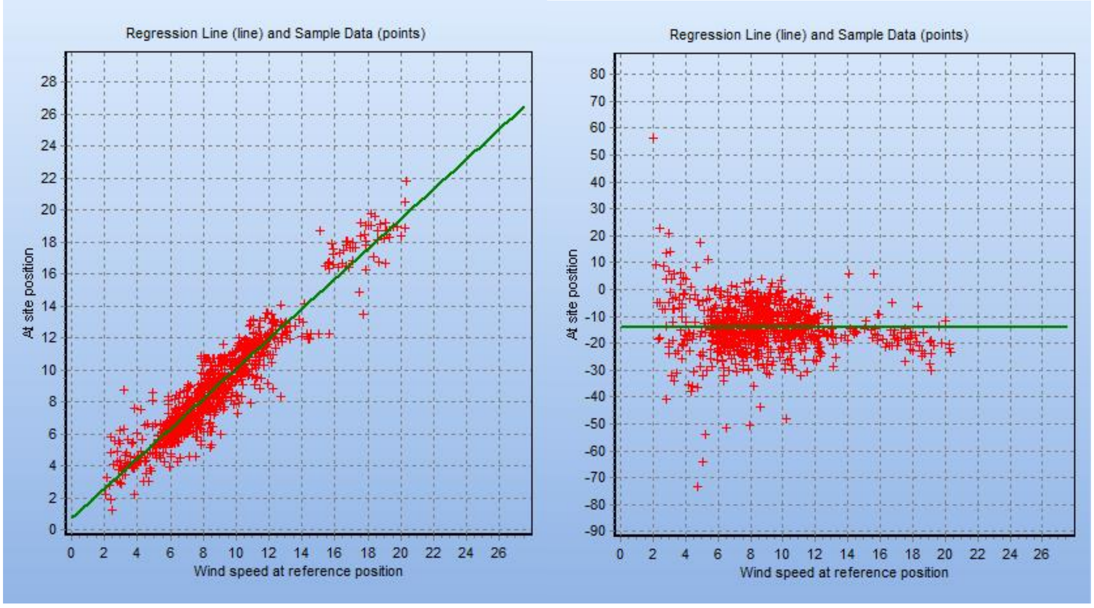

Figure 93. Correlation of wind speed (left) and wind veer (right) for wake direction 300º (5.4D distance).

Sectors wake-affected show also a very good correlation agreement. Their std. dev. is also larger than for free-wind offshore sectors.

Residuals are also plotted in MCP module and the results follow the same description for all sectors: there is no pattern, they are randomly distributed around zero.

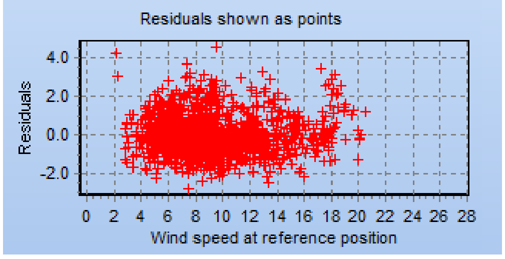

Annex V – Modifying the Q1 file

WindSim Q1 file is located in the root folder WindSim/bin/Phoenics. To set an input value of Turbulent Kinetic Energy (KE) as an initial value for the boundary conditions the parameter KEIN is modified.

Line 64: KEIN = 0.1323

The substitution above will force an initial value of KE to 0.1323. However, after one iteration the initial value will have evolved and the solution the CFD solver will converge to will move away from that inputted value.

To force the KE value remain the same during iterations a fix value has to be inputted in lines 703 and 710:

Line 703: VALUE (IN1, KE, 0.1323)
Line 710: VALUE (IN2, KE, 0.1323)

Replacing the GRND function for the desired value the KE value at the boundary remains constant though iterations.

It is also possible to force a constant wind speed vertical profile as a boundary condition by modifying the GRBET parameter from line 76:

GRBET = 1 —force constant vertical wind profile (unrealistic)
GRBET = 2 —initialize wind profile from log wind profile

When GRBET is set to 1 (force constant wind profile) the value of SPEED can be inputted in the Q1 file (line 60), otherwise the SPEED value is always read from WindSim user interface.

Annex VI – Results analytical models: Case 270º with 7D spacing.

Wind speed: 6 m/s

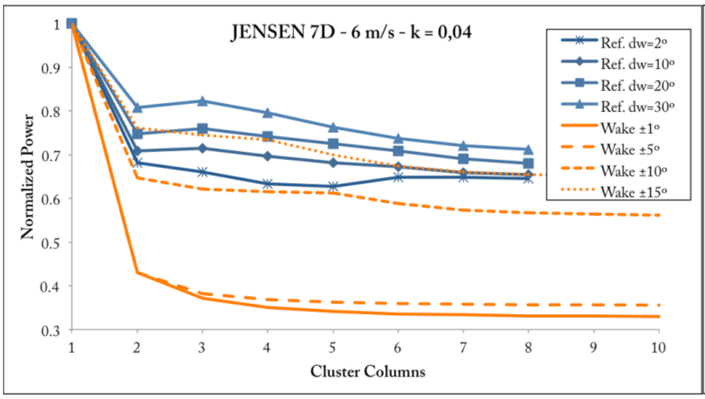

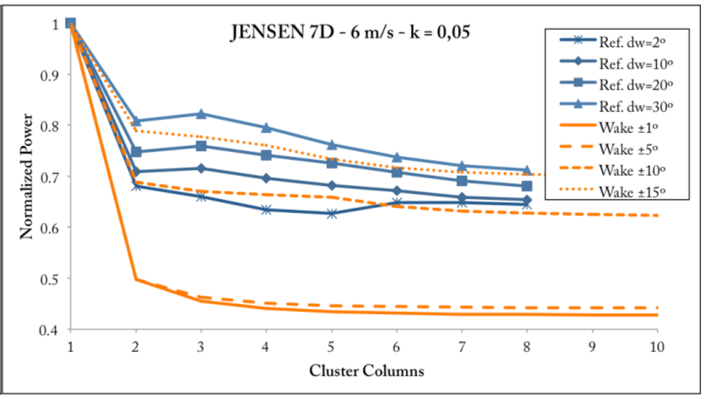

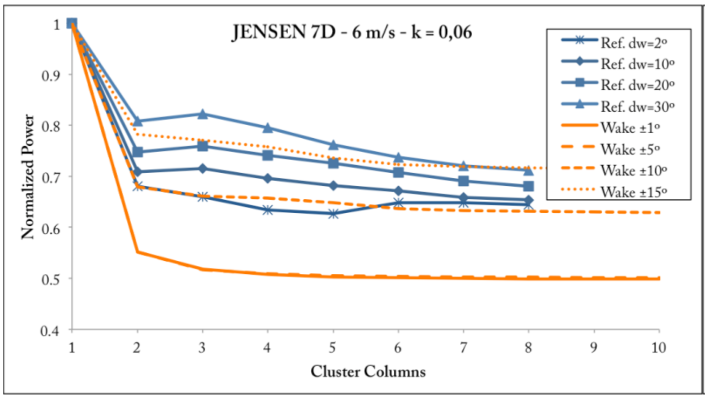

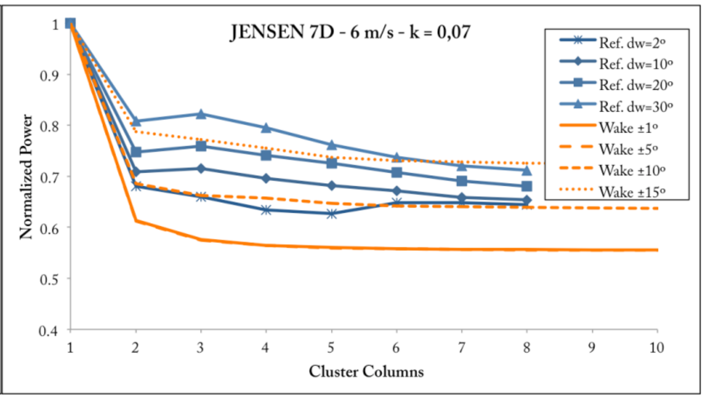

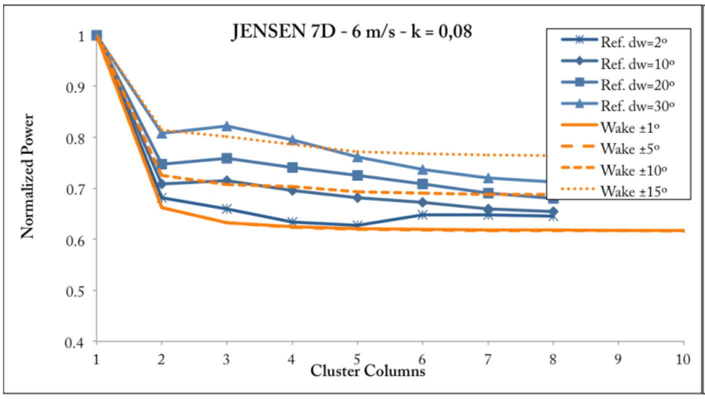

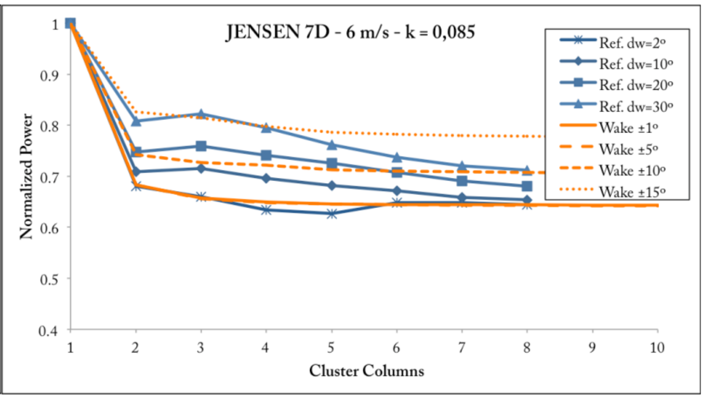

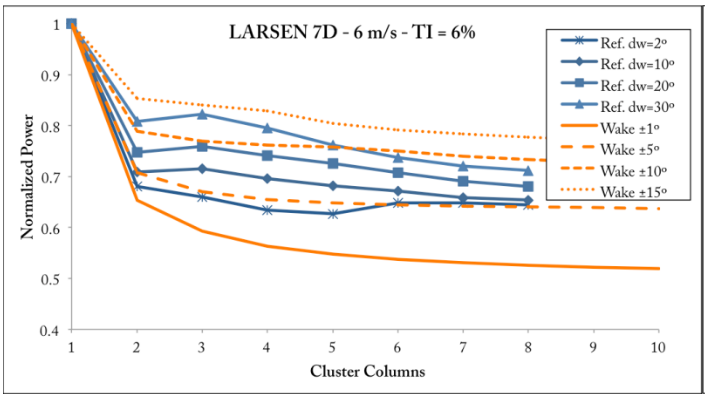

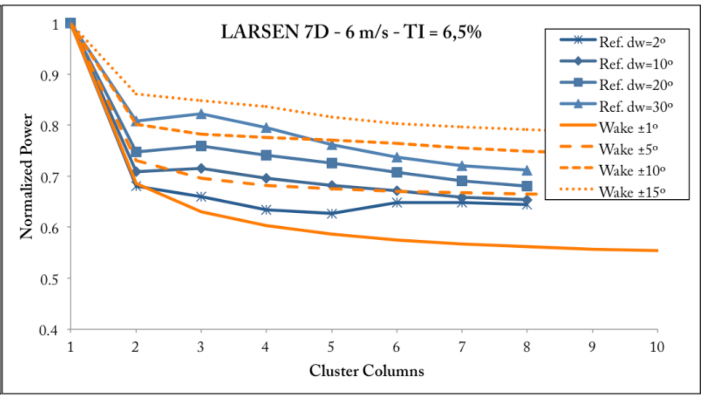

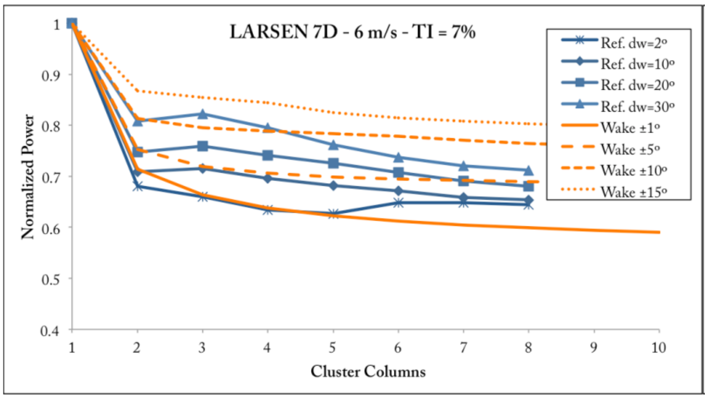
LARSEN 7D - 6 m/s - TI = 7%
Normalized Power
Cluster Columns
1
0.9
0.8
0.7
0.6
0.5
0.4
1 2 3 4 5 6 7 8 9 10
Ref. dw=2º
Ref. dw=10º
Ref. dw=20º
Ref. dw=30º
Wake ±1º
Wake ±5º
Wake ±10º
Wake ±15º

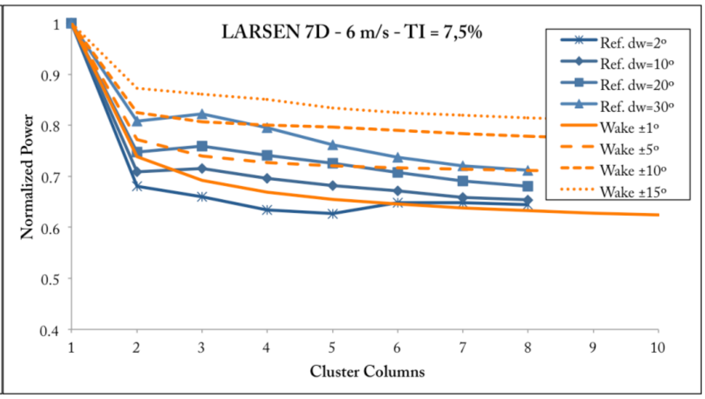
LARSEN 7D - 6 m/s - TI = 7,5%
Normalized Power
Cluster Columns
1
0.9
0.8
0.7
0.6
0.5
0.4
1 2 3 4 5 6 7 8 9 10
Ref. dw=2º
Ref. dw=10º
Ref. dw=20º
Ref. dw=30º
Wake ±1º
Wake ±5º
Wake ±10º
Wake ±15º

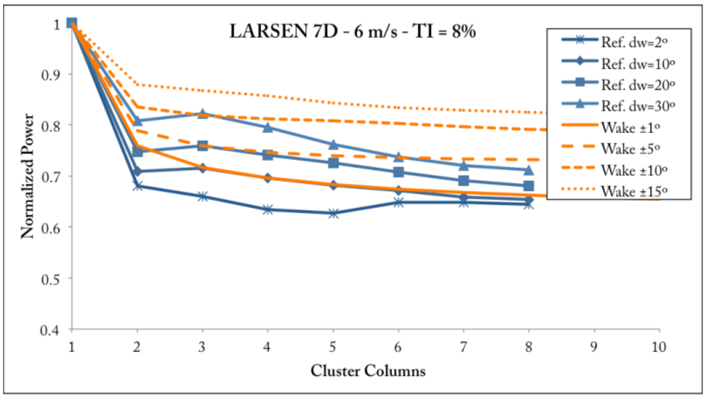
LARSEN 7D - 6 m/s - TI = 8%
Normalized Power
Cluster Columns
1
0.9
0.8
0.7
0.6
0.5
0.4
1 2 3 4 5 6 7 8 9 10
Ref. dw=2º
Ref. dw=10º
Ref. dw=20º
Ref. dw=30º
Wake ±1º
Wake ±5º
Wake ±10º
Wake ±15º

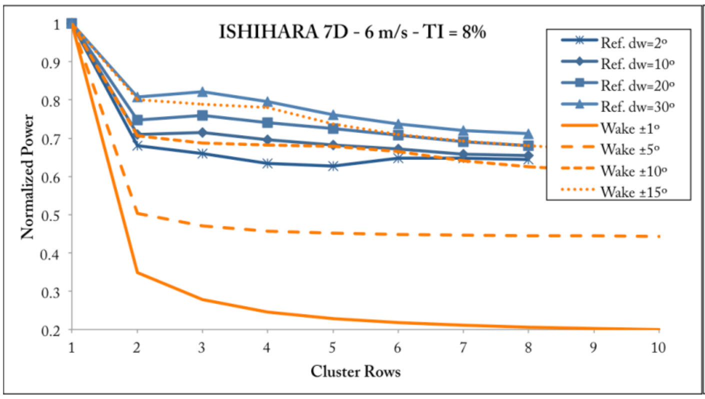
ISHIHARA 7D - 6 m/s - TI = 8%
Normalized Power
Cluster Rows
1
0.9
0.8
0.7
0.6
0.5
0.4
0.3
0.2
1 2 3 4 5 6 7 8 9 10
Ref. dw=2º
Ref. dw=10º
Ref. dw=20º
Ref. dw=30º
Wake ±1º
Wake ±5º
Wake ±10º
Wake ±15º

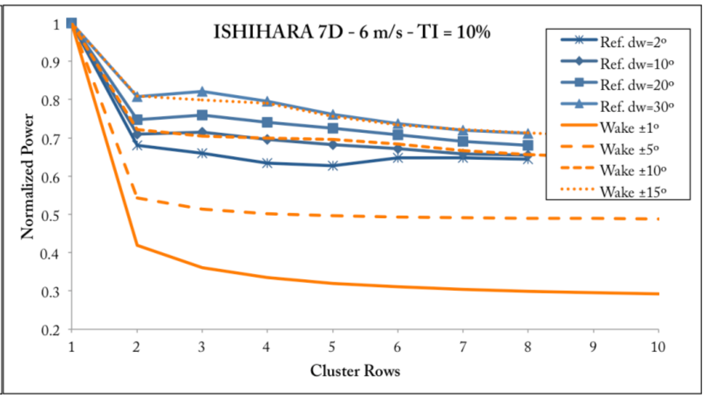
ISHIHARA 7D - 6 m/s - TI = 10%
Normalized Power
Cluster Rows
1
0.9
0.8
0.7
0.6
0.5
0.4
0.3
0.2
1 2 3 4 5 6 7 8 9 10
Ref. dw=2º
Ref. dw=10º
Ref. dw=20º
Ref. dw=30º
Wake ±1º
Wake ±5º
Wake ±10º
Wake ±15º

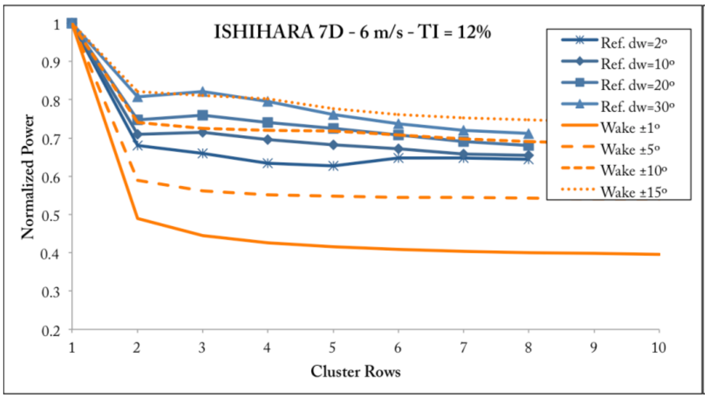
ISHIHARA 7D - 6 m/s - TI = 12%
Normalized Power
Cluster Rows
1
0.9
0.8
0.7
0.6
0.5
0.4
0.3
0.2
1 2 3 4 5 6 7 8 9 10
Ref. dw=2º
Ref. dw=10º
Ref. dw=20º
Ref. dw=30º
Wake ±1º
Wake ±5º
Wake ±10º
Wake ±15º

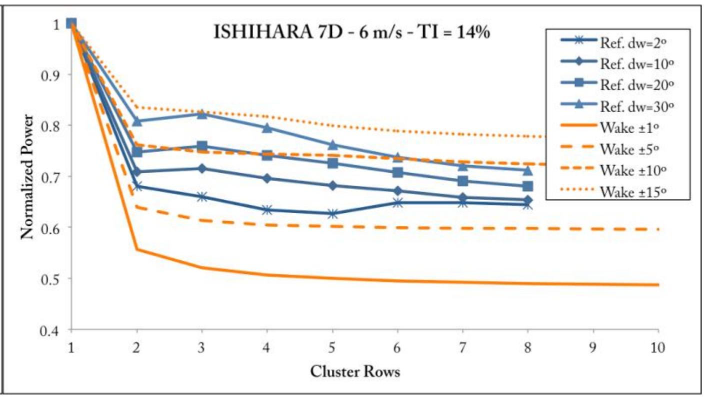
ISHIHARA 7D - 6 m/s - TI = 14%
Normalized Power
Cluster Rows
1
0.9
0.8
0.7
0.6
0.5
0.4
1 2 3 4 5 6 7 8 9 10
Ref. dw=2º
Ref. dw=10º
Ref. dw=20º
Ref. dw=30º
Wake ±1º
Wake ±5º
Wake ±10º
Wake ±15º

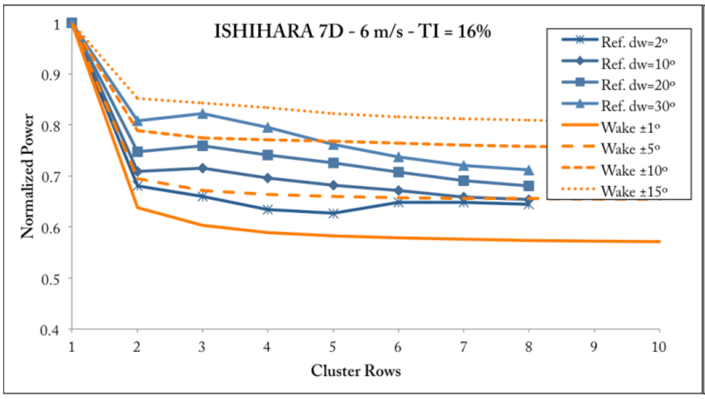

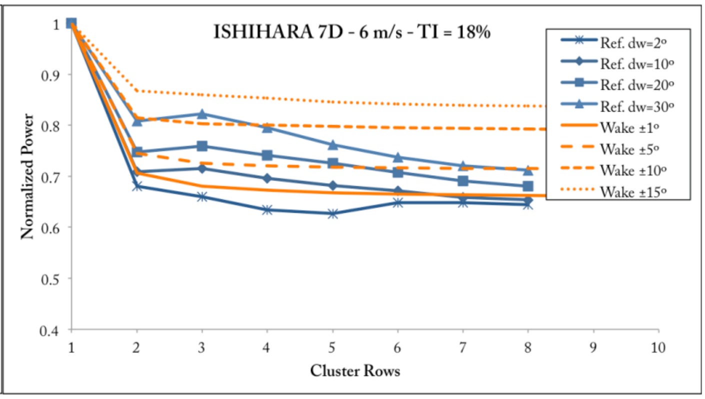

Wind speed: 8 m/s

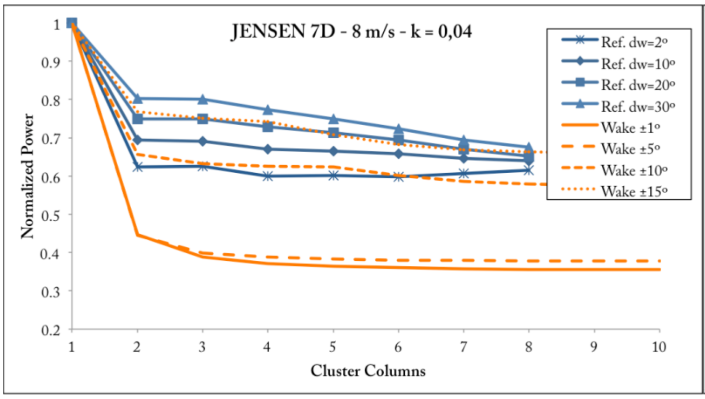

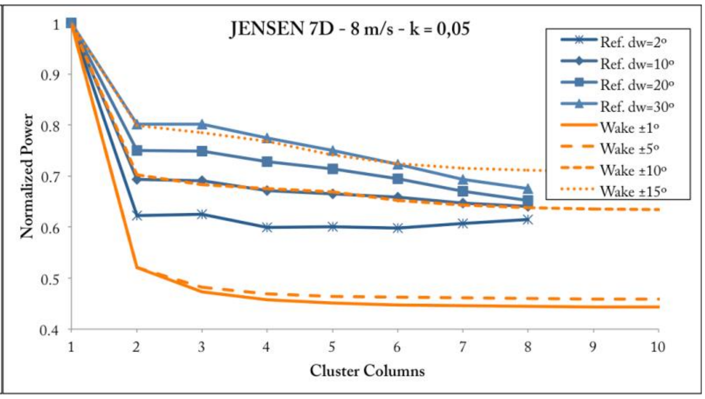

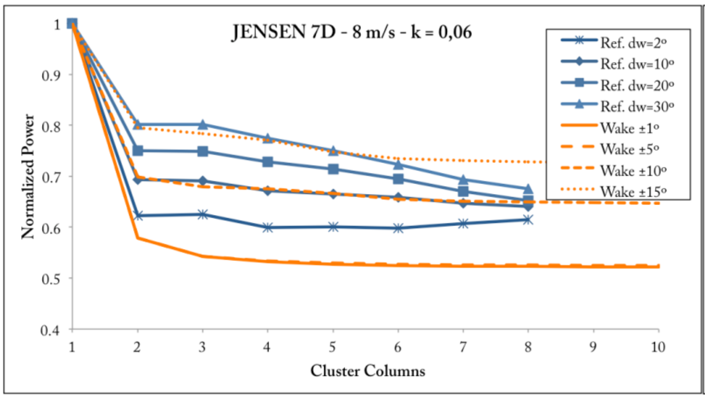

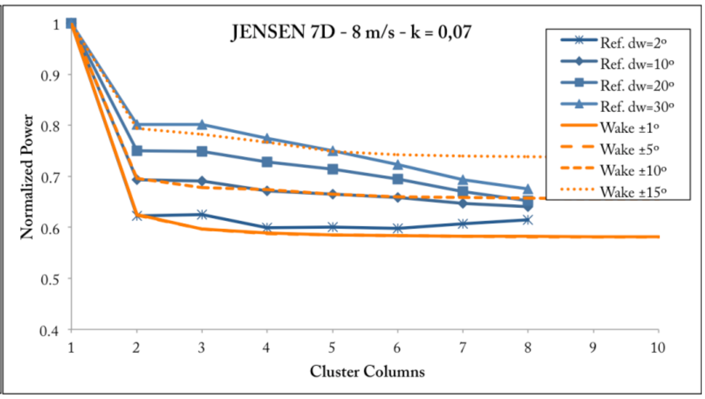

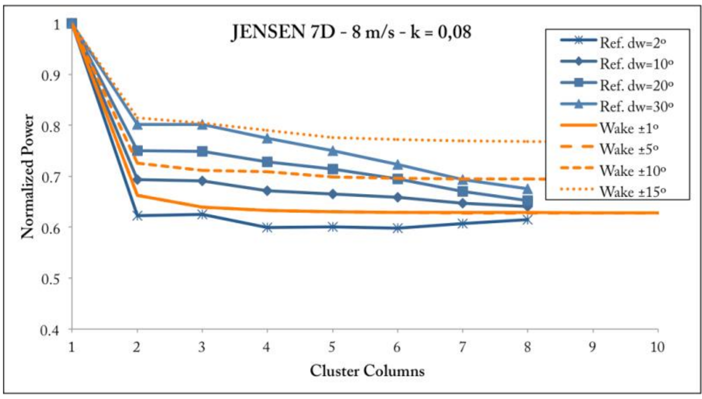

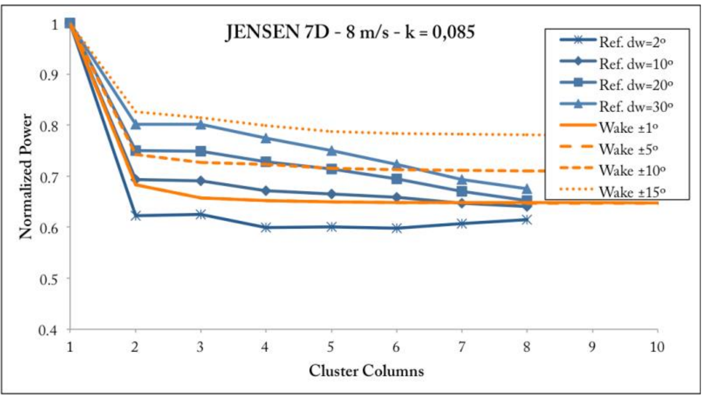

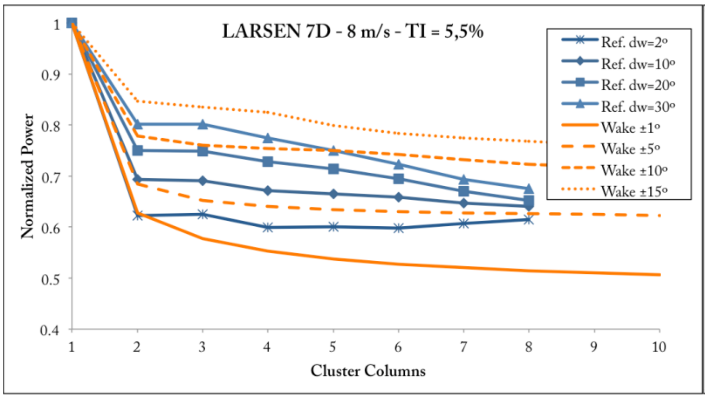
LARSEN 7D - 8 m/s - TI = 5,5%
Normalized Power
1
0.9
0.8
0.7
0.6
0.5
0.4
1 2 3 4 5 6 7 8 9 10
Cluster Columns
Ref. dw=2º
Ref. dw=10º
Ref. dw=20º
Ref. dw=30º
Wake ±1º
Wake ±5º
Wake ±10º
Wake ±15º

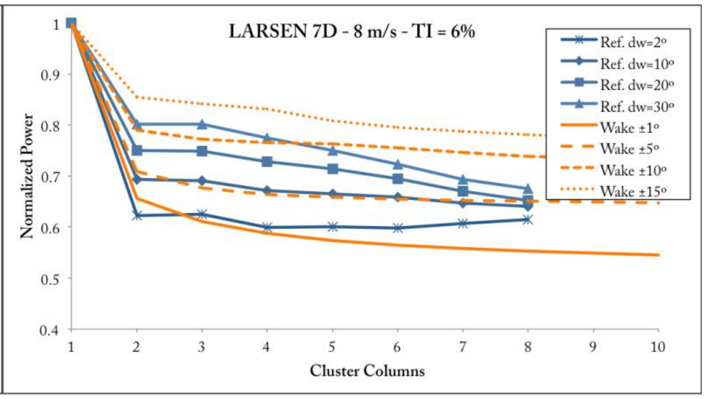
LARSEN 7D - 8 m/s - TI = 6%
Normalized Power
1
0.9
0.8
0.7
0.6
0.5
0.4
1 2 3 4 5 6 7 8 9 10
Cluster Columns
Ref. dw=2º
Ref. dw=10º
Ref. dw=20º
Ref. dw=30º
Wake ±1º
Wake ±5º
Wake ±10º
Wake ±15º

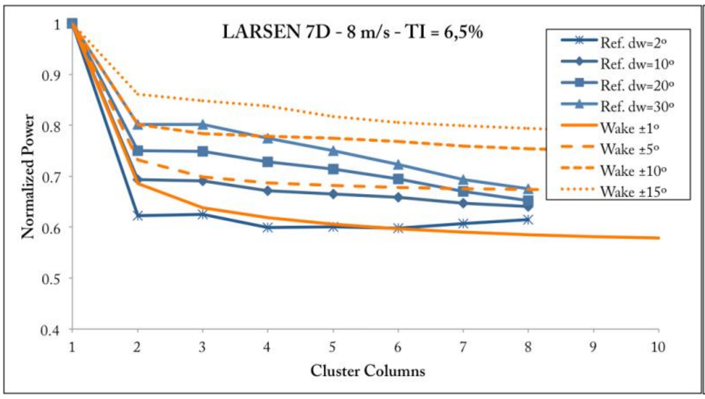
LARSEN 7D - 8 m/s - TI = 6,5%
Normalized Power
1
0.9
0.8
0.7
0.6
0.5
0.4
1 2 3 4 5 6 7 8 9 10
Cluster Columns
Ref. dw=2º
Ref. dw=10º
Ref. dw=20º
Ref. dw=30º
Wake ±1º
Wake ±5º
Wake ±10º
Wake ±15º

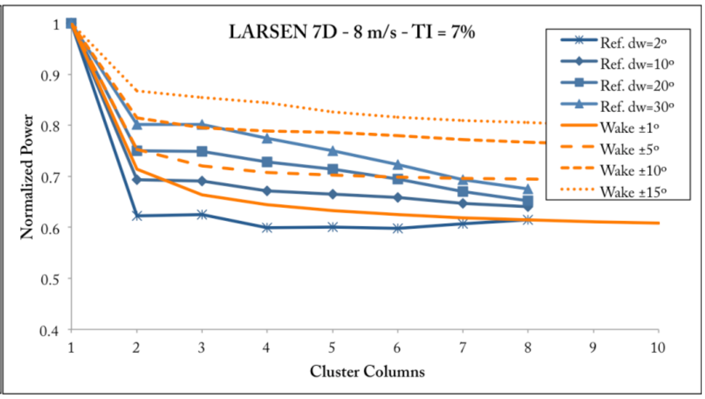
LARSEN 7D - 8 m/s - TI = 7%
Normalized Power
1
0.9
0.8
0.7
0.6
0.5
0.4
1 2 3 4 5 6 7 8 9 10
Cluster Columns
Ref. dw=2º
Ref. dw=10º
Ref. dw=20º
Ref. dw=30º
Wake ±1º
Wake ±5º
Wake ±10º
Wake ±15º

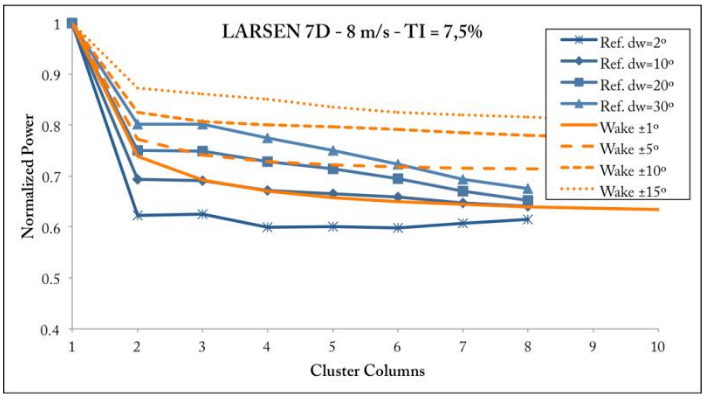
LARSEN 7D - 8 m/s - TI = 7,5%
Normalized Power
1
0.9
0.8
0.7
0.6
0.5
0.4
1 2 3 4 5 6 7 8 9 10
Cluster Columns
Ref. dw=2º
Ref. dw=10º
Ref. dw=20º
Ref. dw=30º
Wake ±1º
Wake ±5º
Wake ±10º
Wake ±15º

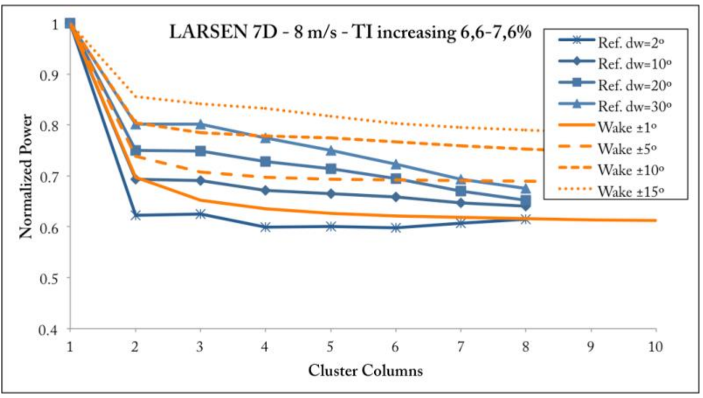
LARSEN 7D - 8 m/s - TI increasing 6,6-7,6%
Normalized Power
1
0.9
0.8
0.7
0.6
0.5
0.4
1 2 3 4 5 6 7 8 9 10
Cluster Columns
Ref. dw=2º
Ref. dw=10º
Ref. dw=20º
Ref. dw=30º
Wake ±1º
Wake ±5º
Wake ±10º
Wake ±15º

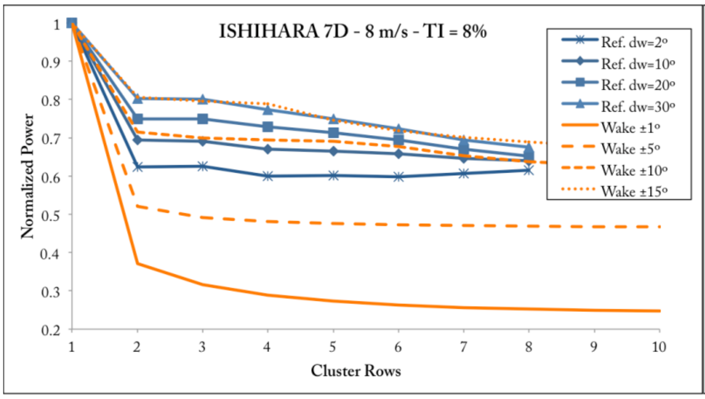
ISHIHARA 7D - 8 m/s - TI = 8%
Normalized Power
1
0.9
0.8
0.7
0.6
0.5
0.4
0.3
0.2
1 2 3 4 5 6 7 8 9 10
Cluster Rows
Ref. dw=2º
Ref. dw=10º
Ref. dw=20º
Ref. dw=30º
Wake ±1º
Wake ±5º
Wake ±10º
Wake ±15º

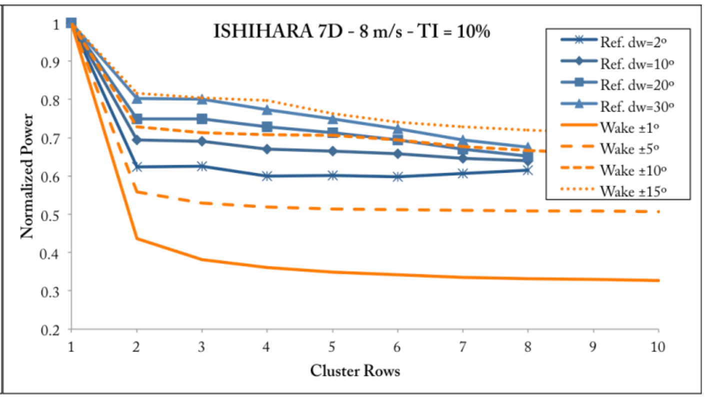
ISHIHARA 7D - 8 m/s - TI = 10%
Normalized Power
1
0.9
0.8
0.7
0.6
0.5
0.4
0.3
0.2
1 2 3 4 5 6 7 8 9 10
Cluster Rows
Ref. dw=2º
Ref. dw=10º
Ref. dw=20º
Ref. dw=30º
Wake ±1º
Wake ±5º
Wake ±10º
Wake ±15º

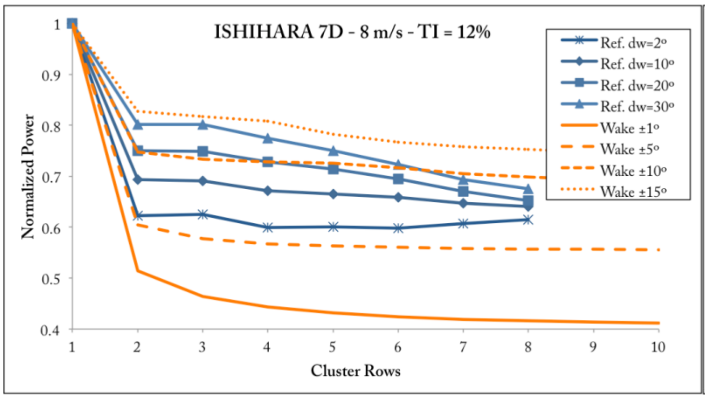

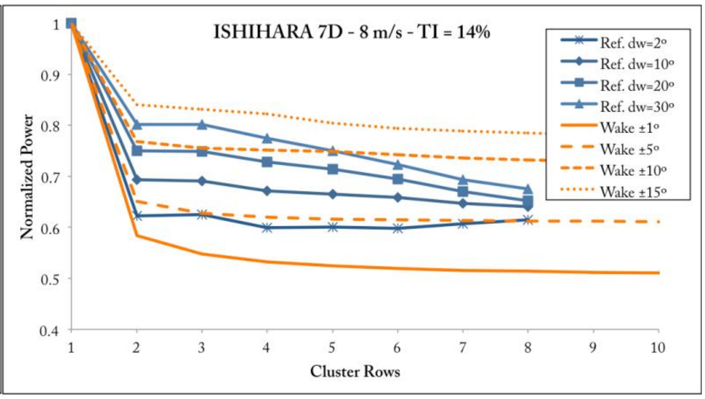

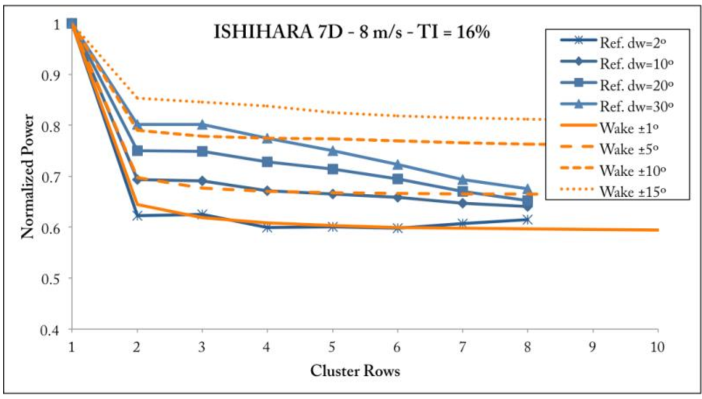

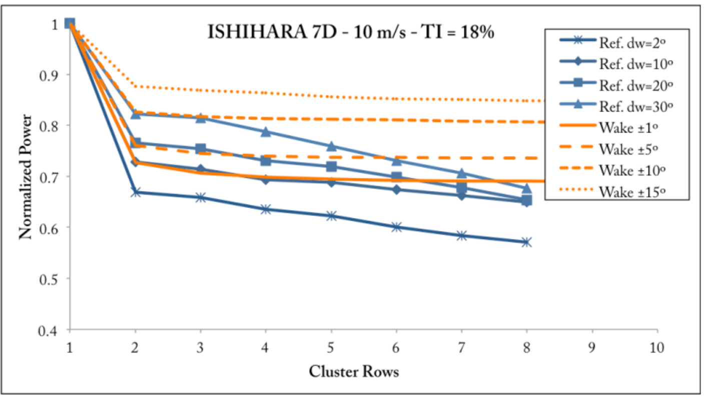

Wind speed: 10 m/s

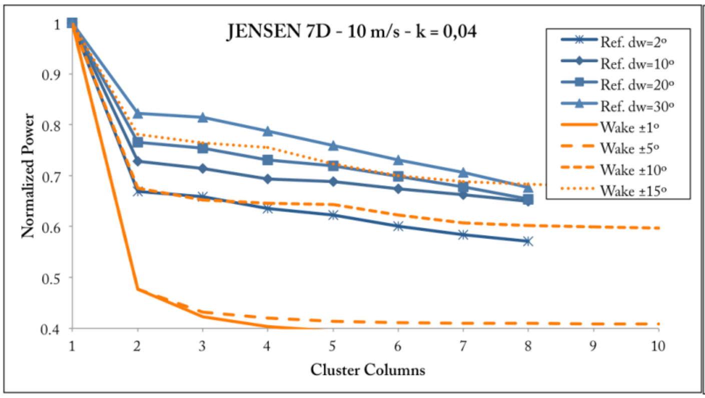

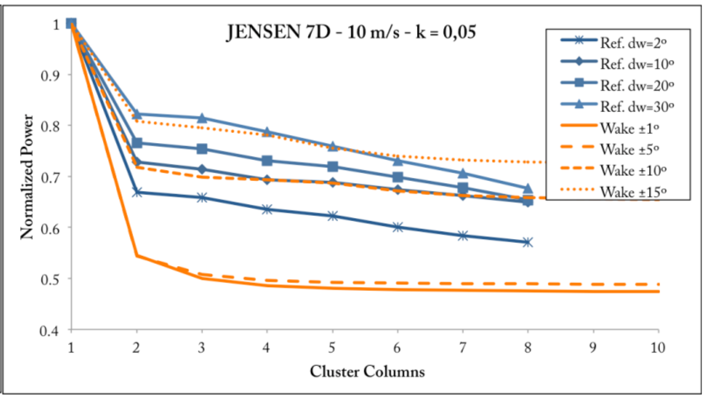

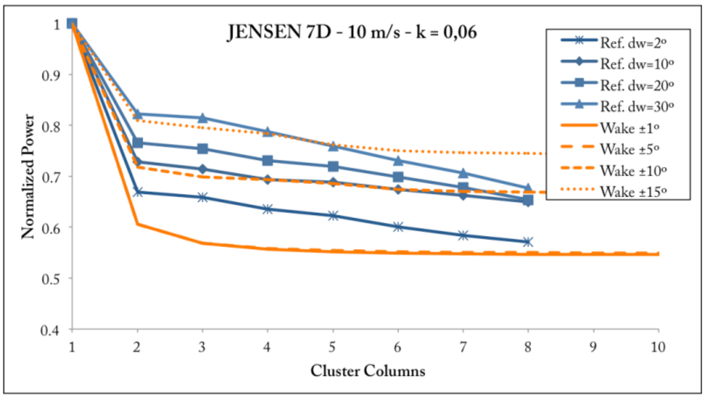

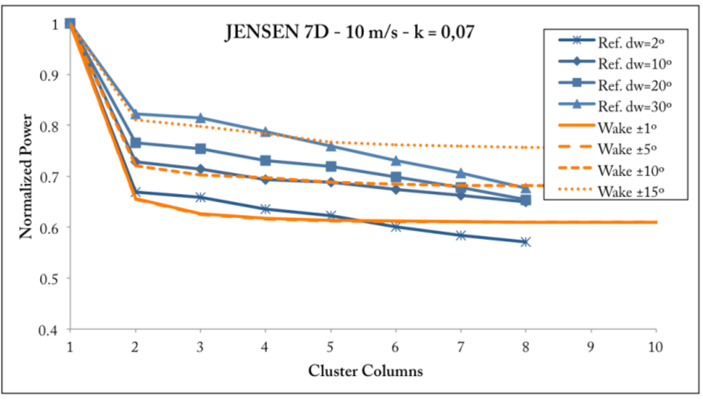

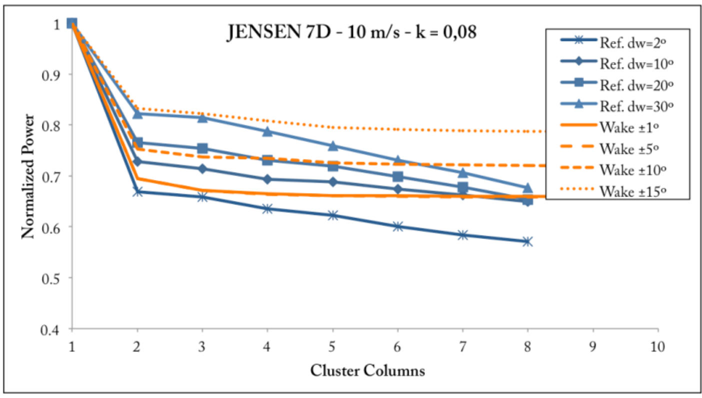
JENSEN 7D - 10 m/s - k = 0,08
Normalized Power
1
0.9
0.8
0.7
0.6
0.5
0.4
1 2 3 4 5 6 7 8 9 10
Cluster Columns
Ref. dw=2º
Ref. dw=10º
Ref. dw=20º
Ref. dw=30º
Wake ±1º
Wake ±5º
Wake ±10º
Wake ±15º

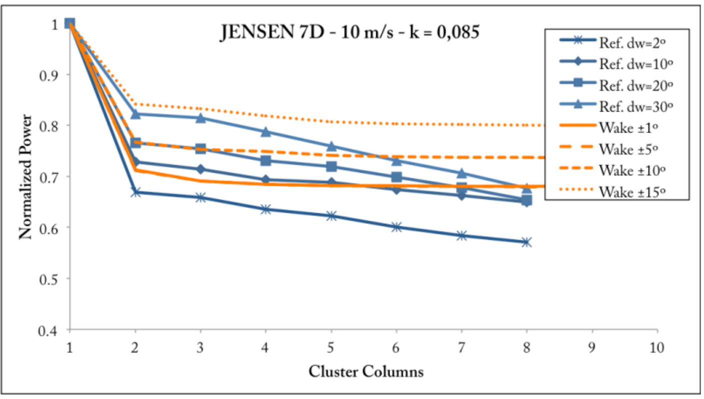
JENSEN 7D - 10 m/s - k = 0,085
Normalized Power
1
0.9
0.8
0.7
0.6
0.5
0.4
1 2 3 4 5 6 7 8 9 10
Cluster Columns
Ref. dw=2º
Ref. dw=10º
Ref. dw=20º
Ref. dw=30º
Wake ±1º
Wake ±5º
Wake ±10º
Wake ±15º

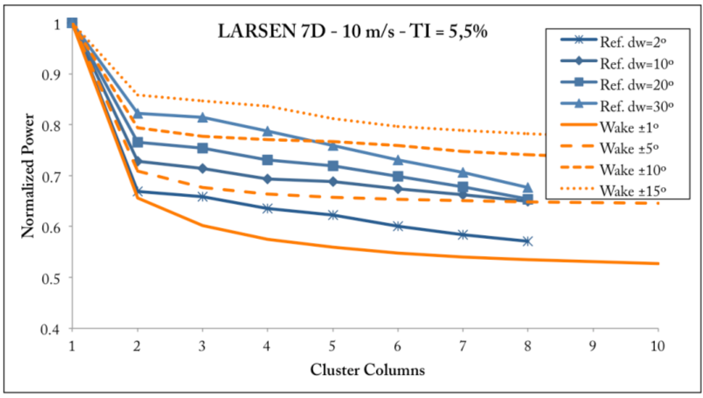
LARSEN 7D - 10 m/s - TI = 5,5%
Normalized Power
1
0.9
0.8
0.7
0.6
0.5
0.4
1 2 3 4 5 6 7 8 9 10
Cluster Columns
Ref. dw=2º
Ref. dw=10º
Ref. dw=20º
Ref. dw=30º
Wake ±1º
Wake ±5º
Wake ±10º
Wake ±15º

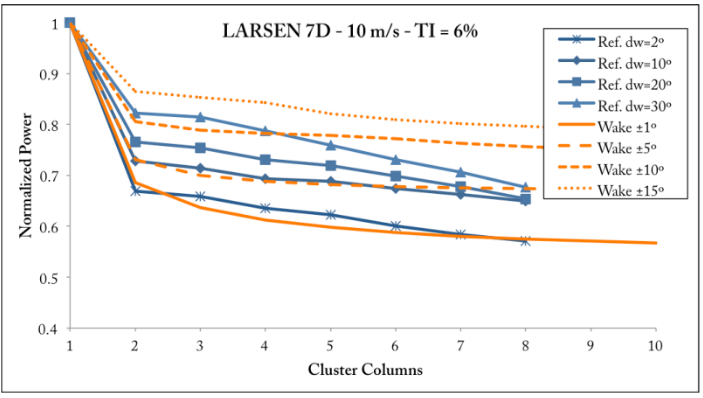
LARSEN 7D - 10 m/s - TI = 6%
Normalized Power
1
0.9
0.8
0.7
0.6
0.5
0.4
1 2 3 4 5 6 7 8 9 10
Cluster Columns
Ref. dw=2º
Ref. dw=10º
Ref. dw=20º
Ref. dw=30º
Wake ±1º
Wake ±5º
Wake ±10º
Wake ±15º

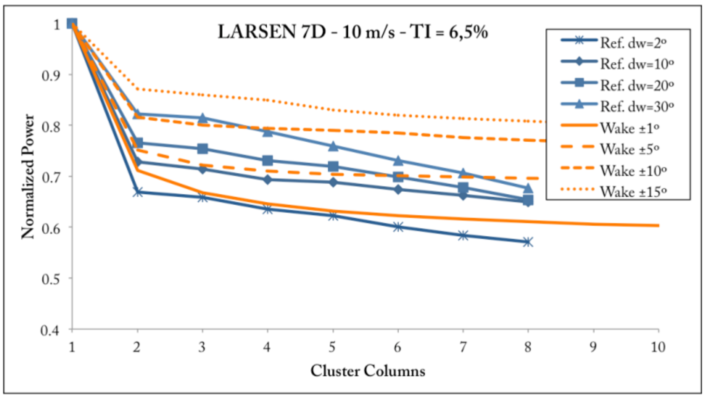
LARSEN 7D - 10 m/s - TI = 6,5%
Normalized Power
1
0.9
0.8
0.7
0.6
0.5
0.4
1 2 3 4 5 6 7 8 9 10
Cluster Columns
Ref. dw=2º
Ref. dw=10º
Ref. dw=20º
Ref. dw=30º
Wake ±1º
Wake ±5º
Wake ±10º
Wake ±15º

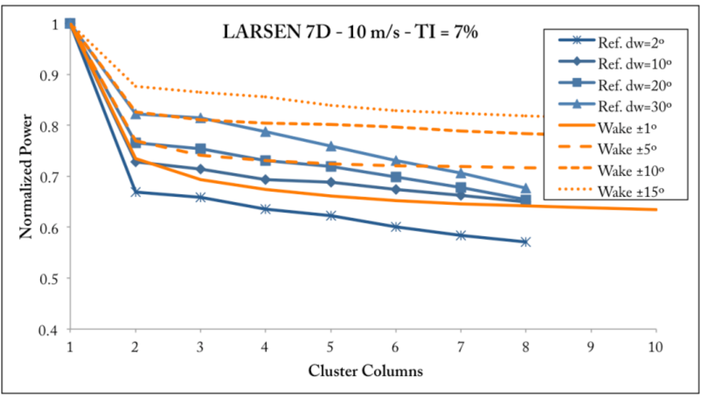
LARSEN 7D - 10 m/s - TI = 7%
Normalized Power
1
0.9
0.8
0.7
0.6
0.5
0.4
1 2 3 4 5 6 7 8 9 10
Cluster Columns
Ref. dw=2º
Ref. dw=10º
Ref. dw=20º
Ref. dw=30º
Wake ±1º
Wake ±5º
Wake ±10º
Wake ±15º

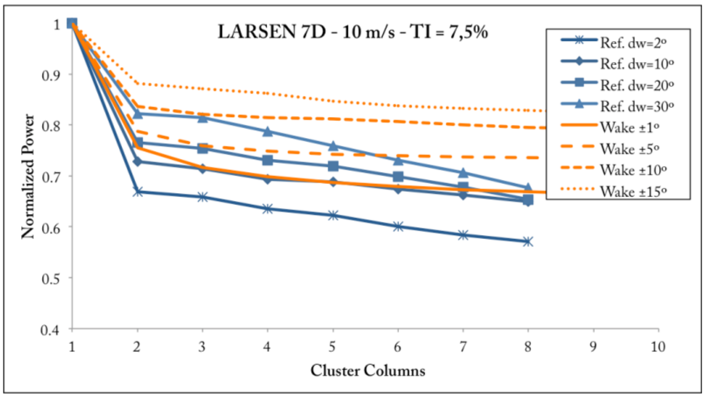
LARSEN 7D - 10 m/s - TI = 7,5%
Normalized Power
1
0.9
0.8
0.7
0.6
0.5
0.4
1 2 3 4 5 6 7 8 9 10
Cluster Columns
Ref. dw=2º
Ref. dw=10º
Ref. dw=20º
Ref. dw=30º
Wake ±1º
Wake ±5º
Wake ±10º
Wake ±15º

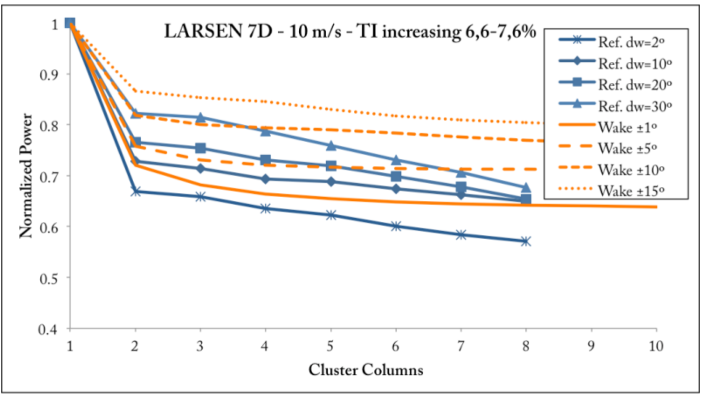
LARSEN 7D - 10 m/s - TI increasing 6,6-7,6%
Normalized Power
1
0.9
0.8
0.7
0.6
0.5
0.4
1 2 3 4 5 6 7 8 9 10
Cluster Columns
Ref. dw=2º
Ref. dw=10º
Ref. dw=20º
Ref. dw=30º
Wake ±1º
Wake ±5º
Wake ±10º
Wake ±15º

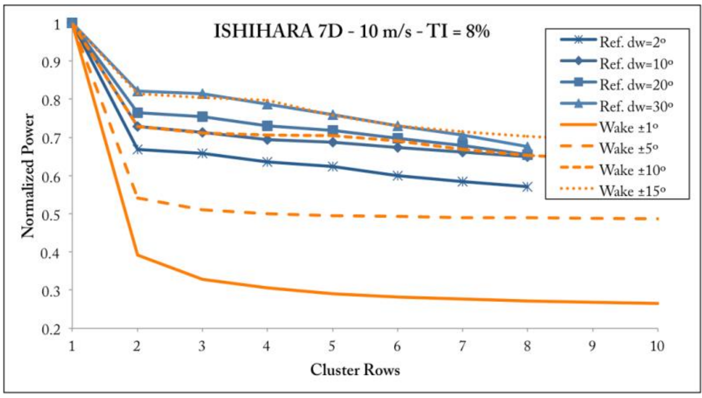
ISHIHARA 7D - 10 m/s - TI = 8%
Normalized Power
Cluster Rows
1
0.9
0.8
0.7
0.6
0.5
0.4
0.3
0.2
1 2 3 4 5 6 7 8 9 10
Ref. dw=2º
Ref. dw=10º
Ref. dw=20º
Ref. dw=30º
Wake ±1º
Wake ±5º
Wake ±10º
Wake ±15º

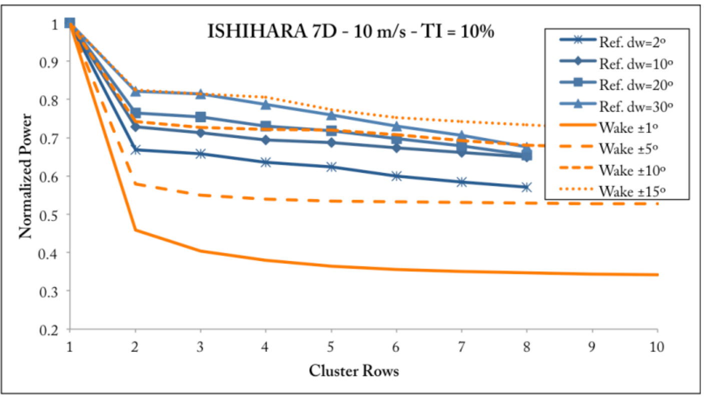
ISHIHARA 7D - 10 m/s - TI = 10%
Normalized Power
Cluster Rows
1
0.9
0.8
0.7
0.6
0.5
0.4
0.3
0.2
1 2 3 4 5 6 7 8 9 10
Ref. dw=2º
Ref. dw=10º
Ref. dw=20º
Ref. dw=30º
Wake ±1º
Wake ±5º
Wake ±10º
Wake ±15º

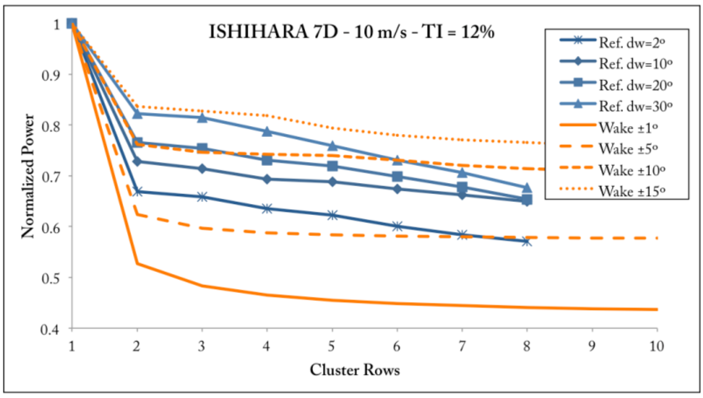
ISHIHARA 7D - 10 m/s - TI = 12%
Normalized Power
Cluster Rows
1
0.9
0.8
0.7
0.6
0.5
0.4
1 2 3 4 5 6 7 8 9 10
Ref. dw=2º
Ref. dw=10º
Ref. dw=20º
Ref. dw=30º
Wake ±1º
Wake ±5º
Wake ±10º
Wake ±15º

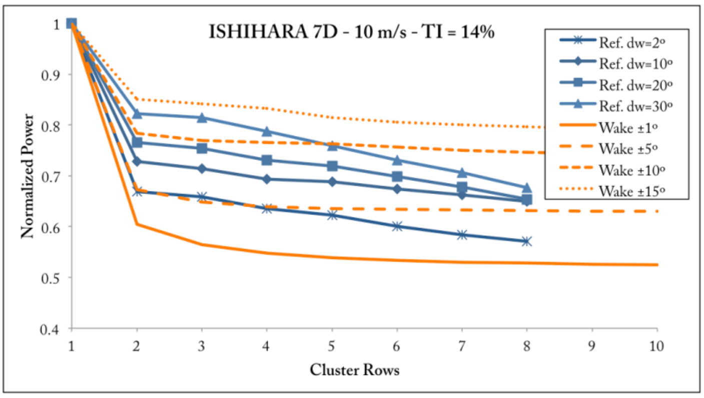
ISHIHARA 7D - 10 m/s - TI = 14%
Normalized Power
Cluster Rows
1
0.9
0.8
0.7
0.6
0.5
0.4
1 2 3 4 5 6 7 8 9 10
Ref. dw=2º
Ref. dw=10º
Ref. dw=20º
Ref. dw=30º
Wake ±1º
Wake ±5º
Wake ±10º
Wake ±15º

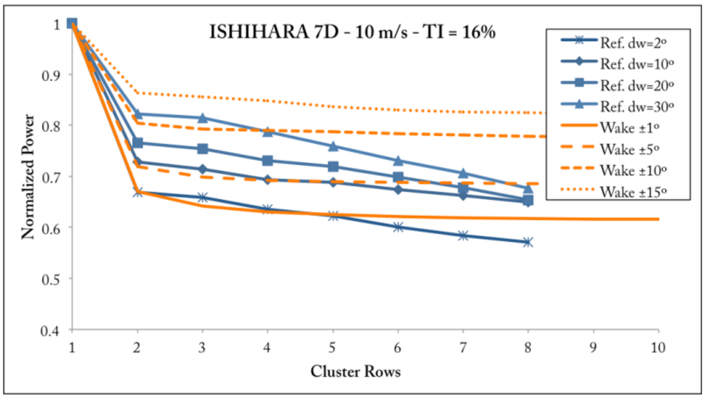
ISHIHARA 7D - 10 m/s - TI = 16%
Normalized Power
Cluster Rows
1
0.9
0.8
0.7
0.6
0.5
0.4
1 2 3 4 5 6 7 8 9 10
Ref. dw=2º
Ref. dw=10º
Ref. dw=20º
Ref. dw=30º
Wake ±1º
Wake ±5º
Wake ±10º
Wake ±15º

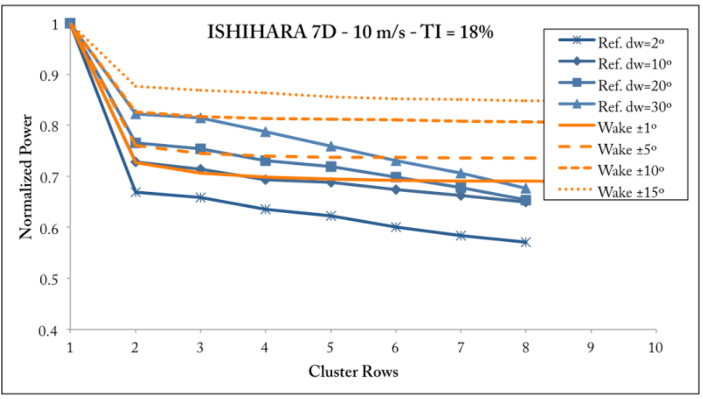
ISHIHARA 7D - 10 m/s - TI = 18%
Normalized Power
Cluster Rows
1
0.9
0.8
0.7
0.6
0.5
0.4
1 2 3 4 5 6 7 8 9 10
Ref. dw=2º
Ref. dw=10º
Ref. dw=20º
Ref. dw=30º
Wake ±1º
Wake ±5º
Wake ±10º
Wake ±15º

Annex VII – Results analytical models: Case 221º with 9,4D spacing.

Wind speed: 6 m/s

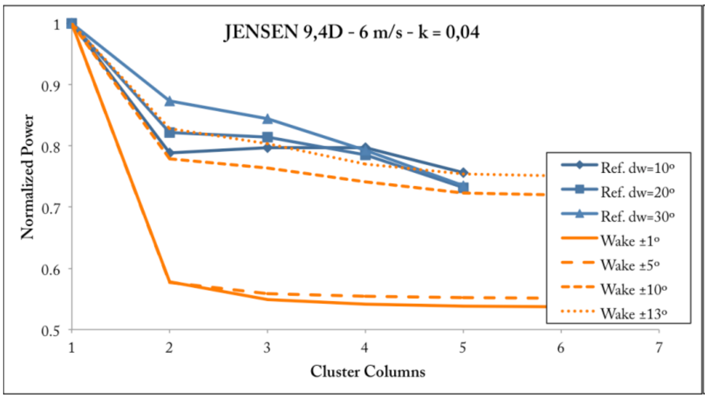
JENSEN 9,4D - 6 m/s - k = 0,04

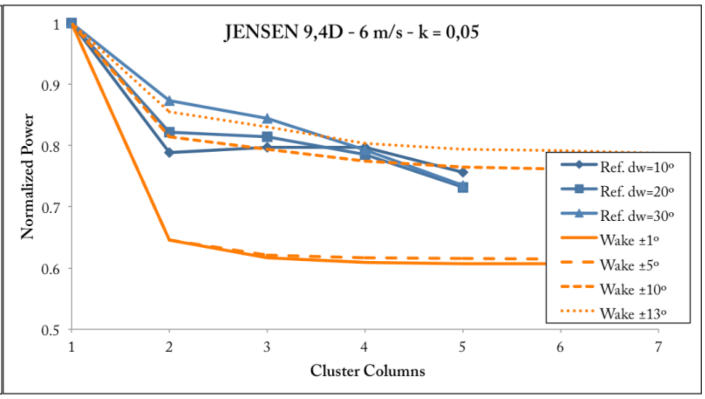
JENSEN 9,4D - 6 m/s - k = 0,05

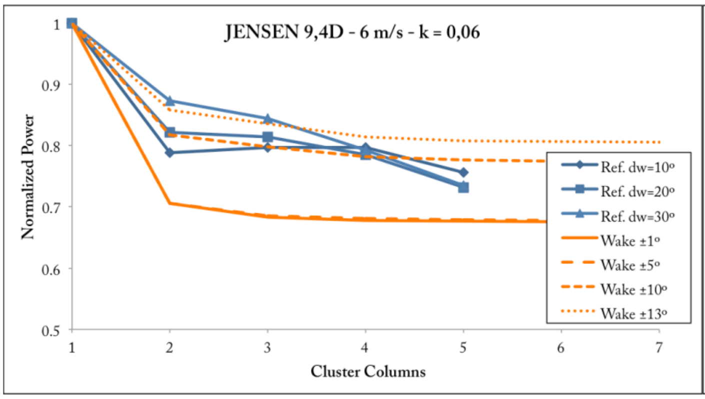
JENSEN 9,4D - 6 m/s - k = 0,06

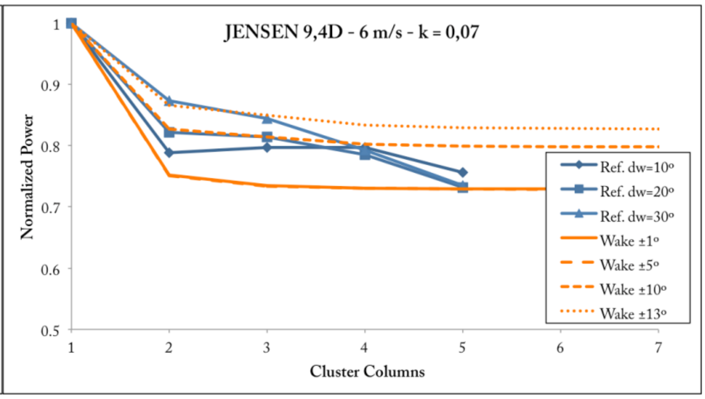
JENSEN 9,4D - 6 m/s - k = 0,07

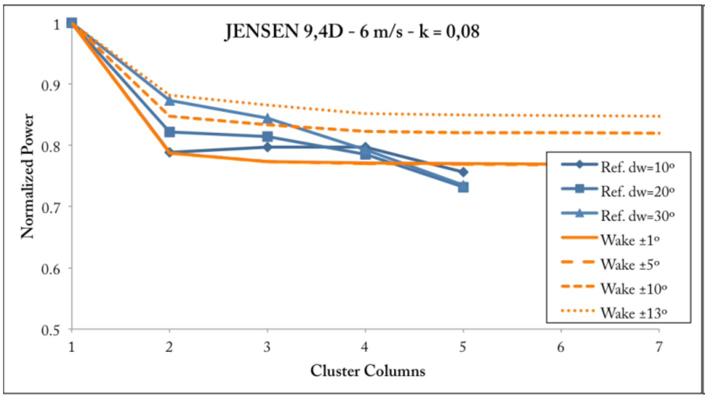
JENSEN 9,4D - 6 m/s - k = 0,08

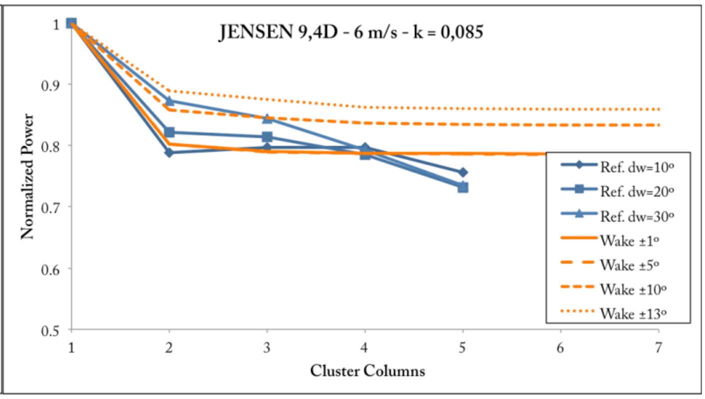
JENSEN 9,4D - 6 m/s - k = 0,085

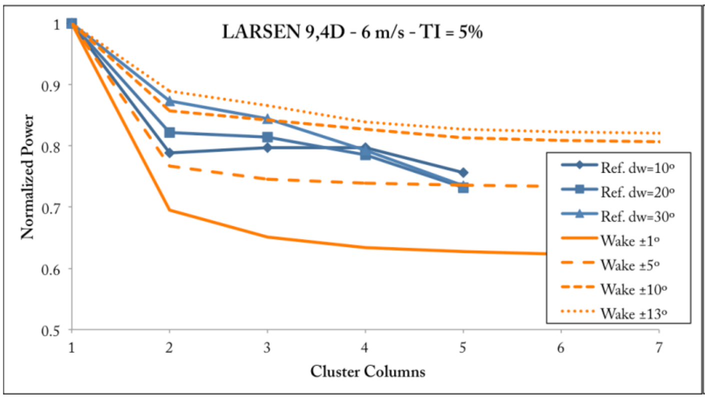
LARSEN 9,4D - 6 m/s - TI = 5%

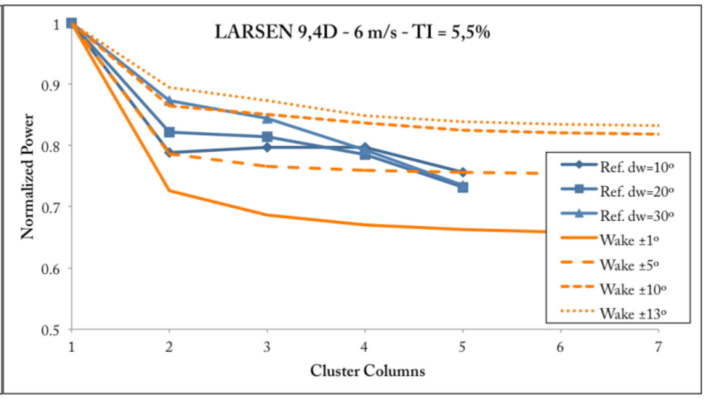
LARSEN 9,4D - 6 m/s - TI = 5,5%

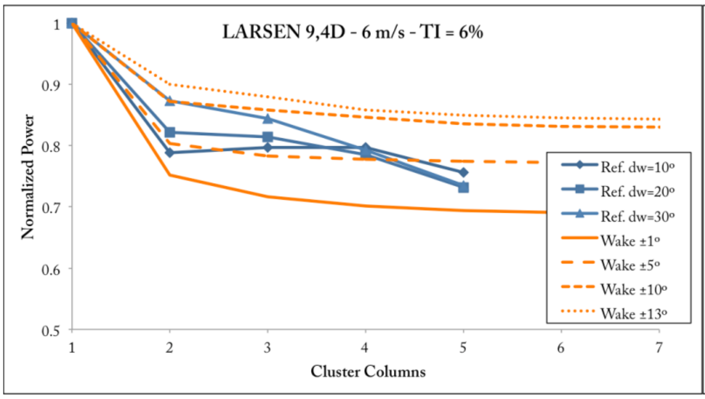
LARSEN 9,4D - 6 m/s - TI = 6%
Normalized Power
1
0.9
0.8
0.7
0.6
0.5
1
2
3
4
5
6
7
Cluster Columns
Ref. dw=10°
Ref. dw=20°
Ref. dw=30°
Wake ±1°
Wake ±5°
Wake ±10°
Wake ±13°

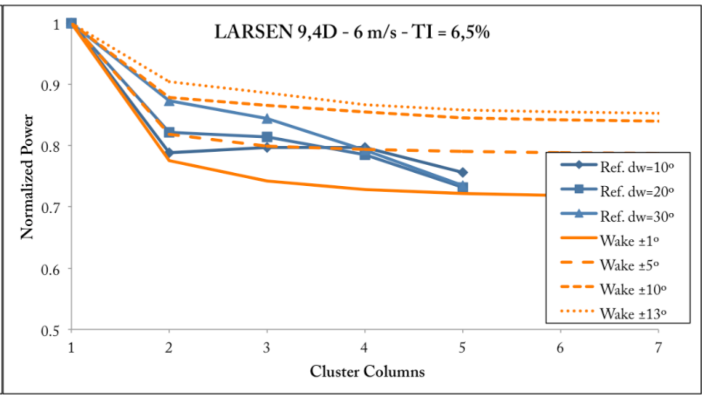
LARSEN 9,4D - 6 m/s - TI = 6,5%
Normalized Power
1
0.9
0.8
0.7
0.6
0.5
1
2
3
4
5
6
7
Cluster Columns
Ref. dw=10°
Ref. dw=20°
Ref. dw=30°
Wake ±1°
Wake ±5°
Wake ±10°
Wake ±13°

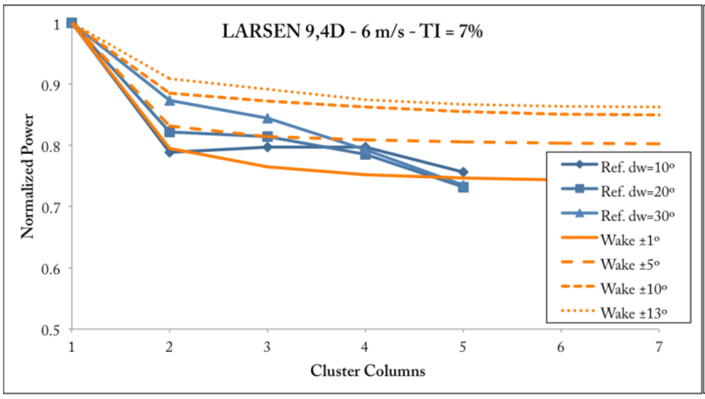
LARSEN 9,4D - 6 m/s - TI = 7%
Normalized Power
1
0.9
0.8
0.7
0.6
0.5
1
2
3
4
5
6
7
Cluster Columns
Ref. dw=10°
Ref. dw=20°
Ref. dw=30°
Wake ±1°
Wake ±5°
Wake ±10°
Wake ±13°

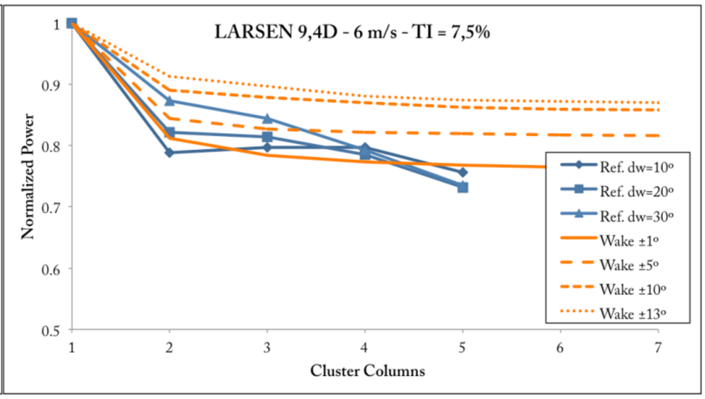
LARSEN 9,4D - 6 m/s - TI = 7,5%
Normalized Power
1
0.9
0.8
0.7
0.6
0.5
1
2
3
4
5
6
7
Cluster Columns
Ref. dw=10°
Ref. dw=20°
Ref. dw=30°
Wake ±1°
Wake ±5°
Wake ±10°
Wake ±13°

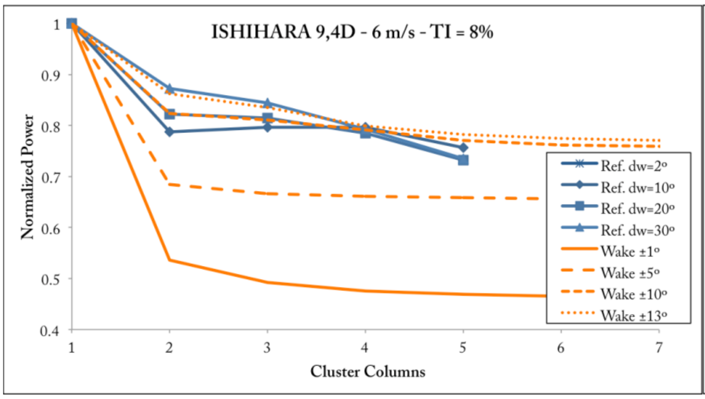
ISHIHARA 9,4D - 6 m/s - TI = 8%
Normalized Power
1
0.9
0.8
0.7
0.6
0.5
0.4
1
2
3
4
5
6
7
Cluster Columns
Ref. dw=2°
Ref. dw=10°
Ref. dw=20°
Ref. dw=30°
Wake ±1°
Wake ±5°
Wake ±10°
Wake ±13°

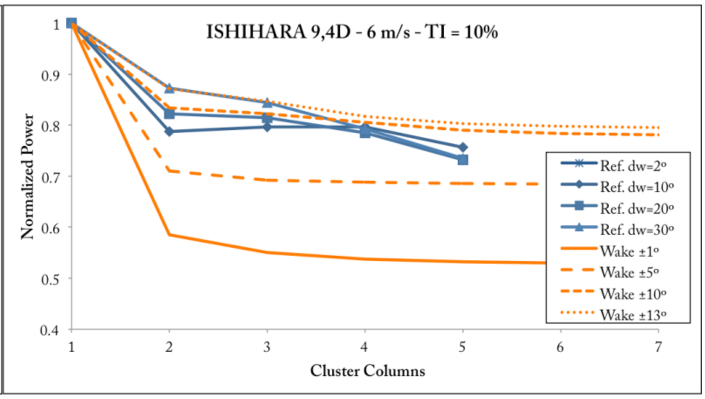
ISHIHARA 9,4D - 6 m/s - TI = 10%
Normalized Power
1
0.9
0.8
0.7
0.6
0.5
0.4
1
2
3
4
5
6
7
Cluster Columns
Ref. dw=2°
Ref. dw=10°
Ref. dw=20°
Ref. dw=30°
Wake ±1°
Wake ±5°
Wake ±10°
Wake ±13°

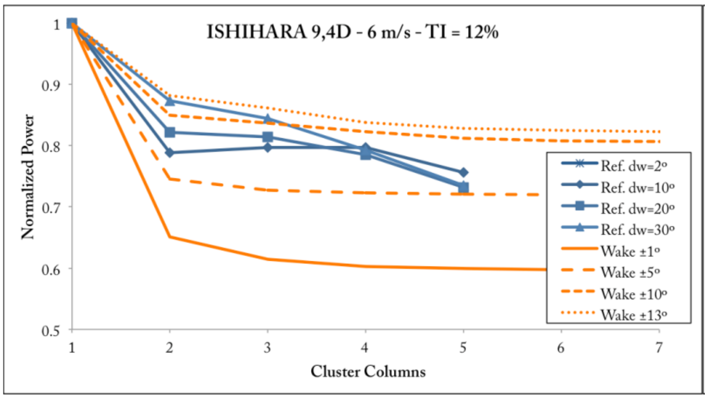
ISHIHARA 9,4D - 6 m/s - TI = 12%
Normalized Power
1
0.9
0.8
0.7
0.6
0.5
1
2
3
4
5
6
7
Cluster Columns
Ref. dw=2°
Ref. dw=10°
Ref. dw=20°
Ref. dw=30°
Wake ±1°
Wake ±5°
Wake ±10°
Wake ±13°

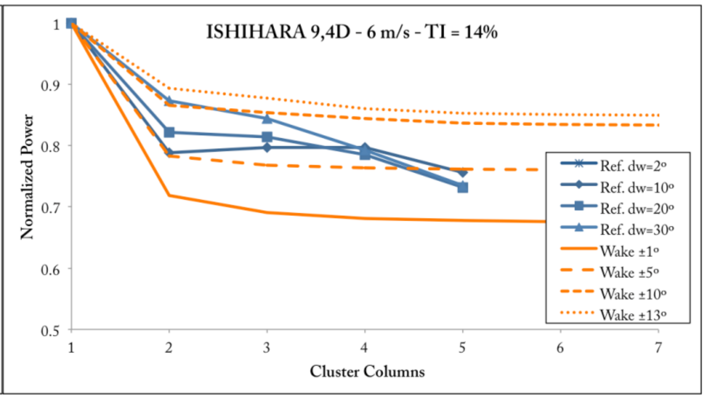
ISHIHARA 9,4D - 6 m/s - TI = 14%
Normalized Power
1
0.9
0.8
0.7
0.6
0.5
1
2
3
4
5
6
7
Cluster Columns
Ref. dw=2°
Ref. dw=10°
Ref. dw=20°
Ref. dw=30°
Wake ±1°
Wake ±5°
Wake ±10°
Wake ±13°

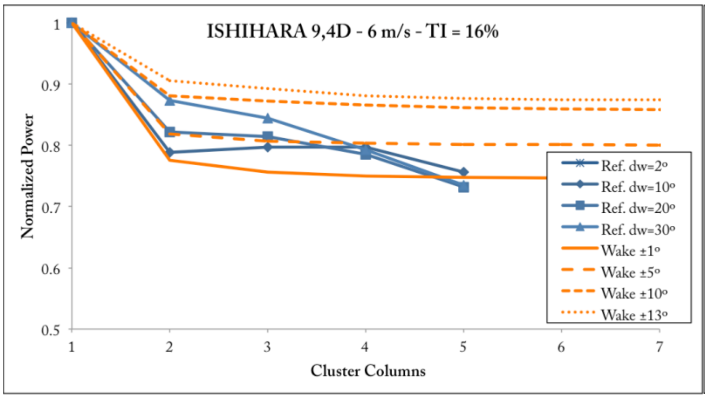

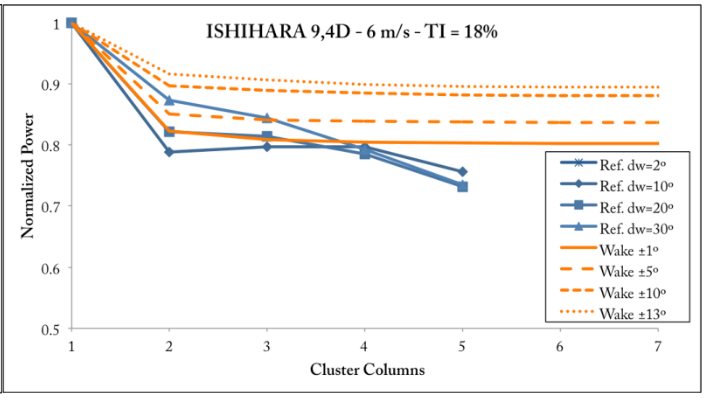

Wind speed: 8 m/s

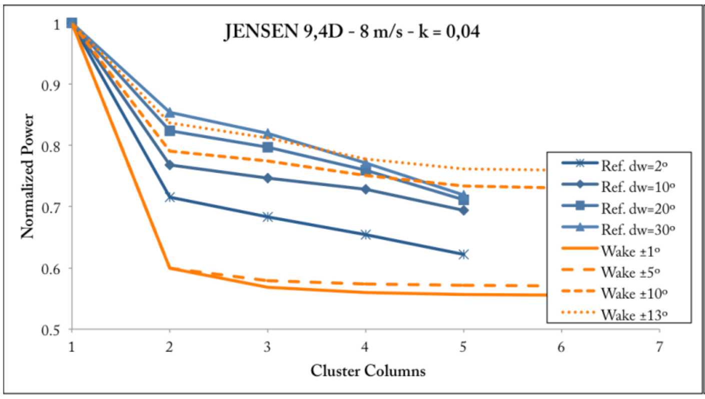

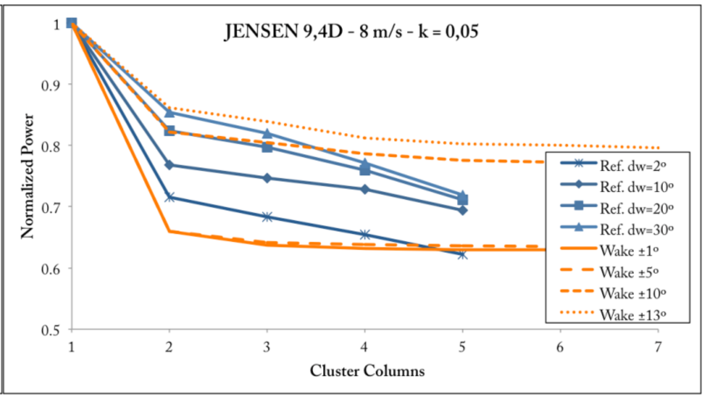

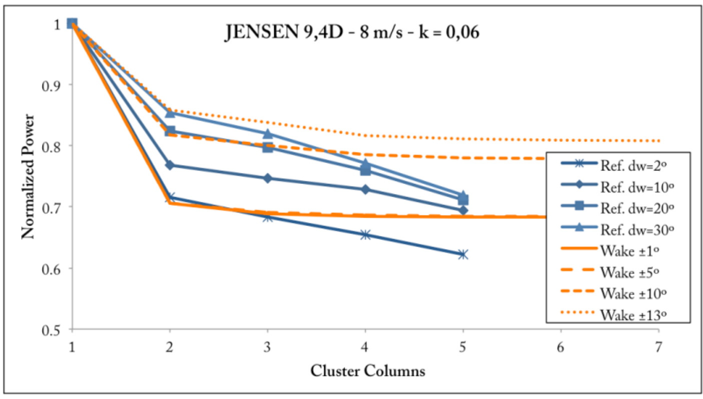

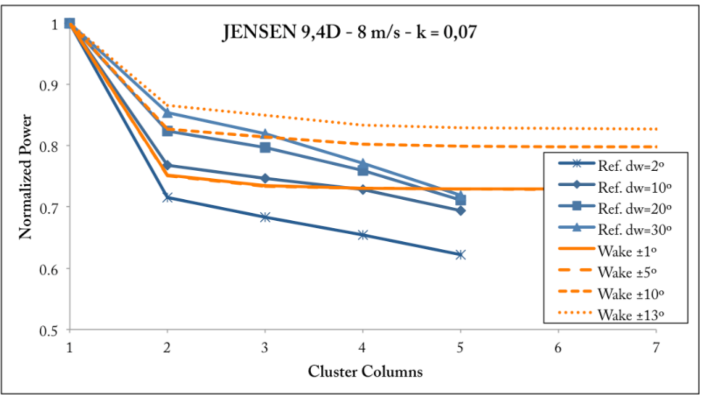

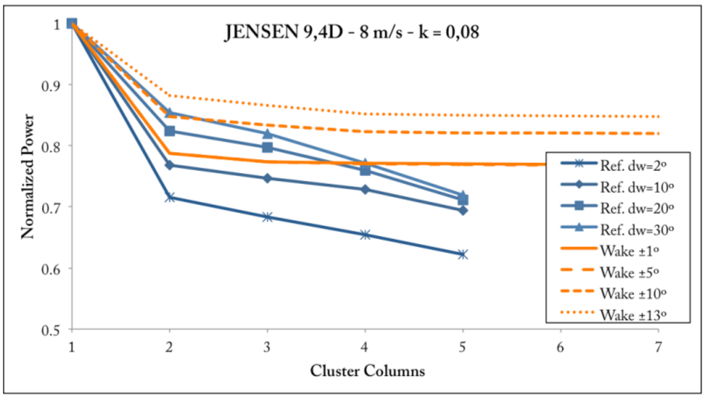

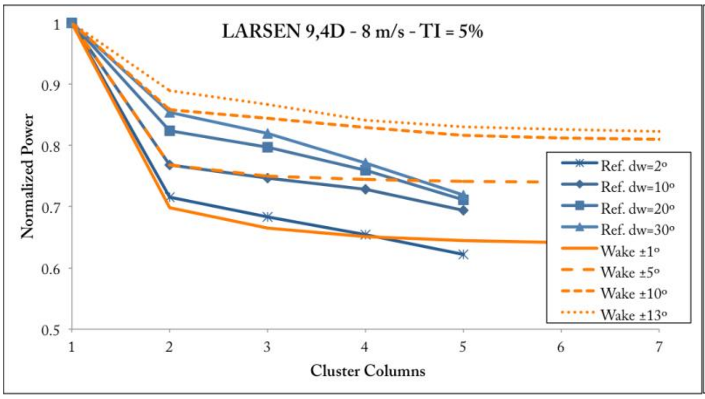
LARSEN 9,4D - 8 m/s - TI = 5%
Normalized Power
1
0.9
0.8
0.7
0.6
0.5
Cluster Columns
1
2
3
4
5
6
7
Ref. dw=2º
Ref. dw=10º
Ref. dw=20º
Ref. dw=30º
Wake ±1º
Wake ±5º
Wake ±10º
Wake ±13º

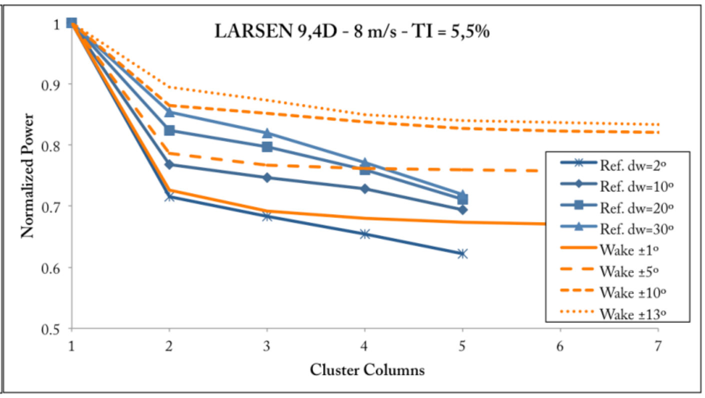
LARSEN 9,4D - 8 m/s - TI = 5,5%
Normalized Power
1
0.9
0.8
0.7
0.6
0.5
Cluster Columns
1
2
3
4
5
6
7
Ref. dw=2º
Ref. dw=10º
Ref. dw=20º
Ref. dw=30º
Wake ±1º
Wake ±5º
Wake ±10º
Wake ±13º

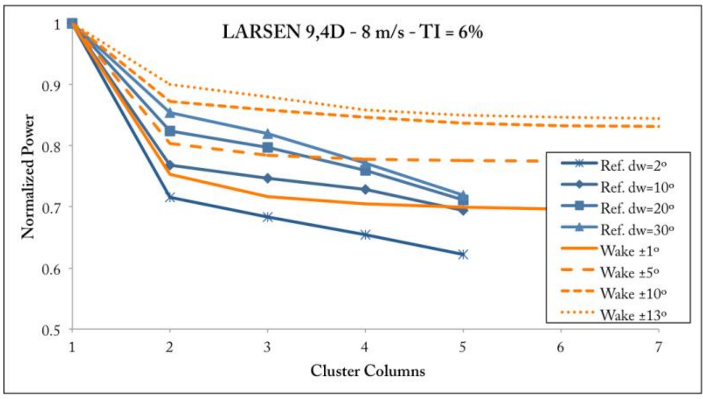
LARSEN 9,4D - 8 m/s - TI = 6%
Normalized Power
1
0.9
0.8
0.7
0.6
0.5
Cluster Columns
1
2
3
4
5
6
7
Ref. dw=2º
Ref. dw=10º
Ref. dw=20º
Ref. dw=30º
Wake ±1º
Wake ±5º
Wake ±10º
Wake ±13º

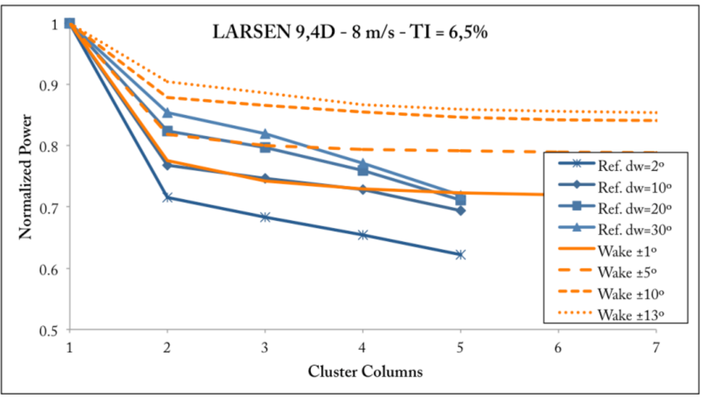
LARSEN 9,4D - 8 m/s - TI = 6,5%
Normalized Power
1
0.9
0.8
0.7
0.6
0.5
Cluster Columns
1
2
3
4
5
6
7
Ref. dw=2º
Ref. dw=10º
Ref. dw=20º
Ref. dw=30º
Wake ±1º
Wake ±5º
Wake ±10º
Wake ±13º

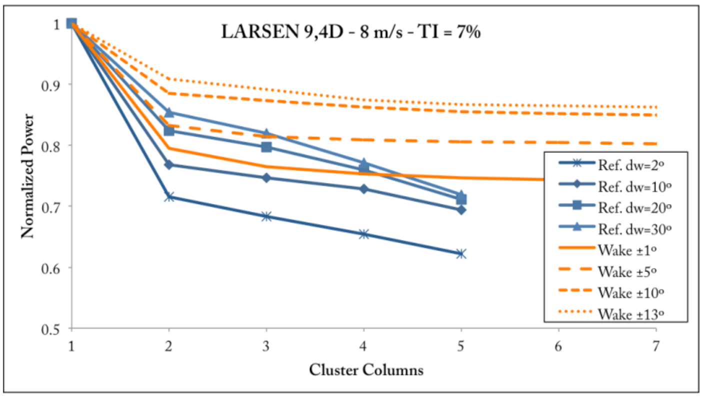
LARSEN 9,4D - 8 m/s - TI = 7%
Normalized Power
1
0.9
0.8
0.7
0.6
0.5
Cluster Columns
1
2
3
4
5
6
7
Ref. dw=2º
Ref. dw=10º
Ref. dw=20º
Ref. dw=30º
Wake ±1º
Wake ±5º
Wake ±10º
Wake ±13º

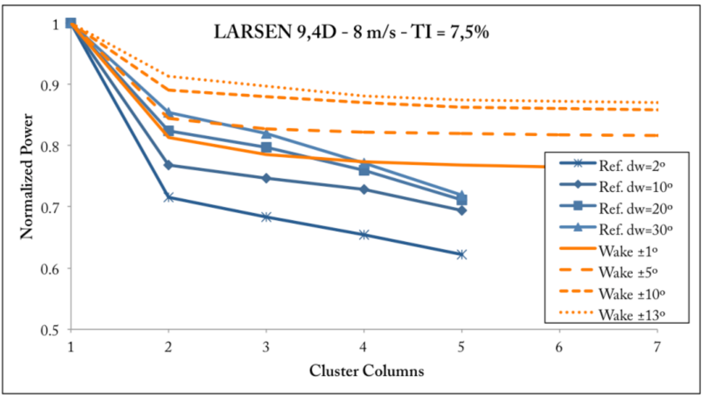
LARSEN 9,4D - 8 m/s - TI = 7,5%
Normalized Power
1
0.9
0.8
0.7
0.6
0.5
Cluster Columns
1
2
3
4
5
6
7
Ref. dw=2º
Ref. dw=10º
Ref. dw=20º
Ref. dw=30º
Wake ±1º
Wake ±5º
Wake ±10º
Wake ±13º

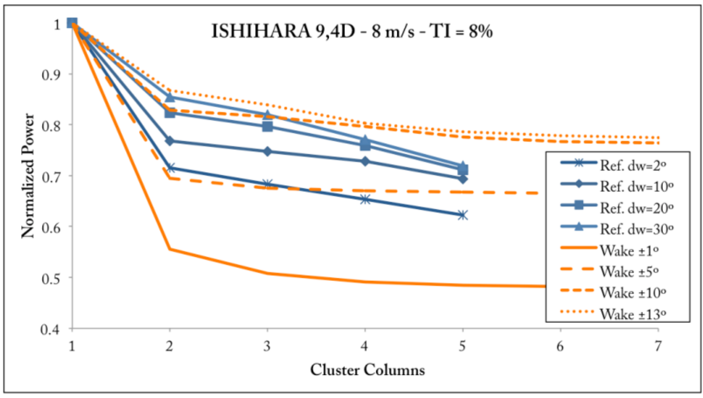
ISHIHARA 9,4D - 8 m/s - TI = 8%
Normalized Power
1
0.9
0.8
0.7
0.6
0.5
0.4
Cluster Columns
1
2
3
4
5
6
7
Ref. dw=2º
Ref. dw=10º
Ref. dw=20º
Ref. dw=30º
Wake ±1º
Wake ±5º
Wake ±10º
Wake ±13º

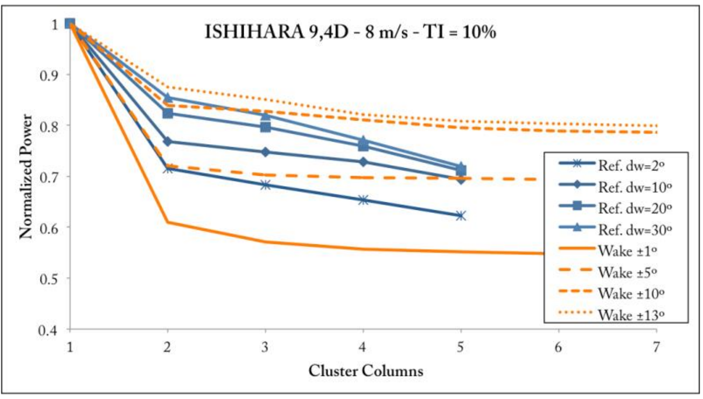
ISHIHARA 9,4D - 8 m/s - TI = 10%
Normalized Power
1
0.9
0.8
0.7
0.6
0.5
0.4
Cluster Columns
1
2
3
4
5
6
7
Ref. dw=2º
Ref. dw=10º
Ref. dw=20º
Ref. dw=30º
Wake ±1º
Wake ±5º
Wake ±10º
Wake ±13º

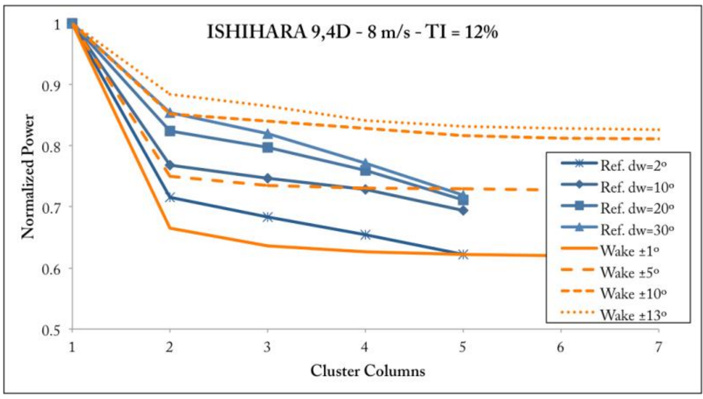

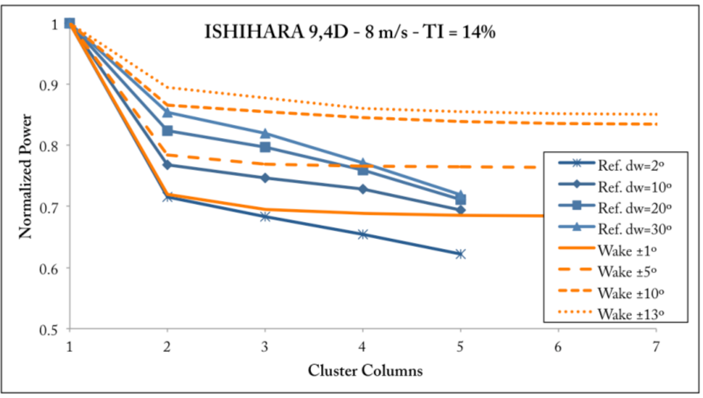

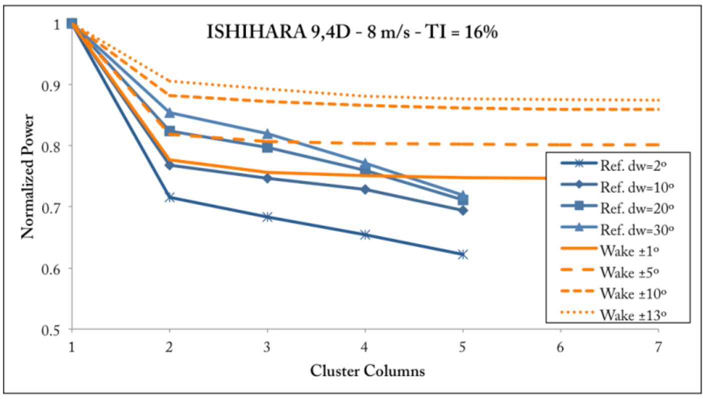

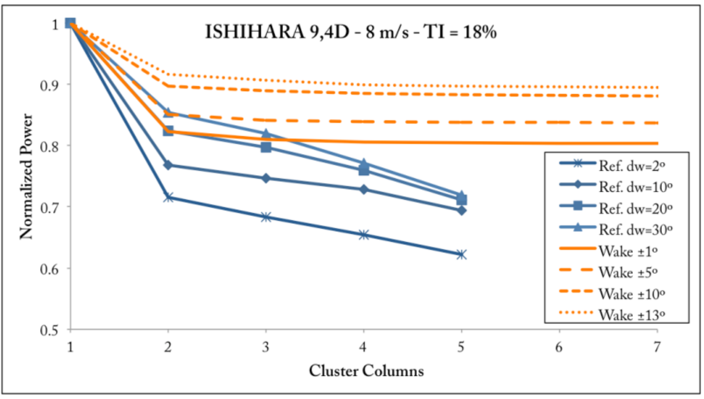

Wind speed: 10 m/s

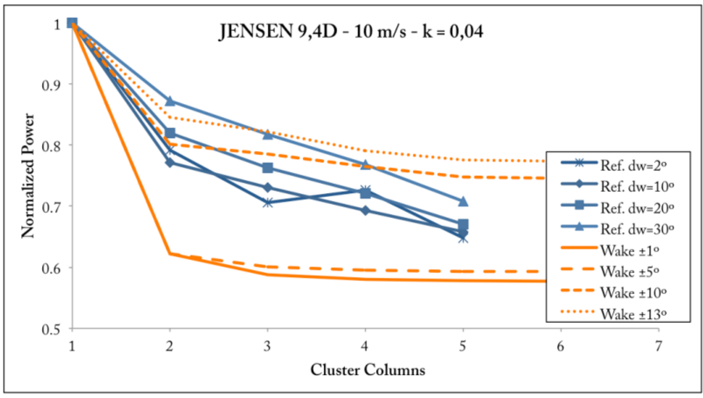

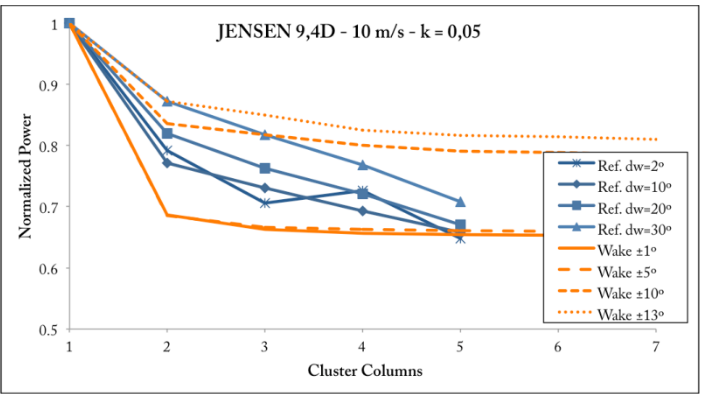

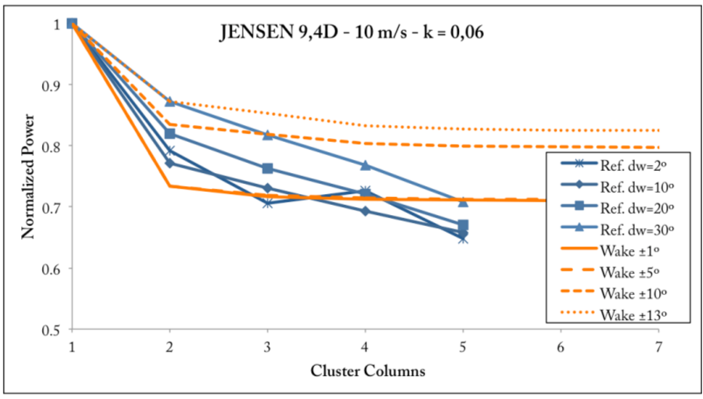

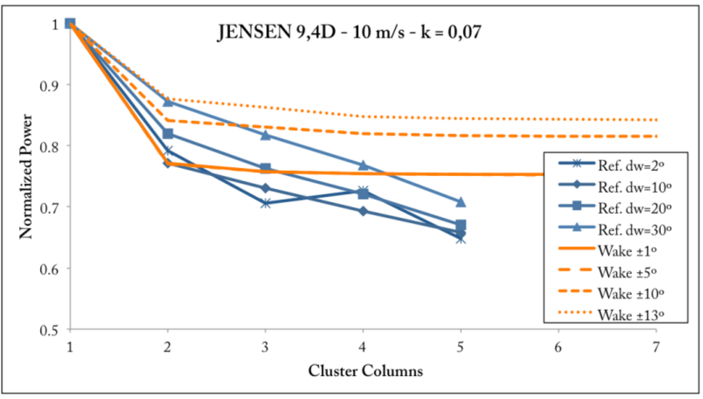

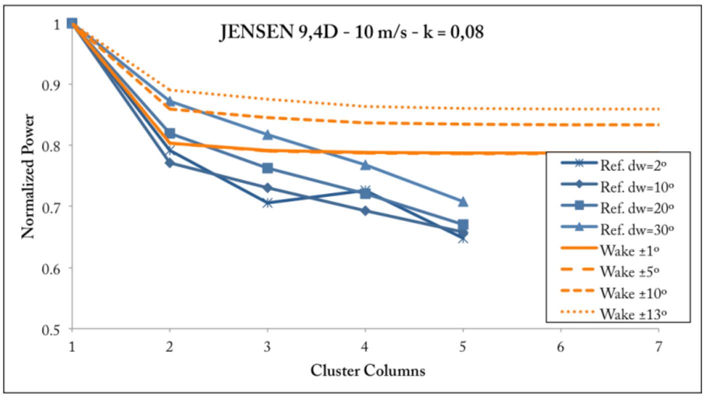
JENSEN 9,4D - 10 m/s - k = 0,08
Normalized Power
1
0.9
0.8
0.7
0.6
0.5
Cluster Columns
1
2
3
4
5
6
7
Ref. dw=2º
Ref. dw=10º
Ref. dw=20º
Ref. dw=30º
Wake ±1º
Wake ±5º
Wake ±10º
Wake ±13º

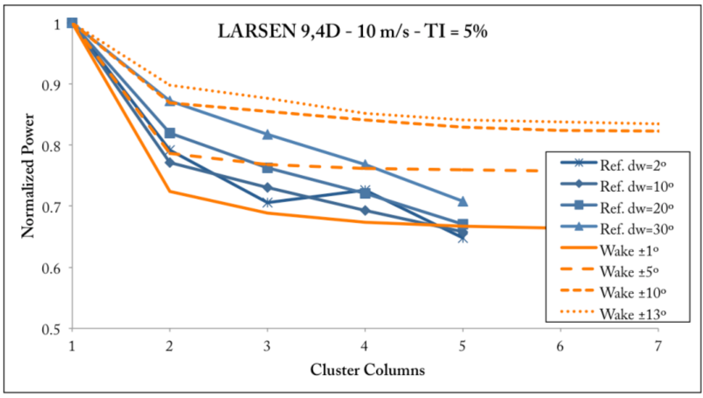
LARSEN 9,4D - 10 m/s - TI = 5%
Normalized Power
1
0.9
0.8
0.7
0.6
0.5
Cluster Columns
1
2
3
4
5
6
7
Ref. dw=2º
Ref. dw=10º
Ref. dw=20º
Ref. dw=30º
Wake ±1º
Wake ±5º
Wake ±10º
Wake ±13º

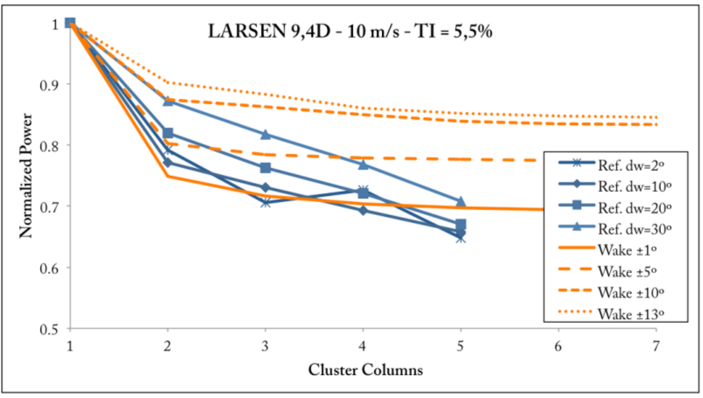
LARSEN 9,4D - 10 m/s - TI = 5,5%
Normalized Power
1
0.9
0.8
0.7
0.6
0.5
Cluster Columns
1
2
3
4
5
6
7
Ref. dw=2º
Ref. dw=10º
Ref. dw=20º
Ref. dw=30º
Wake ±1º
Wake ±5º
Wake ±10º
Wake ±13º

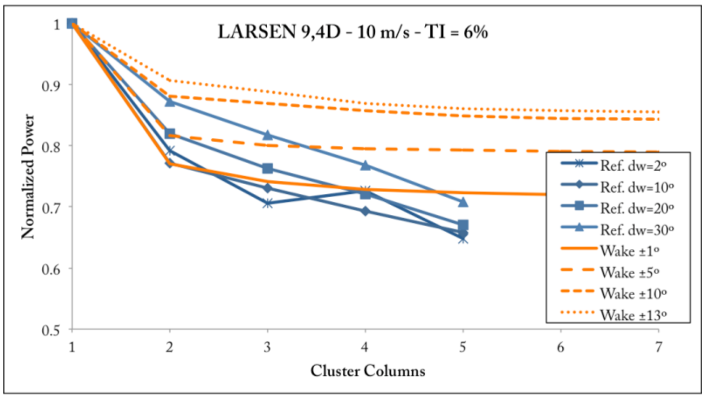
LARSEN 9,4D - 10 m/s - TI = 6%
Normalized Power
1
0.9
0.8
0.7
0.6
0.5
Cluster Columns
1
2
3
4
5
6
7
Ref. dw=2º
Ref. dw=10º
Ref. dw=20º
Ref. dw=30º
Wake ±1º
Wake ±5º
Wake ±10º
Wake ±13º

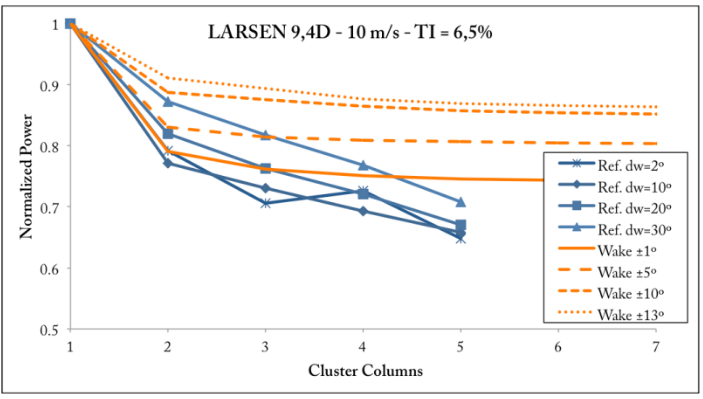
LARSEN 9,4D - 10 m/s - TI = 6,5%
Normalized Power
1
0.9
0.8
0.7
0.6
0.5
Cluster Columns
1
2
3
4
5
6
7
Ref. dw=2º
Ref. dw=10º
Ref. dw=20º
Ref. dw=30º
Wake ±1º
Wake ±5º
Wake ±10º
Wake ±13º

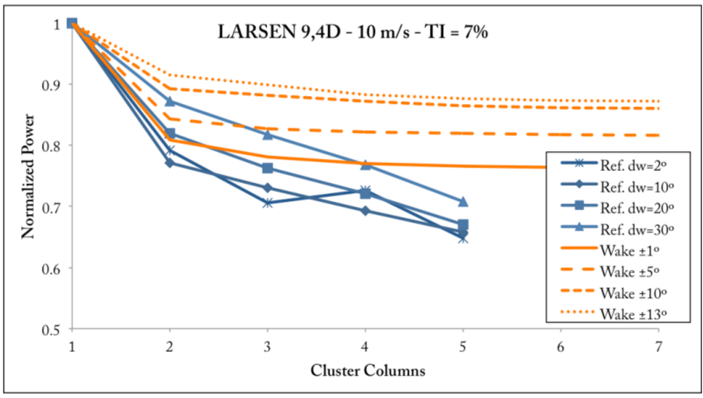
LARSEN 9,4D - 10 m/s - TI = 7%
Normalized Power
1
0.9
0.8
0.7
0.6
0.5
Cluster Columns
1
2
3
4
5
6
7
Ref. dw=2º
Ref. dw=10º
Ref. dw=20º
Ref. dw=30º
Wake ±1º
Wake ±5º
Wake ±10º
Wake ±13º

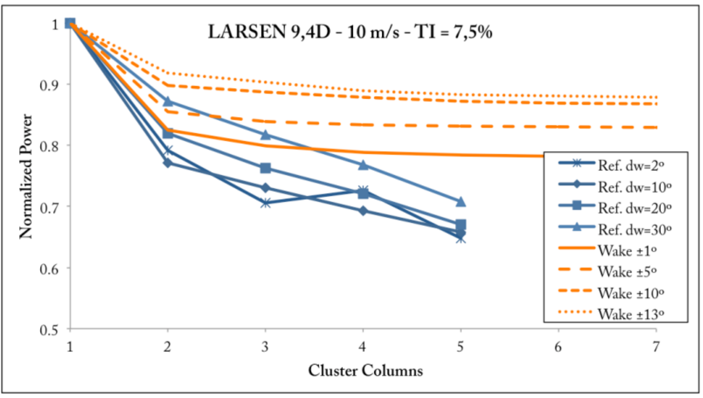
LARSEN 9,4D - 10 m/s - TI = 7,5%
Normalized Power
1
0.9
0.8
0.7
0.6
0.5
Cluster Columns
1
2
3
4
5
6
7
Ref. dw=2º
Ref. dw=10º
Ref. dw=20º
Ref. dw=30º
Wake ±1º
Wake ±5º
Wake ±10º
Wake ±13º

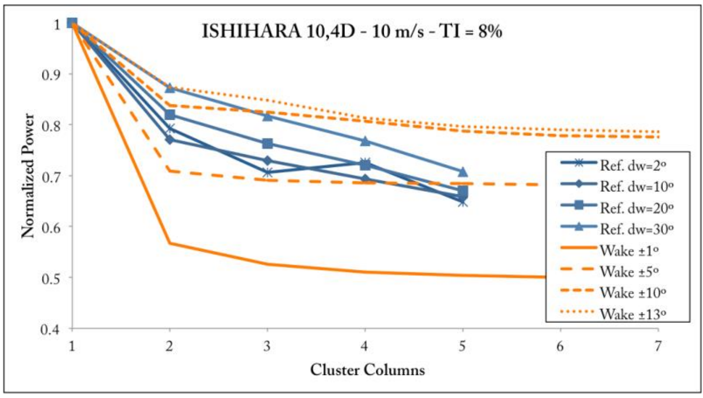
ISHIHARA 10,4D - 10 m/s - TI = 8%
Normalized Power
1
0.9
0.8
0.7
0.6
0.5
0.4
1
2
3
4
5
6
7
Cluster Columns
Ref. dw=2º
Ref. dw=10º
Ref. dw=20º
Ref. dw=30º
Wake ±1º
Wake ±5º
Wake ±10º
Wake ±13º

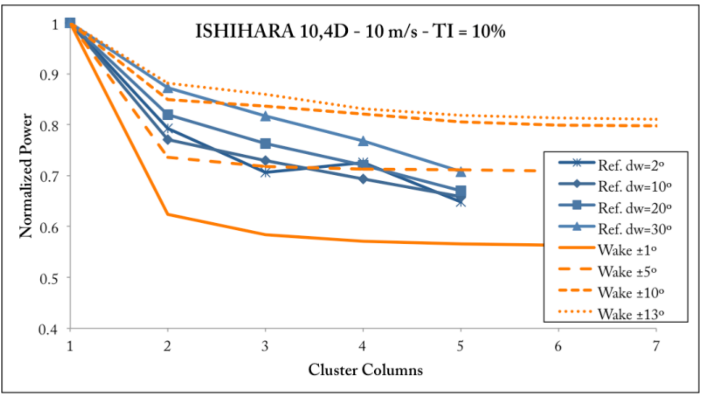
ISHIHARA 10,4D - 10 m/s - TI = 10%
Normalized Power
1
0.9
0.8
0.7
0.6
0.5
0.4
1
2
3
4
5
6
7
Cluster Columns
Ref. dw=2º
Ref. dw=10º
Ref. dw=20º
Ref. dw=30º
Wake ±1º
Wake ±5º
Wake ±10º
Wake ±13º

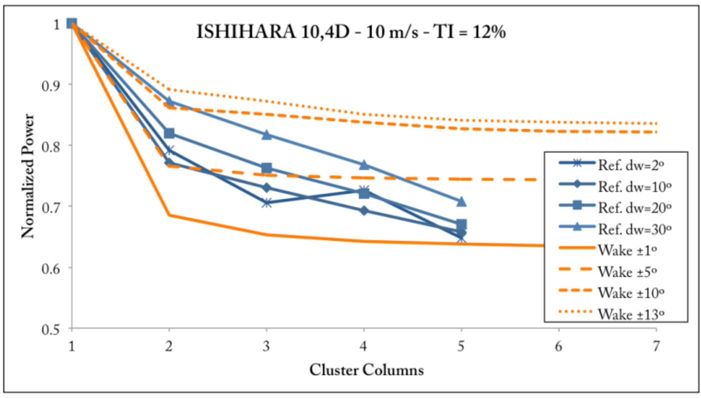
ISHIHARA 10,4D - 10 m/s - TI = 12%
Normalized Power
1
0.9
0.8
0.7
0.6
0.5
1
2
3
4
5
6
7
Cluster Columns
Ref. dw=2º
Ref. dw=10º
Ref. dw=20º
Ref. dw=30º
Wake ±1º
Wake ±5º
Wake ±10º
Wake ±13º

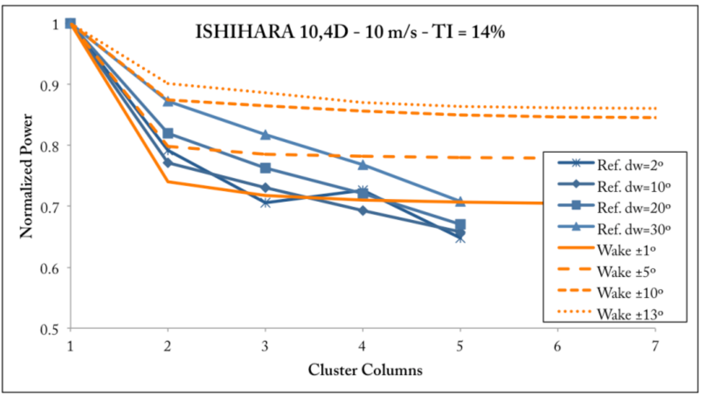
ISHIHARA 10,4D - 10 m/s - TI = 14%
Normalized Power
1
0.9
0.8
0.7
0.6
0.5
1
2
3
4
5
6
7
Cluster Columns
Ref. dw=2º
Ref. dw=10º
Ref. dw=20º
Ref. dw=30º
Wake ±1º
Wake ±5º
Wake ±10º
Wake ±13º

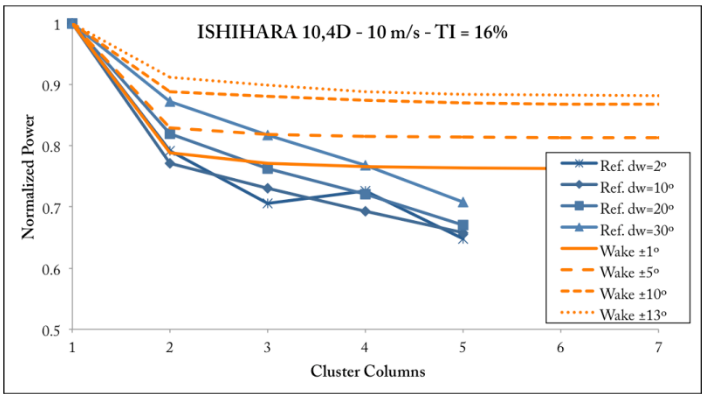
ISHIHARA 10,4D - 10 m/s - TI = 16%
Normalized Power
1
0.9
0.8
0.7
0.6
0.5
1
2
3
4
5
6
7
Cluster Columns
Ref. dw=2º
Ref. dw=10º
Ref. dw=20º
Ref. dw=30º
Wake ±1º
Wake ±5º
Wake ±10º
Wake ±13º

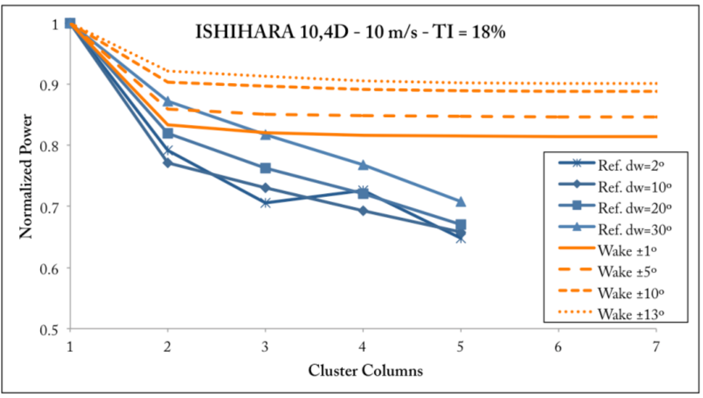
ISHIHARA 10,4D - 10 m/s - TI = 18%
Normalized Power
1
0.9
0.8
0.7
0.6
0.5
1
2
3
4
5
6
7
Cluster Columns
Ref. dw=2º
Ref. dw=10º
Ref. dw=20º
Ref. dw=30º
Wake ±1º
Wake ±5º
Wake ±10º
Wake ±13º

Annex VIII – Results analytical models: Case 312º with 10,4D spacing.

Wind speed: 6 m/s

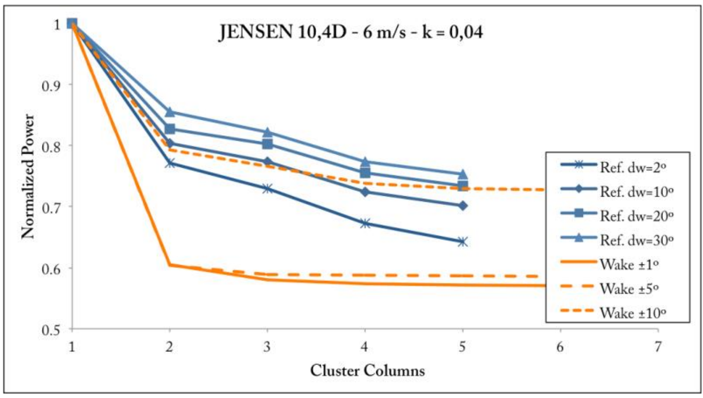

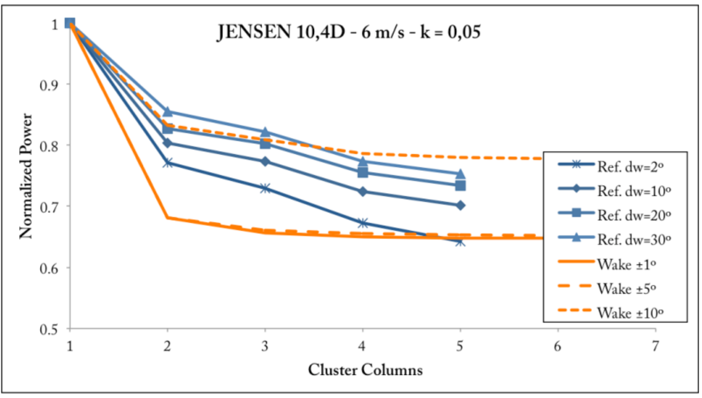

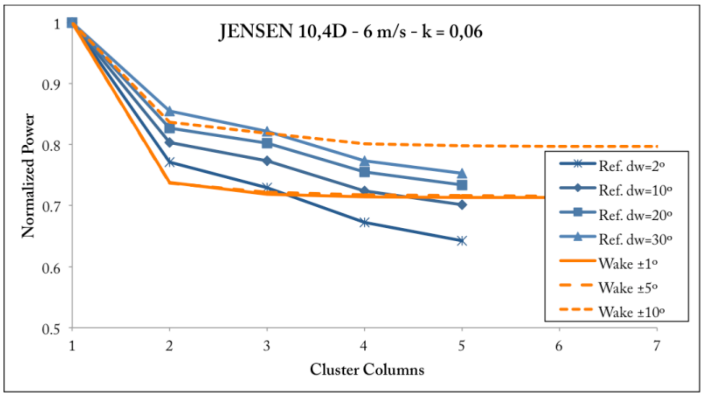

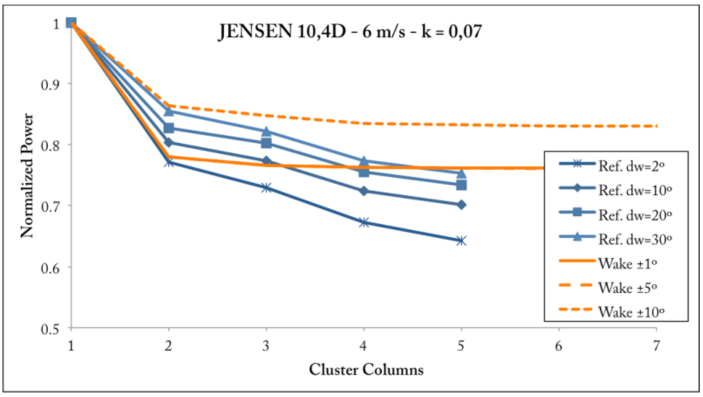

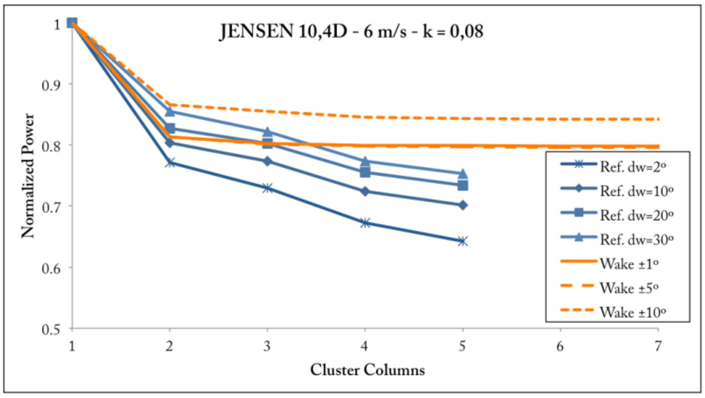

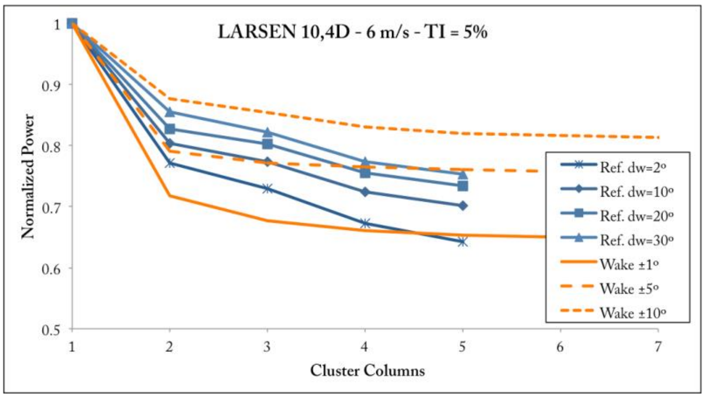

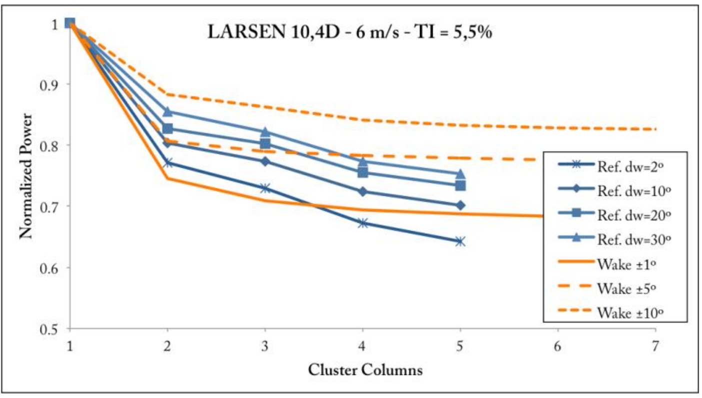

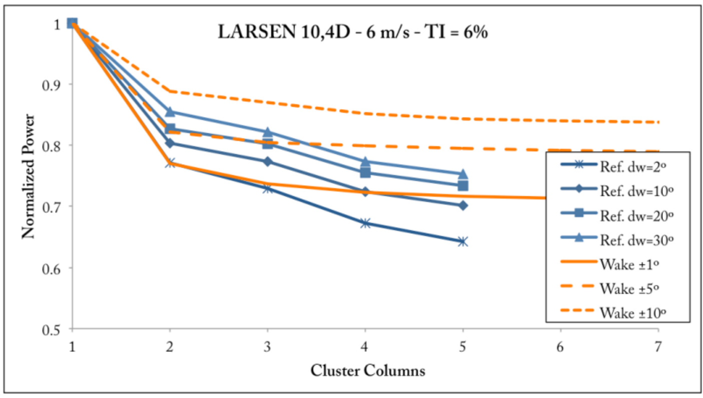
LARSEN 10,4D - 6 m/s - TI = 6%
Normalized Power
1
0.9
0.8
0.7
0.6
0.5
Cluster Columns
1
2
3
4
5
6
7
Ref. dw=2º
Ref. dw=10º
Ref. dw=20º
Ref. dw=30º
Wake ±1º
Wake ±5º
Wake ±10º

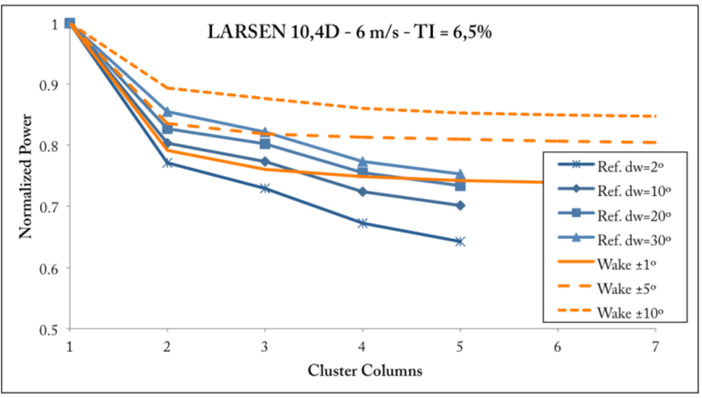
LARSEN 10,4D - 6 m/s - TI = 6,5%
Normalized Power
1
0.9
0.8
0.7
0.6
0.5
Cluster Columns
1
2
3
4
5
6
7
Ref. dw=2º
Ref. dw=10º
Ref. dw=20º
Ref. dw=30º
Wake ±1º
Wake ±5º
Wake ±10º

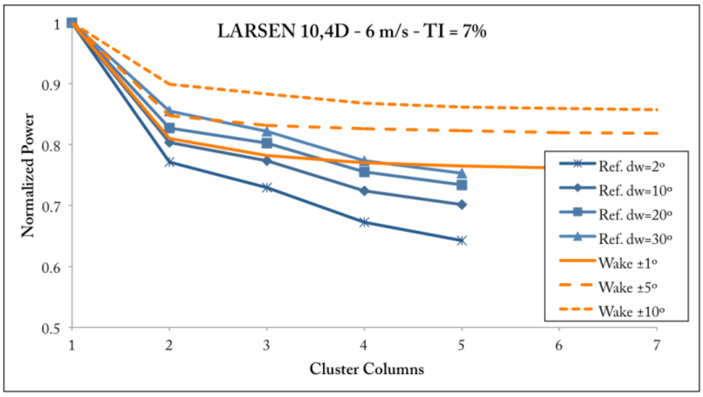
LARSEN 10,4D - 6 m/s - TI = 7%
Normalized Power
1
0.9
0.8
0.7
0.6
0.5
Cluster Columns
1
2
3
4
5
6
7
Ref. dw=2º
Ref. dw=10º
Ref. dw=20º
Ref. dw=30º
Wake ±1º
Wake ±5º
Wake ±10º

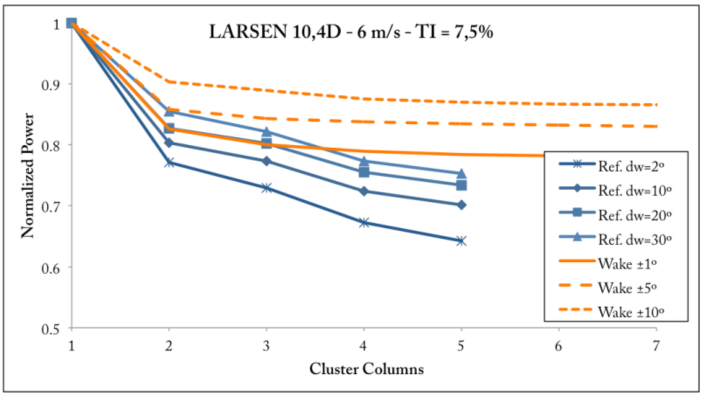
LARSEN 10,4D - 6 m/s - TI = 7,5%
Normalized Power
1
0.9
0.8
0.7
0.6
0.5
Cluster Columns
1
2
3
4
5
6
7
Ref. dw=2º
Ref. dw=10º
Ref. dw=20º
Ref. dw=30º
Wake ±1º
Wake ±5º
Wake ±10º

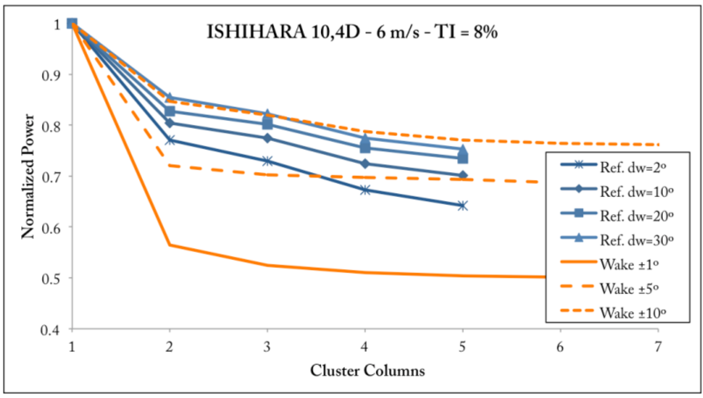
ISHIHARA 10,4D - 6 m/s - TI = 8%
Normalized Power
1
0.9
0.8
0.7
0.6
0.5
0.4
Cluster Columns
1
2
3
4
5
6
7
Ref. dw=2º
Ref. dw=10º
Ref. dw=20º
Ref. dw=30º
Wake ±1º
Wake ±5º
Wake ±10º

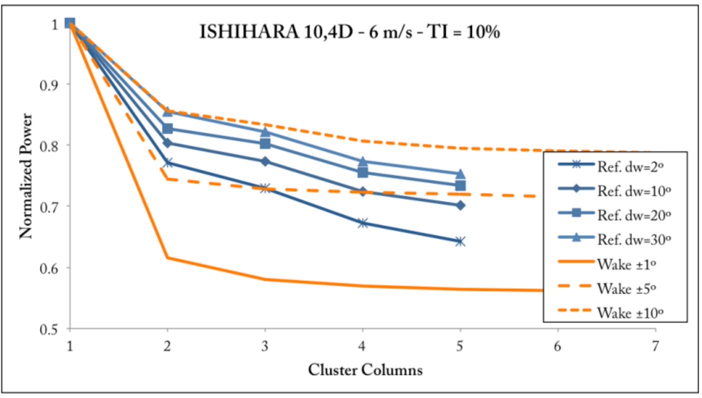
ISHIHARA 10,4D - 6 m/s - TI = 10%
Normalized Power
1
0.9
0.8
0.7
0.6
0.5
Cluster Columns
1
2
3
4
5
6
7
Ref. dw=2º
Ref. dw=10º
Ref. dw=20º
Ref. dw=30º
Wake ±1º
Wake ±5º
Wake ±10º

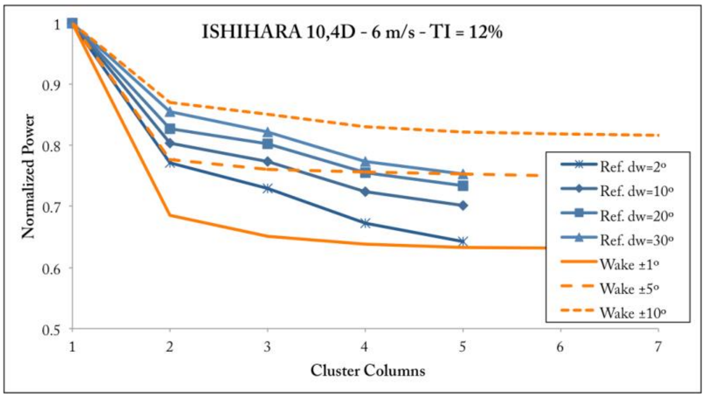
ISHIHARA 10,4D - 6 m/s - TI = 12%
Normalized Power
1
0.9
0.8
0.7
0.6
0.5
Cluster Columns
1
2
3
4
5
6
7
Ref. dw=2º
Ref. dw=10º
Ref. dw=20º
Ref. dw=30º
Wake ±1º
Wake ±5º
Wake ±10º

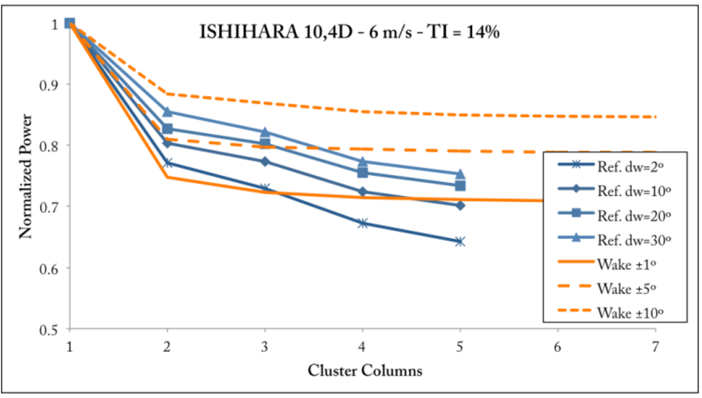
ISHIHARA 10,4D - 6 m/s - TI = 14%
Normalized Power
1
0.9
0.8
0.7
0.6
0.5
Cluster Columns
1
2
3
4
5
6
7
Ref. dw=2º
Ref. dw=10º
Ref. dw=20º
Ref. dw=30º
Wake ±1º
Wake ±5º
Wake ±10º

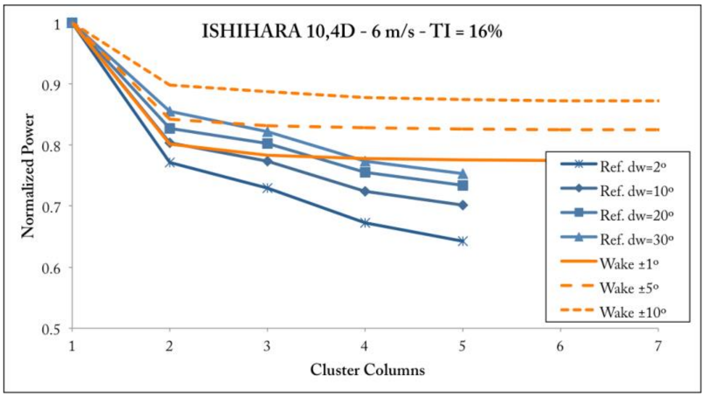

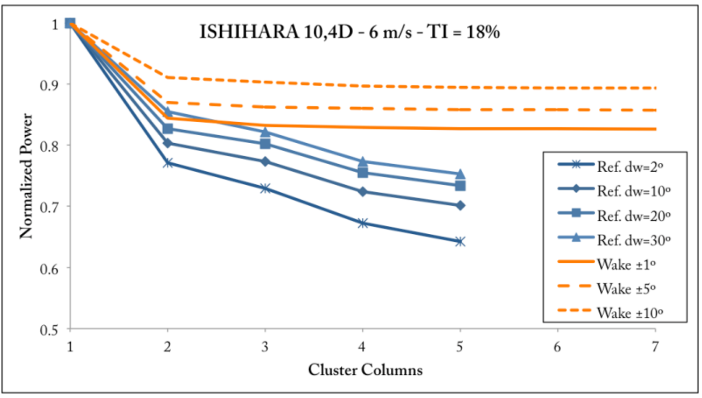

Wind speed: 8 m/s

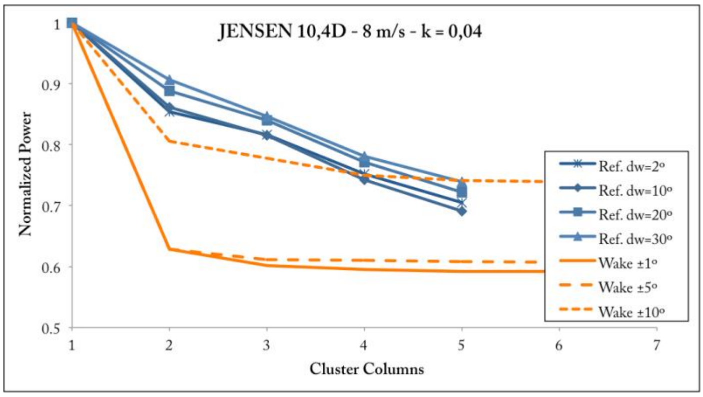

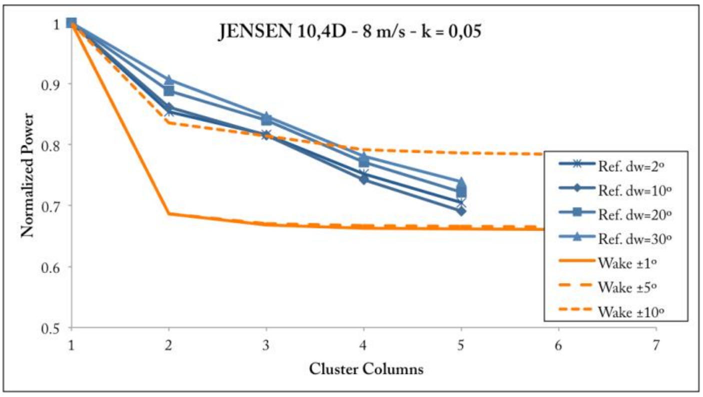

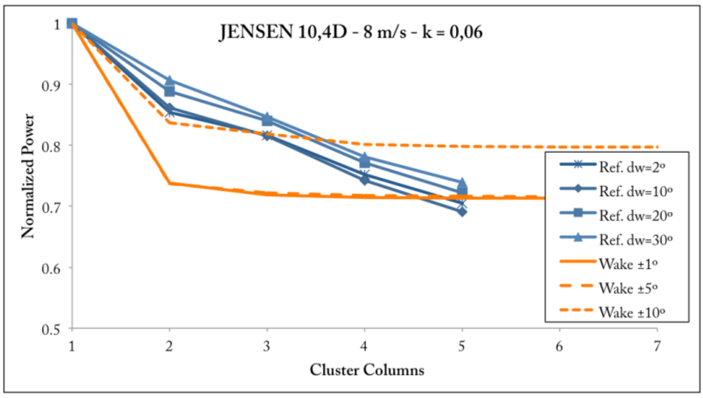

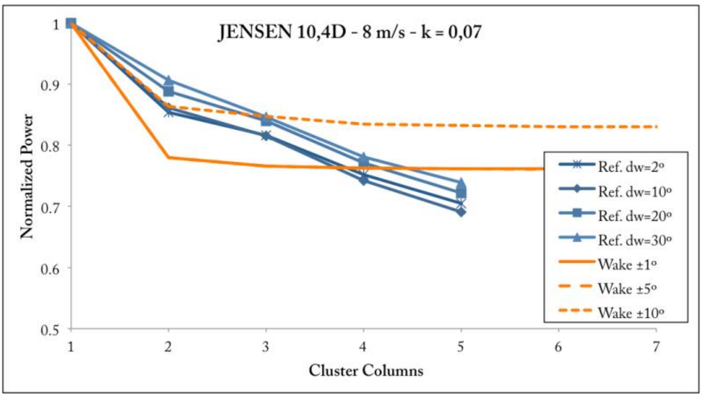

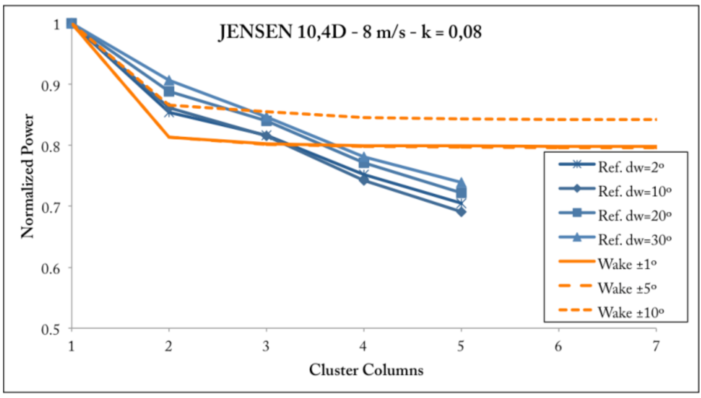

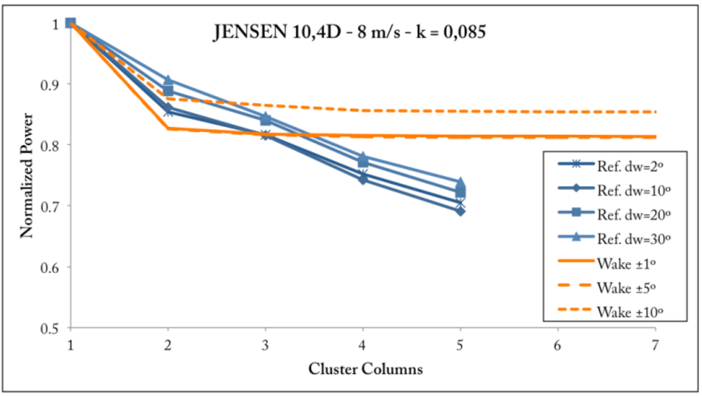

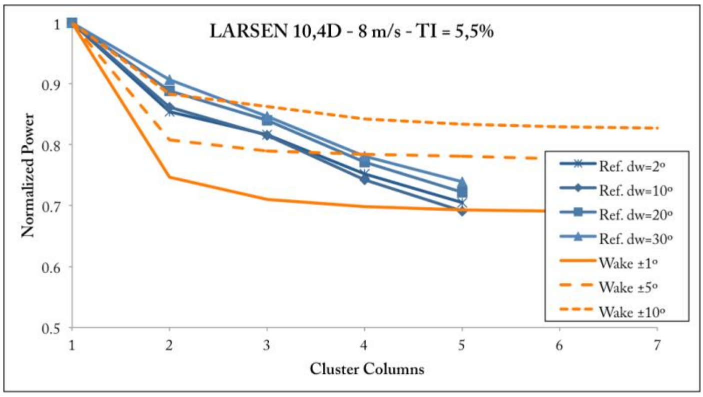
LARSEN 10,4D - 8 m/s - TI = 5,5%
Normalized Power
1
0.9
0.8
0.7
0.6
0.5
Cluster Columns
1
2
3
4
5
6
7
Ref. dw=2º
Ref. dw=10º
Ref. dw=20º
Ref. dw=30º
Wake ±1º
Wake ±5º
Wake ±10º

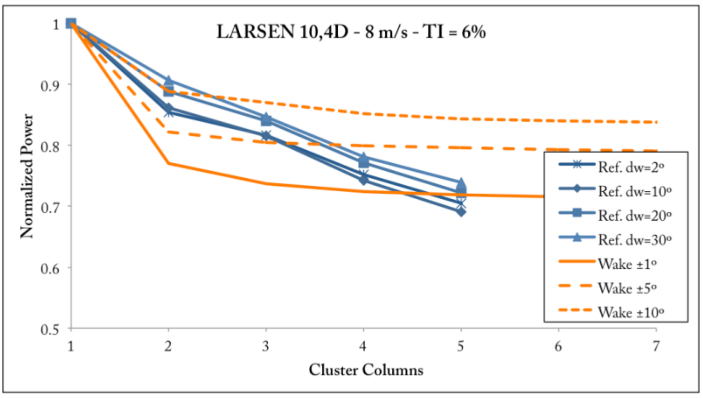
LARSEN 10,4D - 8 m/s - TI = 6%
Normalized Power
1
0.9
0.8
0.7
0.6
0.5
Cluster Columns
1
2
3
4
5
6
7
Ref. dw=2º
Ref. dw=10º
Ref. dw=20º
Ref. dw=30º
Wake ±1º
Wake ±5º
Wake ±10º

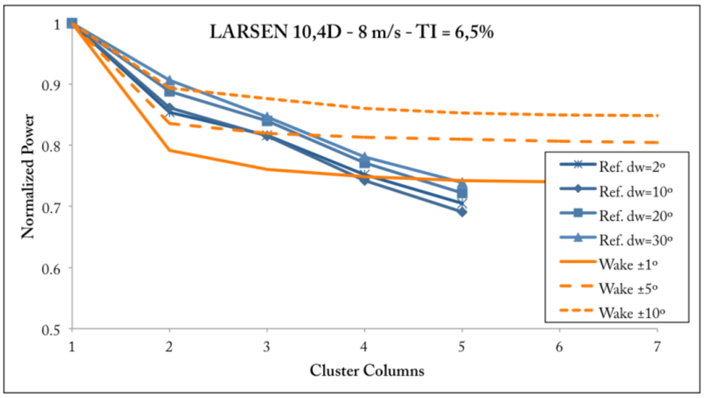
LARSEN 10,4D - 8 m/s - TI = 6,5%
Normalized Power
1
0.9
0.8
0.7
0.6
0.5
Cluster Columns
1
2
3
4
5
6
7
Ref. dw=2º
Ref. dw=10º
Ref. dw=20º
Ref. dw=30º
Wake ±1º
Wake ±5º
Wake ±10º

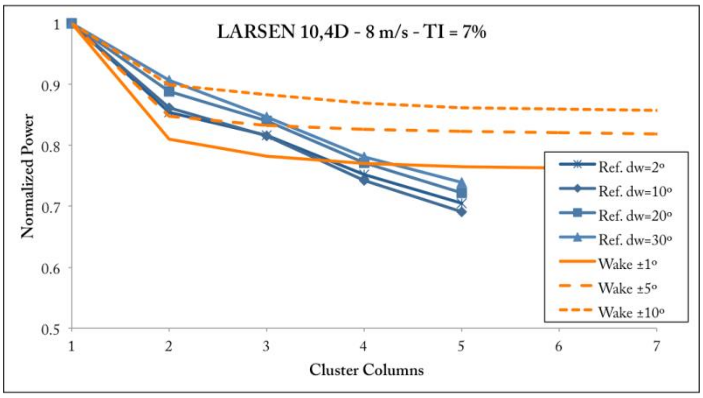
LARSEN 10,4D - 8 m/s - TI = 7%
Normalized Power
1
0.9
0.8
0.7
0.6
0.5
Cluster Columns
1
2
3
4
5
6
7
Ref. dw=2º
Ref. dw=10º
Ref. dw=20º
Ref. dw=30º
Wake ±1º
Wake ±5º
Wake ±10º

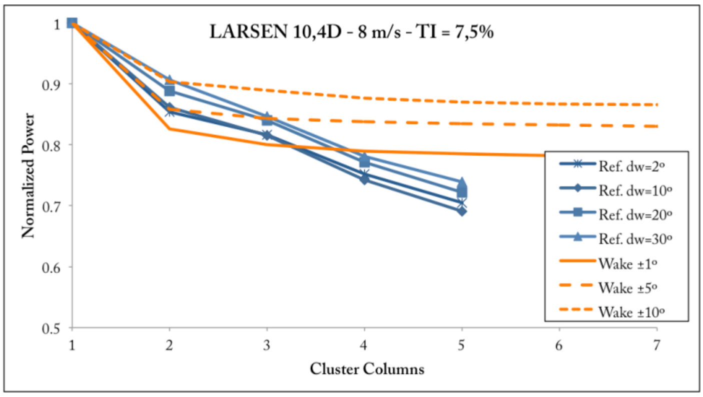
LARSEN 10,4D - 8 m/s - TI = 7,5%
Normalized Power
1
0.9
0.8
0.7
0.6
0.5
Cluster Columns
1
2
3
4
5
6
7
Ref. dw=2º
Ref. dw=10º
Ref. dw=20º
Ref. dw=30º
Wake ±1º
Wake ±5º
Wake ±10º

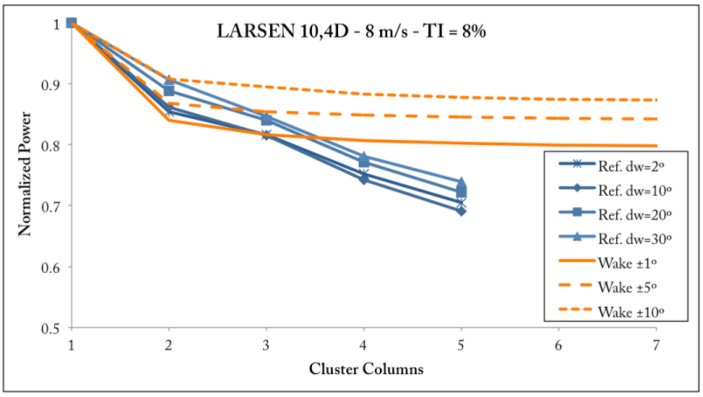
LARSEN 10,4D - 8 m/s - TI = 8%
Normalized Power
1
0.9
0.8
0.7
0.6
0.5
Cluster Columns
1
2
3
4
5
6
7
Ref. dw=2º
Ref. dw=10º
Ref. dw=20º
Ref. dw=30º
Wake ±1º
Wake ±5º
Wake ±10º

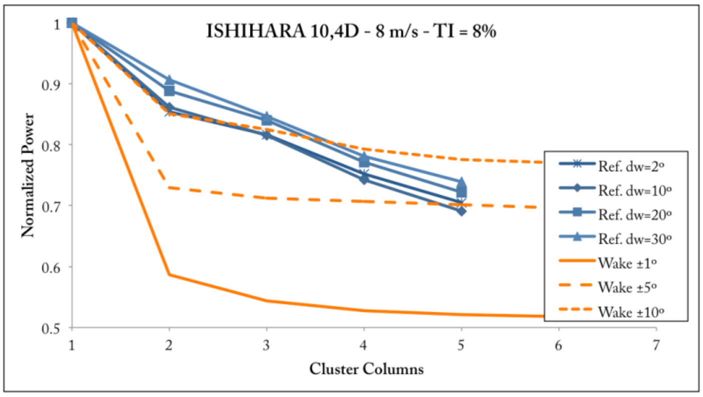
ISHIHARA 10,4D - 8 m/s - TI = 8%
Normalized Power
1
0.9
0.8
0.7
0.6
0.5
Cluster Columns
1
2
3
4
5
6
7
Ref. dw=2º
Ref. dw=10º
Ref. dw=20º
Ref. dw=30º
Wake ±1º
Wake ±5º
Wake ±10º

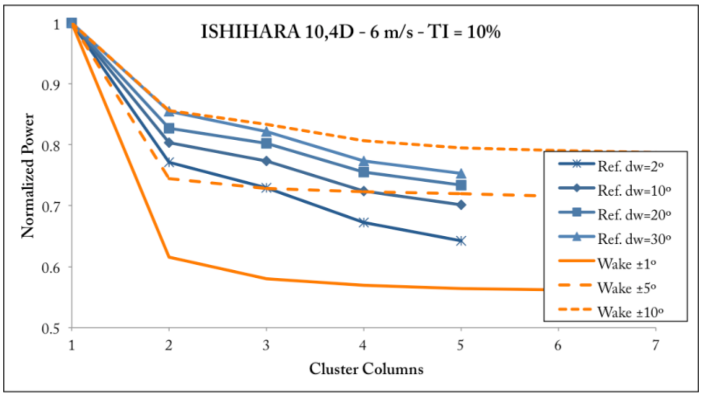
ISHIHARA 10,4D - 6 m/s - TI = 10%
Normalized Power
1
0.9
0.8
0.7
0.6
0.5
Cluster Columns
1
2
3
4
5
6
7
Ref. dw=2º
Ref. dw=10º
Ref. dw=20º
Ref. dw=30º
Wake ±1º
Wake ±5º
Wake ±10º

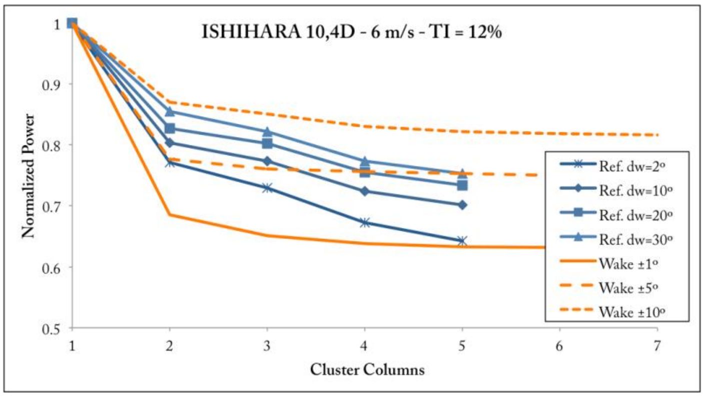

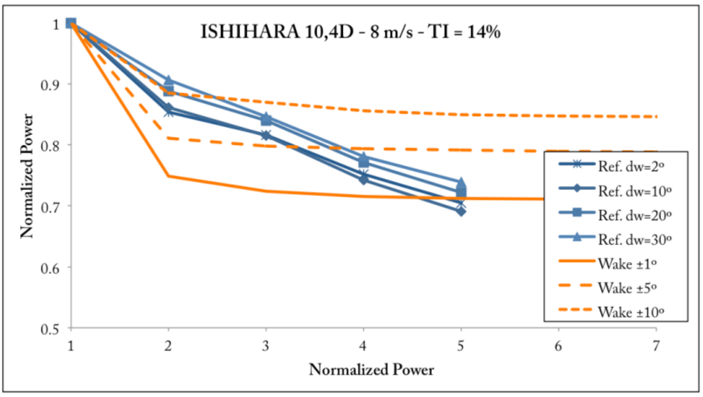

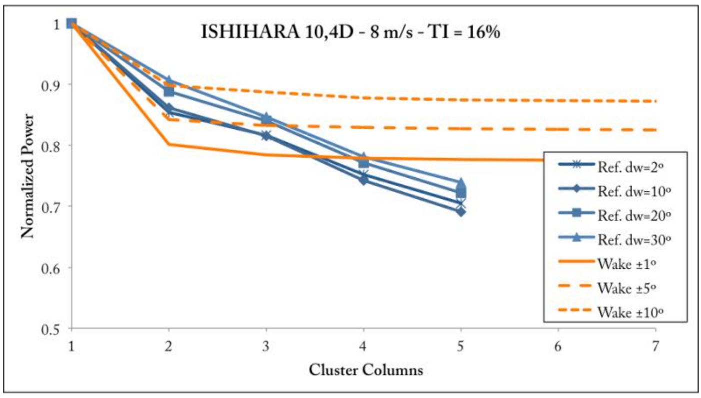

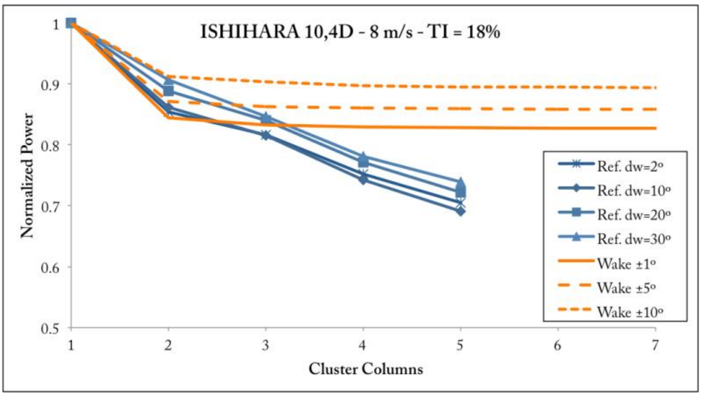

Wind speed: 8 m/s

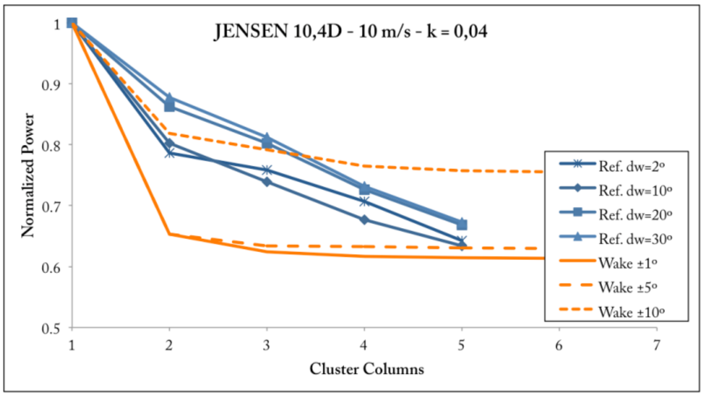

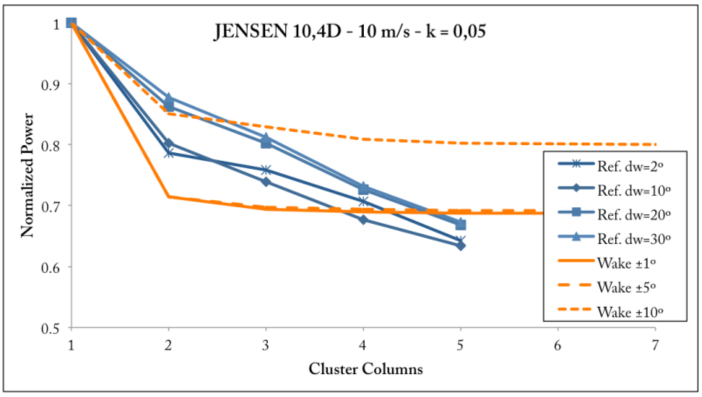

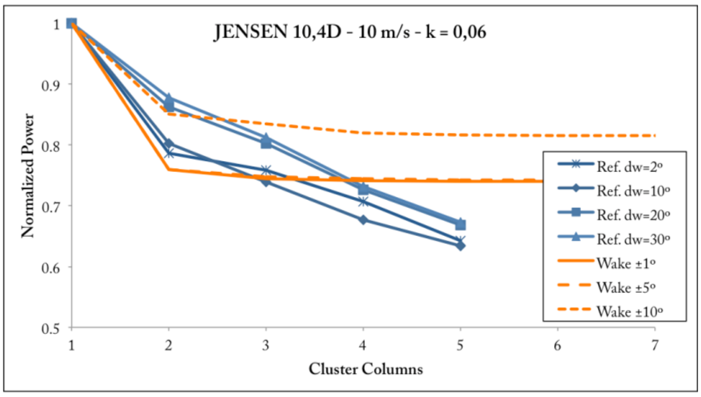

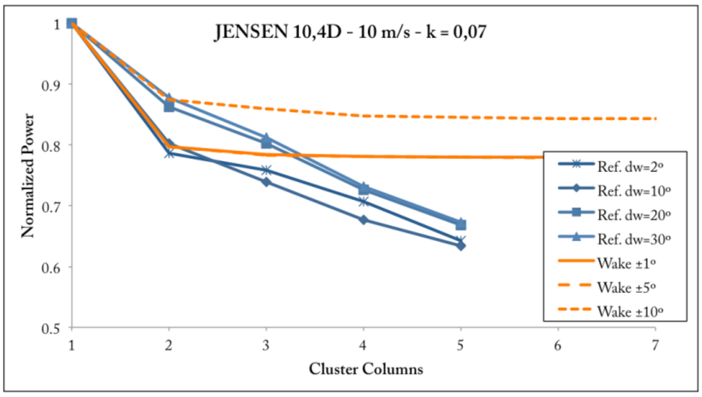

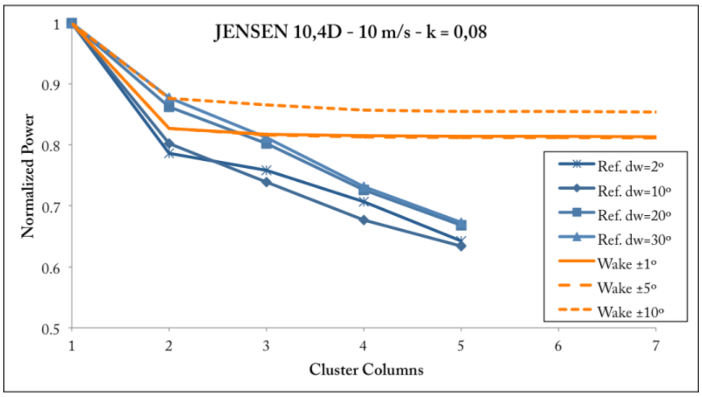
JENSEN 10,4D - 10 m/s - k = 0,08
Normalized Power
Cluster Columns
1
0.9
0.8
0.7
0.6
0.5
1 2 3 4 5 6 7
Ref. dw=2º
Ref. dw=10º
Ref. dw=20º
Ref. dw=30º
Wake ±1º
Wake ±5º
Wake ±10º

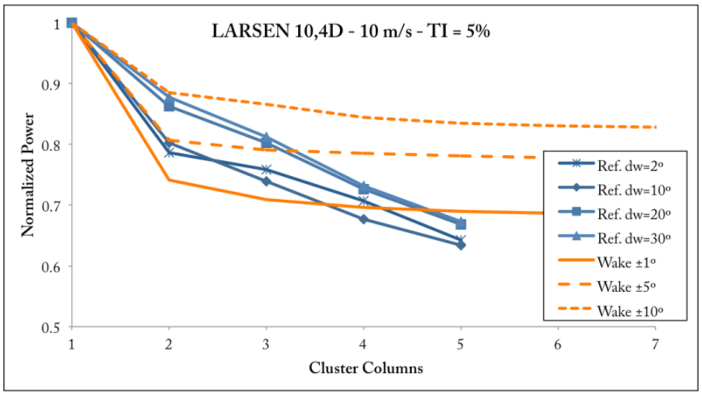
LARSEN 10,4D - 10 m/s - TI = 5%
Normalized Power
Cluster Columns
1
0.9
0.8
0.7
0.6
0.5
1 2 3 4 5 6 7
Ref. dw=2º
Ref. dw=10º
Ref. dw=20º
Ref. dw=30º
Wake ±1º
Wake ±5º
Wake ±10º

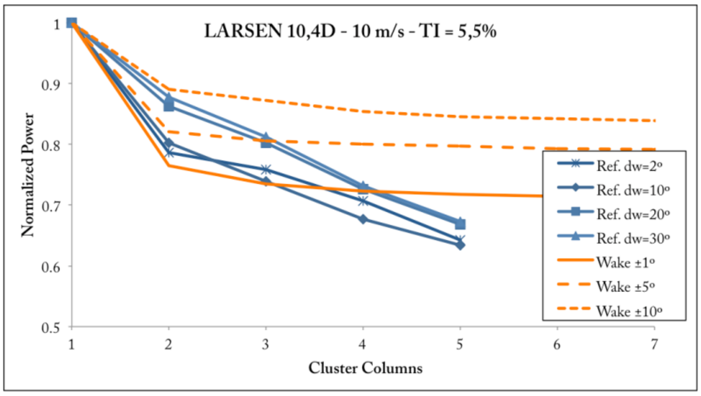
LARSEN 10,4D - 10 m/s - TI = 5,5%
Normalized Power
Cluster Columns
1
0.9
0.8
0.7
0.6
0.5
1 2 3 4 5 6 7
Ref. dw=2º
Ref. dw=10º
Ref. dw=20º
Ref. dw=30º
Wake ±1º
Wake ±5º
Wake ±10º

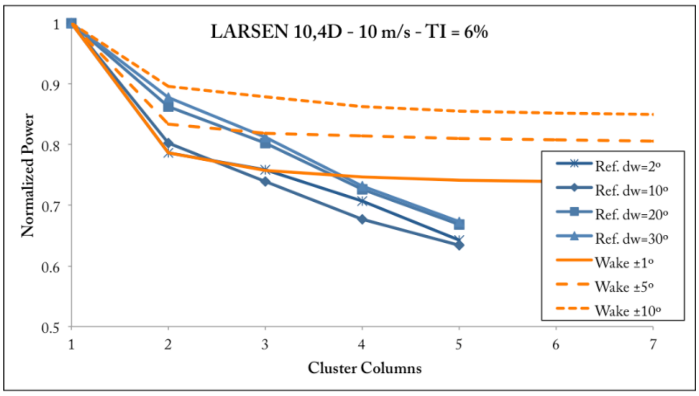
LARSEN 10,4D - 10 m/s - TI = 6%
Normalized Power
Cluster Columns
1
0.9
0.8
0.7
0.6
0.5
1 2 3 4 5 6 7
Ref. dw=2º
Ref. dw=10º
Ref. dw=20º
Ref. dw=30º
Wake ±1º
Wake ±5º
Wake ±10º

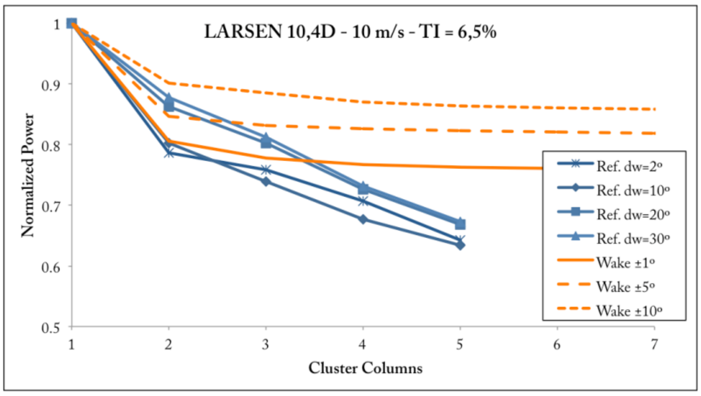
LARSEN 10,4D - 10 m/s - TI = 6,5%
Normalized Power
Cluster Columns
1
0.9
0.8
0.7
0.6
0.5
1 2 3 4 5 6 7
Ref. dw=2º
Ref. dw=10º
Ref. dw=20º
Ref. dw=30º
Wake ±1º
Wake ±5º
Wake ±10º

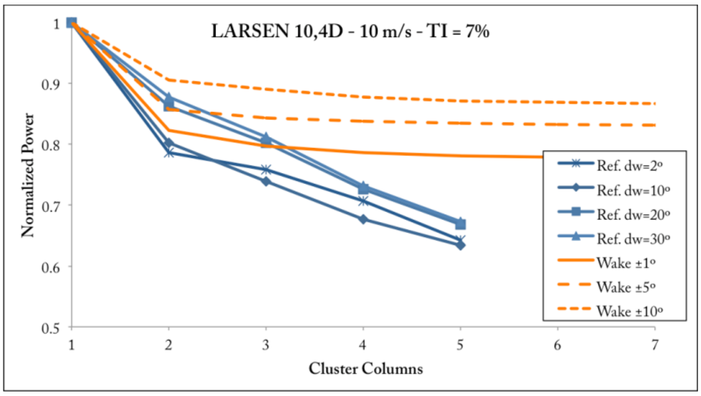
LARSEN 10,4D - 10 m/s - TI = 7%
Normalized Power
Cluster Columns
1
0.9
0.8
0.7
0.6
0.5
1 2 3 4 5 6 7
Ref. dw=2º
Ref. dw=10º
Ref. dw=20º
Ref. dw=30º
Wake ±1º
Wake ±5º
Wake ±10º

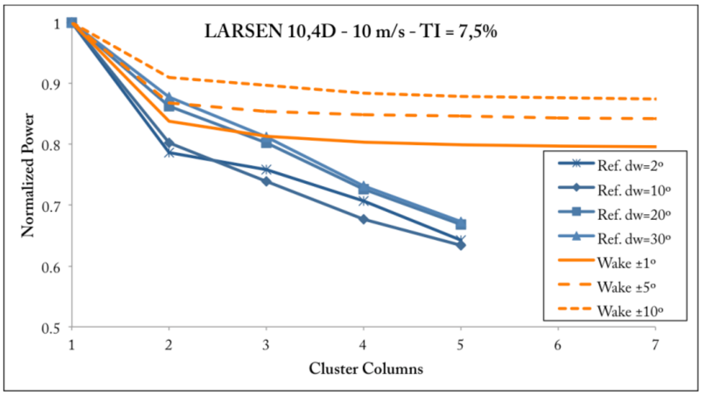
LARSEN 10,4D - 10 m/s - TI = 7,5%
Normalized Power
Cluster Columns
1
0.9
0.8
0.7
0.6
0.5
1 2 3 4 5 6 7
Ref. dw=2º
Ref. dw=10º
Ref. dw=20º
Ref. dw=30º
Wake ±1º
Wake ±5º
Wake ±10º

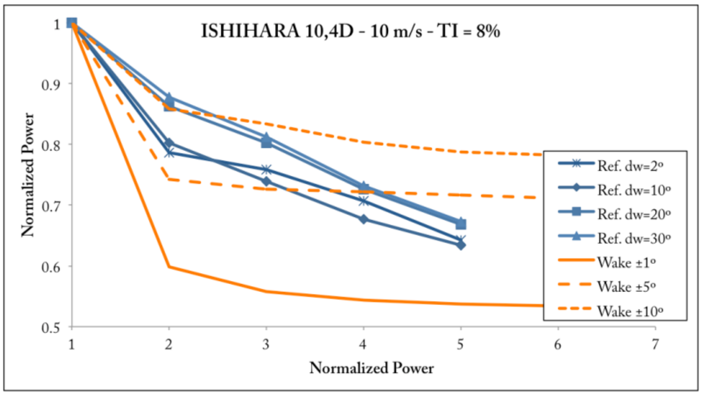
ISHIHARA 10,4D - 10 m/s - TI = 8%
Normalized Power
1
0.9
0.8
0.7
0.6
0.5
1
2
3
4
5
6
7
Normalized Power
Ref. dw=2º
Ref. dw=10º
Ref. dw=20º
Ref. dw=30º
Wake ±1º
Wake ±5º
Wake ±10º

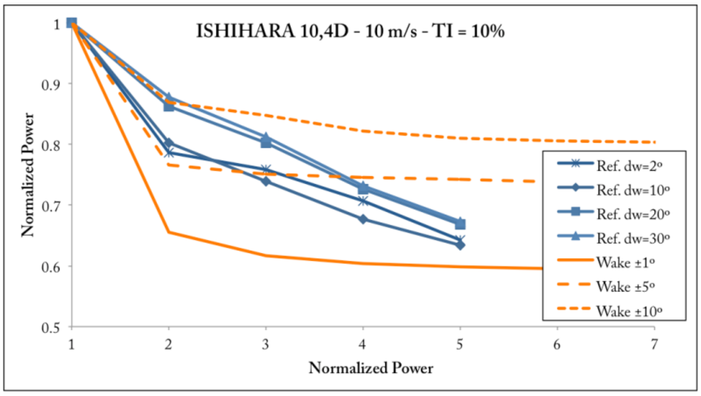
ISHIHARA 10,4D - 10 m/s - TI = 10%
Normalized Power
1
0.9
0.8
0.7
0.6
0.5
1
2
3
4
5
6
7
Normalized Power
Ref. dw=2º
Ref. dw=10º
Ref. dw=20º
Ref. dw=30º
Wake ±1º
Wake ±5º
Wake ±10º

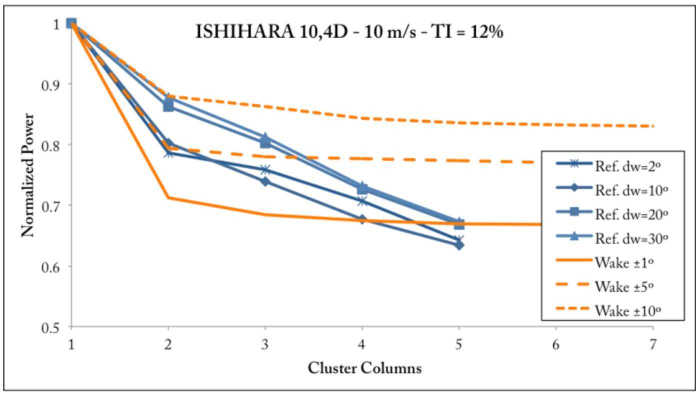
ISHIHARA 10,4D - 10 m/s - TI = 12%
Normalized Power
1
0.9
0.8
0.7
0.6
0.5
1
2
3
4
5
6
7
Cluster Columns
Ref. dw=2º
Ref. dw=10º
Ref. dw=20º
Ref. dw=30º
Wake ±1º
Wake ±5º
Wake ±10º

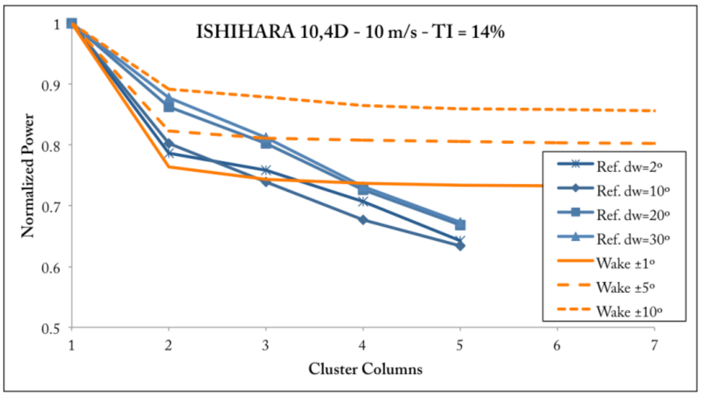
ISHIHARA 10,4D - 10 m/s - TI = 14%
Normalized Power
1
0.9
0.8
0.7
0.6
0.5
1
2
3
4
5
6
7
Cluster Columns
Ref. dw=2º
Ref. dw=10º
Ref. dw=20º
Ref. dw=30º
Wake ±1º
Wake ±5º
Wake ±10º

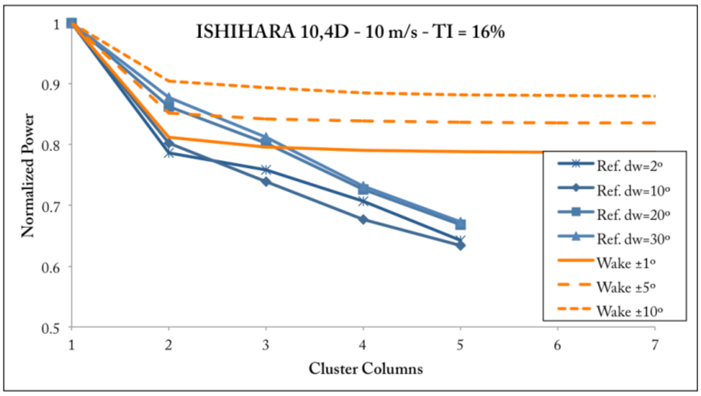
ISHIHARA 10,4D - 10 m/s - TI = 16%
Normalized Power
1
0.9
0.8
0.7
0.6
0.5
1
2
3
4
5
6
7
Cluster Columns
Ref. dw=2º
Ref. dw=10º
Ref. dw=20º
Ref. dw=30º
Wake ±1º
Wake ±5º
Wake ±10º

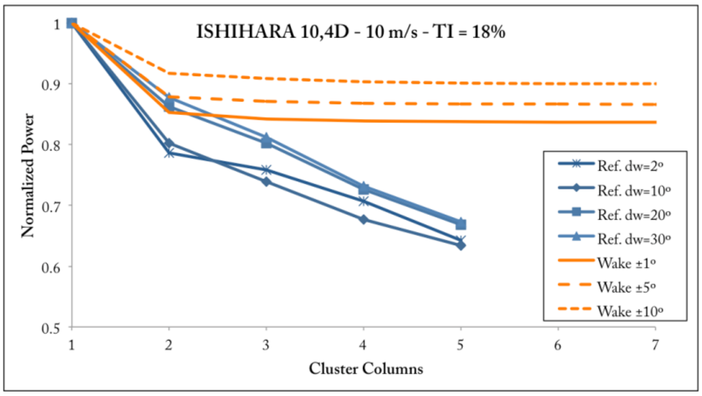
ISHIHARA 10,4D - 10 m/s - TI = 18%
Normalized Power
1
0.9
0.8
0.7
0.6
0.5
1
2
3
4
5
6
7
Cluster Columns
Ref. dw=2º
Ref. dw=10º
Ref. dw=20º
Ref. dw=30º
Wake ±1º
Wake ±5º
Wake ±10º

Annex IX – Power Deficit at the 1st turbine downwind

For the results at 6 m/s see Section 12.1.

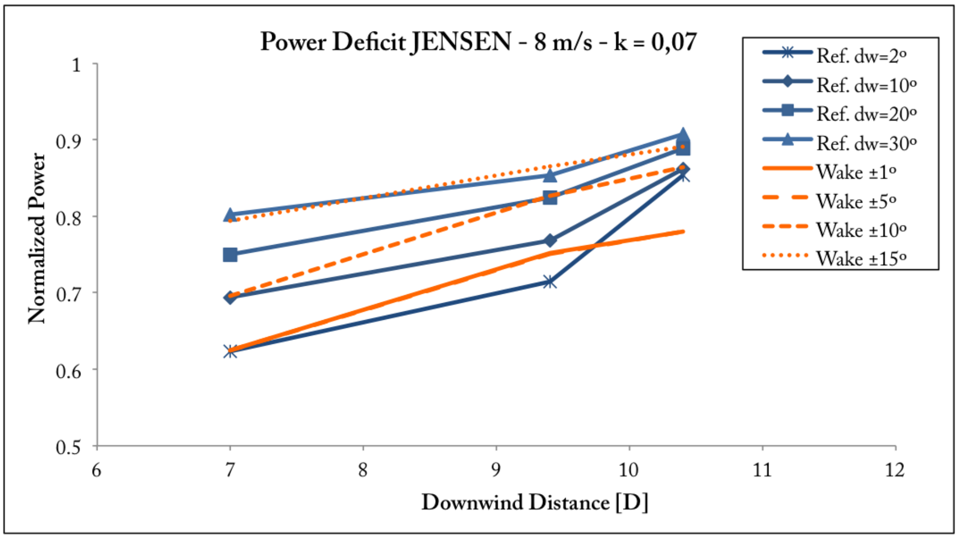

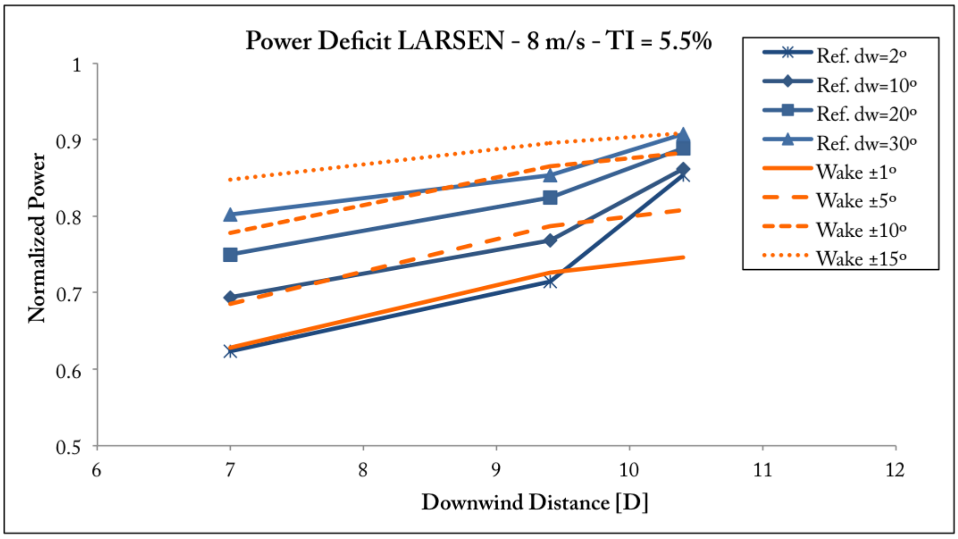

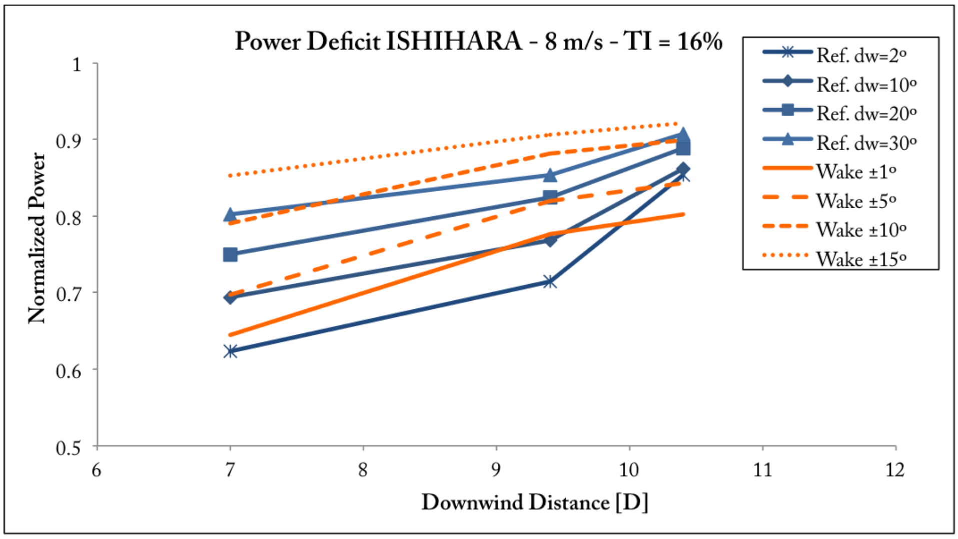

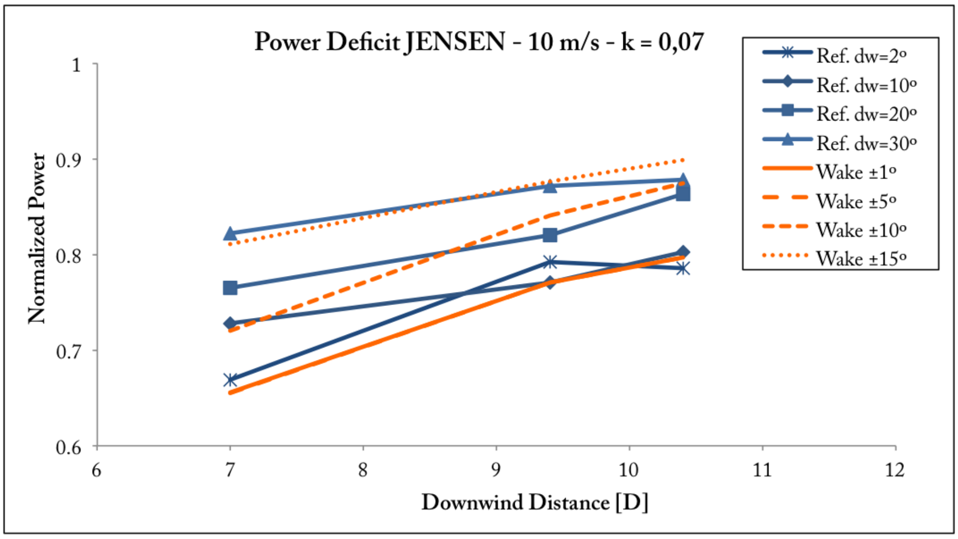
Power Deficit JENSEN - 10 m/s - k = 0,07
Normalized Power
1
0.9
0.8
0.7
0.6
6
7
8
9
10
11
12
Downwind Distance [D]
Ref. dw=2º
Ref. dw=10º
Ref. dw=20º
Ref. dw=30º
Wake ±1º
Wake ±5º
Wake ±10º
Wake ±15º

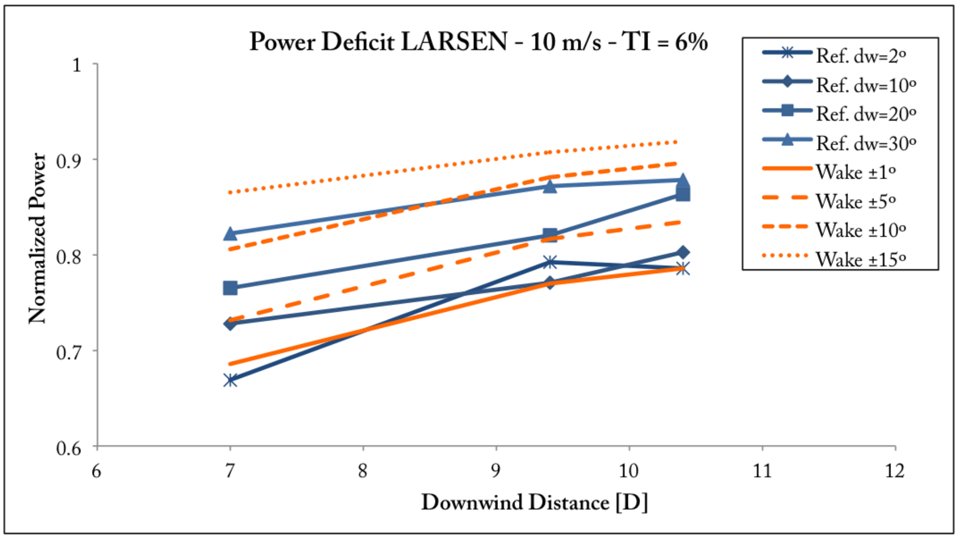
Power Deficit LARSEN - 10 m/s - TI = 6%
Normalized Power
1
0.9
0.8
0.7
0.6
6
7
8
9
10
11
12
Downwind Distance [D]
Ref. dw=2º
Ref. dw=10º
Ref. dw=20º
Ref. dw=30º
Wake ±1º
Wake ±5º
Wake ±10º
Wake ±15º

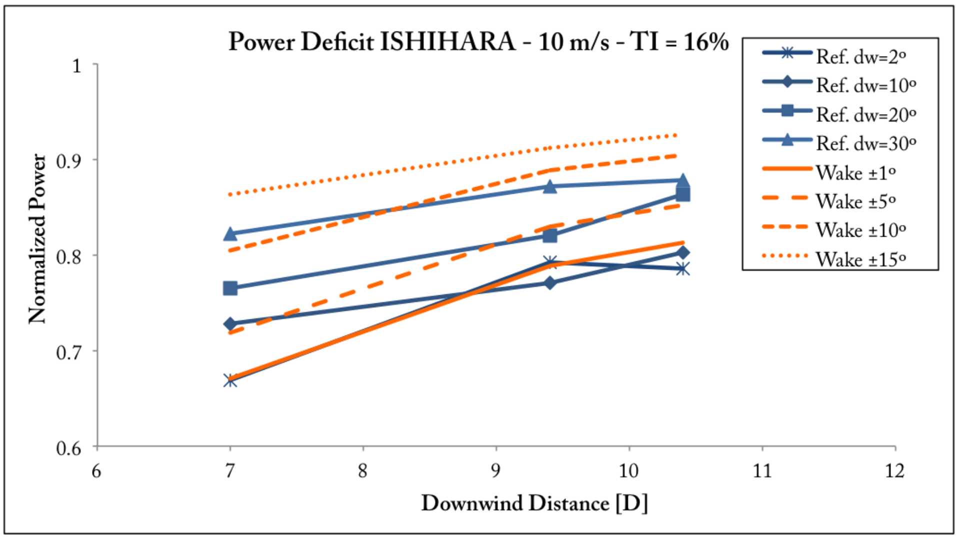
Power Deficit ISHIHARA - 10 m/s - TI = 16%
Normalized Power
1
0.9
0.8
0.7
0.6
6
7
8
9
10
11
12
Downwind Distance [D]
Ref. dw=2º
Ref. dw=10º
Ref. dw=20º
Ref. dw=30º
Wake ±1º
Wake ±5º
Wake ±10º
Wake ±15º

Annex X – Simulated and experimental vertical wind profiles at Bockstigen

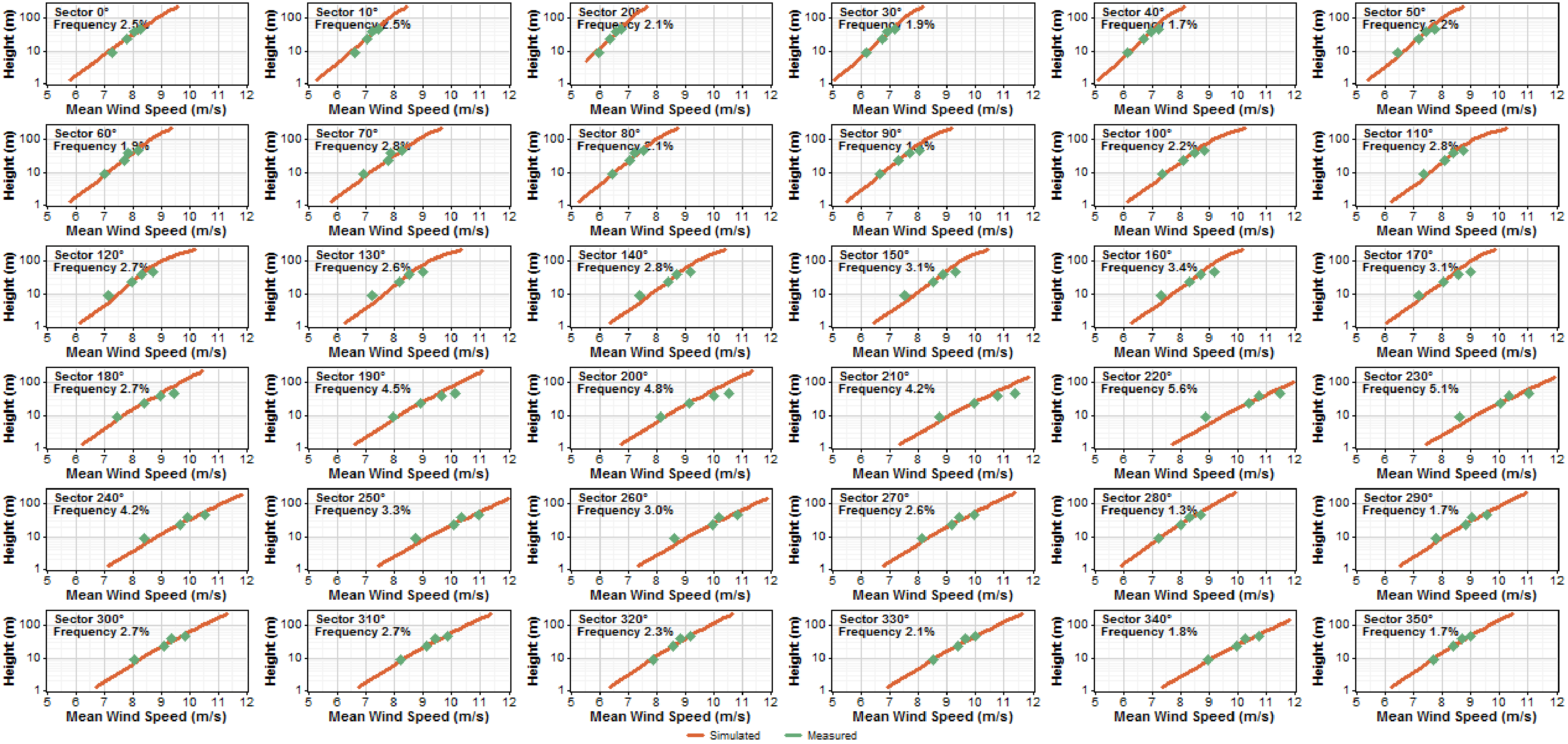

Figure 94. Vertical wind profiles plotted on a logarithmic chart for 36 sectors at Havsmast. Green dots show anemometer measurements and orange line the wind profile simulated using WindSim. Sea roughness: 0,0002 m. Neutral atmosphere.

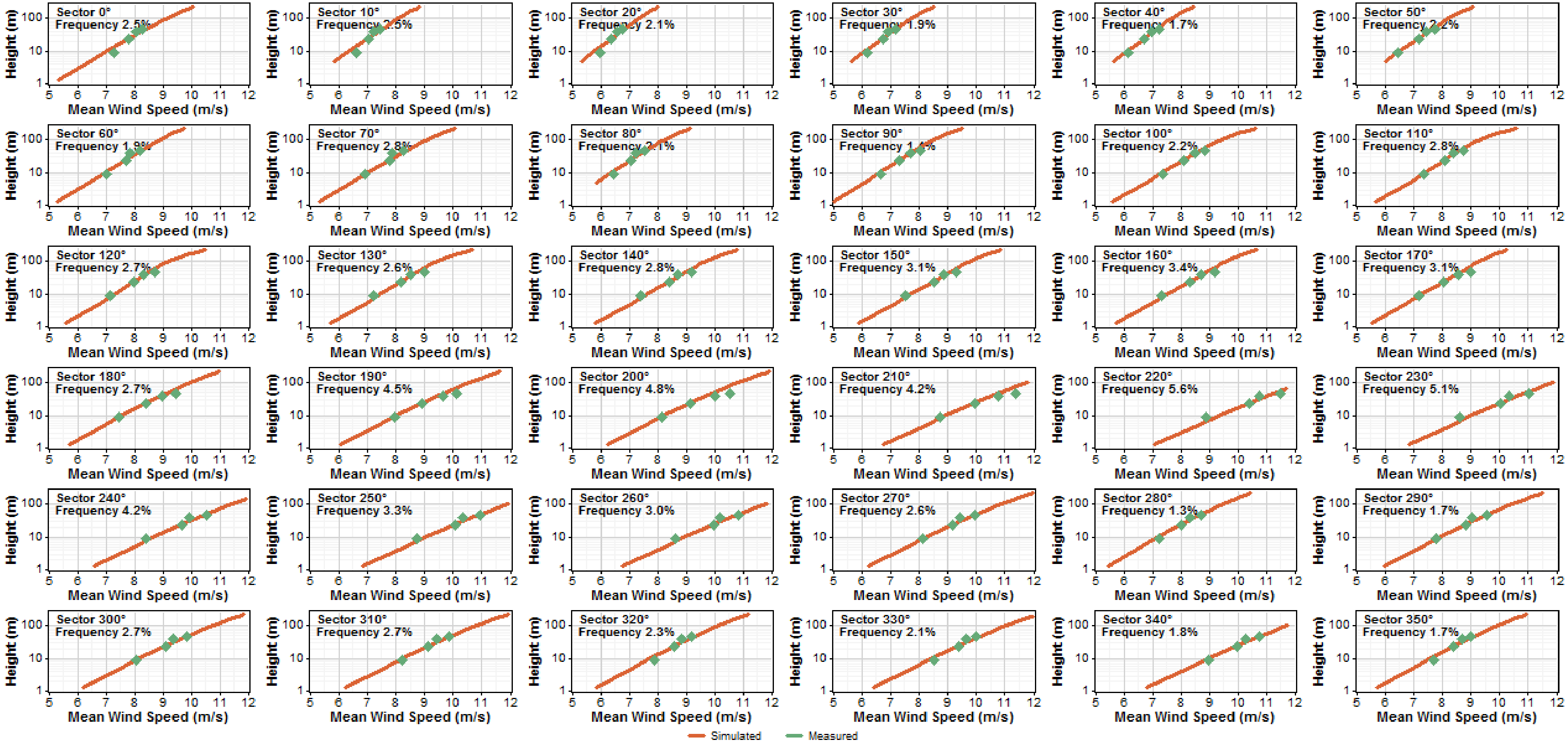

Figure 95. Vertical wind profiles plotted on a logarithmic chart for 36 sectors at Havsmast. Green dots show anemometer measurements and orange line the wind profile simulated using WindSim. Sea roughness: 0,002 m. Neutral atmosphere.